

**Systems metabolic engineering
upgrades *Corynebacterium glutamicum*
to selective high-level production of
the L-lysine derivatives
L-pipecolic acid and 5-aminovalerate**

Dissertation

Zur Erlangung des Grades

Der Doktorin der Naturwissenschaften

Der Naturwissenschaftlich-Technischen Fakultät

Der Universität des Saarlandes

von

Sarah Pauli

Saarbrücken

2023

Tag des Kolloquiums:	26. Januar 2024
Dekan:	Prof. Dr. Ludger Santen
Berichterstatter 1:	Prof. Dr. Christoph Wittmann
Berichterstatter 2:	Prof. Dr. Andriy Luzhetskyy
Vorsitz:	Prof. Dr. Uli Kazmaier
Akad. Mitarbeiter:	Dr. Markus Neuber

Publications

Partial results of this work have been published previously. This was authorized by the Institute of System Biotechnology (Saarland University), represented by Prof. Dr. Christoph Wittmann.

Peer-reviewed articles

Rohles CM*, **Pauli S***, Giesselmann G, Kohlstedt M, Wittmann C (2022). Systems metabolic engineering of *Corynebacterium glutamicum* eliminates all by-products for selective and high-yield production of the platform chemical 5-aminovalerate. *Metab. Eng.* **73**: 168-181. DOI: 10.1016/j.ymben.2022.07.005

*contributed equally

Pauli S, Kohlstedt M, Lamber J, Weiland F, Becker J, Wittmann C (2023). Systems metabolic engineering upgrades *Corynebacterium glutamicum* to selective high-level production of the chiral drug precursor and cell-protective extremolyte L-pipecolic acid. *Metab. Eng.* **77**: 100-117. DOI: 10.1016/j.ymben.2023.03.006

Patent application

Wittmann, C, **Pauli S**, Kohlstedt M (2023). Methods For Producing L-Pipecolic Acid. EP23159532.

Conference contributions

Pauli S, Rohles CM, Giesselmann G, Kohlstedt M, Becker J, Wittmann C (2020). Systems metabolic engineering of *Corynebacterium glutamicum* for the production of L-lysine derived chemicals. March 2020, 6th Joint Conference of the DGHM & VAAM – 72nd Annual Meeting of the DGHM & Annual Meeting of the VAAM, Leipzig, Germany.

Pauli S, Rohles CM, Gläser L, Kohlstedt M, Giesselmann G, Pearson S, del Campo A, Becker J, Wittmann C (2020). Systems metabolic engineering of *Corynebacterium glutamicum* for the production of L-Lysine derived carbon five chemicals. September 2020, German Conference on Synthetic Biology -The 4th GASB, online, Germany.

Pauli S, Kohlstedt M, Lamber J, Weiland F, Becker J, Wittmann C (2023). Selective high-level production of the chiral drug precursor and cell-protective extremolyte L-pipecolic acid by metabolically engineered *Corynebacterium glutamicum*. June 2023, The Metabolic Engineering Conference (ME15), Singapore.

Danksagung

Vorweg möchte ich mich bei Herrn Prof. Dr. Christoph Wittmann für die herzliche und wissenschaftlich hochwertige Betreuung bedanken. Danke, dass ich an einem so spannenden Projekt arbeiten durfte und die Chance bekommen habe, unser Institut vor anderen Wissenschaftlern zu vertreten. Vielen Dank für lobende aber auch mutmachende Worte, kreative Interpretationen von missglückten Versuchen und angenehme private Gespräche. Danke für deine Unterstützung. Ein herzliches Dankeschön auch an Frau Dr. Judith Becker. Du hast mit deiner exzellenten Forschung nicht nur den Grundstein für dieses Projekt gelegt, sondern mir auch immer wieder mit wertvollen Ratschlägen, besonders bei den Enzymassays, zur Seite gestanden und mir damit Mut gemacht, nicht aufzugeben.

Herrn Prof. Dr. Andriy Luzhetskyy danke ich für die Anfertigung des Zweitgutachtens meiner Arbeit. Vielen Dank auch an das restliche Prüfungskomitee für die Übernahme von Prüfungsvorsitz sowie akademischen Beisitz.

Danke an das ganze iSBio für hilfreiche Tipps im Labor, gute Gespräche und eine angenehme Arbeitsatmosphäre. Ein großes Dankeschön geht an Frau Susanne Haßdenteufel für unkonventionelle Lösungen bei dringenden Bestellungen sowie Gespräche fernab der Laborwelt. Vielen Dank auch an Herrn Dr. Michael Kohlstedt für die Unterstützung bei den Fermentationen und Herrn Michel Fritz für geduldige Stunden zur gemeinsamen Etablierung von Messmethoden. Großes Danke auch an Fabia, Jens und Lukas. Danke, dass ihr nicht nur eure Expertise mit mir geteilt habt, sondern auch großartige Begleiter auf Dienstreisen und Stadtfesten wart. Herzlichen Dank auch an meine drei Bachelor-Studentinnen Jessica Lamber, Margaux Mager und Annalena Sommer. Danke auch an Herrn PD Dr. Michael Hutter für die enzymatischen Modellierungen.

Zuletzt ein herzliches Dankeschön an meine Familie, ihr wart immer da und habt an mich geglaubt. Danke!

Table of contents

Summary	IX
Zusammenfassung	X
1 Introduction	1
1.1 General introduction	1
1.2 Main Objectives	4
2 Theoretical background	5
2.1 <i>Corynebacterium glutamicum</i> as industrial work horse	5
2.1.1 Central carbon metabolism and branching-off synthetic pathways.....	6
2.1.2 Systems metabolic engineering strategies	9
2.1.3 Metabolically engineered <i>C. glutamicum</i> as industrial cell factory.....	16
2.1.4 Fermentative production of the amino acid L-lysine.....	18
2.2 L-lysine derivatives as value-added products	23
2.2.1 5-Aminovalerate - a L-lysine degradation intermediate and its application	26
2.2.2 Applications and biosynthesis of the L-lysine derivative L-pipecolic acid	29
3 Materials and Methods	34
3.1 Microorganisms, genes, and plasmids	34
3.2 Genetic engineering	38
3.2.1 Plasmid-based operons for L-pipecolic acid production.....	40
3.2.2 Integrative genetic modules for L-pipecolic acid production	43
3.2.3 Integrative genetic module for 5-aminovalerate production.....	44
3.2.4 Generation of synthetic promoter variants for fine-tuned gene expression ...	45
3.3 Media.....	45
3.3.1 Batch medium.....	45
3.3.2 Fed-batch medium.....	46
3.4 Cultivation.....	47

3.4.1 Cultivation in miniaturized microtiter plate system	47
3.4.2 Cultivation in lab scale bioreactors	48
3.5 Analytics	49
3.5.1 Quantification of cell concentration	49
3.5.2 Quantification of substrates and extracellular products	49
3.5.3 Extraction and quantification of intracellular intermediates.....	50
3.5.4 GC-MS analysis of L-pipecolic acid	51
3.5.5 Analysis of enzymatic activities.....	51
3.5.6 Extraction and quantification of redox metabolites	53
3.5.7 Global gene expression analysis using DNA microarray	53
4 Results and Discussion	55
4.1 Metabolic engineering at the level of product secretion exemplary using 5-aminovalerate producing strains	55
4.1.1 Construction and evaluation of export mutants	56
4.1.2 Monitoring intracellular amino acid availability in the producing strains.....	58
4.2 Harnessing of the L-lysine 6-dehydrogenase route for L-pipecolic acid production.	60
4.2.1 Construction and analysis of a basic L-pipecolic acid producer.....	61
4.2.2 Transcriptional analysis of <i>C. glutamicum</i> PIA-1A	63
4.2.3 Metabolome analysis of <i>C. glutamicum</i> PIA-1A.....	65
4.2.4 Evaluation of alternative heterologous expression strategies.....	67
4.2.5 L-lysine 6-dehydrogenase displays a major metabolic bottleneck.....	69
4.3 Evaluation of pathway alternatives for L-pipecolic acid biosynthesis.....	80
4.4 Systems metabolic engineering of <i>C. glutamicum</i> PIA-7	84
4.4.1 L-lysine 6-aminotransferase exhibits high catalytic efficiency <i>in vivo</i>	85
4.4.2 PIA-7 exhibits optimal redox supply.....	85
4.4.3 Metabolic engineering of product transport.....	86
4.5 High-level fed-batch production of L-pipecolic acid	88
4.5.1 Optimization of process conditions	88

4.5.2 Fed-batch process of <i>C. glutamicum</i> PIA-7	90
4.6 Fine-tuning of <i>lat</i> expression towards maximized production	93
4.6.1 Native promoter replacement for <i>lat</i> expression	93
4.6.2 Synthetic promoter variants enhance productivity	94
4.6.3 Benchmarking <i>C. glutamicum</i> PIA-10B in a fed-batch process	96
5 Conclusion and Outlook	100
6 Appendix.....	107
6.1 Abbreviations and symbols.....	107
6.2 Molecular tools	116
6.3 Supplementary data	122
7 References	135

Summary

The non-proteinogenic amino acid L-pipecolic acid (PIA) plays a crucial role in both plant-acquired immunity and cellular protection and exhibits commercial potential as agrochemical and chiral precursor for a variety of pharmaceuticals. Historically, fossil resources have served as the primary source for this molecule. Towards improved sustainability, however, bio-based production routes from renewable raw materials are desired. Biosynthetically, PIA is derived via the L-lysine pathway, suggesting L-lysine producing *Corynebacterium glutamicum* as promising cellular factory.

Leveraging the principles of systems metabolic engineering, the L-lysine-hyperproducer *C. glutamicum* LYS-12 was successively optimized to enable PIA biosynthesis. First producers, based on incorporating the heterologous L-lysine 6-dehydrogenase pathway from *Ruegeria pomeroyi*, however, failed to efficiently provide the desired product. Comprehensive systems biology analyses then revealed a general incompatibility between the cellular environment and the demand of the pivotal enzyme within the foreign pathway.

Out of several alternatives, the integration of the L-lysine 6-aminotransferase pathway from *Flavobacterium lutescens* enabled a breakthrough in performance, culminating in an impressive L-pipecolic acid yield of 0.562 mol mol⁻¹. The finally created strain, *C. glutamicum* PIA-10B, comprising all beneficial changes, generated 93 g L⁻¹ PIA via a glucose-based fed-batch process.

Zusammenfassung

Die nicht-proteinogene Aminosäure L-Pipecolinsäure (PIA) spielt sowohl bei der Pflanzenimmunität als auch beim Zellschutz eine entscheidende Rolle und hat ein kommerzielles Potenzial als Agrochemikalie und chirale Vorstufe für eine Vielzahl an Arzneimitteln. Bislang dienten fossile Ressourcen als Hauptquelle für dieses Molekül. Im Sinne einer verbesserten Nachhaltigkeit werden biobasierte Produktionswege aus erneuerbaren Rohstoffen angestrebt. Biosynthetisch wird PIA über den L-Lysin-Weg gewonnen, weshalb das L-Lysin produzierende Bakterium *Corynebacterium glutamicum* als vielversprechende zelluläre Fabrik erscheint.

Mittels Systems Metabolic Engineering wurde der L-Lysin-produzierende Stamm *C. glutamicum* LYS-12 sukzessive für die PIA-Biosynthese optimiert. Erste Produzenten, die den heterologen L-Lysin 6-Dehydrogenase-Stoffwechselweg aus *Ruegeria pomeroyi* exprimierten, konnten das gewünschte Produkt jedoch nicht effizient herstellen. Systembiologische Analysen zeigten eine generelle Inkompatibilität zwischen der zellulären Umgebung und dem Bedarf des zentralen Enzyms im fremden Stoffwechselweg.

Unter mehreren Alternativen ermöglichte die Integration des L-Lysin 6-Aminotransferase-Stoffwechsels aus *Flavobacterium lutescens* eine massive Steigerung der Produktion bis zu einer PIA-Ausbeute von $0.562 \text{ mol mol}^{-1}$. Die Zellfabrik *C. glutamicum* PIA-10B, die alle vorteilhaften Veränderungen enthielt, erzeugte 93 g L^{-1} PIA in einem glukosebasierten Fed-Batch-Verfahren.

1 Introduction

1.1 General introduction

The concept of green and sustainable industry resonates deeply, particularly as escalating costs associated with environmentally detrimental extraction and processing, coupled with the dwindling reserves of fossil resources, stand in stark contrast to the holistic utilization of renewable raw materials (Kohlstedt et al, 2022; Becker et al, 2013a). Bio-based processes not only present healthier alternatives for both human well-being and the environment but also facilitate the targeted syntheses of optically pure molecule that find applications in pharmaceuticals and cosmetics (Wolf et al, 2021). Contributing to a more favorable carbon footprint (Nielsen et al, 2019), biotechnological production pathways liberate themselves from the volatility of fossil resource pricing and processing, thereby mitigating their impact on the environment (Rohles et al, 2018).

Among the successes within the realm of biotechnology, the production of valuable molecules using the extensively studied soil bacterium *Corynebacterium glutamicum* stand out as a prominent example (Wittmann & Becker, 2007). Originally isolated seven decades ago during the pursuit of L-glutamate producing strains (Kinoshita et al, 2004), the repertoire of products has steadily expanded over time, owing much to strategies that integrate systems and synthetic biology with genetic engineering and editing tools (Becker & Wittmann, 2019b). This expansion has been driven by a continuous influx of new tools and methodologies, ranging from sequencing techniques (Pfeifer-Sancar et al, 2013) and omics approaches (Becker & Wittmann, 2018; Zha et al, 2023), to precise chromatography and spectrometry methods (Kiefer et al, 2004; Mohd Kamal et al, 2022), and even *in silico* pathway prediction and design (Krömer et al, 2006), all of which provide comprehensive insights into cellular processes and enable tailored engineering.

The synthesis of the essential amino acid L-lysine stands as a monumental biotechnological achievement (Eggeling & Bott, 2015; Wittmann & Becker, 2007). Systematically engineered cell factories, exemplified by *C. glutamicum* LYS-12 have now reached an economically viable stage in the production of this molecule (Becker et al, 2011; Becker et al, 2018b), surpassing a global annual output of two million metric tons (Cheng et al, 2018a; Ikeda, 2017). Sustainable carbon sources such as lignocellulose (Buschke et al, 2013a) and mannitol enriched algae (Hoffmann et al, 2018) have emerged as alternatives to glucose derived from food crops, thereby enhancing the sustainability of the process (Prasad & Ingle, 2019).

Beyond its direct utilization as a feed and food additive, L-lysine has garnered significant interest in the form of derivatives. Compounds like 1,5-diaminopentane (Kind et al, 2010), glutarate (Rohles et al, 2018) and 5-aminovalerate (Rohles et al, 2016) contribute to the expanding landscape of bio-based building blocks for polymers. Notably, these biopolymers not only offer reduced carbon dioxide emission (Nielsen et al, 2019), benefiting environmental health, but also introduce novel material characteristics, effectively supplanting their petrochemical counterparts (Adkins et al, 2013; Rohles et al, 2018). Additionally, L-lysine serves as a valuable precursor for medically relevant molecules, including posttranslationally hydroxylated forms that play a role in stabilizing collagens (Herbert et al, 2012). Biotechnological synthesis routes allow for creation of isoforms not found in nature, opening avenues beyond collagen therapies (Shetty et al, 2009; Hara et al, 2017; Prell et al, 2022; Mager, 2022).

Meanwhile, the L-lysine derivative L-pipecolic acid serves as drug precursor (Roura Padrosa et al, 2020), a disease indicator (Mihalik et al, 1989), a cell protectant (Gouffi et al, 2000; Perez-Garcia et al, 2019), and a pivotal player in the systemic acquired resistance of plants (Shan & He, 2018), offering potential as a chemical priming agent (Westman et al, 2019).

Although 1,5-diaminopentane and glutarate can be obtained with reasonable yields (Buschke et al, 2011; Rohles et al, 2018), the conversion efficiency of L-lysine into other derivatives like 5-aminovalerate and L-pipecolic acid remains modest (Rohles et al, 2016; Perez-Garcia et al, 2017). Consequently, there is a pressing need to enhance the biotechnological routes to achieve higher yields and titers, ultimately enabling the long-term substitution of chemically derived molecules.

1.2 Main Objectives

The central objective of this project was to construct an enhanced microbial cell factory derived from *C. glutamicum*, specialized for the efficient and selective production of L-pipecolic acid. The L-lysine producer *Corynebacterium glutamicum* LYS-12 should be taken the starting point.

To realize *de novo* L-pipecolic acid production via *Corynebacterium glutamicum* LYS-12 as the host, a comprehensive range of techniques was to be established and harnessed. The construction, analysis, and further refinement of L-pipecolic acid producing strains were driven primarily by the distinct characteristics of enzymes involved. The foundational step encompassed the incorporation of designed biosynthetic modules into the L-lysine hyperproducing strain LYS-12, expressing various enzymes responsible for L-lysine conversion into L-pipecolic acid. A holistic understanding of the strains should be obtained through an integration of transcriptomic, metabolomic, and proteomic insights, thereby delineating the state of the most promising L-pipecolic acid producing strain and guiding further optimization.

Ultimately, the best created producers should be benchmarked in fed-batch production processes to evaluate and compare their potential.

2 Theoretical background

2.1 *Corynebacterium glutamicum* as industrial work horse

The gram positive soil bacterium *Corynebacterium glutamicum* (*C. glutamicum*) was isolated almost 70 years ago, when screening for natural L-glutamate producers (Fig. 1) (Kinoshita et al, 2004; Kalinowski et al, 2003).

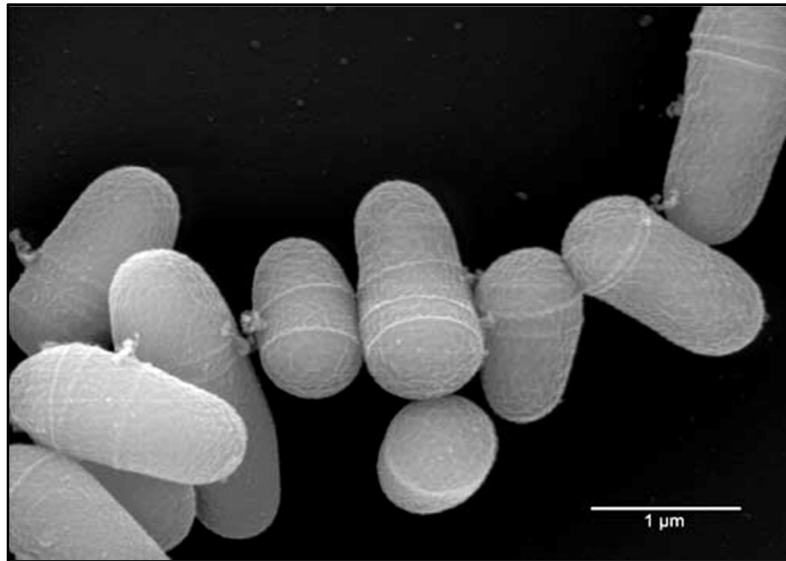


Fig. 1: Scanning electron microscope picture of *C. glutamicum* ATCC 13032 (Wittmann & Becker, 2007).

The microbe exhibits a short rod-like morphology. It is non-endotoxic and non-sporulating and has been therefore certified as “Generally Recognized As Safe” (GRAS) organism (Wolf et al, 2021). *C. glutamicum* is fully sequenced and is well accessible for genetic modification (Ikeda & Nakagawa, 2003; Kalinowski et al, 2003), allowing tailored metabolic engineering strategies (Kirchner & Tauch, 2003; Sahm et al, 1995). Its flexible metabolism, high robustness, genomic accessibility, and genetic stability has made *C. glutamicum* one of the most important chassis strains in industrial biotechnology (Nakamura et al, 2003). Over the years, systems metabolic engineering approaches that integrate efficient genomic engineering tools with systems biology and computational modeling and simulation has provided a range of high-efficiency *C. glutamicum* cell factories for industrial application, traditionally providing amino acids, but meanwhile almost hundred compounds of commercial interest (Becker et al, 2018b; Becker & Wittmann, 2012b).

2.1.1 Central carbon metabolism and branching-off synthetic pathways

Today, the sugars glucose, sucrose and fructose, derived from starch hydrolysates and molasses, respectively, are still more widely used for production than second and third generation feedstocks and therefore display important industrial substrates of *C. glutamicum* (Anaya-Reza & Lopez-Arenas, 2017). The uptake of glucose into the cell is mediated by phosphoenolpyruvate-dependent phosphotransferase (PTS) systems (Xu et al, 2019b), as well as, in certain isolates, ATP-dependent permeases and glucokinases (Moon et al, 2007). However, fructose and sucrose are exclusively assimilated by PTS transporters (Ikeda, 2012). All three sugars differ in the yield for certain products, (Georgi et al, 2005), due to different points of entry into metabolism and different pathway use (Kiefer et al, 2004) (Fig. 2).

During transport, the sugars are activated by phosphorylation, resulting in glucose 6-phosphate (glucose), fructose 1-phosphate and fructose 6-phosphate (fructose), and sucrose 6-phosphate (sucrose). Subsequently, the phosphorylated intermediates enter the central catabolism, comprising the Emden-Meyerhof-Parnas (EMP) pathway, the pentose phosphate (PP) pathway, the tricarboxylic acid (TCA) cycle and the glyoxylate shunt as the major routes (Fig. 2) (Wittmann & Becker, 2007; Kalinowski et al, 2003). Herby, the oxidative part of the PP pathway supplies NADPH, (Sahm et al, 2000) which involves glucose 6-phosphate dehydrogenase and 6-phosphogluconate dehydrogenase (Moritz et al, 2000). This pathway has shown relevance to overproduce different amino acids demanding for efficient supply of NADPH. As example, the biosynthesis of one molecule of L-lysine biosynthesis requires four molecules of NADPH (Moritz et al, 2002). In addition, NADPH is supplied by the TCA cycle enzymes isocitrate dehydrogenase (Chen & Yang, 2000) and malic enzyme (Gourdon et al, 2000). In addition, the PP pathway mediates the breakdown of specific sugars and provides anabolic building blocks for nucleotides (Kamada et al, 2003), vitamins, and other essential intermediates (Ikeda & Katsumata, 1999; Stincone et al, 2015). Carbon from the PP pathway is partially channeled back to the EMP route, for further breakdown. In a stepwise manner, a set of

EMP pathway enzymes then yields the three-carbon intermediate pyruvate, which is further metabolized within TCA cycle, while generating energy, FADH, and NADH (Sahm et al, 2000). Alternatively, pyruvate is carboxylated to oxaloacetate (Bott, 2007). This anaplerotic route provides anabolic precursors to fuel different biosynthetic pathways (Wittmann & Becker, 2007; Sahm et al, 2000). Within the TCA cycle, oxaloacetate and α -ketoglutarate display important anabolic intermediates (Sheng et al, 2021). Depending on the carbon source, e. g. during growth on acetate, the glyoxylate shunt contributes to the anaplerotic supply of the TCA cycle (Gerstmeir et al, 2003; Wendisch et al, 1997). The shunt involves the two enzymes isocitrate lyase and malate synthase, by-passing the formation of α -ketoglutarate and succinyl-CoA (Yang et al, 2022). The three metabolic nodes around acetyl-CoA, phosphoenolpyruvate-pyruvate-oxaloacetate, and α -ketoglutarate are important with regard to the allocation of flux and metabolic control (Sauer & Eikmanns, 2005; Sheng et al, 2021). The nodes offer flexibility and may redirect carbon flux towards EMP pathway and gluconeogenesis via different decarboxylation reactions (Wittmann & Becker, 2007; Yang et al, 2022), catalyzed by malic enzyme (Gourdon et al, 2000), phosphoenol-pyruvate carboxykinase (Riedel et al, 2001), and oxaloacetate decarboxylase (Klaffl & Eikmanns, 2010; Kappelmann et al, 2020). The cyclic linkage of the different carboxylating and decarboxylating enzymes can be used by the cell to balance the ATP level (Wittmann & Becker, 2007). At various stages, the central catabolism branches off into anabolic pathways (Wittmann et al, 2004a).

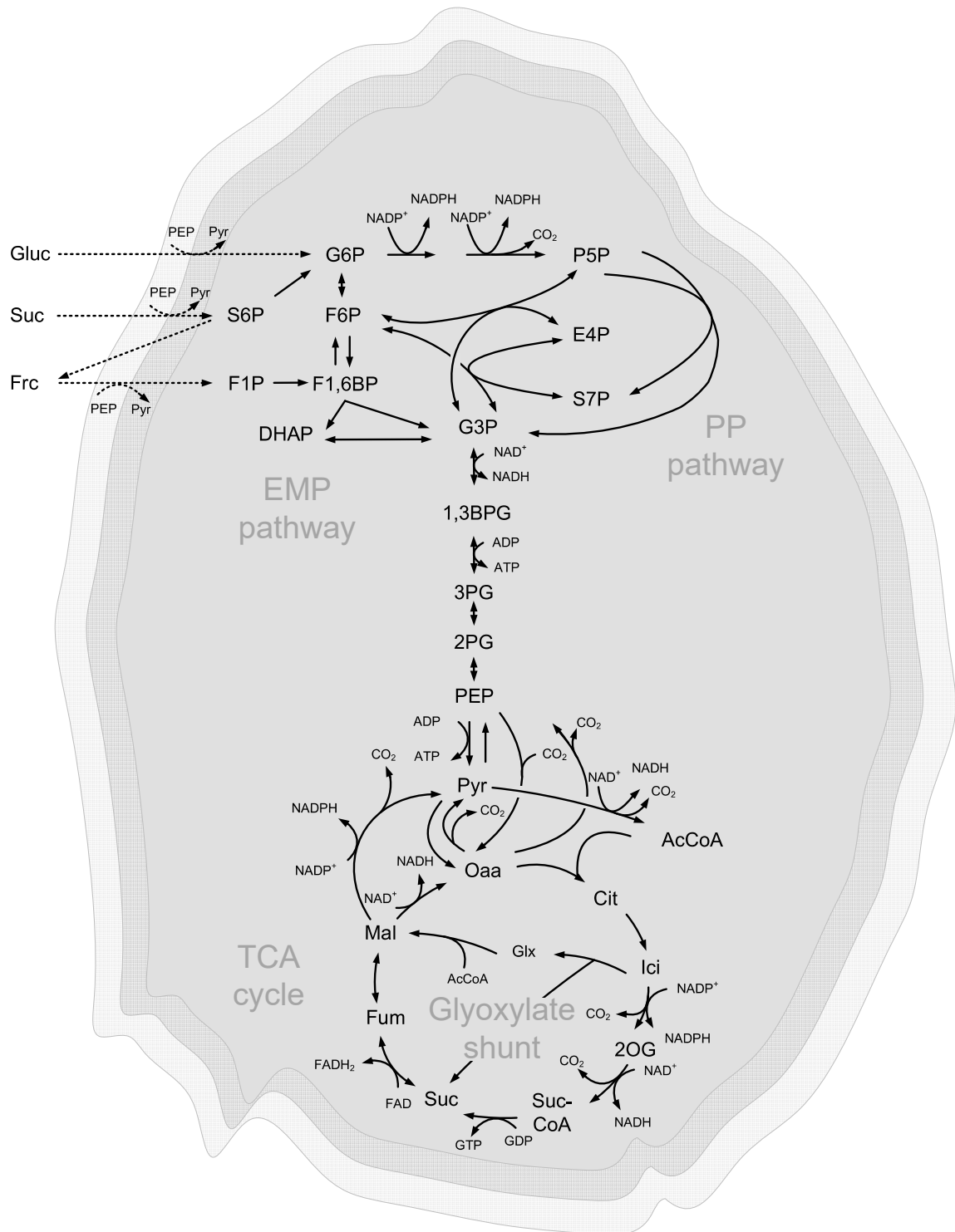


Fig. 2: Central carbon metabolism of *C. glutamicum*. The sugars glucose (gluc), sucrose (suc) and fructose (frc) are channeled into the central carbon metabolism which comprises the Emden-Meyerhof-Parnas (EMP) pathway, the pentose phosphate (PP) pathway, the tricarboxylic acid (TCA) cycle and the glyoxylate shunt as major routes. G6P: Glucose 6-phosphate; P5P: Pentose 5-phosphate; F6P: Fructose 6-phosphate; F1P: Fructose 1-phosphate; F1,6BP: Fructose 1,6-bisphosphate; E4P: Erythrose 4-phosphate; S7P: Sedoheptulose 7-phosphate; DHAP: Dihydroxyacetone phosphate; G3P: Glyceraldehyde 3-phosphate; 1,3BPG: 1,3-bisphosphoglycerate; 3PG: 3-phosphoglycerate; 2PG: 2-phosphoglycerate; PEP: Phosphoenolpyruvate; Pyr: Pyruvate; Oaa: Oxaloacetate; AcCoA: Acetyl coenzyme A; Cit: Citrate; Ici: Isocitrate; Glx: Glyoxylate; 2OG: 2-Oxoglutarate; Suc-CoA: Succinyl coenzyme A; Suc: Succinate; Fum: Fumarate; Mal: Malate. The figure was adapted from previous work (Moon et al, 2007; Tsuge & Yamaguchi, 2021; Litsanov et al, 2012; Kiefer et al, 2004).

Many of these anabolic routes can be harnessed to overproduce valuable compounds (Becker & Wittmann, 2015), such as amino acids and related derivatives (Kinoshita et al, 2004), organic acids (Briki et al, 2020), and fatty acids (Takeno et al, 2013), respectively. As example, pyruvate can be converted to L-alanine (Jojima et al, 2010) and L-valine (Hasegawa et al, 2013), respectively, but yields also organic acids such as D-lactate (Okino et al, 2008) and alcohols such as isobutanol (Smith et al, 2010). Moreover, TCA-cycle-based intermediates display important precursors to derive fatty acids (Takeno et al, 2013), carotenoids (Henke et al, 2018), as well as other amino acids and their derivatives (Becker & Wittmann, 2015). Prominent examples are L-lysine (Becker et al, 2011), L-glutamate (Guo et al, 2013), L-arginine (Park et al, 2014a; Zhao et al, 2022), and cadaverine (Kang & Choi, 2022; Kind et al, 2010).

2.1.2 Systems metabolic engineering strategies

Systems metabolic engineering is a comprehensive approach that integrates classical genetic and metabolic engineering tools with systems and synthetic biology as well as evolutionary engineering approaches (Fig. 3) (Becker & Wittmann, 2019b). The concept has strongly promoted the efficient and rapid development of high-performance cell factories (Ko et al, 2020). On the systems biology side, the analysis of the different omics layers allows to successively unravel the typically complex biological systems and gain valuable knowledge for their targeted optimization (Weighill et al, 2019). For the latter, sophisticated genomic approaches meanwhile allow genetic modification of microbial cells à la carte (Kim et al, 2023; Wang et al, 2021b; Nešvera & Pátek, 2011).

Systems biology of *C. glutamicum*

The whole genome of *C. glutamicum* ATCC13032 was sequenced 20 years ago using clone-by-clone method and the combination of cosmid and bacterial artificial chromosome libraries (Kalinowski et al, 2003). Hereby, overlaps between the obtained genetic fragments allowed complete genome mapping (Tauch et al, 2002) and yielded the complete circular genome structure with more than 3,300,000 base pairs. Different software based prediction tools and similarity analysis then predicted about 3000 protein-coding genes, providing a valuable source for further research (Ikeda & Nakagawa, 2003). To date, 3056 open reading frames have been identified in the microbe (Inui et al, 2007). With regard to transcriptomics, focus aiming at the analysis of the complete set of expressed RNA transcripts, profiling techniques such as microarrays, Northern blots, reverse-transcriptase qPCR and rapid amplification of cDNA ends provide accurate and streamlined approaches. RNA sequencing even tackles background and saturation effects, supporting the quantitative analysis of the transcripts but comes at higher costs and bioinformatic effort for data treatment (Pfeifer-Sancar et al, 2013). Consequently, these methods help to identify new sequence segments and their functions in *C. glutamicum*, and quantify the up- or downregulation of transcripts when comparing related strains and different culture conditions (Loos et al, 2001). RNA sequencing methods can be also used to identify transcriptional start sites, promoter regions, and other genetic elements replacing elaborative primer extension analysis and cDNA amplification techniques (Patek et al, 2003; Pfeifer-Sancar et al, 2013).

With regard to proteomics, global changes in protein expression can be monitored in bottom-up and top-down approaches offering e.g. insights into translational modifications such as phosphorylation, glycosylation, and N-terminal processing (Melo et al, 2023). The top-down approach involves dimensional gel electrophoreses and 2D-chromatography (Kendrick et al, 2019) (Hermann et al, 2000) to separate the protein fractions (Krömer et al, 2008). Further detection via peptide mass fingerprints (PMFs) with matrix-

assisted laser desorption ionization/time-of-flight mass spectrometry (MALDI-TOF-MS), electrospray ionization, tandem-mass spectrometry (ESI-MS/MS) (Encarnacion et al, 2005) provides high-throughput and high-resolution data sets from complex biological samples (Lohnes et al, 2016). Alternatively, smaller proteoforms below 30 kDa can be efficiently pre-fractionated by the combination of Gel-eluted Liquid Fraction Entrapment Electrophoresis (GELFrEE) and SDS-PAGE, followed by LC-MS/MS detection (Melo et al, 2023). In a recent approach quantitative proteomic analysis enabled the study of fatty acid ester surfactant triggered membrane proteins and by that highlighted the impact of proteome analysis on genetic engineering strategies (Jiang et al, 2020). Monitoring enzymes, which are part of the proteome, not only helps to understand strain performance (Giesselmann et al, 2019), and open up further optimization potential (Becker et al, 2011) but also creates valuable knowledge connections between proteins, metabolites, and pathway fluxes.

Metabolomics, i.e. the quantitative assessment of metabolite levels, is based on various high-resolution chromatography methods such as high-performance liquid chromatography tandem-mass spectrometry (HPLC-MS/MS), and gas chromatography mass spectrometry (GC-MS) and other technologies such as nuclear magnetic resonance (NMR) spectroscopy (Mohd Kamal et al, 2022) and specific enzymatic assays (Hoffmann et al, 2021). Specific sampling protocols avoid loss of the sensitive metabolites and have been found crucial to study the microbe accurately (Wittmann & Heinzle, 2001a; Bolten et al, 2007). Important applications examples have unraveled the redox state as response to oxidative stress (Krömer et al, 2008) and during growth on different substrates (Hoffmann et al, 2021). Moreover, metabolite levels displayed precursor supply under semi-anaerobic growth conditions (Goldbeck et al, 2021), reflect the impact of expression of enzymes on intermediates of biosynthetic pathways (Kind et al, 2011) and illustrated the effect of extracellularly supplied protective molecules (Jungmann et al, 2022).

Finally, ^{13}C metabolic flux (fluxome) analysis has proven most valuable to assess *C. glutamicum* (Becker & Wittmann, 2014; Becker & Wittmann, 2020b; Hoffmann et al, 2018). Hereby, the use of isotopic tracers yields complex ^{13}C labelling patterns in various cellular components which provide valuable information to assess the pathway fluxes (Becker & Wittmann, 2020b; Heinzle et al, 2008; Schwechheimer et al, 2018). Assuming steady-state of the metabolism, *in vivo* reaction rates can be calculated using a stoichiometric model and ^{13}C labelling information (Wittmann et al, 2004a; Wittmann et al, 2004b). This technology has allowed to unravel the pathway fluxes of *C. glutamicum* during growth on glucose (Kiefer et al, 2002; Kiefer et al, 2004), fructose (Kiefer et al, 2002; Kiefer et al, 2004), sucrose (Kiefer et al, 2002; Wittmann et al, 2004a), xylose (Buschke et al, 2013a), and mannitol (Hoffmann et al, 2018; Hoffmann et al, 2021), respectively, and compare different mutants during strain development (Wittmann & Heinzle, 2002; Hoffmann et al, 2018), extract carbon source related differences in metabolic networks (Buschke et al, 2013a), and study the response to stress conditions (Krömer et al, 2008; Becker et al, 2008).

Finally, also dry lab technologies have proven valuable to study the *C. glutamicum*, as example, computational modelling and stoichiometric network simulations were used to predict theoretical yields, metabolic bottlenecks, and superior pathways (Becker et al, 2007; Nielsen, 2017). Over the years, elementary flux mode analysis (Melzer et al, 2009) was used to design strains and pathway for the biosynthesis of L-methionine in *C. glutamicum* (Krömer et al, 2005), enhance the production of 1,5-diaminopentane from xylose (Buschke et al, 2013a), design a blueprint for strain engineering for high-level production of L-lysine from glucose (Becker et al, 2011) and understand pathway limitations for the production of L-lysine from mannitol (Hoffmann et al, 2018) and lignocellulose (Chen et al, 2019) in *C. glutamicum*. *In silico* computational tools further support the design of translation efficiency, e.g. in optimizing ribosomal binding sites, 5'-untranslated regions (UTR), and spacer sequences (Kim et al, 2023; Shi et al, 2018).

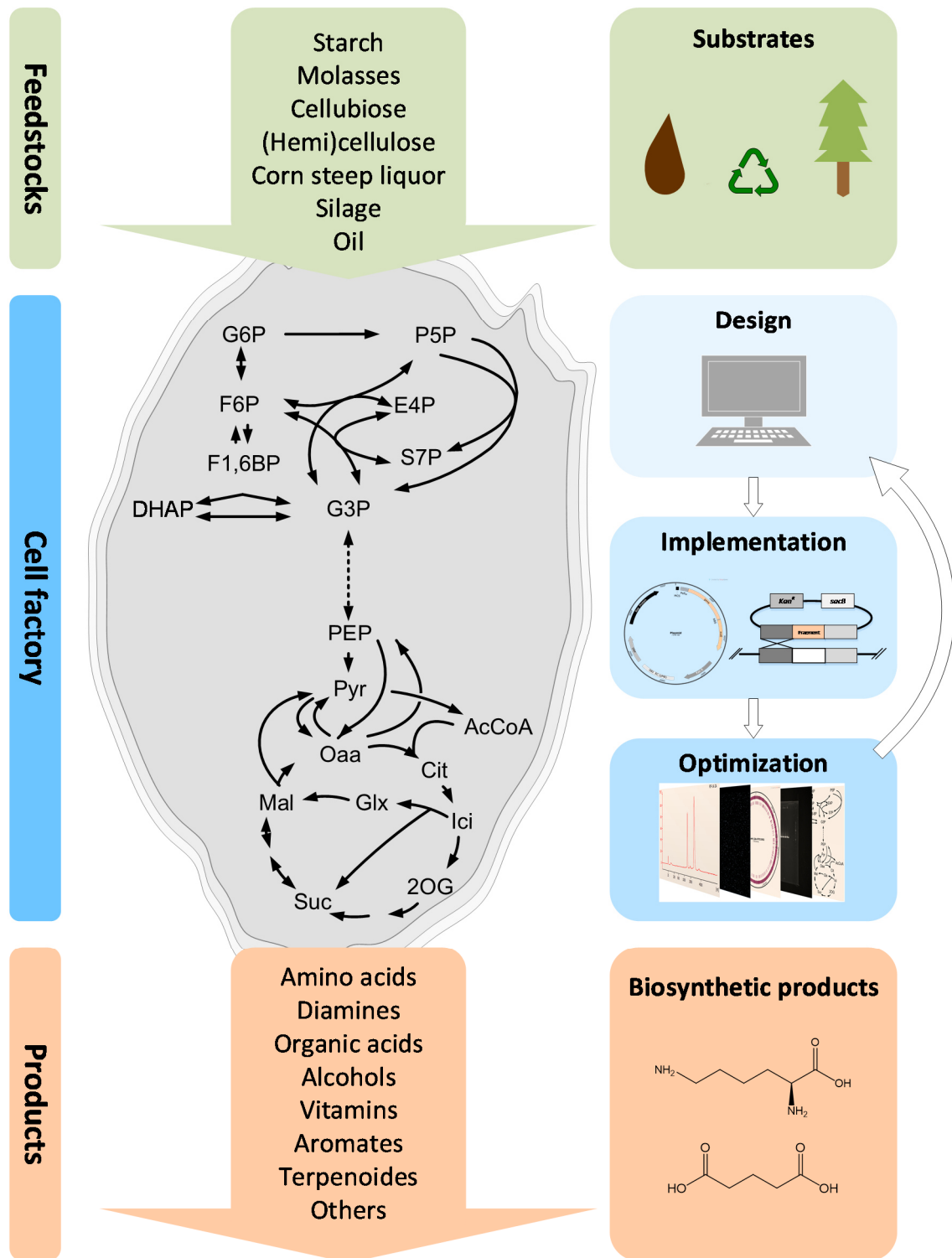


Fig. 3: Systems metabolic engineering of *Corynebacterium glutamicum* to produce biosynthetic molecules from sustainable feedstocks. The tailor-made cell factory was obtained using *in silico* pathway design tools and databases, genetic engineering techniques for DNA implementation and multi-omics analysis for the identification of further optimization targets, iteratively (white arrows). G6P: Glucose 6-phosphate; P5P: Pentose 5-phosphate; F6P: Fructose 6-phosphate; F1,6BP: Fructose 1,6 bisphosphate; E4P: Erythrose 4-phosphate; S7P: Sedoheptulose 7-phosphate; DHAP: Dihydroxyacetone phosphate; G3P: Glyceraldehyde 3-phosphate; PEP: Phosphoenolpyruvate; Pyr: Pyruvate; Oaa: Oxaloacetate; AcCoA: Acetyl Coenzyme A; Cit: Citrate; Ici: Isocitrate; Glx: Glyoxylate; 2OG: 2-Oxoglutarate; Suc: Succinate; Fum: Fumarate; Mal: Malate. The figure was adapted from previous work (Becker et al, 2018b; Choi et al, 2019).

Genetic engineering and genome editing tools of *C. glutamicum*

While initially, random mutagenesis and selection was applied to obtain improved production strains (Sahm et al, 1995), the onset of recombinant DNA technologies allowed for rational site-directed changes of the genetic repertoire (Schwarzer & Pühler, 1991). First, episomal replicating plasmids were used to express heterologous genes in *C. glutamicum* (Kind et al, 2010; Kirchner & Tauch, 2003), and these vectors are still widely used today (Jungmann et al, 2022; Christmann et al, 2023). In addition, genomic modifications were enabled by the use of homologous recombination (Becker et al, 2005; Ikeda & Katsumata, 1998). Based on suicide vectors which were not able to replicate in corynebacterial hosts, single crossovers between homologous sites were enforced to integrate the plasmid DNA into the genome at a desired site in a first recombination event (Becker et al, 2005). A second recombination event then enforced by selection pressure to remove the plasmid backbone while the genome-based modification maintained in *C. glutamicum* (Kirchner & Tauch, 2003). The most frequently used system for the selection was based on the counter-selectable marker gene *sacB* encoding levansucrase from *Bacillus* (Jäger et al, 1992) in addition to a standard antibiotic resistance marker-cassette. This technology has allowed various genomic modifications over the past decade (Becker et al, 2018b). Still today, homologous recombination is a preferred method for genomic engineering (Weiland et al, 2023).

In addition, other methods have been established for genomic engineering of *C. glutamicum*. This includes CRISPR-Cas naturally occurring clustered regularly interspaced short palindromic repeats (CRISPR) in the genome as part of an antiviral system. These sequences can be used in combination with specifically designed guiding RNAs (gRNAs) and a CRISPR-associated (Cas) endonuclease (e.g., Cpf1 or Cas9) to introduce double strand breaks into the genome at a desired position. Cell survival is then relying on non-homologous end-joining, a natural DNA repair mechanism, which allows targeted genomic modifications (Kim et al, 2023; Jiang et al, 2017). While this approach is

fast and allows multiplexed genomic changes, it suffers from uncovered site mutations (Becker & Wittmann, 2018), complicating its use for precise stepwise strain engineering.

In addition to episomal and integrative vectors, a set of genetic elements have become available. For fine-tuned stable gene expression of native or heterologous genes, constitutive promoters have become popular, including promoter of the corynebacterial elongation factor tu (*tuf*) (Becker et al, 2005) and of superoxide dismutase (*sod*), respectively (Becker et al, 2009). In addition, synthetic promoter libraries provide opportunities to choose the optimal promoter strength (Giesselmann et al, 2019). For inducible gene expression, the strong hybrid promoters P_{tac} (Christmann et al, 2023; Goldbeck et al, 2021) and P_{trc} offer inducer-associated regulation (Kirchner & Tauch, 2003). Besides synthetic transcription regulators, *C. glutamicum* requires naturally expressed regulatory elements which account for about 5.3 % of the total predicted protein-coding regions (Schröder & Tauch, 2010). Transcription of the L-lysine exporter gene *lysE* for example is positively affected by its regulator LysG whose expression in turn depends on the intracellular level of L-lysine and L-arginine (Bellmann et al, 2001). Another key player in post-transcriptional regulation of the gene expression is non-coding RNA (Parise et al, 2021) which has been successfully used as genome editing tool in other bacteria due to interaction with target mRNA (Papenfort & Vanderpool, 2015; Copeland et al, 2014; Zemanova et al, 2008). Libraries of RBS (Zhang et al, 2015) and modulated assembly of bicistronic RBS parts together with synthetic promoters (Giesselmann et al, 2019) contributed to optimal interplay of the regulatory elements. As a starting point, 16 S rRNA studies identified Shine Dalgarno sequences as part of ribosomal binding sites (Martin et al, 2003).

Furthermore, important for expression of a protein is the translational efficiency (Becker et al, 2010) which, among other factors, relies on the translational start codon of the gene to be expressed. Notably, the replacement of the naturally weak GTG triplet by ATG enhanced the expression of enzymes from central carbon metabolism (Becker et al,

2010). Vice versa, the use of weaker start codons allowed reduced gene expression TCA related enzymes (Becker et al, 2009). Finally, the adaption of the codon usage enables to modulate the translational efficiency (Kind et al, 2010; Hoffmann et al, 2018). Regarding plasmid based expression, the origin of replication (ORI) determines the plasmid copy number within the cell, another possibility to influence gene expression (Hashiro & Yasueda, 2018). Hereby, plasmid selection by auxotrophies as opposed to antibiotics can provide an additional benefit for strain stability and vitality (Li et al, 2020).

Different to these rational engineering efforts, also untargeted approaches have been developed and applied. As example, transposon-mediated mutagenesis was shown to provide a library of mutants with different modification sites. Covering nearly 80 % of all open reading frames and thereby inactivating the affected genes, its use contributed to the overall understanding of *C. glutamicum* cell factories (Suzuki et al, 2006) and enabled the identification of unknown genes in biosynthetic pathways (Mormann et al, 2006). In addition, adaptive evolution has been successfully used to generate growth-improved hosts (Graf et al 2019) and faster-growing glutarate production strains (Prell et al, 2021). Coupled to a biosensor system, the underlying mutation rate could be translated into detectable signals, e. g. from a fluorescence protein depending on intracellular metabolite concentrations (Yu et al, 2021).

2.1.3 Metabolically engineered *C. glutamicum* as industrial cell factory

C. glutamicum is most famous for its capability to overproduce amino acids, and these products, including L-glutamate and L-lysine, are produced at industrial level since almost 50 years (Becker & Wittmann, 2012b). Today, amino acid world market, largely driven by *C. glutamicum* cell factories displays a multi-billion dollar business (Becker et al, 2018b). In addition, strains of *C. glutamicum* have been metabolically engineered to produce a variety of more than 70 other products (Becker et al, 2018b). In the recent years, *C. glutamicum* has been continuously improved and adapted to produce fine and bulk

chemicals at industrial scale (Becker & Wittmann, 2020b). Furthermore, the microbe was upgraded to synthesize high-value and new product classes (Becker et al, 2018b) (Wolf et al, 2021). Prominent examples for bulk products are organic acids such as glutarate (Rohles et al, 2018), lactate (Inui et al, 2004), succinate (Becker et al, 2015), and *cis,cis*-muconate (Becker et al, 2018a; Weiland et al, 2023), diamines such as 1,5-diaminopentane (Buschke et al, 2011), and alcohols like ethanol (Jojima et al, 2015) and isobutanol (Blombach et al, 2011). Moreover, the microbe was upgraded to synthesize high-value cell protective molecules for cosmetic and medical applications, including ectoine (Becker et al, 2013b; Becker & Wittmann, 2020a), 5-hydroxyectoine (Jungmann et al, 2022), mannosyl-glycerate (Becker & Wittmann, 2020a), and L-pipecolic acid (Perez-Garcia et al, 2016; Becker et al, 2018b). Recently, cell factories of *C. glutamicum* also proven value to efficiently produce antimicrobial peptides for food preservation such as Pediocin PA-1 (Christmann et al, 2023; Goldbeck et al, 2021) and nisin (Weixler et al, 2022). In many cases titers, yields and productivities have reached economically attractive levels (Becker et al, 2018b; Becker et al, 2015).

On the raw material side, *C. glutamicum* was modified towards an extended substrate spectrum (Becker et al, 2018b; Buschke et al, 2013b). Metabolic engineering of the microbe to the use of xylose (Buschke et al, 2013a) and arabinose (Schneider et al, 2011) has enable processes based on hemicellulose (Buschke et al, 2011; Becker et al, 2018b), while the extension of the substrate spectrum to glycerol (Zahoor et al, 2012) and mannitol (Hoffmann et al, 2018; Hoffmann et al, 2021) has opened the possibility of production from raw sugar alcohols from the biodiesel industry (Buschke et al, 2013b) and seaweed (Poblete-Castro et al, 2020; Hoffmann et al, 2021), respectively, all displaying environmentally friendly and sustainable carbon source alternatives. In contrast to glucose, fructose, and sucrose, these alternatives are not competing with food supply (Buschke et al, 2013b; Inderwildi & King, 2009). This also beneficially applies to lignin-based aromatics representing a globally available, substantially underutilized resource (Becker & Wittmann, 2019a). Notably, engineering strains of *C. glutamicum* exhibit a high

capability to use aromatics and lignin-based hydrolysates, allowing the production of commercially attractive chemicals (Weiland et al, 2023; Weiland et al, 2022). As example, the engineered strain *C. glutamicum* MA-2 formed 1.8 g L⁻¹ *cis,cis*-muconic acid from softwood lignin hydrolysate (Becker et al, 2018a). Hereby, the excellent breakdown of complex raw materials, typically containing elevated levels of inhibitors, especially aromatic compounds and furfurals, demonstrated a high stress tolerance of *C. glutamicum*, adding an excellent trait to its performance as industrial host (Buschke et al, 2013b; Weiland et al, 2022; Sakai et al, 2007).

2.1.4 Fermentative production of the amino acid L-lysine

The production of the essential amino acid L-lysine is a traditional industrial application of *C. glutamicum* (Wittmann & Becker, 2007). Advantageously, the organism is naturally able to synthesize L-lysine from glucose (Wittmann & Heinzle, 2001b), involving the precursors oxaloacetate and pyruvate, and redox power in the form of NADPH (Wittmann & Becker, 2007). At the start of the biosynthetic pathway, oxaloacetate is transaminated into L-aspartate. Subsequent phosphorylation into aspartyl phosphate mediated by aspartokinase represents a key step of L-lysine synthesis due to the feedback regulation of the enzyme by L-lysine and L-threonine that has to be overcome for enhanced L-lysine production (Kalinowski et al, 1991). A subsequent reduction step then forms L-aspartate semialdehyde which is condensed with pyruvate to L-2,3-dihydrodipicolinate and then reduced into L- Δ^1 -tetrahydrodipicolinate. This intermediate is then converted to DL-meso-diaminopimelate, involving two parallel routes in *C. glutamicum*, the succinylase pathway and the dehydrogenase pathway (Wehrmann et al, 1998). Depending on nitrogen availability (Sahm et al, 2000), DL-meso-diaminopimelate is either formed via the succinylase pathway, including L-glutamate as amino group donor, or via the dehydrogenase pathway which involves ammonia instead (Wehrmann et al, 1998). L-lysine is finally obtained by decarboxylation of DL-meso-diaminopimelate

(Wittmann & Becker, 2007). Transport out of the cells is mediated by the endogenous and specific translocator LysE (Bellmann et al, 2001; Vrljic et al, 1996). In general, *C. glutamicum* possesses also an antiport uptake system (Broer & Krämer, 1990). However, high pH and L-lysine auxotrophy are required to force substantial import so that this process is negligible as soon as larger quantities of L-lysine are produced (Broer & Krämer, 1990).

After several decades of modest improvement using rational genetic engineering of single targets (Eggeling & Sahm, 1999), global strain optimization using systems metabolic engineering strategies provided the tailor-made high-level L-lysine overproducer *C. glutamicum* LYS-12 (Fig. 4) that competed in performance with classically derived industrial strains (Table 1) (Becker et al, 2011).

The strain benefited from a total of 12 coordinated genomic modifications. The modifications synergistically targeted, among other things, improved NADPH supply by increasing flux via the pentose phosphate pathway, maximized availability of pyruvate and oxaloacetate by reducing flux via opposing reactions, and increased flux via the biosynthetic pathway of L-lysine (Becker et al, 2011).

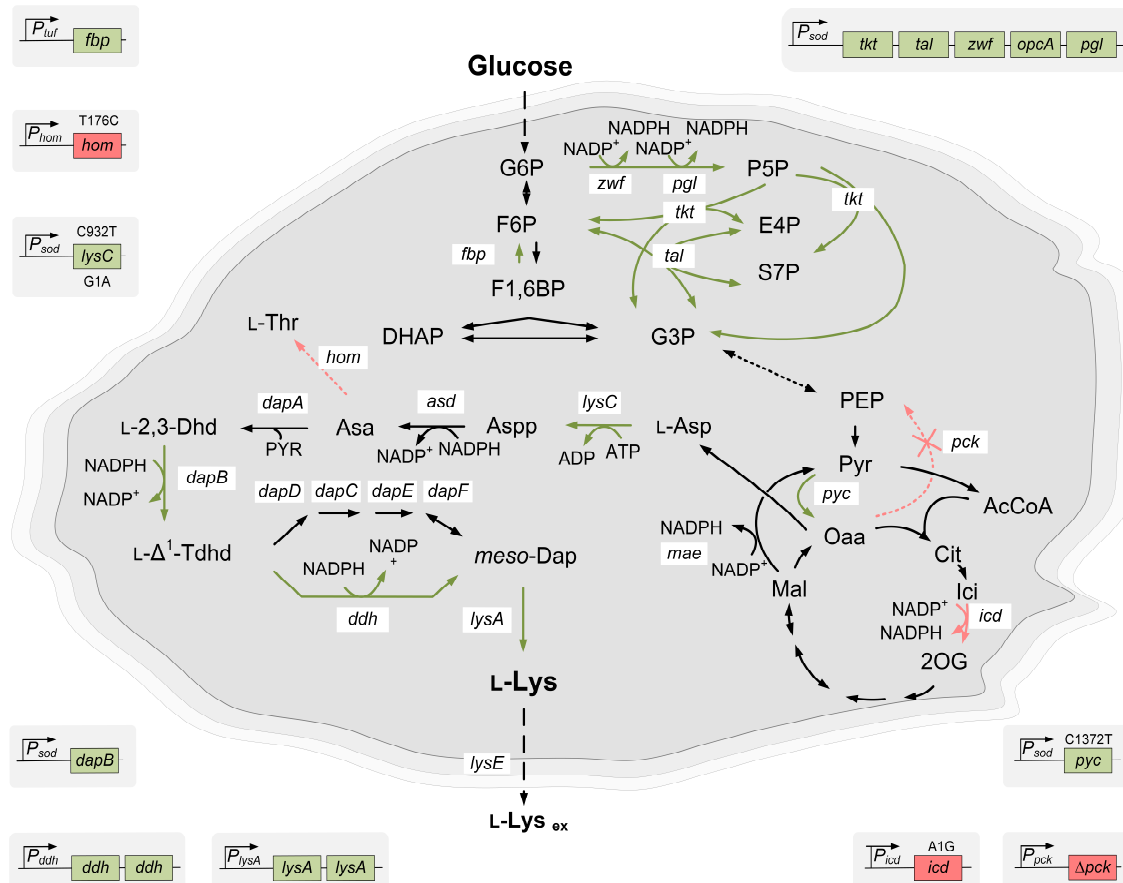


Fig. 4: Metabolic pathway design for *de novo* production of the essential amino acid L-lysine in *Corynebacterium glutamicum*. The chassis strain *C. glutamicum* LYS-12 previously derived from the wildtype strain ATCC13032 possessed twelve genomic modifications. These covered overexpression of fructose 1,6-bisphosphatase (P_{luf} *fbp*), attenuation of homoserine dehydrogenase (*hom*^{V59A}), introducing a point mutation in aspartokinase and replacing original promoter (P_{sod} *lysC*^{T311I}), promoter exchange of 4-hydroxy-tetrahydrodipicolinate reductase (P_{sod} *dapB*), duplication of meso-diaminopimelate dehydrogenase (*dhh*) and of meso-diaminopimelate decarboxylase (*lysA*), overexpression of the *tkt* operon (P_{sod} *tkt*) comprising glucose 6-phosphate dehydrogenase (*zwf*), transketolase (*tkt*) and transaldolase (*tal*), 6-phosphogluconolactonase (*pgl*) and the putative subunit of glucose 6-phosphate dehydrogenase (*opcA*), introducing a point mutation in pyruvate carboxylase and replacing original promoter (P_{sod} *pycA*^{P458S}), deletion of phosphoenolpyruvate carboxykinase (Δpck), and attenuation of isocitrate dehydrogenase (*icd*^{GT6}) (Becker et al, 2011). Enhancing modifications are displayed in green, weakened reactions are illustrated in red. G6P: Glucose 6-phosphate; P5P: Pentose 5-phosphate; F6P: Fructose 6-phosphate; F1,6BP: Fructose 1,6-bisphosphate; E4P: Erythrose 4-phosphate; S7P: Sedoheptulose 7-phosphate; DHAP: Dihydroxyacetone phosphate; G3P: Glyceraldehyde 3-phosphate; PEP: Phosphoenolpyruvate; Pyr: Pyruvate; Oaa: Oxaloacetate; AcCoA: Acetyl CoA; Cit: Citrate; Ici: Isocitrate; 2OG: 2-Oxoglutarate; Mal: Malate; L-Asp: L-Aspartate; AspP: Aspartyl phosphate; Asa: Aspartate semialdehyde; L-2,3-Dhd: L-2,3 dihydrodipicolinate; L- Δ^1 -Tdh: L- Δ^1 -Tetrahydrodipicolinate; meso-Dap: meso-Diaminopimelate; L-Lys: L-Lysine; ex: exported.

In the first step, feedback inhibition of the aspartokinase (encoded by *lysC*) was removed via amino acid exchange T311I (Becker et al, 2005). The key anaplerotic enzyme pyruvate carboxylase (encoded by *pycA*) was disrupted by promoter exchange and replaced with a feedback-resistant variant with the amino acid exchange P485S (Becker et al, 2009). Together with the deletion of the counter-reaction catalyzed by phosphoenolpyruvate

carboxykinase (encoded by *pck*), an adequate supply of precursors was ensured (Becker et al, 2009). Downregulation of TCA cycle by replacing the start codon of isocitrate dehydrogenase (encoded by *icd*) and introducing the point mutation V59A into homoserine dehydrogenase (encoded by *hom*) contributed to the reduction of carbon loss in the L-lysine synthesis pathway (Becker et al, 2009).

Furthermore, overexpression of the enzymes aspartokinase (encoded by *lysC*), 4-hydroxy-tetrahydrodihydrodipicolinate reductase (encoded by *dapB*) and diaminopimelate decarboxylase (encoded by *lysA*) resulted in increased carbon flux through the L-lysine synthesis pathway (Becker et al, 2009). In addition, duplication of the gene for diaminopimelate decarboxylase (encoded by *ddh*) enhanced the diaminopimelate pathway relative to the succinylase route. NADPH supply was increased by replacing the promoter of the gene *fbp*, encoding fructose-1,6-bisphosphatase, and the transketolase operon with the genes *zwf*, *tkt*, *tal*, *pgl*, and *opcA* (encoding glucose 6-phosphate dehydrogenase, transketolase, transaldolase, 6-phosphogluconolactonase, and a putative subunit of glucose 6-phosphate dehydrogenase) (Becker et al, 2011). The final cell factory *C. glutamicum* LYS-12 achieved a remarkable titer of 120 g L⁻¹ (Becker et al, 2011).

Although having been created more than 10 years ago and many efforts have been carried out since then, *C. glutamicum* LYS-12 is still among the best L-lysine hyperproducing strains (Table 1). Moreover, the smart iterative strain optimization strategy and the immense knowledge, gained during strain engineering by fluxome analysis and *in silico* pathway modeling, have laid the foundation for further strain improvement (Becker et al, 2011).

Table 1: L-lysine overproducing *C. glutamicum* strains with the corresponding genotypic information and the achieved performance in terms of titer, yield, and productivity.

<i>C. glutamicum</i> strain	Genotype and modifications	Titer [g L ⁻¹]	Yields [g g ⁻¹]	Productivity [g L ⁻¹ h ⁻¹]	Source
B-6 ^a	Derived through stepwise mutagenesis of ATCC13032 using N-nitro-N'-nitro-N-nitrosoguanidine, selection due to resistance to D,L-S-(2-aminoethyl) L-cysteine, rifampicin, streptomycin and 6-azauracil	100	n. d.	2.1	(Hirao et al, 1989)
MH20-22B ^a	Derived through stepwise mutagenesis of ATCC13032 using N-nitro-N'-nitro-N-nitrosoguanidine, selection due to resistance to L-threonine, D,L-S-(2-aminoethyl) L-cysteine, plus <i>lysC^{ibr}</i> , <i>ΔleuD</i>	44	0.44*	n. d.	(Schrum pf et al, 1992)
h-8241 ^a	Derived through stepwise mutagenesis of FERM BP-1655 using N-nitro-N'-nitro-N-nitrosoguanidine, resistance to 3,3',35-triiodo L-thyronine	48	0.48*	n. d.	(Nakano et al, 1994)
ATCC 21513 (Hom-, Leu-)	ATCC21513 with L-leucin and L-homoserine auxotrophy, resistance to D,L-S-(2-aminoethyl) L-cysteine	48.5	0.37	1.47	(Sassi et al, 1996)
MH20-22B/pJC23 <i>dapA</i>	MH20-22B ^a , overexpression of <i>dapA</i>	39.8*	n. d.	n. d.	(Eggeling et al, 1998)
AK-31833	ATCC31833, <i>lysC^{T3111}</i>	59	n. d.	2.1	(Ohnishi & Ikeda, 2006)
RE2A/pCAK311	ATCC13032, <i>lysC^{T3111}</i> , <i>gapA</i> replaced by <i>gapN</i> from <i>S. mutans</i>	3.4	0.11*	n. d.	(Takeno et al, 2010)
AHPΔptsH320d <i>eIA</i>	ATCC31833, <i>hom^{V59A}</i> , <i>lysC^{T3111}</i> , <i>pyc^{P458S}</i> , activation of <i>iolT1</i> -system	8.8*	0.29*	n. d.	(Ikeda et al, 2011)
LYS-12	ATCC13032, <i>lysC^{T3111}</i> , <i>pyc^{P458S}</i> , <i>hom^{V59A}</i> , <i>icd^{A1G}</i> ; <i>Δpck</i> ; over-expression: <i>lysC</i> , <i>pyc</i> , <i>ddh</i> , <i>lysA</i> , <i>dapB</i> , <i>fbp</i> , <i>tkl</i>	120	0.55	4	(Becker et al, 2011)
DM1933 <i>murE</i> -G81E	DM1933, <i>murE^{G81E}</i> , <i>pyc^{P458S}</i> , <i>hom^{V59A}</i> , <i>Δpck</i> ; 2x: <i>lysC^{T3111}</i> , <i>asd</i> , <i>dapA</i> , <i>dapB</i> , <i>ddh</i> , <i>lysA</i> , <i>lysE</i>	10.0*	n. d.	n. d.	(Binder et al, 2012)
AGL-6	ATCC31833, <i>hom^{V59A}</i> , <i>lysC^{T3111}</i> , <i>pyc^{P458S}</i> , <i>mgo224 (W224opal)</i> , <i>leuC456</i>	100	0.4	3.3	(Ikeda & Takeno, 2013)
Lys5-8	ATCC13032, <i>gapC</i> from <i>C. acetobutylicum</i> 2x: <i>lysC^{C932T}</i> , <i>asd</i> , <i>dapA</i> , <i>dapB</i> , <i>ddh</i> , <i>lysA</i> ; <i>pyc^{G1A, C1372T}</i> , <i>hom^{T176C}</i> , <i>murE^{G242A}</i> ; <i>Δ: aceE</i> , <i>alaT</i> , <i>avtA</i> , <i>ldhA</i> , <i>mdh</i> , <i>ilvNc-τ</i> , <i>pck</i>	130	0.47	2.73	(Xu et al, 2014)
RE2A <i>iol lysC gapN</i>	ATCC13032 <i>gapN</i> ; <i>hom^{T176C}</i> , <i>lysC^{T3111}</i> , <i>pyc^{P458S}</i>	9.55	0.19	n. d.	(Takeno et al, 2016)
JL-6Δ <i>dapB</i> :: <i>Ec-dapBC115G,G116C</i>	Strain JL-6 ^b plus replacement of <i>dapB</i> gene by mutated <i>dapB^{C115G,G116C}</i> from <i>E. coli</i>	117.3	0.44	2.93	(Xu et al, 2018b)

Continuation of table 1.

JL-69P _{tac-M} gdh	Strain JL-6 ^b , Δpck , $\Delta dodx$; overexpression: <i>pyc</i> , <i>ppc</i> , <i>gltA</i>	181.5	0.65	3.78	(Xu et al, 2018a)
RGI	Strain JL-6 ^b , replacement of <i>icd</i> and <i>gapA</i> gene by <i>S. mutans</i> genes <i>icd</i> and <i>gapC</i>	121.4	0.46	n. d.	(Xu et al, 2019a)
ZL-92	Strain ZL-9 ^c <i>iolT1</i> -A113G, -C112G, overexpression: <i>iolT2</i> and <i>ppgK</i> (2x)	201.6	0.65	5.04	(Xu et al, 2019b)
ATCC 21543 PaASPDH, TmASADH, EcDHDPR	ATCC 21543, replacement of NADPH-dependent dehydrogenases by NADH-utilizing enzymes PaASPDH, TmASADH, EcDHDPR	27.7	0.35	n. d.	(Wu et al, 2019a)
K-8	Strain JL-6 ^b , <i>scrK</i> , $\Delta ptsG$, <i>DptsF</i> , <i>iolT1</i> -A113G, -C112G; overexpression: <i>iolT2</i> (2x), <i>ndh</i> ; replacement of <i>glk</i> gene by <i>glk</i> from <i>B. subtilis</i> , codon-optimized <i>glk</i> from <i>M. maripaludis</i>	221.3	0.71 ^e	5.53	(Xu et al, 2020)
XQ-5-W4	Strain XQ-5 ^d , pEC-XK99E- <i>ddh</i> , $\Delta amtR$, weakening of <i>dapD</i> .	189	n. d.	n. d.	(Liu et al, 2021)
Cg $\Delta exeR$ *Pst	Strain 0206 ^f with ~1 kb deletion of <i>exeR</i> replaced by <i>P_{eftu} ptxDPst</i> .	41	n. d. ^g	n. d.	(Lei et al, 2021)
SEA-7	LYS-12, $\Delta mtlR$, modified <i>mak</i> gene and <i>pntAB</i> from <i>E. coli</i> , codon-optimized <i>gapN</i> from <i>S. mutans</i> .	76	0.21 ^{*,h}	2.1	(Hoffman et al, 2021)
LJ01-pP _{eftu} -PntAB	Strain B253 $\Delta ldhA::xylAB$, plus <i>P_{eftu} pntAB</i> .	31.3	0.23	n. d.	(Jin & Bao, 2021)
KT ₄₅₋₆ S-5	K-8 which grows at 45 °C, fusion gene <i>amyA-glaA</i> .	23.9	n. d. ^k	n. d.	(Li et al, 2022)

n. d. not defined

* Calculated from provided data.

^a Classically derived strain with unknown genotype.

^b JL-6: classically derived from *C. glutamicum* ATCC13032 after multiple rounds of random mutagenesis, selected by resistance to S-2-aminoethyl-L-cysteine and sulfadiazine, sensitive to β -fluoro-pyruvate and leaky for L-methionine.

^c ZL-9: classically derived from *C. glutamicum* ATCC13032 after multiple rounds of random mutagenesis, selected by resistance to S-2-aminoethyl-L-cysteine, sulfadiazine, monofluoroacetate and 2-thiazoalanine, sensitive to L-threonine and L-methionine.

^d XQ-5: classically derived from *C. glutamicum* ATCC13032 after multiple rounds of random mutagenesis, selected by resistance to S-2-aminoethyl-L-cysteine, monofluoroacetate and 2-thiazoalanine, sensitive to L-methionine.

^e Fermentation using a sugar mix as carbon sources.

^f 0206: classically derived from *C. glutamicum* CICC21763.

^g Fermentation using beet molasses as additional carbon source, phosphite instead of phosphate was used to supply phosphorus source.

^h Fermentation using mannitol as carbon source.

ⁱ K-8: Derived from JL-6 after genome breeding.

^k Fermentation using raw starch as main feedstock.

Merely, strains derived from combinatorial strain design including rational and classical approaches were able to surpass the performance (Xu et al, 2020; Xu et al, 2018a; Xu et al, 2018b; Xu et al, 2019b; Liu et al, 2022). Further strain engineering mainly aimed at optimization of substrate uptake (Xu et al, 2020), modifications of L-lysine associated transporters (Malla et al, 2022) and reconstruction of the diaminopimelic acid pathway

(Liu et al, 2021). On the other hand, metabolic engineering for the utilization of regenerative feedstocks created further adaptation and application potential (Hoffmann et al, 2021) (Jin & Bao, 2021). Additionally, the cultivation temperature was discovered as interesting feature to affect L-lysine productivity in *C. glutamicum* based processes (Li et al, 2022), including the L-lysine hyperproducer LYS-12 (Giesselmann, 2018; Schäfer, 2016). Beneficially, *C. glutamicum* LYS-12 has proven value as chassis strain for the synthesis of commercially attractive L-lysine derivatives, including 1,5-diaminopentane, glutarate and 5-aminovalerate (Kind et al, 2014; Rohles et al, 2016; Rohles et al, 2018).

2.2 L-lysine derivatives as value-added products

Beyond its direct value as a feed and food additive (Wittmann & Becker, 2007), L-lysine serves as precursor for different value-added compounds (Becker et al, 2018b). Prominently, the L-lysine overproducer *C. glutamicum* LYS-12 has been successfully modified to produce 1,5-diaminopentane (Kind et al, 2010), glutarate (Rohles et al, 2018) and 5-aminovalerate (Rohles et al, 2016), all building blocks for bio-based polymers such as polyamides, polyesters, and polyurethanes, respectively.

As example, basic production of 1,5-diaminopentane was enabled by genomic expression of the heterologous L-lysine decarboxylase (*ldcC*) from *E. coli* in *C. glutamicum* LYS-12 (Kind et al, 2010). Increased *in vivo* activity of the newly implemented L-lysine decarboxylase enzyme was then realized by expression enhancement due to promoter exchange and codon-optimization, resulting in improved performance (Kind et al, 2010). Metabolic engineering at the level of the cellular transport and by-product formation then increased the product yield in *C. glutamicum* DAP-3C to 20 %, while simultaneously reducing the formation of the undesired by-product N-acetyl-diaminopentane (Kind et al, 2011). The combination of all beneficial modifications yielded strain *C. glutamicum* DAP-16 which achieved a diaminopentane a yield of 41 % in shake flask.

In a fed-batch process, *C. glutamicum* DAP-16 accumulated 1,5-diaminopentane to a titer of 88 g L⁻¹ at a molar yield of 50 % and a productivity of 2.2 g L⁻¹ h⁻¹ (Kind et al, 2014). Subsequent extraction and distillation provided pure 1,5-diaminopentane. The product was co-polymerized with sebacic acid to a novel bio-nylon PA5.10 (Kind et al, 2014). Furthermore, heterologous expression of the *E. coli* genes *xylA* and *xylB* enabled the utilization of hemicellulose fractions, rich in xylose (Buschke et al 2011). Further strain optimization strategies involved metabolic flux analysis and global transcriptome profiling to identify potential bottlenecks. Subsequent deletion of the genes involved in the formation of L-lysine and N-acetyl diaminopentane, the attenuation of isocitrate dehydrogenase, and the overexpression of fructose-1,6-bisphosphatase and the transketolase operon yielded a superior strain that achieved a 1,5-diaminopentane titer of 103 g L⁻¹ from xylose at a product yield of 32 % in a fed-batch process (Buschke et al, 2013a).

Similar approaches allowed production of 5-aminovalerate and glutarate. By implementing the operon *davBA* from *P. putida* into *C. glutamicum* LYS-12, the conversion of L-lysine into 5-aminovalerate was enabled. The deletion of counteracting pathways yielded strain *C. glutamicum* AVA-3 which produced 28 g L⁻¹ of 5-aminovalerate at productivity of 0.9 g L⁻¹ h⁻¹ (Rohles et al, 2016). The synthesis of glutarate built on the formation of 5-aminovalerate, as *C. glutamicum* was found to possess a natural pathway for 5-aminovalerate degradation toward glutarate (Rohles et al, 2016). Starting from *C. glutamicum* AVA-2, the endogenous pathway was overexpressed. The product selectivity was increased by enhancing the re-import of 5-aminovalerate into the cell. The final strain *C. glutamicum* GTA-4 accumulated more than 90 g L⁻¹ of glutarate from molasses-based at a yield of 0.7 mol mol⁻¹ and a productivity of 1.8 g L⁻¹ h⁻¹. The formed glutarate was purified and used to form the bio-based polymer bionylon-6,5 (Rohles et al, 2018).

Moreover, L-lysine is also regarded as interesting precursor for molecules with medical relevance. As example, hydroxylysine (Prell et al, 2022; Mager, 2022) and L-pipecolic acid

(Perez-Garcia et al, 2016) production routes have been recently implemented into *C. glutamicum*. Whereas the optimization of the hydroxylysine pathway focused on increasing precursor supply (Prell et al, 2022), modifications for enhanced L-pipecolic acid production intended to diminish counteracting L-lysine export and increase the expression of L-lysine degradation enzymes (Perez-Garcia et al, 2017).

Independent from availability, pricing and processing of fossil resources, the biotechnological production of these molecules contributes to satisfying the increasing demand for fossil resource-derived everyday products and at the same time reduce the impact on nature (Rohles et al, 2018; Nielsen et al, 2019). The need for environmentally friendly and sustainable production strategies becomes particular clear (Adkins et al, 2012; Andrady & Neal, 2009; Becker & Wittmann, 2015) when looking at the estimated plastic production, surpassing 500 million tons by 2050 (Chen & Yin, 2020). Beyond conservation of resources and environment bio-based syntheses also guarantee high product selectivity without time- and cost-consuming purification processes (Rohles et al, 2018; Clemente-Jimenez et al, 2008). In contrast to chemical processes, microbial production enables high optical purity of the products due to tailor-made enzymatic reactions, especially attractive for medical and pharmaceutical applications (Lemire & Charette, 2010).

2.2.1 5-Aminovalerate - a L-lysine degradation intermediate and its application

Eco-friendly polymers derived from bio-based monomers are predicted to achieve a market share of 2.43 million tons in 2024 (Hauptka et al, 2020). Starch blends, polylactic acid, polyamides and polyester hereby represent the most frequent bioplastics produced (European Bioplastics, 2022). While starch-based blends are traditionally synthesized by additions of plasticizer and heat (Jayarathna et al, 2022), building blocks for other polymers could be obtained from microbial production.

Natural producers as *Basfia succiniciproducens* (Lange et al, 2017), members of the *Pasteurellaceae* family (Kuhnert et al, 2010) and *Lactobacilli* (Akermann et al, 2020) together with tailor-made microorganisms provide an extensive product portfolio in the field of bio-based polymer precursors: diamines such as 1,5-diaminopentane (Kind et al, 2010; Buschke et al, 2011; Kind et al, 2014) and 1,3-diaminopropane (Chae et al, 2015); lactames such as ϵ -caprolactam (Thompson et al, 2020); polyester forming alcohols such as 1,3-propanediol (Saxena et al, 2009; Becker et al, 2018b), dicarboxylic acids such as succinate (Kuhnert et al 2010; Lange et al, 2017), adipate (Vardon et al, 2015; Becker et al, 2015), *cis,cis*-muconate (Kohlstedt et al, 2022; Barton et al, 2018) (Becker et al, 2018a) and glutarate (Rohles et al, 2018), hydroxyl acids such as 3-hydroxybutyrate (Atakav et al, 2021), and ω -amino acids such as 6-aminocaproate (Turk et al, 2016).

In addition, the non-proteinogenic amino acid 5-aminovalerate is another important carbon-5 platform chemical belonging to the latter group (Cheng et al, 2021). Besides direct use for polymerization of nylon-5 to replace petroleum based nylon-4,6 (Adkins et al, 2013; Bermudez, 2000), 5-aminovalerate serves as precursor for the synthesis of glutarate (Rohles et al, 2018), δ -valerolactam (Zhang et al, 2017b), 5-hydroxyvalerate (Liu et al, 2014; Cheng et al, 2021) and 1,5-pentanediol (Park et al, 2014b). Co-polymerizations of these 5-aminovalerate derivatives expand the nylon spectrum (Adkins et al, 2013; Park et al, 2014b) and prove ecological production by maintaining or even improving polymer characteristics (Rohles et al, 2018; Adkins et al, 2013; Kind et al, 2014).

The versatile monomer 5-aminovalerate has become available through both chemical and microbial synthesis. An example of chemical synthesis with relatively high yields up to over 90 % is the oxidation of piperidine (Dairo et al, 2016). Besides petroleum feedstocks and expensive catalyzers, the process also includes demanding process properties and high environmental impact (Dairo et al, 2016). For this reason biotechnological production

routes of 5-aminovalerate and others became more attractive to cover the increasing demand (Hauptka et al, 2020; Hong et al, 2018).

Microbial production processes for 5-aminovalerate are based on degradation of L-lysine. In the soil bacterium *Pseudomonas putida* KT2440, DL-lysine is degraded to 5-aminovalerate and glutarate to yield nitrogen, carbon and energy (Chang & Adams, 1974). First, the oxidative decarboxylation of L-lysine into 5-aminovaleramide involves L-lysine 2-monooxygenase (DavB). The subsequent hydrolyzation of the intermediate 5-aminovaleramide into 5-aminovalerate is catalyzed by 5-aminovaleramide amidase (DavA) (Fig. 5) (Revelles et al, 2005). In *Pseudomonas putida* 5-aminovalerate transaminase (DavT) and glutarate semialdehyde dehydrogenase (DavD) further convert 5-aminovalerate into glutarate (Revelles et al, 2005).

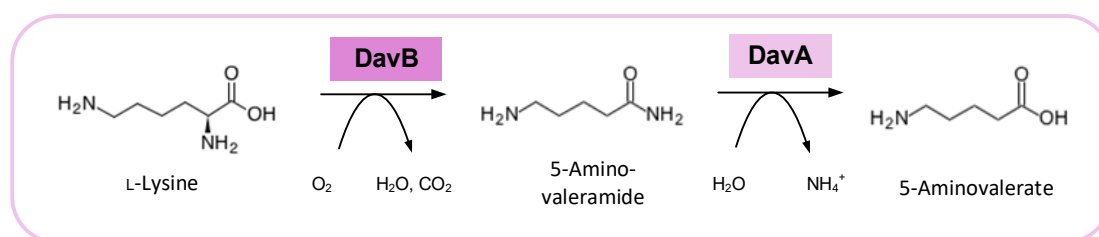


Fig. 5: Biosynthetic pathway for the degradation of L-lysine into 5-aminovalerate in *P. putida*. L-lysine 2-monooxygenase DavB and 5-aminovaleramide amidase DavA catalyze the conversion. Adapted from Revelles et al, 2005.

Taking advantage of this natural pathway, several cell factories were previously designed to synthesize 5-aminovalerate from L-lysine. Whole cell *E. coli* catalysts express the pseudomonal *davBA* operon to produce 5-aminovalerate from L-lysine as precursor in a biotransformation (Park et al, 2013; Wang et al, 2016). Fed-batch biotransformation processes, reached a conversion yield of almost 87 % at a titer of 240 g L⁻¹ 5-aminovalerate but required upstream supply of L-lysine (Wang et al, 2016). While biotransformation processes turned out to achieve high yields, they rely on the addition of L-lysine so that the overall conversion is disadvantageous in terms of sustainability and long-term efficiency, but also production costs (Adkins et al, 2013). Also, enzymatic

production of 5-aminovalerate was investigated (Liu et al, 2014). Other approaches aimed to produce 5-aminovalerate *de novo*. To this end, L-lysine hyperproducing *C. glutamicum* strains were further modified. They either expressed the heterologous *davBA* operon (Fig. 6) (Rohles et al, 2016; Joo et al, 2017; Shin et al, 2016) or enzymes of the cadaverine degradation pathway from *E. coli*, i.e. L-lysine decarboxylase (LdcC), cadaverine transaminase (PatA) and 4-aminobuyraldehyde dehydrogenase (PatD) (Jorge et al, 2017). Very recently, 5-aminovalerate was also microbially synthesized in *E. coli* via a 2-keto-6-aminocaproate-mediated route (Cheng et al, 2021).

Similar to *P. putida*, *C. glutamicum* can also convert 5-aminovalerate into glutarate by using 5-aminovalerate transaminase *gabT* and glutarate semialdehyde dehydrogenase *gabD* (Rohles et al, 2016). For this reason the genes of the L-lysine exporter *lysE* and the 5-aminovalerate transaminase *gabT* were deleted and yielded an 5-aminovalerate titer of 28 g L⁻¹ plus 7 g L⁻¹ glutarate (Rohles et al, 2016). Similar approaches resulted in titers of 33 g L⁻¹ 5-aminovalerate with significantly longer process run times and by-product accumulation (Shin et al, 2016). Efficient formation of the 5-aminovalerate derivative glutarate (Rohles et al, 2018) uncovers improvement potential of the 5-aminovalerate synthesis route.

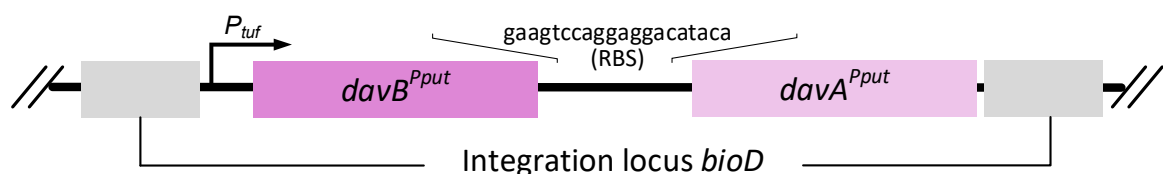


Fig. 6: *davBA* integration module. The genes *davB* and *davA* amplified from *P. putida* KT2440 are organized in an operon with additional RBS as separator. Controlled by the corynebacterial promoter *tuf*, the module is flanked by homologous recombination sites for stable integration in *bioD* locus of *C. glutamicum*. Adapted from Rohles et al. 2016.

2.2.2 Applications and biosynthesis of the L-lysine derivative L-pipecolic acid

L-pipecolic acid is a non-proteinogenic amino acid (Neshich et al, 2013) also known as the ring homologue of L-proline, so-called homoproline (Ankri et al, 1996; Perez-Garcia et al, 2019). The molecule naturally occurs in both microorganisms and

plants but also in human beings as osmoprotectant and important marker. In plants L-pipecolic acid plays a functional role in inducible plant immunity by enabling cell-cell communication during pathogen infection (Bernsdorff et al, 2016; Navarova et al, 2012) and triggering the systemic acquired resistance by its derivatives (Shan & He, 2018) in tomatoes for example (Holmes et al, 2019). L-pipecolic acid can increase the robustness of plants by inducing the adaptive priming strategy and leads simultaneously to a reduction of agrochemical usage to defeat plant pests and diseases (Westman et al, 2019; Conrath et al, 2015). Bacteria also make use of the protective mechanism of L-pipecolic acid. *Sinorhizobium meliloti* and the marine *Ruegeria pomeroyi* for example synthesize the amino acid naturally in order to protect the cells from external stress factors as high salinity of the growing milieu (Gouffi et al, 2000; Neshich et al, 2013). Not only natural producers use L-pipecolic acid as osmoprotectant (Vranova et al, 2013; Becker & Wittmann, 2020a). Accumulation in *Corynebacterium glutamicum* for example increases tolerance towards higher salt concentrations while maintaining cell viability (Perez-Garcia et al, 2019). L-pipecolic acid thus performs a similar function to the structurally very close osmoprotectants ectoine (Becker et al, 2018b) and L-proline (Peter et al, 1998). Unlike in bacteria, accumulation of L-pipecolic acid is harmful in the human body, since a lack of degradation, for example in the liver, indicates a defective function of the L-pipecolate oxidase (Rao & Chang, 1990). As diagnostic marker naturally produced in the brain (Mihalik et al, 1989), L-pipecolic acid helps to detect peroxisomal disorders as for example epilepsy (Plecko et al, 2005), Zellweger syndrome (Mihaliketal, 1989), brain associated dysfunctions (Bernasconi et al, 1986; Gutierrez & Delgado-Coello, 1989; Qi et al, 2022), liver and gallbladder diseases (Qiu et al, 2022). Furthermore, the molecule also serves as a precursor molecule for pharmaceuticals. It is used to produce the peptide antibiotic virginiamycin which is active against *Staphylococcus aureus* and *Enterococcus* (He, 2006) and immunosuppressive and antitumor acting drugs such as immunosuppressants rapamycin (Gatto et al, 2006) and Tacrolimus FK506 (Ireland et al, 1996), the amide anesthetic drugs Mepivacaine and Ropivacaine (Adger et al, 1996; Roura Padrosa et al,

2020) and the antitumor agents swainsonine (He, 2006) and Biricodar VX-710 (Germann et al, 1997). The multifaceted applications together with an estimated market price up to 30,000 \$ per ton (Cheng et al, 2018b) make L-pipecolic acid an interesting precursor molecule.

The use in the pharmaceutical and the food industry requires a high optical purity of the molecule (Maddess et al, 2008). Chemically synthesized L-pipecolic acid is preceded either by a complex stereoselective process or racemates of D- and L-pipecolic acid have to be cleaned up costly and time-consuming yielding low amounts of the pure product (Lemire & Charette, 2010). In contrast biotechnological production routes via enzymatic pathways enable high optical purity (Clemente-Jimenez et al, 2008).

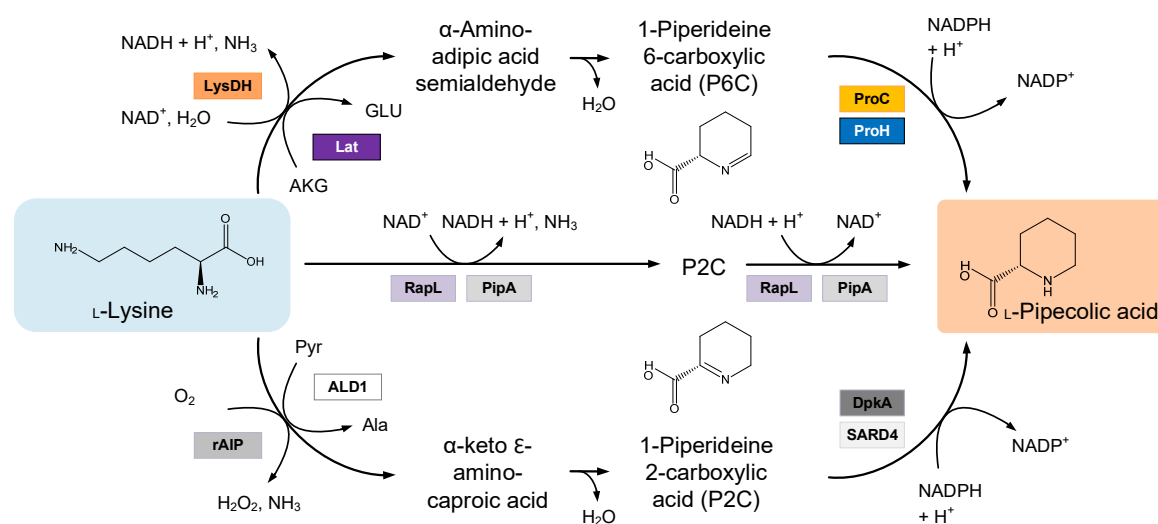


Fig. 7: L-lysine degradation routes to L-pipecolic acid. Two pathways either via 1-piperidine 6-carboxylic acid or 1-piperidine 2-carboxylic acid enable L-pipecolic acid synthesis from L-lysine. L-lysine cyclodeaminases PipA from *Streptomyces pristinaespiralis* and RapL from *Streptomyces hygroscopicus* catalyze the complete reaction. L-lysine 6-dehydrogenase from *R. pomeroyi* and L-lysine 6-aminotransferase from *F. lutescens* transform L-lysine into α -amino-adipic semialdehyde which is spontaneously converted into 1-piperidine 6-carboxylic acid. The Δ^1 -pyrroline 5-carboxylate reductases from *C. glutamicum*, *E. coli* and *B. subtilis* intervene at this point and mediate the last conversion step. Like that apoptosis-inducing protein rAIP from *Scomber japonicus* and aminotransferase AGD2-like defense response protein 1 from *A. thaliana* catalyze first degradation step of 1-piperidine 2-carboxylic acid route where the Δ^1 -pyrroline 2-carboxylate reductases DpkA from *P. putida* and the systemic acquired resistance-deficient 4 from *A. thaliana* take over. Adapted from Han et al, 2020.

Starting from L-lysine, L-pipecolic acid can be synthesized by one- or two-step pathways (Fig. 7). One step synthesis relies on L-lysine cyclodeaminases which are found to catalyze

the degradation of L-lysine into L-pipecolic acid and recycling cofactor simultaneously (Gatto et al, 2006; Poupin et al, 1999). Known genes to encode L-lysine cyclodeaminase are e.g. *rapL* from the rapamycin gene cluster of *Streptomyces hygroscopicus* (Khaw et al, 1998; Molnar et al, 1996; Gatto et al, 2006) and *pipA* from *Streptomyces pristinaespiralis* (Tsotsou & Barbirato, 2007; Ying et al, 2017). Heterologous expression of *pipA* in *E.coli* yielded a titer of 93.5 g L⁻¹ whereby 72 % of the added L-lysine was converted into L-pipecolic acid after 5 days (Han et al, 2020). Up to 90 % conversion was achieved (Tsotsou & Barbirato, 2007). Although the price of L-lysine (1,500 € per ton) is below the estimated market value of L-pipecolic acid (Cheng et al, 2018b), it adds significantly to the production costs and reduces to overall yield (Leuchtenberger et al, 2005).

De novo production thus appears more cost-effective and compatible with existing markets. *E. coli*, expressing *pipA*, reached a L-pipecolic acid titer of 61 g L⁻¹, at a glucose conversion efficiency of almost 30 % (Xu et al, 2022). Alternatively to L-lysine cyclodeaminase, other enzymes catalyze the degradation of L-lysine into L-pipecolic acid via the intermediates α -amino adipic acid semialdehyde and 1-piperidine 6-carboxylic acid, or α -keto- ϵ -amino-caproic acid and 1-piperidine 2-carboxylic acid (He, 2006). Different enzymes can catalyze this two-step synthesis (Fig. 7). The degradation pathway via the intermediate 1-piperidine 6-carboxylic acid can be initiated by co-expression of L-lysine 6-dehydrogenase and Δ^1 -pyrroline 5-carboxylate reductase (Perez-Garcia et al, 2016) but also by the combination of L-lysine 6-aminotransferase and Δ^1 -pyrroline 5-carboxylate reductase (Fujii et al, 2002b). The two first enzymes differ in terms of their cofactor choices, L-lysine 6-dehydrogenase uses NAD⁺ or NADP⁺ (Perez-Garcia et al, 2017) and L-lysine 6-aminotransferase requires α -ketoglutarate and pyridoxal phosphate (Fujii et al, 2002b). After a spontaneous hydrolysis into 1-piperidideine 6-carboxylate, NADPH + H⁺ is necessary for further reduction into L-pipecolic acid by Δ^1 -pyrroline 5-carboxylate reductase (Fujii et al, 2002b). Previous efforts, however, revealed only minor potential of this pathway. Engineered *E. coli*, heterologously expressing the L-lysine 6-aminotransferase from *F. lutescens* and the endogenous Δ^1 -pyrroline 5-carboxylate

reductase, yielded only 3.9 g L⁻¹ L-pipecolic acid (Fujii et al, 2002b). On the other hand, *C. glutamicum*, heterologously expressing L-lysine 6-dehydrogenase from *Ruegeria pomeroyi* and endogenous Δ^1 -pyrroline 5-carboxylate reductase, reached a titer of 14.4 g L⁻¹ (Perez-Garcia et al, 2017). Further dehydrogenases could be found in the gram-negative phytopathogen *Agrobacterium tumefaciens* (Misono et al, 1989) and the gram-positive thermophilic *Geobacillus staerothermophilus* (Heydari et al, 2004) providing valuable enzyme characteristics as temperature and pH optimum of the L-lysine 6-dehydrogenase (Heydari et al, 2004). Cell-free approaches hereby illustrate the high efficiency of the biocatalytic pathway reaching space-time yields up to 2.5 g L⁻¹ h⁻¹ (Roura Padrosa et al, 2020).

The alternative pathway via intermediate 1-piperidine 2-carboxylic acid was also used for biotechnological production. Starting from L-lysine the L-lysine alpha-oxidase catalyzes the first degradation step. Further conversion into L-pipecolic acid is performed by 1-piperidine-2-carboxylate reductase. Co-expression of the L-lysine alpha-oxidase from *Trichoderma viride* and 1-piperidine 2-carboxylic acid in *Pseudomonas putida* enabled the L-lysine degradation up to an L-pipecolic titer of 27 g L⁻¹ (Muramatsu et al, 2006). One-pot fermentation in *E. coli* yielded titers up to 46.7 g L⁻¹ by co-expressing *Scomber japonicus* and 1-piperidine 2-carboxylate reductase from *Pseudomonas putida* (Cheng et al, 2018a; Tani et al, 2015). Recently, the L-pipecolic acid pathway via 1-piperidine-2-carboxylate from *Arabidopsis thaliana* was reconstructed in *E. coli* and thus represents another interesting route for biotechnological production (Ding et al, 2016).

3 Materials and Methods

3.1 Microorganisms, genes, and plasmids

E. coli DH10B and NM522 (Invitrogen, Carlsbad, CA, USA) were used as hosts for plasmid amplification and corynebacterial-specific methylation (Becker et al, 2011; Kind et al, 2010). The chassis strains *Corynebacterium glutamicum* LYS-12 (Becker et al, 2011) and *C. glutamicum lysC^{fbr} ΔlysE* (Giesselmann et al, 2019) were taken from previous work. For cloning purposes, DNA templates from *Ruegeria pomeroyi* DSS-3 (DSM 15171) and *Streptomyces hygroscopicus* NRRL 5491 (DSM 41530) were obtained from the German Collection of Microorganisms and Cell Cultures (DSMZ, Braunschweig, Germany). DNA of *Bacillus subtilis* K168 was obtained from previous work (Kohlstedt et al, 2014). Heterologous genes of interest from *Geobacillus stearothermophilus* UTB1103, *Agrobacterium tumefaciens*, *Flavobacterium lutescens* IFO 3084, *Escherichia coli* K12-MG1655, and *Streptomyces mutans* UA159, respectively, were synthesized based on digital sequence information (GenScript, Piscataway Township, NJ, USA) or taken from previous work (Hoffmann et al, 2018; Hoffmann et al, 2021).

The plasmid *pClik5a MCS* was used for episomal gene expression in *C. glutamicum* (Buschke et al, 2011), while the plasmid *pClik int sacB* served as integrative vector for genome-based modifications (Becker et al, 2005). During cloning, integrative plasmids were co-expressed in *E. coli* NM522 together with *pTC* to obtain the corynebacterial-specific methylation pattern (Kind et al, 2010). All strains and plasmids used are listed in Table 2.

Table 2: Strains and plasmids.

Strains	Description	Reference
<i>E. coli</i>		
DH10B	Cloning host	Invitrogen
NM522	Cloning host	Invitrogen
<i>C. glutamicum</i>		
ATCC 13032	Wild type	Becker et al, 2011
LYS-12	L-Lysine hyperproducing strain with 12 genome-based modifications	Becker et al, 2011
LYS-12 <i>P_{tuf} pntAB^{Ecol}</i>	LYS-12 with genome-based expression of <i>P_{tuf} pntAB^{Ecol}</i>	Hoffmann et al, 2018
LYS-12 Δ <i>mtlR</i> <i>P_{tuf} gapN^{Smut, opt}</i>	LYS-12 with genome-based expression of Δ <i>mtlR</i> <i>P_{tuf} gapN^{Smut, opt}</i>	Hoffmann et al, 2021
<i>lysC^{fbr} ΔlysE</i>	Non-L-lysine secreting chassis strain	Giesselmann et al, 2019
PIA-0	LYS-12 <i>pClik5a</i>	This work
PIA-1A	LYS-12 <i>pClik5a P_{tuf} lysDH^{Rpom} proC^{Cglu}</i>	This work
PIA-1A <i>LysDH^{I81K}</i>	LYS-12 <i>pClik5a P_{tuf} lysDH^{Rpom I81K} proC^{Cglu}</i>	This work
PIA-1A <i>LysDH^{Q114D}</i>	LYS-12 <i>pClik5a P_{tuf} lysDH^{Rpom Q114D} proC^{Cglu}</i>	This work
PIA-1A <i>LysDH^{S228A}</i>	LYS-12 <i>pClik5a P_{tuf} lysDH^{Rpom S228A} proC^{Cglu}</i>	This work
PIA-1A <i>LysDH^{G286D}</i>	LYS-12 <i>pClik5a P_{tuf} lysDH^{Rpom G286D} proC^{Cglu}</i>	This work
PIA-1B	LYS-12 <i>pClik5a P_{tuf} lysDH^{Geo} proC^{Cglu}</i>	This work
PIA-1C	LYS-12 <i>pClik5a P_{tuf} lysDH^{Atum} proC^{Cglu}</i>	This work
PIA-2A	LYS-12 <i>pClik5a P_{tuf} lysDH^{Rpom, opt} proC^{Cglu, opt}</i>	This work
PIA-2B	LYS-12 <i>pClik5a P_{tuf} proC^{Cglu} P_{tuf} lysDH^{Rpom} proC^{Cglu}</i>	This work
PIA-2C	LYS-12 <i>P_{tuf} lysDH^{Rpom} proC^{Cglu}</i>	This work
PIA-3	LYS-12 <i>pClik5a P_{tuf} lysDH^{Rpom, opt} proH^{Bsub}</i>	This work
PIA-4	LYS-12 <i>P_{tuf} pntAB^{Ecol} pClik5a P_{tuf} lysDH^{Rpom} proC^{Cglu}</i>	This work
PIA-5	LYS-12 <i>P_{tuf} gapN^{Smut, opt} pClik5a P_{tuf} lysDH^{Rpom} proC^{Cglu}</i>	This work
PIA-6	LYS-12 <i>pClik5a P_{tuf} rapL^{Shyg}</i>	This work
PIA-7	LYS-12 <i>pClik5a P_{tuf} lat^{Flut} proC^{Cglu}</i>	This work
PIA-8A	LYS-12 <i>P_{tuf} pntAB^{Ecol} pClik5a P_{tuf} lat^{Flut} proC^{Cglu}</i>	This work
PIA-8B	LYS-12 <i>P_{tuf} gapN^{Smut, opt} pClik5a P_{tuf} lat^{Flut} proC^{Cglu}</i>	This work
PIA-8C	<i>lysC^{fbr} ΔlysE pClik5a P_{tuf} lat^{Flut} proC^{Cglu}</i>	This work
PIA-8D	LYS-12 Δ <i>proP</i> <i>pClik5a P_{tuf} lat^{Flut} proC^{Cglu}</i>	This work
PIA-9	LYS-12 <i>pClik5a P_{sod} lat^{Flut} proC^{Cglu}</i>	This work

Continuation Table 2

Strains	Description	Reference
PIA-10A	LYS-12 <i>pClik5a P_{sod}^{opt1} lat^{Flut} proC^{Cglu}</i>	This work
PIA-10B	LYS-12 <i>pClik5a P_{sod}^{opt2} lat^{Flut} proC^{Cglu}</i>	This work
AVA-5A	AVA-4C with deleted <i>gabTDP</i> operon and genomic expression of <i>P_{tuf} gabP^{Pput}</i>	Rohles, 2021
AVA-5B	AVA-5A with a second copy of <i>P_{tuf} gabP^{Pput}</i>	This work
AVA-7	AVA-6B with genomic expression of <i>P_{tuf} gabP^{Pput}</i>	Rohles, 2021
AVA-8	AVA-7 with a second copy of <i>P_{tuf} gabP^{Pput}</i>	This work
Plasmids	Description	Reference
<i>pTC</i>	Cloning vector, ORI for <i>E. coli</i> , <i>tet^R</i>	Becker et al, 2011
<i>pClik5a</i>	Episomal vector, ORI for <i>E. coli</i> and <i>C. glutamicum</i> , <i>kan^R</i>	Buschke et al, 2011
<i>pClik5a P_{tuf} lysDH^{Rpom} proC^{Cglu}</i>	Episomal expression of <i>lysDH</i> from <i>R. pomeroyi</i> DSS-3 (Acc. No. SPO0234) and <i>proC</i> from <i>C. glutamicum</i> (Acc. No. P0C1E4) under control of <i>P_{tuf}</i>	This work
<i>pClik5a P_{tuf} lysDH^{Rpom} I81K proC^{Cglu}</i>	Episomal expression of <i>lysDH</i> from <i>R. pomeroyi</i> DSS-3 (Acc. No. SPO0234) with point mutation I81K and <i>proC</i> from <i>C. glutamicum</i> (Acc. No. P0C1E4) under control of <i>P_{tuf}</i>	This work
<i>pClik5a P_{tuf} lysDH^{Rpom} Q114D proC^{Cglu}</i>	Episomal expression of <i>lysDH</i> from <i>R. pomeroyi</i> DSS-3 (Acc. No. SPO0234) with point mutation Q114D and <i>proC</i> from <i>C. glutamicum</i> (Acc. No. P0C1E4) under control of <i>P_{tuf}</i>	This work
<i>pClik5a P_{tuf} lysDH^{Rpom} S228A proC^{Cglu}</i>	Episomal expression of <i>lysDH</i> from <i>R. pomeroyi</i> DSS-3 (Acc. No. SPO0234) with point mutation S228A and <i>proC</i> from <i>C. glutamicum</i> (Acc. No. P0C1E4) under control of <i>P_{tuf}</i>	This work
<i>pClik5a P_{tuf} lysDH^{Rpom} G286D proC^{Cglu}</i>	Episomal expression of <i>lysDH</i> from <i>R. pomeroyi</i> DSS-3 (Acc. No. SPO0234) with point mutation G286D and <i>proC</i> from <i>C. glutamicum</i> (Acc. No. P0C1E4) under control of <i>P_{tuf}</i>	This work
<i>pClik5a P_{tuf} lysDH^{Atum} proC^{Cglu}</i>	Episomal expression of <i>lysDH</i> from <i>A. tumefaciens</i> (Acc. No. C5NM90) and <i>proC</i> from <i>C. glutamicum</i> under control of <i>P_{tuf}</i>	This work

Continuation Table 2

Plasmids	Description	Reference
<i>pClik5a P_{tuf} lysDH^{Gste} proC^{Cglu}</i>	Episomal expression of <i>lysDH</i> from <i>G. stearothermophilus</i> (Acc. No. Q9AJC6) and <i>proC</i> from <i>C. glutamicum</i> under control of <i>P_{tuf}</i>	This work
<i>pClik5a P_{tuf} lysDH^{Rpom, opt} proC^{Cglu, opt}</i>	Episomal expression of codon-optimized <i>lysDH</i> from <i>R. pomeroyi</i> DSS-3 and codon-optimized <i>proC</i> from <i>C. glutamicum</i> under control of <i>P_{tuf}</i>	This work
<i>pClik5a P_{tuf} proC^{Cglu} P_{tuf} lysDH^{Rpom} proC^{Cglu}</i>	Episomal expression of <i>lysDH</i> from <i>R. pomeroyi</i> DSS-3 and 2 copies of <i>proC</i> from <i>C. glutamicum</i> under control of <i>P_{tuf}</i>	This work
<i>pClik5a P_{tuf} lysDH^{Rpom} proH^{Bsub}</i>	Episomal expression of <i>lysDH</i> from <i>R. pomeroyi</i> DSS-3 and <i>proH</i> from <i>B. subtilis</i> K168 (Acc. No. P0CI77) under control of <i>P_{tuf}</i>	This work
<i>pClik5a P_{tuf} lat^{Flut} proC^{Cglu}</i>	Episomal expression of <i>lat</i> from <i>F. lutescens</i> IFO 3084 (Acc. No. Q9EVJ7) and <i>proC</i> from <i>C. glutamicum</i> under control of <i>P_{tuf}</i>	This work
<i>pClik5a P_{tuf} mCherry</i>	Episomal expression of mCherry under control of <i>P_{tuf}</i>	This work
<i>pClik5a P_{sod} mCherry</i>	Episomal expression of mCherry under control of <i>P_{sod}</i>	This work
<i>pClik5a P_{sod}^{opt1} mCherry</i>	Episomal expression of mCherry under control of <i>P_{sod}^{opt1}</i>	This work
<i>pClik5a P_{sod}^{opt2} mCherry</i>	Episomal expression of mCherry under control of <i>P_{sod}^{opt2}</i>	This work
<i>pClik5a P_{sod} lat^{Flut} proC^{Cglu}</i>	Episomal expression of <i>lat</i> from <i>F. lutescens</i> IFO 3084 (Acc. No. Q9EVJ7) and <i>proC</i> from <i>C. glutamicum</i> under control of <i>P_{sod}</i>	This work
<i>pClik5a P_{sod}^{opt1} lat^{Flut} proC^{Cglu}</i>	Episomal expression of <i>lat</i> from <i>F. lutescens</i> IFO 3084 (Acc. No. Q9EVJ7) and <i>proC</i> from <i>C. glutamicum</i> under control of <i>P_{sod}^{opt1}</i>	This work
<i>pClik5a P_{sod}^{opt2} lat^{Flut} proC^{Cglu}</i>	Episomal expression of <i>lat</i> from <i>F. lutescens</i> IFO 3084 (Acc. No. Q9EVJ7) and <i>proC</i> from <i>C. glutamicum</i> under control of <i>P_{sod}^{opt2}</i>	This work
<i>pClik5a P_{tuf} lat^{Flut} proC^{Cglu} CM</i>	Episomal expression of <i>lat</i> from <i>F. lutescens</i> IFO 3084 (Acc. No. Q9EVJ7) and <i>proC</i> from <i>C. glutamicum</i> under control of <i>P_{tuf}</i> , kanamycin selection marker replaced by chloramphenicol cassette	This work
<i>pClik int SacB ΔlysE</i>	Partial deletion of <i>lysE</i> (Acc. No. P94633)	Kind et al, 2011

Continuation Table 2

Plasmids	Description	Reference
<i>pClik int SacB ΔlysE</i> <i>CM</i>	Partial deletion of <i>lysE</i> (Acc. No. P94633), kanamycin selection marker replaced by chloramphenicol cassette	This work
<i>pClik int SacB P_{tuf}</i> <i>lat^{Flut} proC^{Cglu} ΔlysE</i>	Partial deletion of <i>lysE</i> (Acc. No. P94633) and simultaneous integration of <i>P_{tuf} lat^{Flut} proC^{Cglu}</i>	This work
<i>pClik int sacB P_{tuf}</i> <i>lysDH^{Rpom} proC^{Cglu}</i>	Genomic integration of <i>lysDH</i> from <i>R. pomeroyi</i> DSS-3 and <i>proC</i> from <i>C. glutamicum</i> under control of <i>P_{tuf}</i> into <i>bioA</i> (NCg2604l)	This work
<i>pClik int sacB ΔproP</i>	Complete deletion of <i>proP</i> (Acc. No. Q79VC4)	This work
<i>pClik int sacB P_{tuf}</i> <i>pntAB</i>	Genomic integration of <i>pntAB</i> from <i>E. coli</i> K12-MG1655 (Acc. No. P07001, P0AB67) under control of <i>P_{tuf}</i> into <i>crtB</i> (NCgl0598)	Hoffmann et al, 2021
<i>pClik int sacB P_{tuf}</i> <i>gapN</i>	Genomic integration of codon-optimized <i>gapN</i> from <i>S. mutans</i> UA159 (Acc. No. Q59931) under control of <i>P_{tuf}</i> into <i>crtI2</i> (NCgl0597)	Hoffmann et al, 2018
<i>pClik int SacB P_{tuf}</i> <i>PP2911 (crtI2)</i>	Genomic integration of a second copy of the GABA permease PP2911 from <i>P. putida</i> (Acc. No. Q88IT8) under control of <i>P_{tuf}</i> into <i>crtI2</i> (NCgl0597)	This work

3.2 Genetic engineering

The software SnapGene (Version 5.3.2 GSL Biotech, Chicago, IL, USA) was used to design the cloning strategies. In an initial step, vectors were linearized using the restriction enzymes *SmaI*, *AscI*, *XbaI*, *NdeI* and *KpnI*, respectively (FastDigest, Thermo Fisher Scientific, Waltham, MA, USA). Fragments of interest were amplified from genomic DNA using PCR (Table S1 and S2, Phusion High-Fidelity PCR Master Mix with HF Buffer, New England Biolabs, Frankfurt am Main, Germany) and primers with specific overlaps (Table S3) (Rohles et al, 2016). The obtained fragments were separated (1 % agarose gel, TAE buffer (40 mM TrisBase, 20 mM glacial acetic acid, 1 mM EDTA, pH 8)), purified (Wizard SV Gel and PCR Clean-Up System, Walldorf, Germany), analyzed (Nanodrop ND-1000 spectrophotometer, software ND-1000 V 3.8.1, PEQLAB Biotechnology GmbH, Erlangen, Germany) and assembled *in vitro* for 1 h at 50 °C (Table S4) (Gibson et al, 2009).

E. coli was transformed with plasmids by heat-shock (Inoue et al, 1990). For that, competent *E. coli* cells were prepared from 100 mL BHI medium culture, pre-grown in a 500 mL shake flask at 37 °C, harvested at an optical density (OD₆₀₀) between 0.25 and 0.3 (5000 x g, 4 °C), chilled on ice for 15 minutes, washed with 80 mL ice-cold 0.1 M CaCl₂, chilled again (30 min, 4 °C) and resuspended in 10 mL ice-cold 0.1 M CaCl₂ solution containing 15 % glycerol (The Filion lab, version 0.5, March 24 2012). For transformation these cells were incubated with 10 µL of Gibson assembly mix (30 min, 4 °C), heat-shocked (45 sec, 45 °C), chilled on ice (2 min, 4 °C) and incubated in 900 µL BHI medium at 37 °C for 1 hour (850 rpm ThermoMixer C, Eppendorf, Hamburg, Germany). Subsequently, cells were plated out on BHI agar, containing appropriate amounts of antibiotics (50 µg mL⁻¹ kanamycin, 12.5 µg mL⁻¹ tetracycline), and incubated at 37 °C for 12 h. Plasmids were verified for correctness using colony PCR (Table S1 and S2, Phire Green Hot Start II PCR Master Mix, ThermoFisher Scientific) and isolated (Qiagen Plasmid Mini Kit, Hilden, Germany).

C. glutamicum cells were transformed by electroporation. In short, exponentially growing cells were harvested (4 min, 4732 x g, 4 °C), washed twice with 5 mL of 10 % (v/v) glycerol (4 min, 4732 x g, 4 °C) and resuspended in 8 mL of 10 % (v/v) glycerol per gram cell wet weight. Then, 200 µL of electro-competent cells were mixed with plasmid DNA (500 ng for episomal plasmids, 5,000 ng for integrative plasmids) in electroporation cuvettes (0.2 cm, Gene Pulser/ MicroPulser Electroporation Cuvettes, Bio-Rad Laboratories, Hercules, California, USA), incubated (2 min, 4 °C), overlaid with 400 µL 10 % (v/v) glycerol, pulsed (3kV, 25 µF, 200 Ω, GenePulser XCell, Bio-Rad Laboratories, Hercules, California, USA) and heat-shocked in 4 mL BHIS medium (6 min, 46 °C). The cells were then regenerated for 2 h in an orbital shaker (30 °C, 230 rpm, 5 cm, HT Infors Multitron, Bottmingen, Switzerland), harvested (5962 x g, 3 min, room temperature) plated on BHIS-Kan medium (50 µg ml⁻¹), and incubated at 30 °C for 36 h to 48 h (Becker et al, 2010). For integrative plasmids the further procedure included two recombination events (Becker et al, 2005). Selection is based on kanamycin and sucrose which would be further converted to toxic

levan by the levansucrase *sacB* (Jäger et al, 1992). PCR (Table S1 and S2, Phire Green Hot Start II PCR Master Mix, ThermoFisher Scientific) and Sanger sequencing (Azenta, Chelmsford, MA, USA) were used to verify correct clones.

3.2.1 Plasmid-based operons for L-pipecolic acid production

L-pipecolic acid operons based on L-lysine 6-dehydrogenase variants and Δ^1 -pyrroline 5-carboxylate reductase. For L-pipecolic acid production several combinations and layouts of genetic elements were tested (Fig. 8). All operons comprised the promoter of the *tuf* gene (200 bp upstream of *tuf*) and two genes separated by the 20 bp sized ribosomal binding site of P_{tuf} (Rohles et al, 2016). Final assembly with the vector *pClik5a* MCS and preparation was conducted as described above.

In a first approach three different *lysDH* were individually combined with *proC*. For the amplification of the native *lysDH* gene of *R. pomeroyi* DSS-3 (Acc. No. SPO0234, 1,107 bp) genomic DNA served as template. The native *lysDH* genes of *Geobacillus stearothermophilus* UTB1103 (Acc. No. Q9AJC6, 1,158 bp) and *Agrobacterium tumefaciens* (Acc. No. C5NM90, 1,101 bp) were synthesized from digital data (Azenta). The second gene *proC* was isolated from *C. glutamicum* (Acc. No. P0C1E, 813 bp). Additionally, another biosynthetic design comprised the combination of codon-optimized variants of the *lysDH* from *R. pomeroyi* DSS-3 and *proC* from *C. glutamicum* (Eurofins, Ebersberg, Germany). In a further bicistronic operon two copies of *proC* were introduced. The second copy under control of P_{tuf} was cloned upstream of the previous operon *lysDH^{Rpom} proC^{Cglu}*. In a sixth alternative, the native *proC* from *C. glutamicum* (Acc. No. P0C1E, 813 bp) was replaced by the native *proH* gene from *B. subtilis* (Acc. No. Q62U84, 894 bp). The final operon comprised the promoter *tuf*, the native *lysDH* gene from *R. pomeroyi* (1,107 bp), the additional RBS from P_{tuf} and *proH* from *B. subtilis*.

L-pipecolic acid operons based on L-lysine 6-aminotransferase and Δ^1 -pyrroline 5-carboxylate reductase. In the next approach *lat* was combined with *proC*. The native *lat* gene from *F. lutescens* IFO 3084 (Acc. No. Q9EVJ7, 1,479 bp) and the second gene *proC* originally isolated from *C. glutamicum* (Acc. No. P0C1E, 813 bp) were synthesized based on digital sequence (Azenta). In an advanced approach the promoter *tuf* was replaced by native and synthetic variants of *sod* promoter (Acc. No. Q9APY3, 180 bp).

L-pipecolic acid module based on L-lysine cyclodeaminase. In another approach, the native L-lysine cyclodeaminase gene *rapL* from *S. hygrosopicus* (Acc. No. Q54304, 1,032 bp) was amplified from genomic template. The genetic element was assembled with the promoter *tuf* and further prepared as described above.

Computational modelling-based modifications of the LysDH protein sequence. To change pH preference of LysDH, a structural model of LysDH from *R. pomeroyi* was derived from the template models A0A0P1II55_9RHOB (SWISS-MODEL, Biozentrum, University of Basel) from *Ruegeria denitrificans* and A0A1Y5TAF1_9RHOB (SWISS-MODEL) from *Pseudoruegeria aquimaris*. Protein sequence alignments were used to identify potential modification sites. Structural modeling and alignment were conducted by Michael Hutter (Saarland University). The QuikChange Kit (Agilent Technologies) and specific primers (Table S3) were used to introduce the identified mutations.

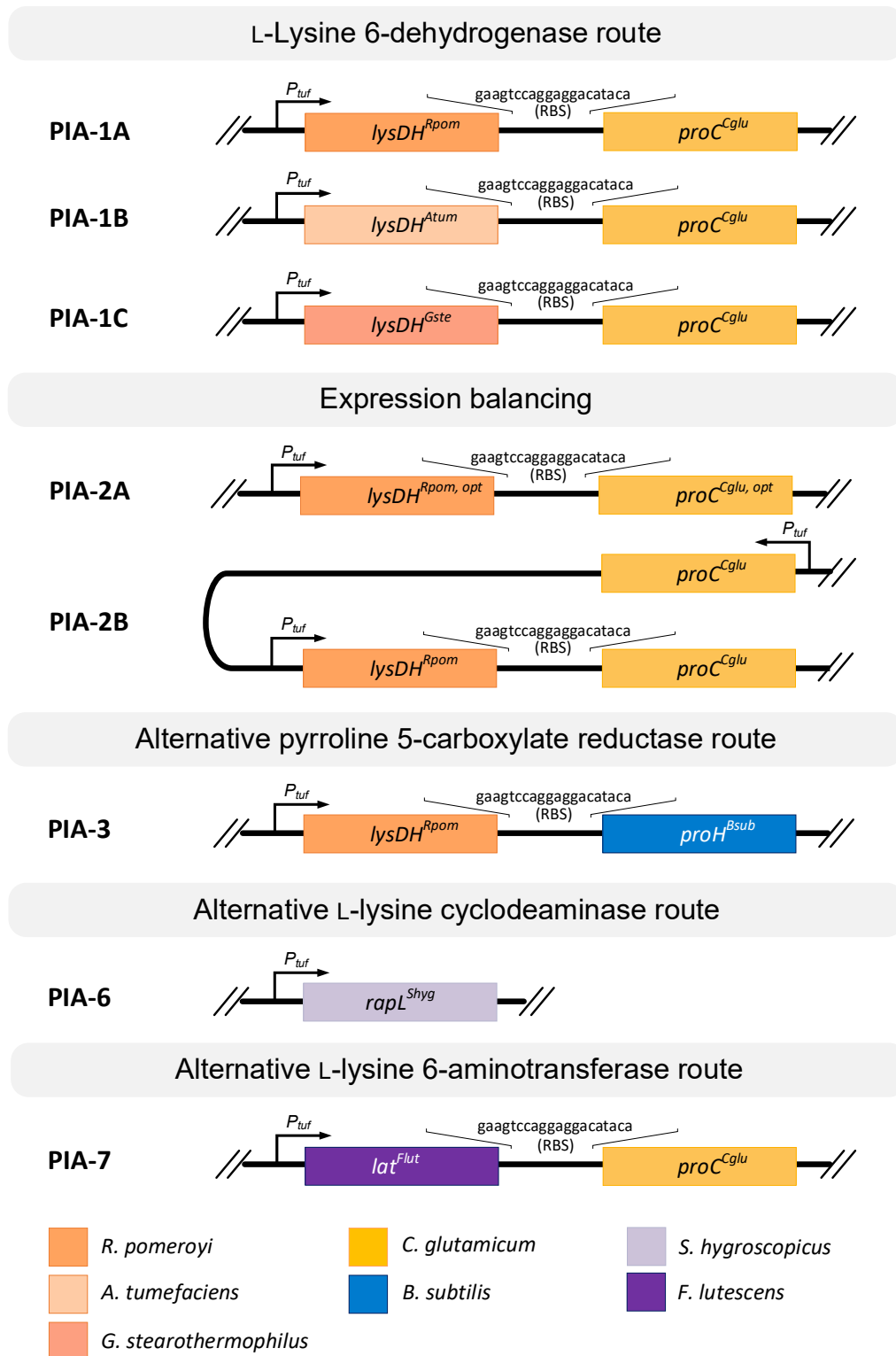


Fig. 8: Plasmid-based operons for L-pipecolic acid production. Several combinations and layouts of genetic elements were tested. All operons comprised the *tuf* promoter and two genes separated by the 20-bp sized ribosomal binding site of *P_{tuf}*. For the L-lysine 6-dehydrogenase (*lysDH*) *R. pomeroyi*, *A. tumefaciens* and *G. stearothermophilus* served as donor. *C. glutamicum* and *B. subtilis* provided two different Δ^1 -pyrroline 5-carboxylate reductases (*proC* and *proH*). L-lysine cyclodeaminase and L-lysine 6-aminotransferase were isolated from *S. hygroscopicus* and *F. lutescens*, respectively.

3.2.2 Integrative genetic modules for L-pipecolic acid production

Genome-based integration of L-lysine 6-dehydrogenase and Δ^1 -pyrroline 5-carboxylate reductase operon in *C. glutamicum*. First, the operon $P_{tuf} lysDH^{Rpom} proC^{Cglu}$ (2,180 bp) was amplified from the plasmid described above. Additional flanking regions, intended to insert the operon into the *bioA* locus (Acc. No. P46395), were fused upstream (606 bp) and downstream (591 bp) with the construct. The linked genetic elements were then introduced into the linearized vector *pClik int SacB* and further processed as described above. Two integration events were used to integrate the operon into the genome of *C. glutamicum*.

Genome-based integration of supporting modules for enhanced redox supply. In order to improve the redox supply in L-pipecolic acid producing strains, two genome-based expression modules were tested: the native transhydrogenase gene *pntAB* (Hoffmann et al, 2021) and a codon-optimized version of NADP-dependent glyceraldehyde 3-phosphate dehydrogenase gene *gapN* (Hoffmann et al, 2018). Final assembly with the vector *pClik int sacB* and preparation was conducted as described above and included two recombination events in *C. glutamicum*.

For the integration of the membrane-bound transhydrogenase *pntAB* (Acc. No. P07001, P0AB67, 2,932 bp) from *E. coli* K12-MG1655, the operon was fused with the promoter P_{tuf} (Acc. No. P42439, 200 bp) and flanked by two homologous sites (600 bp each). Flanking regions were designed to integrate into *crtB* locus (Acc. No. Q93QX6) (Hoffmann et al, 2018; Hoffmann et al, 2021).

The *gapN* gene from *S. mutans* UA159 (SMU 676) was codon-optimized for *C. glutamicum* and synthesized (Hoffmann et al, 2018; Hoffmann et al, 2021). Optimization included exchange of the weak native translational start codon GTG by ATG (Hoffmann et al, 2018). The *gapN* gene was fused with the promoter P_{tuf} (Acc. No. P42439, 200 bp) and flanked by two homologous regions (483 bp and 447 bp) to be introduced into the *crtI2* gene locus (Acc. No. Q8NSP5) in *C. glutamicum* (Hoffmann et al, 2018).

The recombinant strains LYS-12 $P_{tuf} pntAB^{EcoI}$ and LYS-12 $\Delta mtlR P_{tuf} gapN^{SmuT, opt}$ were taken from previous work (Hoffmann et al, 2018; Hoffmann et al, 2021).

Genomic deletion of genes encoding competing transporters. To diminish by-product formation and re-import L-pipecolic acid, the gene *lysE*, encoding the L-lysine exporter and *prop*, potentially encoding an L-pipecolic acid importer should be deleted in L-pipecolic acid producing strains. In a first round, the L-pipecolic acid module, comprising the promoter *tuf* and the genes *lat* and *proC*, were flanked by homologous sites (500 bp), designed to delete *lysE*. Due to beneficial episomal expression of the L-pipecolic acid genetic elements, the already existing plasmids *pClik int SacB $\Delta lysE$* and *pClik5a P_{tuf} lat^{Flut} proC^{Cglu}* were modified. A chloramphenicol resistance cassette including the promoter (820 bp), was introduced into each plasmid using the restriction sites *SmaI* and *AscI* to ensure simultaneous episomal expression as well as selection.

For deletion of the potential L-pipecolic acid importer, flanking sites of *proP* (500 bp each, upstream and downstream of Acc. No. Q79VC4) were assembled with the *SmaI*-linearized-vector *pClik int SacB*.

3.2.3 Integrative genetic module for 5-aminovalerate production

A second copy of GABA permease PP2911 from *P. putida* (Acc. No. Q88IT8) was integrated into *C. glutamicum* AVA-5A and AVA-7. The assembled plasmid, based on *SmaI*-linearized *pClik int sacB* vector, comprised the *tuf* promoter (200 bp) and the *gabP* gene (1,389 bp), flanked by two homologous sites (500 bp each) to be integrated into the *crtI2* (Q8NSP5) locus.

3.2.4 Generation of synthetic promoter variants for fine-tuned gene expression

The *mCherry* gene was used as reporter (Kohlstedt et al, 2018). The gene was amplified using *pSEVA247R* as template (Silva-Rocha et al, 2013) and assembled with the *NdeI*-linearized vector *pClik 5a MCS*. For further promoter cloning, the primer pair PR_{mCherry_1} and PR_{mCherry_2} used to amplify *mCherry* gene in a first round, introduced an additional *NdeI* upstream of the *mCherry* gene.

For random mutagenesis of the promoter *sod* (Acc. No. Q9APY3, 180 bp) (Becker et al, 2007) a two-step PCR-protocol and the instructions of the JBS dNTP-Mutagenesis Kit (Jena Bioscience, Jena, Germany) were followed. The first PCR step was used to amplify the promoter in co-presence of dNTP analogs with varying PCR cycles (10, 20, 30). In a second PCR, specific overlaps were introduced to subclone the mutagenized promoter variants into the newly derived vector *pClik 5a MCS mCherry* by using *NdeI* restriction site and Gibson assembly. Plasmids were processed as described above and used to transform *C. glutamicum*. Plasmids with the native *sod* (Acc. No. Q9APY3, 180 bp) and *tuf* promoter, respectively, served as reference (Acc. No. P42439, 200 bp). The two *sod* promoter derivatives used here, were generated, and kindly provided by Fabia Weiland (Saarland University).

3.3 Media

3.3.1 Batch medium

E. coli cultures and first-step pre-cultures of *C. glutamicum* were prepared in BHI medium (37 g L⁻¹, Brain heart Infusion, Becton Dickinson, Heidelberg, Germany). For the regeneration of transformed *C. glutamicum* cells, BHI medium was enriched with 0.5 M sorbitol. Second-step pre-cultures and main cultures of *C. glutamicum* were grown in minimal medium which contained per liter: 10 g of glucose, 15 g of (NH₄)₂SO₄, 1 g of NaCl, 200 mg of MgSO₄·7H₂O, 55 mg of CaCl₂, 20 mg of FeSO₄·7H₂O, 1 mg of thiamin HCl,

1 mg of calcium pantothenate, 0.5 mg of biotin, 100 mL of 2 M potassium phosphate buffer (pH 7.8), 10 mL of a trace element solution (200 mg L⁻¹ of FeCl₃·6H₂O, 200 mg L⁻¹ of MnSO₄·H₂O, 50 mg L⁻¹ of ZnSO₄·7H₂O, 20 mg L⁻¹ of CuCl₂·2H₂O, 20 mg L⁻¹ of Na₂B₄O₇·10H₂O, 10 mg L⁻¹ of (NH₄)₆Mo₇O₂₄·4H₂O, adjusted to pH 1.0 with HCl), and 30 µg L⁻¹ of 3,4-dihydroxybenzoic acid. To grow strains with episomal plasmids, kanamycin (50 µg mL⁻¹) and tetracycline (12.5 µg L⁻¹) were added to the medium. Solid media were obtained by mixing liquid formulations with 20 g L⁻¹ of Difco agar (Becton Dickinson).

3.3.2 Fed-batch medium

For fed-batch processes, the initial batch medium (300 mL) contained per liter: 90 g of glucose, 25 g of (NH₄)₂SO₄, 15 g of yeast extract (Becton Dickinson), 2 g of citric acid, 1.25 g of KH₂PO₄, 1.25 g of Na₂HPO₄, 1.25 g of MgSO₄ · 7 H₂O, 168 mg of CaSO₄ · 2 H₂O, 70 mg of FeSO₄ · 7 H₂O, 30 mg of ZnSO₄ · 7 H₂O, 9.1 mg of MnSO₄ · H₂O, 15 mL of a vitamin stock (300 mg L⁻¹ biotin, 500 mg L⁻¹ thiamin · HCl, 600 mg L⁻¹ nicotinamide, 2 g L⁻¹ calcium pantothenate), and 1.43 mL of a trace element stock (2.1 g L⁻¹ citric acid, 228 mg L⁻¹ CuSO₄ · 5 H₂O, 214 mg L⁻¹ CoSO₄ · 7 H₂O, 169 mg L⁻¹ NiSO₄ · 6 H₂O, 150 mg L⁻¹ Na₂B₄O₇·10 H₂O, 29.5 mg L⁻¹ Na₂MoO₄ · 2 H₂O). In addition, 50 µg mL⁻¹ kanamycin, 13 mg L⁻¹ pyridoxal-5-phosphate monohydrate (Sigma Aldrich, St. Louis, MI, USA), and 1 mL antifoam 204 (Sigma Aldrich, St. Louis, MI, USA) was added.

The feed solution for the second phase of the process contained per liter: 500 g of glucose, 200 g of (NH₄)₂SO₄, 15 g of yeast extract (Becton Dickinson), 14 g of urea (Grüssing Analytica, Filsum, Germany), 2 g of citric acid, 1.25 g of KH₂PO₄, 1.25 g of Na₂HPO₄, 1.25 g of MgSO₄ · 7 H₂O, 168 mg of CaSO₄ · 2 H₂O, 70 mg of FeSO₄ · 7 H₂O, 30 mg of ZnSO₄ · 7 H₂O, 9.1 mg of MnSO₄ · H₂O, 15 mL of vitamin stock (300 mg L⁻¹ biotin, 500 mg L⁻¹ thiamin · HCl, 600 mg L⁻¹ nicotinamide, 2 g L⁻¹ calcium pantothenate), 1.43 mL of a trace element stock (2.1 g L⁻¹ citric acid, 228 mg L⁻¹ CuSO₄ · 5 H₂O, 214 mg L⁻¹ CoSO₄

· 7 H₂O, 169 mg L⁻¹ NiSO₄ · 6 H₂O, 150 mg L⁻¹ Na₂B₄O₇·10H₂O, 29.5 mg L⁻¹ Na₂MoO₄ · 2 H₂O), and 13 mg L⁻¹ pyridoxal-5-phosphate monohydrate.

3.4 Cultivation

E. coli was pre-grown on BHI agar at 37 °C for 12 h. Then, one loop of cells was used to inoculate the main culture in 100 mL shake flasks, filled with 10 mL BHI medium which was incubated on an orbital shaker (37 °C, 230 rpm, 85 % humidity, Multitron, Infors AG, Bottmingen, Switzerland).

The first pre-culture of *C. glutamicum* (10 mL BHI medium in 100 mL baffled shake flask) was inoculated with a colony from an agar plate culture that had been pre-incubated at 30 °C for 48 h. It was grown overnight on an orbital shaker. Harvested cells (3 min, 8,800 x g, room temperature) served as inoculum for the second pre-culture in minimal medium (25 mL in 250 mL baffled shake flask) When reaching mid exponential growth phase, cells were harvested and used to inoculate the main culture in minimal medium (5m mL medium in 500 mL baffled shake flasks). All liquid cultures were conducted in an orbital shaker (230 rpm, 85 % humidity, Multitron, Infors AG). Different temperatures were used, as described below. Main cultures were conducted in biological triplicate.

3.4.1 Cultivation in miniaturized microtiter plate system

A miniaturized bioreactor system (1,300 rpm, 85 % humidity, Beckman Coulter GmbH, Baesweiler, Germany) was used to screen *C. glutamicum* strains. The cultures were grown in 48-well flower plates, filled with 1 mL medium and inoculated to an initial OD₆₂₀ of 0.2. Cell growth was monitored online at 620 nm (OD₆₂₀) (Becker et al, 2018a; Weiland et al, 2023). The pre-cultures were prepared as described before. The system was also used to quantify the strength of promoters. The analysis was based on reporter strains that expressed mCherry and the online measurement of fluorescence (580/610 nm). The

specific strength of a promoter was calculated from the slope of the recorded fluorescence signal against the increase of biomass over time and expressed as specific fluorescence unit (SFU) (Kohlstedt et al, 2018). All main cultures were conducted in biological triplicate.

3.4.2 Cultivation in lab scale bioreactors

A first pre-culture was inoculated from a BHI agar plate, pre-incubated for 2 days at 30 °C. For this purpose, a colony was inoculated into 50 mL BHI medium in a 500 mL shake flask. The pre-culture was grown overnight at 34 °C (230 rpm, 85 % humidity, Multitron, Infors AG). Then, the cells were harvested (3 min, 8,800 x g, room temperature), re-suspended in 2 L shake flasks, filled with 200 mL batch medium to an initial OD₆₆₀ of 0.2, and incubated over 20 h at 34 °C (230 rpm, 85 % humidity, Multitron, Infors AG). Then, the cells were again harvested as described above and re-suspended in 50 mL batch medium each, which was then added to the bioreactor, pre-filled with 250 mL batch medium (1 L lab scale bioreactor, Eppendorf, Hamburg, Germany). For each bioreactor, a separate pre-culture was prepared.

Fed-batch processes were monitored and controlled by DASGIP control software (SR0700ODLS, Eppendorf). The pH value was kept at 7.0 ± 0.2 using a pH probe (405-DPAS-SC-K8S/225, Mettler Toledo, Giessen, Germany) and automatic addition of 6 M NaOH (MP8 pump system, Eppendorf). The initial stirring rate was set to 800 rpm. An optical sensor (VisiFerm DO 225, Hamilton, Höchst, Germany) measured the dissolved oxygen (DO) level in the bioreactor. During the process, the DO level was controlled above 30 % of saturation by automatic adjustment of the stirring rate. The aeration rate was maintained constant at 1 vvm. The content of CO₂ and O₂ in the exhaust gas was monitored online (GA4, Eppendorf). The feed phase was initiated when glucose was depleted. The sudden increase of DO signal that resulted from consumption of the sugar was used as trigger to automatically add 20 mL feed pulses.

Different process configurations were tested. In a first set-up, the temperature was kept at $34\text{ °C} \pm 0.1$ (CWD4 Bioblock, Eppendorf). In a second set-up, the initial batch phase was controlled at 30 °C , and the temperature was increased to 34 °C at the beginning of the feed phase. A third set-up was conducted at $30\text{ °C} \pm 0.1$. Each condition was performed in duplicate. The deviation between duplicates was in the range of 5 %.

3.5 Analytics

3.5.1 Quantification of cell concentration

The optical density of the cells was measured at 660 nm (OD_{660}) using photometry (UV-1600PC Spectrophotometer, VWR, Darmstadt International, Germany). The cell dry weight (CDW) was calculated from optical density readings using a previously established correlation ($CDW\ [g\ L^{-1}] = 0.32 \times OD_{660}$) (Rohles et al, 2016).

3.5.2 Quantification of substrates and extracellular products

Glucose and gluarate were quantified by HPLC (1260 Infinity Series, Agilent Technologies) using an Aminex HPX-87H column (7.8 mm x 300 mm x 9 μm , 55 $^{\circ}\text{C}$, Bio-Rad Laboratories, Hercules, CA, USA) as the stationary phase and 3.5 mM H_2SO_4 as the mobile phase (0.8 mL min^{-1}) (Rohles et al, 2016; Rohles et al, 2018). Glucose was measured using refractive index analysis (1260 RID, G1362A, Agilent Technologies), and its quantification was based on external standards.

The concentration of L-pipecolic acid was determined by HPLC (1290 Infinity Series, Agilent Technologies) using an Eclipse Plus C18 column (4.6 mm x 100 mm x 3.5 μm , Agilent Technologies), kept at 10 $^{\circ}\text{C}$, and a gradient of water (A) and acetonitrile (B) at a flow rate of 0.7 mL min^{-1} as the eluent (0 min: 100 % A, 0-3 min: 90 % A, 3-3.5 min: 0 % A, 3.5-4 min: 100 % A, 4–7 min: 100 % A). For detection, a diode array detector was used (194 nm, 1290 Infinity II Diode Array Detector, Agilent Technologies). External standards

were used for quantification. The quantification of L-lysine and 5-aminovalerate was conducted by HPLC (1200 Series, Agilent Technologies) as described previously (Krömer et al, 2005; Rohles et al, 2016). Prior to analysis, samples were diluted with α -aminobutyric acid (220 μ M) as an internal standard (Krömer et al, 2008).

The phosphate level was determined by ion chromatography (Thermo Scientific, Karlsruhe, Germany) using an anion exchange column (IonPac AS9-HC, 2 mm x 250 mm x 9 μ m, Thermo Scientific) at 30 °C as the stationary phase and 12 mM Na₂CO₃ as the mobile phase (0.25 mL min⁻¹) (Kuhl et al, 2020). Trehalose, lactate, and acetate were analyzed via HPLC (1260 Infinity Series, Agilent Technologies) (Hoffmann et al, 2018).

3.5.3 Extraction and quantification of intracellular intermediates

Intracellular metabolites were collected using fast filtration and extraction in boiling water (Bolten et al, 2009). The obtained cell extract was diluted 1:10 with α -aminobutyric acid as an internal standard (Krömer et al, 2008). Subsequently, L-pipecolic was quantified in the obtained cell extract by HPLC (1260 Infinity Series, Agilent) using a C18 column (4.6 mm x 100 mm x 3.5 μ m, Gemini Phenomenex, Phenomenex, Torrance, CA, USA) at 40 °C, a gradient of eluent A (10 mM NaH₂PO₄, 0.125 g L⁻¹ sodium azide, pH 7.8) and eluent B (70 % acetonitrile, 20 % methanol, 10 % water) as the mobile phase (1 mL min⁻¹, 0 min: 56 % A, 0-1 min: 56 % A, 1-7.5 min: 36.5 % A, 7.5-8 min: 0 % A, 8-10 min: 0% A, 10-13 min: 56 % A, 13-15 min: 56 % A) and fluorescence detection (266/305 nm, G1321 A, Agilent Technologies). Prior to analysis, the analytes were derivatized with fluorenylmethoxycarbonyl (FMOC) under reducing conditions (0.5 % 2-mercaptopropionate in 500 mM bicine, pH 9.0) using the HPLC autosampler and a predefined sample sequence. External standards were used for quantification. All other intracellular intermediates were quantified as described above (Rohles et al, 2016; Rohles et al, 2018; Krömer et al, 2005). Intracellular concentrations were estimated based on a correlation factor of 1.95 (μ L cytoplasm) mg_{CDW}⁻¹ (Krömer et al, 2004).

3.5.4 GC-MS analysis of L-pipecolic acid

First, the culture supernatant (20 μL) was dried under nitrogen. Then, the obtained solid was dissolved in 50 μL of dimethyl formamide (0.1 % pyridine) and 50 μL of N-methyl-N-*t*-butyldimethylsilyl-trifluoroacetamide (Macherey-Nagel, Düren, Germany), followed by incubation for 30 min at 80 °C, clarification from debris and GC–MS analysis (Kiefer et al, 2004). The setup comprised a gas chromatograph (GC 7890B, Agilent Technologies), an HP-5MS column (5 % phenyl-methylpolysiloxane, 30 m x 250 μm x 0.25 μm , Agilent Technologies) as the stationary phase, Helium 5.0 as the carrier gas (1.2 mL min⁻¹), and a quadrupole detector (MSD 5977A, Agilent Technologies) (Krömer et al, 2008; Schwechheimer et al, 2018). For analysis, a 2 μL sample was injected at a split ratio of 1:10. The column temperature was initially kept at 120 °C (0-2 min) and then increased to 300 °C at a rate of 10 °C min⁻¹. The instrument was operated at the following temperature settings: inlet: 300 °C, ion source: 230 °C, interface: 300 °C, and quadrupole: 150 °C. Using this protocol, L-pipecolic acid eluted after 10.6 minutes. Structural identification was based on a library search (MassHunter Library version NIST08.L, Agilent Technologies) and analysis of a commercial standard.

3.5.5 Analysis of enzymatic activities

L-Lysine 6-dehydrogenase. Exponentially growing cells were harvested (5 min, 8000 x *g*, 4 °C) and washed twice with 100 mM glycine-KOH buffer (pH 10.0, 0.5 mM dithiothreitol) or 100 mM potassium phosphate buffer (pH 7.8, 0.5 mM dithiothreitol) depending on the desired pH for the later assay. Then, the cells were resuspended in the same buffer to a final concentration of 1 g (cell wet mass) mL⁻¹, and aliquots were placed in lysing matrix B tubes (MP Biomedicals, Eschwege, Germany). Cell disruption was then performed in a ribolyser (Precellys 24, Bertin Technologies, Ile de France, France) with a 2 min cooling step on ice between two disruption cycles (30 s, 5500 x *g*). Subsequently, cell debris was removed by centrifugation (8,000 x *g*, 4 °C, 20 min). The master mix for the enzyme assay

was based either on glycine-KOH (pH 10.0) or on potassium phosphate (pH 7.8). Each sample contained 10 mM L-lysine HCl, 2 mM NAD⁺, and 50 $\mu\text{L mL}^{-1}$ of diluted cell extract. To investigate the enzyme kinetics, the concentrations of L-lysine and NAD⁺ were varied as specified below. Unless stated otherwise, all assays were performed at 30 °C. Negative controls without NAD⁺, L-lysine, and cell extract were included in all experiments. Enzymatic activity was assayed as the change in absorbance at 340 nm over time (Hoffmann et al, 2018).

L-Lysine 6-aminotransferase. Exponentially growing cells were harvested (5 min, 8000 $\times g$, 4 °C) and washed twice with 100 mM Tris-HCl buffer (pH 8.5, 0.5 mM dithiothreitol, 0.5 mM pyridoxal phosphate) or 100 mM potassium phosphate buffer (pH 7.8, 0.5 mM dithiothreitol, 0.5 mM pyridoxal phosphate), depending on the pH desired for the subsequent analysis. Then, cells were resuspended in the same buffer to a final concentration of 1 g (cell wet mass) mL^{-1} , and aliquots were placed in lysing matrix B tubes (MP Biomedicals, Eschwege, Germany). Mechanical cell disruption was performed as described above. Subsequently, cell debris was removed by centrifugation (8,000 $\times g$, 4 °C, 20 min). The master mix for enzymatic analysis comprised either 100 mM Tris-HCl (pH 8.5) or 100 mM potassium phosphate (pH 7.8) buffer plus L-lysine HCl (0 - 30 mM), 10 mM α -ketoglutarate, 0.5 mM pyridoxal phosphate, and 50 $\mu\text{L mL}^{-1}$ cell extract. A volume of 10 mL of reaction mix was placed in a shake flask (100 mL) and incubated for 1 h at 30 °C on an orbital shaker (230 rpm, 5 cm, HT Infors Multitron). Samples were taken every 5 minutes, followed by immediate inactivation (100 °C, 15 min, ThermoMixer C, Eppendorf Deutschland, Wesseling-Berzdorf, Germany). Protein debris was removed (8,000 $\times g$, 4 °C, 3 min). Enzymatic activity was then inferred from the linear decrease in the L-lysine concentration, which was quantified via HPLC as described above. In all cases, the total protein concentration of the cell extract was estimated using the Bradford method (Protein Assay Dye Reagent Concentrate, Bio-Rad Laboratories) and bovine serum albumin as a standard (Becker et al, 2008).

3.5.6 Extraction and quantification of redox metabolites

Culture samples were quenched using a protocol from previous work (Hoffmann et al, 2021). In short, 5 mL of culture broth was mixed with 10 mL of precooled methanol (-58 °C, 60 % v/v), centrifuged (9,400 x g, -10 °C, 5 min) and resuspended in 1.1 mL phosphate-buffered saline. To obtain separate samples for NAD⁺ and NADH analysis, the suspension was split into two fractions of 500 µL each, and each fraction was centrifuged (10,000 x g, 4 °C, 5 min). The intracellular NAD⁺ and NADH levels were then determined using an assay kit (EnzyChrom NAD⁺/NADH Assay Kit, BioAssay System, Hayward, CA, USA) following the manufacturer's protocol. Finally, this yielded the NADH to NAD⁺ ratio.

3.5.7 Global gene expression analysis using DNA microarray

A customized microarray (SurePrint G3 Custom GE 8x60 K, part number G4863A, Agilent Technologies) was designed using the eArray workspace (Agilent Technologies) (Christmann et al, 2023). Three different probes (45 to 60 bp) covered each gene of the *C. glutamicum* ATCC 13032 genome (entry number: # T00102, KEGG database) plus heterologous genes of interest: *lysDH* from *R. pomeroyi* in native and codon-optimized forms, native *lysDH* from *Agrobacterium tumefaciens* and *Geobacillus stearothermophilus*, native *lat* from *Flavobacterium lutescens*, and the codon-optimized *proC* from *C. glutamicum*, respectively. Each probe was applied as 6 replicates and randomized to different locations on the slide using SurePrint technology (Agilent Technologies).

First, RNA was isolated, cleaned up (RNeasy Mini Kit, Qiagen, Hilden, Germany) and quantified (NanoDrop 1000, PEQLAB Biotechnology, Erlangen, Germany). Then, the RNA quality was evaluated (RNA 6000 Nano Kit, 2100 Bioanalyzer System, Agilent Technologies). All samples exhibited an RNA integrity number (RIN) > 9.9. In the next step, fluorescent cRNA was generated (Low Input Quick Amp WT Labeling One-Color Kit, Agilent Technologies, RNA Spike-In One-Color Kit, Agilent Technologies, and RNeasy Mini Kit, Qiagen). Fifty nanograms of total RNA served as the starting material and yielded

> 825 ng of labeled cRNA with a specific Cy3 activity of 15 pmol Cy3 per μg cRNA. A total of 600 ng of labeled cRNA was hybridized onto the microarray (Gene Expression Hybridization Kit, hybridization gasket slides, SureHyb chamber, hybridization oven, all Agilent Technologies). Subsequently, the slide sandwiches were disassembled (Gene Expression Wash Buffer Kit, Agilent Technologies). Scanning was then conducted by the SureScan Microarray Scanner (G4900DA, SureScan Microarray Scanner Control Software, Version 9.1.11.13, Agilent Technologies). Transcriptomic data extraction was performed with microarray and feature extraction software (Version 12.1.1.1, Agilent Technologies). The results were visualized and further evaluated using GeneSpring software (Version 14.9, Agilent Technologies). For statistical analysis, a moderated t test was applied, using asymptotic computation of p-values adjusted for multiple testing according to the Benjamini–Hochberg method and a q-value cutoff of 0.05 (Kohlstedt et al, 2022). The data were then filtered for genes with a \log_2 -fold change ≥ 1 (p-value ≤ 0.05). RNA extraction and analysis were conducted in biological triplicate for each condition. The entire transcriptome dataset is available at GEO (GSESE216736).

4 Results and Discussion

4.1 Metabolic engineering at the level of product secretion exemplary using 5-aminovalerate producing strains

The chemical 5-aminovalerate is an L-lysine derivative with widespread applications for bio-polymer production (Rohles et al, 2016; Adkins et al, 2013; Park et al, 2014b). Meanwhile, biotechnological routes promise sustainable production of this interesting chemical (Rohles et al, 2016). These routes make use of catabolic pathways which involve 5-aminovalerate as intermediate from the degradation of L-lysine (Revelles et al, 2005). A prominent recent example was based on the implementation of the *davBA* operon from *P. putida*, encoding for two enzymes to convert L-lysine into 5-aminovalerate, L-lysine hyperproducing strain *C. glutamicum* LYS-12 (Rohles et al, 2016). After the elimination of competing pathways via deletion of the genes *lysE* and *gabT*, the created producer AVA-3 yielded 28 g L⁻¹ 5-aminovalerate with major shares of glutarate in a fed-batch process (Rohles et al, 2016). Subsequent attempts aimed to modulate the expression level of *davB* and *davA* by codon-optimization (Pauli, 2018) and identified a monocistronic layout based on the native codon usage as optimum (Pauli, 2018). Hereby, the analysis of the 5-aminovalerate-producing strain AVA-1 revealed high, well-balanced enzyme activity of DavB and DavA (above 1 U mg⁻¹ *in vitro*), whereas the other mutants that expressed either codon-optimized or bi-cistronic operons exhibited imbalanced and decreased enzyme activities (Pauli, 2018).

Further strain optimization strategies were therefore based on *C. glutamicum* AVA-3 with the native *davBA* operon and deleted *lysE* and *gabT* genes (Rohles, 2021). During further development, metabolome analysis of 5-aminovalerate producers unraveled a high intracellular concentration of the product up to 340 mM (Rohles, 2021), suggesting a limitation in product export.

4.1.1 Construction and evaluation of export mutants

Towards improved production, heterologous expression of 5-aminovalerate transport proteins was evaluated. The GABA permease from *P. putida* KT2440 GabP-III appeared as promising candidate (Li et al, 2016; Rohles, 2021). The corresponding gene was expressed in the 5-aminovalerate overproducer *C. glutamicum* AVA-4C (LYS-12 *davBA* Δ *lysE*, Δ *gabTDP*) under control of the constitutive promotor *P_{tuf}* (Rohles, 2021). Beneficially, the newly derived strain *C. glutamicum* AVA-5A elevated amounts of 18.9 mM of 5-aminovalerate (Rohles, 2021).

Based on the positive outcome, another round of metabolic engineering aimed at further streamlining product export. Therefore, a second copy of GabP-III from *P. putida* was implemented to increase 5-aminovalerate export. The gene was integrated into the *crtI2* locus. The correctness of the modification was verified by colony PCR (2755 bp integration mutant, 2970 bp original integration locus) and Sanger sequencing. Due to the already integrated copy of *gabP-III* in AVA-5A, the recombination event was also possible at this locus, increasing the screening effort significantly. Therefore, by choosing *crtI2* as integration locus of the second copy, successful recombination was also confirmed by phenotypic change to a brighter cell color (Fig. 9) due to its natural function in the carotenoid biosynthesis (Heider et al, 2012).



Fig. 9: Phenotypic evidence of successful integration into the *crtI2* locus. Left: Cell pellet of *C.-glutamicum* AVA-5A possessing native *crtI2* locus. Right: Cell pellet *C. glutamicum* AVA-5B possessing *gabP-III* from *P. putida* instead of *crtI2*.

The newly derived strain was designated *C. glutamicum* AVA-5B. It was characterized in comparison to strain AVA-5A which carried a single copy of the *gabP-III* gene (Rohles, 2021) (Fig. 10). The double-exporter mutant accumulated 21.4 mM 5-aminovalerate, slightly more than the parent strain (19.8 mM) and exhibited a higher

5-aminovalerate yield of 382 mmol mol⁻¹ (Table 3). However, at the same time, the strain fitness seemed somewhat reduced (Table 3), suggesting that the massive overexpression of the exporter caused undesired side effects, as also observed before (Kind et al, 2011). A single genomic copy of the 5-aminovalerate transporter therefore appeared optimal at this stage of engineering.

In addition, the cultivation of *C. glutamicum* AVA-5A was characterized by high reproducibility. The cultivation profile and representative values such as titers, yields and rates of the two independent cultivations deviate from each other by only 5 % (Fig. 10) (Rohles, 2021). When used on an industrial scale at a later stage, this ensures consistent quality of the cell factory.

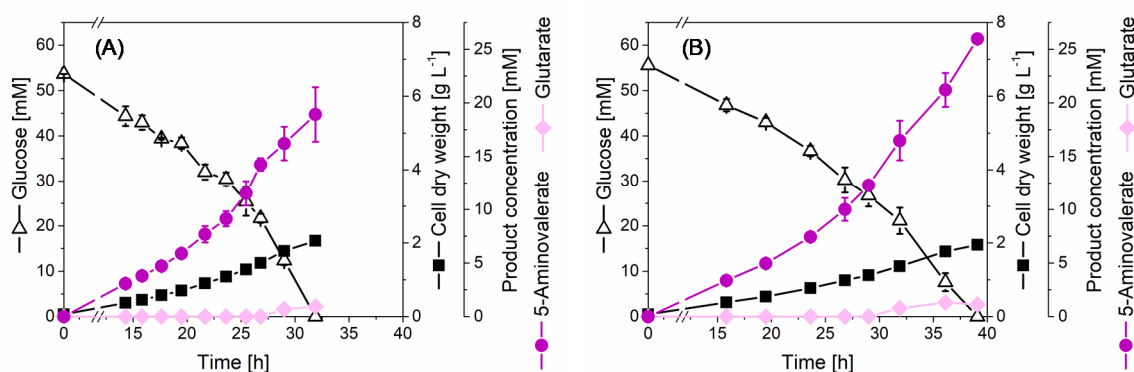


Fig. 10: Cultivation profiles of *C. glutamicum* AVA-5A and AVA-5B. The strains express one (AVA-5A, (A)) and two (AVA-5B, (B)) genomic copies of the GABA permease GabP-III from *P. putida* in addition to *P_{tuf}* controlled *davBA* operon, *lysE* and *gabTDP* operon were eliminated. Batch was performed in glucose minimal medium at 30 °C using shake flasks. The cultivation profile shows glucose depletion (empty symbols), product formation of 5-aminovalerate (violet symbols) and glutarate (rose symbols), and biomass formation (black symbols). Mean values and standard errors were calculated from biological triplicate.

Subsequently, the strategy was also applied to the advanced strain *C. glutamicum* AVA-7 that exhibited glutarate free 5-aminovalerate production due to deletion of the *argD* gene (Rohles, 2021). To this end, a second copy of the permease was integrated into *crt12* locus of AVA-7. The correctness of the genetic modification was verified by colony PCR (2755 bp integration mutant, 2970 bp original integration locus) and Sanger sequencing.

The new mutant, designated AVA-8, however, did not achieve better performance (Fig. 11, Table 3). Conclusively, *C. glutamicum* AVA-7 was proven to be the best *de novo* cell factory for 5-aminovalerate production.

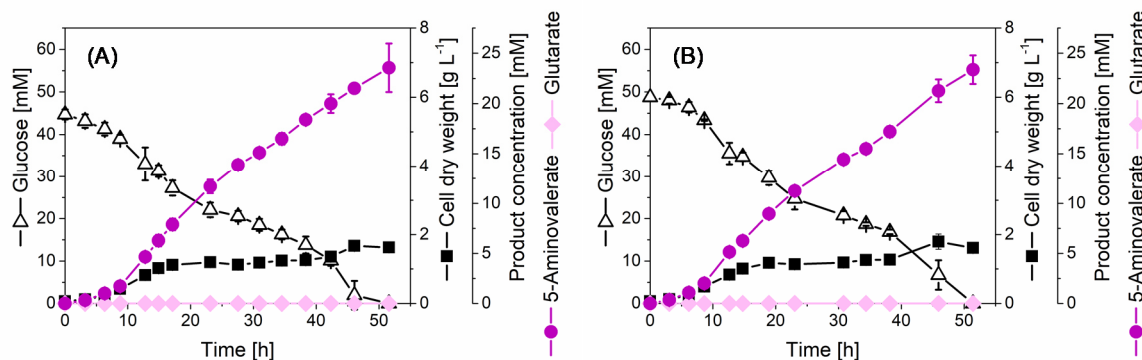


Fig. 11: Cultivation of the selective 5-aminovalerate hyperproducing strains AVA-7 and AVA-8. The strains express one (AVA-7, (A)) and two (AVA-8, (B)) genomic copies of the GABA permease GabP-III from *P. putida* in addition to P_{tuv} controlled *davBA* operon, *lysE*, *gabTDP*, operon and *argD* were eliminated. Batch was performed in glucose minimal medium at 30 °C using shake flasks. The cultivation profile shows glucose depletion (empty symbols), product formation of 5-aminovalerate (violet symbols) and glutamate (rose symbols), and biomass formation (black symbols). Mean values and standard errors were calculated from biological triplicate.

Table 3: Kinetics and stoichiometry of growth and product formation in advanced 5-aminovalerate-producing *C. glutamicum* strains. The strains all express either one (AVA-5A, AVA-7) or two copies (AVA-5B, AVA-8) of GABA permease GabP-III from *P. putida*. In AVA-7 and AVA-8 counteracting ArgD was additionally deleted. The strains were cultivated in glucose minimal medium in shake flask at 30 °C. The data comprise growth rates (μ), substrate consumption and product formation rate (q) and yields (Y). The added yeast extract represented 7 % of the total carbon and was included accordingly to determine the yields. Mean values and standard deviations were calculated from biological triplicates. GLC = glucose; AVA = 5-aminovalerate, GTA = glutamate, X = biomass. * n.d. = not detected.

	AVA-5A	AVA-5B	AVA-7	AVA-8
Rates				
μ [h ⁻¹]	0.10 ± 0.00	0.08 ± 0.00	0.10 ± 0.00	0.09 ± 0.00
q_{GLC} [mmol g ⁻¹ h ⁻¹]	2.41 ± 0.03	2.36 ± 0.02	3.12 ± 0.19	2.67 ± 0.16
q_{AVA} [mmol g ⁻¹ h ⁻¹]	0.87 ± 0.01	0.91 ± 0.01	1.74 ± 0.05	1.61 ± 0.05
q_{GTA} [mmol g ⁻¹ h ⁻¹]	0.03 ± 0.00	0.03 ± 0.00	n.d.	n.d.
Yields				
$Y_{X/GLC}$ [g mol ⁻¹]	42.7 ± 1.9	35.8 ± 3.2	31.3 ± 1.5	42.5 ± 1.5
$Y_{AVA/GLC}$ [mmol mol ⁻¹]	361.6 ± 2.9	382.1 ± 0.0	557.3 ± 26.6	532.4 ± 8.3
$Y_{GTA/GLC}$ [mmol mol ⁻¹]	13.5 ± 0.3	15.1 ± 0.2	n.d.	n.d.

4.1.2 Monitoring intracellular amino acid availability in the producing strains

To obtain the intracellular amino acid pool, mid-exponentially growing cells were fast filtered and subsequently extracted by boiling (Bolten et al, 2009). D,L-aminobutyric acid served here as an internal standard and was therefore already added during the preparation of the cell extract.

Insights into the metabolome of the advanced 5-aminovalerate producing strains AVA-5A and AVA-5B proofed an efficient conversion of the precursor L-lysine into 5-aminovalerate. Compared to L-lysine hyperproducing strain LYS-12, the intracellular L-lysine pool was significantly decreased (Table 4). The integration of the second copy of the GABA permease in *C. glutamicum* AVA-5B resulted in L-lysine levels even below 10 mM (Table 4).

Different than expected, the integration of the GABA permease GabP-III increased the intracellular availability of 5-aminovalerate (Table 4). Nevertheless, the simultaneous increase of intracellular product concentration and product yield of AVA-5B and AVA-7 demonstrated the capability of the cell factories to channel more carbon towards 5-aminovalerate biosynthetic pathway. Similar conclusions could be drawn for 1,5-diaminopentane production. The analysis of the intracellular 1,5-diaminopentane level helped to identify new engineering targets to improve overall strain performance by also indicating product export as major bottleneck (Kind et al, 2011). Notably, the 5-aminovalerate level, measured in this work, surpassed the previously found intracellular 1,5-diaminopentane amount twenty-fold (Kind et al, 2011).

Whereas several other amino acids not directly linked to 5-aminovalerate pathway could be measured in the cell extracts, glutarate could not be detected, verifying the complete elimination of 5-aminovalerate degradation pathways (Rohles, 2021).

The comparison with the previous data set on the strains AVA-5A and AVA-7 illustrates a high reproducibility for determined 5-aminovalerate levels with deviations of about 4 % between the two elevations (Table 4) (Rohles, 2021). The concentrations of the other listed amino acids differ by more than 10 % (Rohles, 2021) but are higher in the newly collected data set (Table 4).

Table 4: Intracellular amino acid pools in the *C. glutamicum* strains AVA-5A and AVA-7 and their derivatives AVA-5B and AVA-8 linked to the 5-aminovalerate pathway. Samples were extracted from mid-exponentially on glucose growing cells. Based on the correlation factor of 1.95 ($\mu\text{L cytoplasm}$) $\text{mg}_{\text{CDW}}^{-1}$ intracellular concentration were determined (Krömer et al, 2004). Displayed data represent mean values and standard errors of three biological replicates.

Amino acid	AVA-5A	AVA-5B	AVA-7	AVA-8
L-Lysine	11.40 \pm 3.59	7.43 \pm 2.20	5.98 \pm 1.11	9.25 \pm 0.70
L-Aspartic acid	2.66 \pm 0.61	2.66 \pm 0.61	7.57 \pm 1.51	6.85 \pm 1.62
Glycine	13.70 \pm 0.16	14.62 \pm 2.93	9.37 \pm 2.22	10.70 \pm 0.70
L-Alanine	13.24 \pm 0.91	13.55 \pm 1.65	10.26 \pm 2.08	11.25 \pm 0.64
L-Leucine	3.14 \pm 0.44	3.00 \pm 0.49	42.54 \pm 5.38	48.28 \pm 3.77
5-AVA	452.53 \pm 40.51	508.50 \pm 111.88	405.42 \pm 26.21	427.34 \pm 19.99

4.2 Harnessing of the L-lysine 6-dehydrogenase route for L-pipecolic acid production

Encouragingly, *C. glutamicum* LYS-12 overproduced L-lysine (Becker et al, 2011), the precursor of L-pipecolic acid, and was therefore taken as a starting point for strain engineering. To enable L-pipecolic acid production, different genetic modules that each encoded a heterologous L-lysine 6-dehydrogenase (LysDH), and the native Δ^1 -pyrroline 5-carboxylate reductase (ProC) were designed and constitutively expressed (Fig. 12).

The expression of L-lysine 6-dehydrogenase is known to enable the conversion of L-lysine into α -amino adipic acid semialdehyde, which spontaneously transforms into Δ^1 -piperidine 6-carboxylic acid in *C. glutamicum* (Perez-Garcia et al, 2016). The latter intermediate could be converted by ProC, natively part of L-proline biosynthesis, into L-pipecolic acid (Ankri et al, 1996).

4.2.1 Construction and analysis of a basic L-pipecolic acid producer

The L-lysine 6-dehydrogenase variants from three different donors, namely, *Ruegeria pomeroyi* (*R. pomeroyi*), a gram-negative bacterium from the marine environment (Neshich et al, 2013); *Geobacillus stearothermophilus* (*G. stearothermophilus*), a gram-positive thermophilic *Bacillus* (Heydari et al, 2004); and *Agrobacterium tumefaciens* (*A. tumefaciens*), a gram-negative phytopathogen (Misono et al, 1989) were implemented. Each *lysDH* gene was expressed with its native codon usage under the constitutive *tuf* promoter (Becker et al, 2005) on the *pClik5a* vector together with *proC* and an additional RBS (Fig. 12), resulting in the strains *C. glutamicum* PIA-1A, PIA-1B, and PIA-1C.

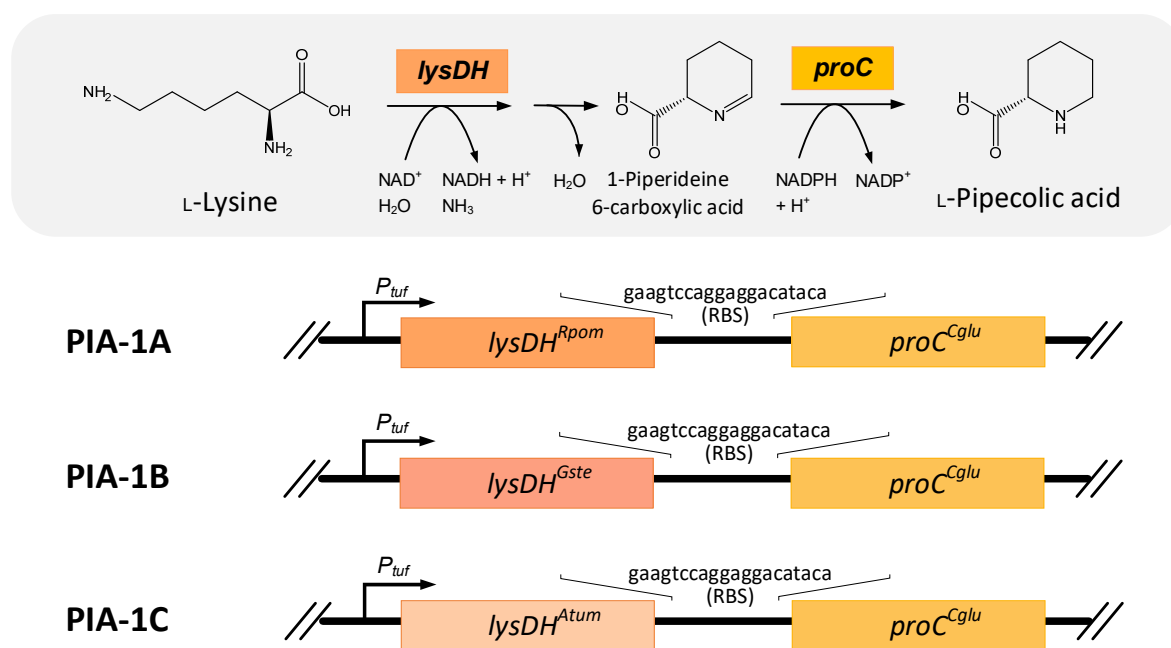


Fig. 12: Modules for L-lysine 6-dehydrogenase route. Biosynthetic modules each comprising the promoter *tuf* (P_{tuf}), the L-lysine 6-dehydrogenase from different donors, an additional RBS and the Δ^1 -pyrroline 5-carboxylate reductase from *Corynebacterium glutamicum*. PIA-1A expresses *lysDH* from *R. pomeroyi*, PIA-1B from *G. stearothermophilus* and PIA-1C from *A. tumefaciens*. The schematic diagram of the conversion of L-lysine into L-pipecolic acid was adapted from Perez-Garcia et al, 2016. Rpom = *R. pomeroyi*, Gste = *G. stearothermophilus*, Atum = *A. tumefaciens*, Cglu = *C. glutamicum*.

In shake flask cultivation, the newly derived strains *C. glutamicum* PIA-1A and PIA-1C formed L-pipecolic acid (Fig. 13, Fig. 31), as confirmed by GC-MS analysis (Fig. S1). In contrast, the PIA-1B mutant did not exhibit production, indicating that the enzyme from

A. tumefaciens was not functionally expressed. *C. glutamicum* PIA-1A performed best, secreted approximately 6 mM L-pipecolic acid into the medium, together with 20 mM L-lysine (Fig. 14). Notably, in relation to the utilized glucose, the L-pipecolic acid yield (88 mmol mol⁻¹) and the specific production rate (0.31 mmol g⁻¹ h⁻¹) remained low (Table 8). Low-level production of L-pipecolic acid in a mixture with large amounts of L-lysine (15.5 mM) matched previous findings from the overexpression of a similar construct in another L-lysine overproducer (Perez-Garcia et al, 2016).

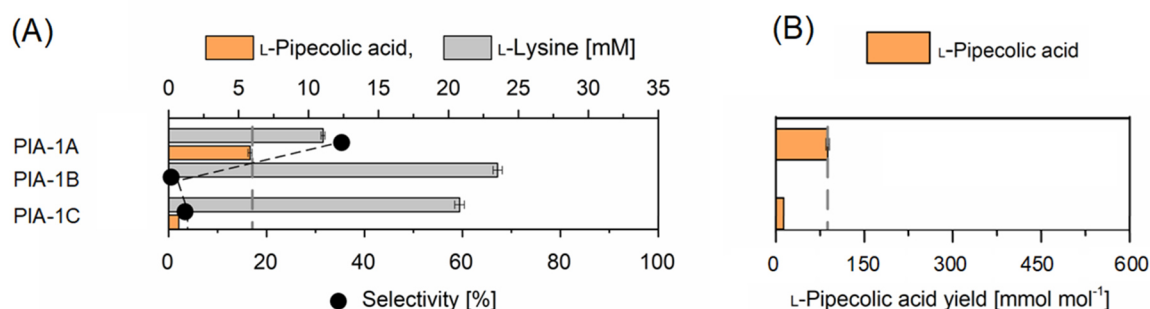


Fig. 13: Basic L-pipecolic acid production in metabolically engineered *C. glutamicum*. The strains express biosynthetic modules each comprising a L-lysine 6-dehydrogenase from different donors, an additional RBS and the Δ^1 -pyrroline 5-carboxylate reductase from *Corynebacterium glutamicum*. Cultivation was performed in miniaturized bioreactor system using glucose minimal medium at 30 °C. Product titers and product selectivity (A) and corresponding L-pipecolic acid yields (B) are displayed. Mean values and standard errors were calculated from three biological replicates.

The performance of strain PIA-1A was poor compared to that of previously engineered derivatives of LYS-12 that had been designed to produce other L-lysine-based chemicals. For example, *C. glutamicum* DAP-13, a LYS-12 descendant that additionally expressed L-lysine decarboxylase, accumulated diaminopentane at 34 % yield without any L-lysine (Kind et al, 2014). Furthermore, *C. glutamicum* AVA-1 (Rohles et al, 2016) and GTA-1 (Rohles et al, 2018), LYS-12 derivatives that additionally expressed L-lysine oxidase plus different downstream pathway enzymes, formed mixtures of L-lysine-derived 5-aminovalerate and glutarate at 22.2 % and 26.5 % yield with only minor amounts of L-lysine, respectively. The three- to fourfold lower L-pipecolic acid yield observed here pointed to severe limitations in the basic producer and indicated substantial space for improvement. *C. glutamicum* PIA-1A, expressing the LysDH variant from *R. pomeroyi* and performing best among the candidates, was further studied.

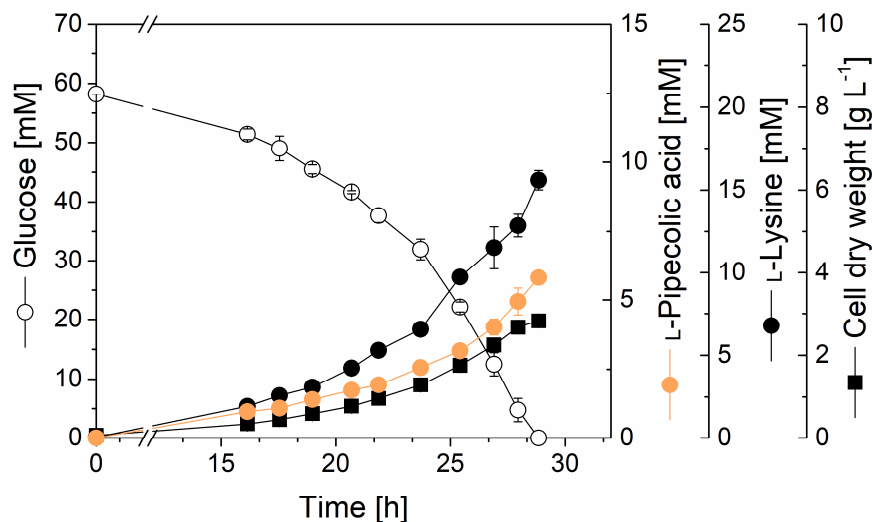


Fig. 14: Performance of basic L-pipecolic acid producing strain PIA-1A. The strain expresses the *lysDH* from *R. pomeroyi* and *proC* from *C. glutamicum* episomally. The operon is controlled by P_{tuf} . The batch was performed at 30 °C in shake flasks using glucose minimal medium. The cultivation profile shows the depletion of glucose, the formation of the products L-pipecolic acid and L-lysine, and the biomass formation. Mean values and standard errors were calculated from three biological replicates.

4.2.2 Transcriptional analysis of *C. glutamicum* PIA-1A

To globally capture eventual metabolic bottlenecks and other unfavorable conditions, e.g., stress-related changes in *C. glutamicum* PIA-1A that could explain its weak performance, its transcriptome was compared to that of the reference strain PIA-0, i.e., LYS-12 expressing the empty *pClik5a* vector (and thereby ruling out plasmid-caused effects). Both strains were harvested during the mid-exponential phase at an OD_{660} of 4.0 and subjected to transcriptome analysis (Table 5). Statistical evaluation by PCA demonstrated excellent data quality (Fig. S2).

In summary, the two genes for L-pipecolic acid biosynthesis, *lysDH* and *proC*, were found to be strongly upregulated, indicating high-efficiency transcription of the heterologous pathway. The relatively weaker activation for *proC* could be well explained by the genomic copy of *proC* that natively existed in *C. glutamicum* (Kalinowski et al, 2003; Perez-Garcia et al, 2016). Nevertheless, the \log_2 -fold change of 6.3 found for this gene revealed that transcription was enhanced almost 80-fold. Mild upregulation resulted for a few TCA cycle-related genes and *catA*, which is involved in the degradation of 3,4-dihydroxybenzoate,

and was added to the medium as an iron chelator (Graf et al, 2019). In *C. glutamicum*, the aromatic is metabolized via catechol and enters the TCA cycle further downstream at the level of succinyl-CoA (Becker et al, 2018a; Weiland et al, 2022).

Table 5: Transcription profiling of L-pipecolic acid-producing *C. glutamicum* PIA-1A. The data comprise significantly up- and downregulated genes compared to *C. glutamicum* PIA-0 expressing the empty plasmid (\log_2 -fold change ≥ 1 and ≤ -1 , $p \leq 0.05$). The samples were taken from glucose-based cultures during mid-exponential growth. The statistical quality of the data was verified by PCA (Fig. S2). $n = 3$. The data represent mean values and standard errors from three biological replicates.

Locus tag	Gene	Function	Log ₂ fold change
	<i>lysDH</i>	L-lysine 6-dehydrogenase	+ 12.6
<i>CGL_RS02095</i>	<i>proC</i>	Δ^1 -pyrroline carboxylate 5-reductase	+ 6.3
<i>CGL_RS01905</i>	<i>sdhA</i>	Succinate dehydrogenase flavoprotein subunit	+ 1.3
<i>CGL_RS01910</i>	<i>sdhB</i>	Succinate dehydrogenase/ fumarate reductase iron-sulfur subunit	+ 1.4
<i>CGL_RS01900</i>	<i>sdhC</i>	Succinate dehydrogenase cytochrome b subunit	+ 1.2
<i>CGL_RS07720</i>	<i>acn</i>	Aconitate hydratase	+ 1.3
<i>CGL_RS11910</i>	<i>catA</i>	Catechol 1,2-dioxygenase	+ 1.3
<i>CGL_RS05735</i>	<i>cydA</i>	Cytochrome ubiquinol oxidase subunit I	+ 1.2
<i>CGL_RS05915</i>	<i>narJ</i>	Nitrate reductase molybdenum cofactor assembly chaperone	+ 1.2
<i>CGL_RS05925</i>	<i>narG</i>	Nitrate reductase alpha subunit	+ 1.2
<i>CGL_RS02010</i>	<i>mtrA</i>	HtaA domain-containing protein	- 4.0
<i>CGL_RS01750</i>	<i>NCgl0329</i>	iron-siderophore ABC transporter substrate- binding protein	- 2.6
<i>CGL_RS04925</i>	<i>hmuT</i>	Helix-turn-helix transcriptional regulator	- 2.2
<i>CGL_RS04045</i>	<i>NCgl0773</i>	Siderophore-interacting protein	- 2.1
<i>CGL_RS00670</i>	<i>NCgl0123</i>	Hypothetical protein	- 2.0
<i>CGL_RS02555</i>	<i>NCgl0483</i>	Iron-chelate uptake ABC transporter family per- mease subunit	- 1.9
<i>CGL_RS10120</i>	<i>NCgl1959</i>	Iron-siderophore ABC transporter substrate- binding protein	- 1.9
<i>CGL_RS02560</i>	<i>NCgl0484</i>	Iron-chelate uptake ABC transporter family per- mease subunit	- 1.9
<i>CGL_RS08590</i>	<i>NCgl1647</i>	Hypothetical protein	- 1.8

On the other hand, a few genes were downregulated, and *mtrA* was the most repressed gene. Interestingly, MtrA is part of a signal transduction system that activates the expression of *betP* and *proP*, encoding importers of the compatible solutes betaine and L-proline (Moker et al, 2004). A previously studied L-pipecolic acid producer exhibited the same downregulation, and it was concluded that the response was due to L-pipecolic acid being itself a compatible solute (Perez-Garcia et al, 2019). Other weakly down-regulated genes emerge in relation to iron transport or in the regulatory level.

Overall, the analysis revealed high expression of the introduced biosynthetic pathway in the basic L-pipecolic acid producer, as desired, but no other significant changes. This outcome suggested that the bottlenecks limiting production in PIA-1A were more likely metabolic than regulatory (Schilling et al, 2007).

4.2.3 Metabolome analysis of *C. glutamicum* PIA-1A

Taken the previous results, the level of intracellular amino acids, including L-pipecolic acid and its cellular precursor L-lysine was analyzed, given the previous value of such data to unravel metabolic bottlenecks in *C. glutamicum* cell factories (Kind et al, 2011; Rohles, 2021).

For this purpose, mid-exponential cells ($OD_{660} = 4.0$) of the L-pipecolic acid producer PIA-1A and its reference PIA-0 were studied (Table 6). Selected amino acids were strongly affected by the heterologous L-pipecolic acid pathway. The intracellular L-lysine pool was almost halved (from 64 to 35 mM). L-Pipecolic acid was present in high amounts inside the cells, which is typical for compatible solutes (Neshich et al, 2013; Perez-Garcia et al, 2019). However, more than 90 % of the product was excreted (Table 6, Table 8). The intracellular concentrations of other amino acids of the L-aspartate family, such as L-threonine, L-methionine, L-asparagine, and L-aspartate itself, were found to be increased, indicating that the supporting pathway network, branching off from central metabolism, was well supplied with carbon. Furthermore, the production (and intracellular

presence) of L-pipecolic acid reduced the intracellular pools of L-proline and L-glutamine (Table 6) other prominent compatible solutes in *C. glutamicum* (Peter et al, 1998; Kawasaki & Martinac, 2020; Wood et al, 2001) and heterologous ectoine and hydroxyectoine production in this microbe (Steger et al, 2004; Becker et al, 2013b; Jungmann et al, 2022).

Table 6: Intracellular amino acid levels in the L-pipecolic acid-producing strains *C. glutamicum* PIA-1A and PIA-7 and the nonproducing control strain PIA-0 The samples were taken from glucose-based cultures during mid-exponential growth. Intracellular concentrations were determined based on the correlation factor of 1.95 ($\mu\text{L cytoplasm}$) $\text{mg}_{\text{CDW}}^{-1}$ (Krömer et al, 2004). With regard to L-pipecolic acid formation, the product accumulated both inside the constantly growing cells and in the broth. For strain PIA-1A, the corresponding specific production rate for intracellular L-pipecolic was estimated on the basis of biomass yield, specific growth rate (Table 6, Table 8) and the intracellular L-pipecolic pool. The calculation yielded a value of $0.025 \text{ mmol g}^{-1} \text{ h}^{-1}$, far below the extracellular accumulation rate ($0.31 \text{ mmol g}^{-1} \text{ h}^{-1}$) (Table 8). More than 90 % of the product was excreted, and the additional amount accumulating inside the cells did not significantly change the overall picture of weak production by strain PIA-1A. The data represent mean values and standard errors from three biological replicates.

Amino acid	PIA-1A [mM]	PIA-0 [mM]
L-Lysine	35.3 ± 05.8	63.5 ± 06.9
L-Aspartic acid	16.6 ± 00.8	12.1 ± 01.3
L-Glutamic acid	227.4 ± 19.8	238.2 ± 19.6
L-Asparagine	7.7 ± 00.5	4.1 ± 00.4
L-Serine	7.7 ± 00.5	4.9 ± 00.5
L-Glutamine	22.0 ± 01.0	42.3 ± 05.8
L-Histidine	0.0 ± 00.0	0.0 ± 00.0
Glycine	11.6 ± 01.2	9.8 ± 01.1
L-Threonine	6.2 ± 00.5	3.2 ± 00.4
L-Arginine	8.0 ± 00.5	5.0 ± 05.0
L-Alanine	14.3 ± 00.9	12.1 ± 01.1
L-Tyrosine	0.0 ± 00.0	0.0 ± 00.0
L-Valine	32.3 ± 02.8	28.4 ± 02.9
L-Methionine	4.5 ± 00.4	1.7 ± 00.1
L-Phenylalanine	8.9 ± 00.7	5.1 ± 00.5
L-Isoleucine	16.7 ± 01.3	14.3 ± 01.5
L-Leucine	11.9 ± 00.8	6.9 ± 00.6
L-Tryptophan	21.7 ± 01.4	11.8 ± 01.0
L-Proline	49.9 ± 05.8	59.1 ± 04.4
L-Pipecolic acid	266.9 ± 48.1	0.0 ± 00.0

4.2.4 Evaluation of alternative heterologous expression strategies

Next, alternative genetic designs of the heterologous pathway module were created and evaluated to improve biocatalytic efficiency (Pauli, 2018). In a first attempt, the codon usage of the heterologous *lysDH^{Rpom}* gene and the endogenous *proC* gene were adapted to that of *C. glutamicum* (resulting in the adapted genes *lysDH^{Rpom, opt}* and *proC^{Cglu, opt}*, Fig. 15, Fig. S3, and Fig. S4), previously proven as helpful feature for 1,5-diaminopentane and L-lysine production for example (Kind et al, 2010) (Hoffmann et al, 2018). Clearly, however, this approach was detrimental. The resulting mutant PIA-2A (*LYS-12 P_{tuf} lysDH^{Rpom, opt} proC^{Cglu, opt}*) formed only approximately 1 mM L-pipecolic acid, 6-fold less than PIA-1A, which carried the native gene sequences (Fig. S5).

Then, a second copy of *proC* was inserted into the plasmid (Fig. 15) because gene duplication had previously doubled the enzymatic capacity in engineered *C. glutamicum* (Becker et al, 2011). Strain PIA-2B (*LYS-12 P_{tuf} proC^{Cglu} P_{tuf} lysDH^{Rpom} proC^{Cglu}*) accumulated 2.2 mM of the desired product, less than 40 % of that obtained from PIA-1A. Moreover, in this strain, less L-lysine was made, pointing to a more general defect (Fig. 16).

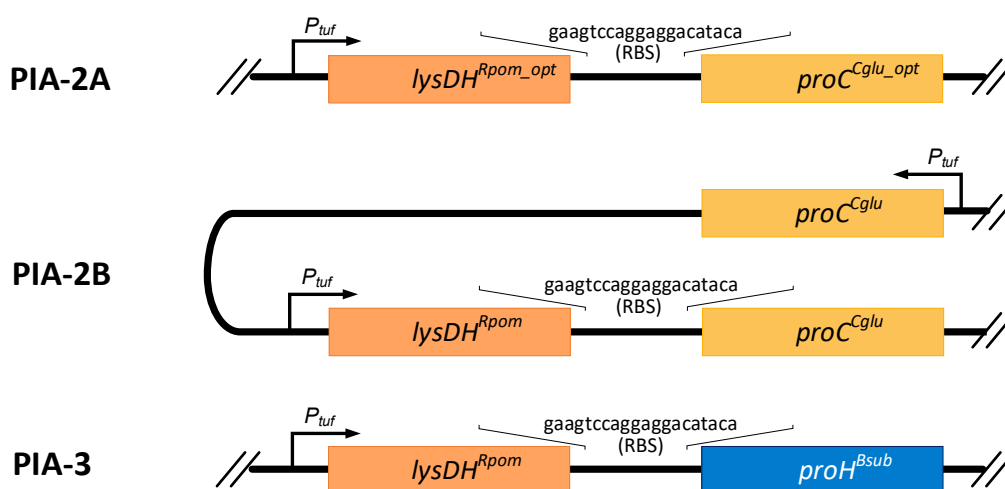


Fig. 15: Modules for expression balancing of L-lysine 6-dehydrogenase route. First biosynthetic module comprises promoter *tuf* (P_{tuf}), codon-optimized L-lysine 6-dehydrogenase from *R. pomeroyi*, additional RBS and codon-optimized Δ^1 -pyrroline 5-carboxylate reductase from *C. glutamicum*. In the second module, native *lysDH* operon was extended upstream by an additional copy of the promoter *tuf* (P_{tuf}) plus native Δ^1 -pyrroline 5-carboxylate reductase from *C. glutamicum*. In the last operon *proC* was replaced by *proH* from *B. subtilis*. Opt = codon-optimized; Rpom = *R. pomeroyi*; Cglu = *C. glutamicum*. Bsub = *B. subtilis*.

Different to *C. glutamicum*, *B. subtilis* possesses two active pyrroline 5-carboxylate reductases: ProG and ProH (Belitsky et al, 2001; Forlani et al, 2017). ProG was known to play a constitutive role and was regarded similar to the ProC from *C. glutamicum*, whereas ProH had been shown to be activated under stress for increased levels of L-proline (Forlani et al, 2017). The protein sequences of ProC and ProH shared only about 35 % of conserved regions (Fig. S6), suggesting ProH as promising alternative. A third strategy therefore involved the use of the Δ^1 -pyrroline 5-carboxylate reductase based on the ProH protein from *B. subtilis* (Fig. S6). However, the corresponding strain PIA-3 (LYS-12 $P_{tuf} lysDH^{Rpom} proH^{Bsub}$) did not yield significant improvement, achieving a product titer of 3.8 mM (Fig. 16).

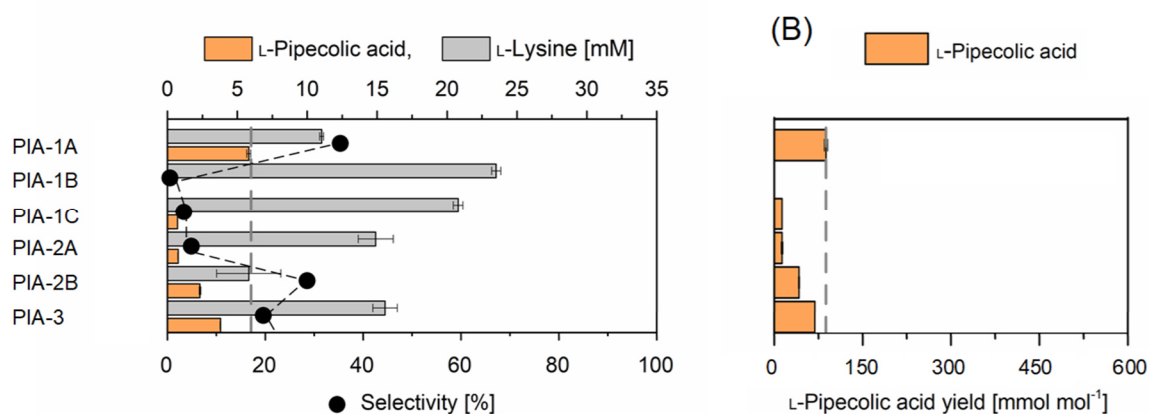


Fig. 16: Evaluation of basic L-pipecolic acid producers. The strains express biosynthetic modules each comprising a L-lysine 6-dehydrogenase from different donors, an additional RBS and Δ^1 -pyrroline 5-carboxylate reductase. Cultivation was performed in miniaturized bioreactor system using glucose minimal medium at 30 °C. Product titers and product selectivity (A) and corresponding L-pipecolic acid yields (B) are displayed. Mean values and standard deviation were calculated from three biological replicates.

Because, different to ProC, ProH was known to work particularly well under stress such as high salt level (Schroeter et al, 2013), PIA-1A and PIA-3 were additionally evaluated under supplementation of NaCl up to 1 M. Normalized to initial titers without additional NaCl, no stress-induced increase of L-pipecolic acid titer in culture supernatants of PIA-3 could be detected in a miniaturized batch (Table 7).

In summary, the monocistronic design with the two native genes *lysDH^{Rpom}* and *proC^{Cglu}* appeared optimal. Genome-based expression of a single copy of $P_{tuf} lysDH^{Rpom} proC^{Cglu}$ in

LYS-12 (*C. glutamicum* PIA-2C), tested in addition to the plasmid-based layout, revealed negligible product formation (Table 8), so the plasmid-based strain PIA-1A was used further.

Table 7: Impact of the salt level on L-pipecolic acid production in *C. glutamicum* PIA-1A and PIA-3. PIA-1A and PIA-3 were evaluated under supplementation of NaCl up to 1 M. The cultivations were performed at 30 °C in a miniaturized microtiter plate reactor on glucose minimal medium, supplemented with NaCl (0 – 1000 mM). In addition to absolute values, the titers are shown as relative values, normalized to production without NaCl supplementation. The data represent mean values and standard errors from three biological replicates.

NaCl [mM]	PIA-1A PIA [mM]	PIA-3 PIA [mM]	PIA-1A PIA [%]	PIA-3 PIA [%]
0	7.63 ± 0.17	4.76 ± 0.08	100.0	100.0
10	7.52 ± 0.56	4.75 ± 0.43	98.5	99.7
50	7.38 ± 0.47	4.91 ± 0.38	96.7	103.1
100	6.54 ± 0.12	4.35 ± 0.19	85.7	91.4
500	6.16 ± 0.26	3.82 ± 0.25	80.7	80.3
1000	0.10 ± 0.01	0.14 ± 0.02	1.3	2.9

4.2.5 L-lysine 6-dehydrogenase displays a major metabolic bottleneck

Integrating enzyme data with flux data indicated that the heterologous L-lysine 6-dehydrogenase from *R. pomeroyi* was a key enzyme that controlled performance. Under assay conditions, its maximum *in vitro* activity was 900 mU (mg protein)⁻¹. This value was in the range of high-flux TCA cycle enzymes of *C. glutamicum* (Becker et al, 2009; Kind et al, 2013), confirming that a high amount of active LysDH was expressed. Assuming a cellular protein content of 50 %, the *in vitro* activity corresponded to a maximum flux capacity of the enzyme for L-pipecolic acid production of 27 mmol g⁻¹ h⁻¹ under optimum conditions. However, the effective L-pipecolic acid flux of PIA-1A, the best strain up to this point, was only 0.31 mmol g⁻¹ h⁻¹. To evaluate whether the reduced L-lysine availability limited the performance of the introduced L-lysine 6-dehydrogenase, the enzyme was

assayed for its affinity (Fig. 18). The kinetic analysis yielded a $K_{M, LYS}$ of 3.1 ± 0.2 mM L-lysine at (cytoplasmic) pH 7.8. The intracellular L-lysine level was more than ten-fold higher (Table 6), suggesting that the cells supplied enough of the precursor due to their massively optimized upstream metabolism. Evidently, L-lysine 6-dehydrogenase operated only at approximately 1 % of its theoretical ability, despite being sufficiently supplied with L-lysine.

The intracellular pH limits the *in vivo* LysDH activity in *C. glutamicum* PIA-1A

Based on this unfavorable underperformance, the properties of LysDH were further investigated. A series of measurements using a crude cell extract of *C. glutamicum* PIA-1A revealed a strong influence of pH on the enzyme (Fig. 17).

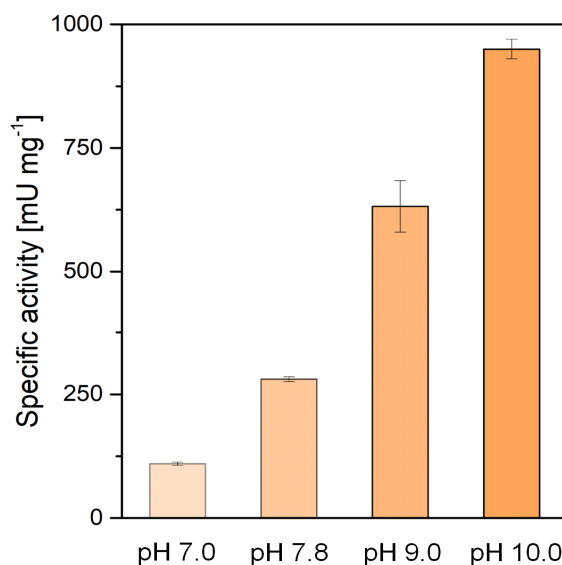


Fig. 17: Impact of the pH value on the activity of LysDH from *R. pomeroyi*. Crude cell extract was obtained from exponentially growing *C. glutamicum* PIA-1A. The master mix for the reaction contained 100 mM buffer, 30 mM L-lysine, 2 mM NAD⁺ and 50 μ l ml⁻¹ cell extract (30 °C). The data represent mean values and standard errors from three biological replicates.

LysDH preferred an alkaline milieu (pH 10.0), similar to LysDH from *G. stearothermophilus* (Heydari et al, 2004) and *Pyrococcus horikoshii* (Yoneda et al, 2010). Under neutral conditions (pH 7.8) mimicking the cytoplasm of *C. glutamicum* (Follmann et al, 2009) however, the specific activity was reduced to 25 %. At pH 7.0, it was reduced to below

10 %. Notably, the resulting *in vitro* capacity of the native enzyme at cytoplasmic pH 7.8 (6.8 mmol g⁻¹ h⁻¹) was still more than twenty-fold higher than the achieved flux *in vivo*.

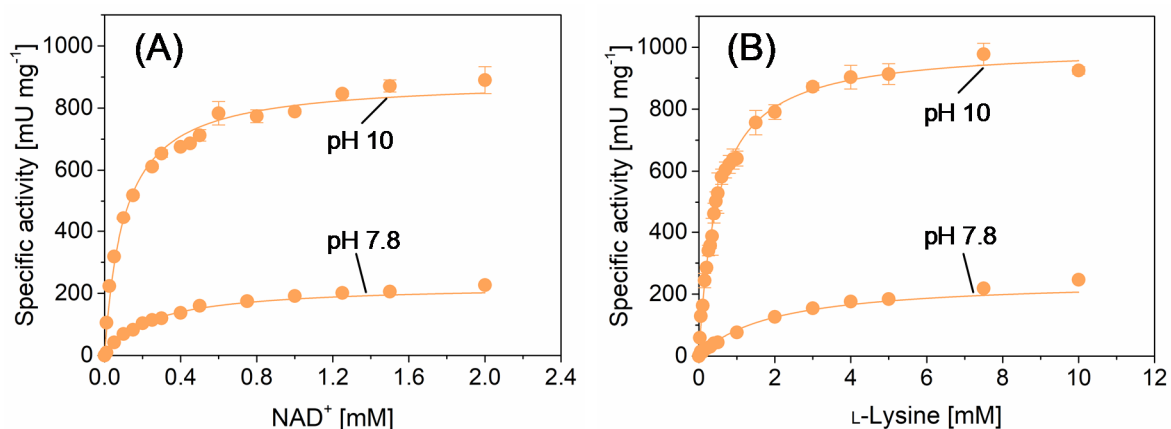


Fig. 18: Characterization of L-lysine 6-dehydrogenase from *R. pomeroyi* in crude cell extract of *C. glutamicum* PIA-1A. Enzyme kinetics at varied NAD⁺ levels, a saturating concentration of 30 mM L-lysine and different pH values: pH 7.8 ($k_{M, NAD^+} = 308 \pm 15 \mu\text{M}$, $v_{max} = 253 \pm 4 \text{ mU mg}^{-1}$) and pH 10.0 ($k_{M, NAD^+} = 104 \pm 9 \mu\text{M}$, $v_{max} = 892 \pm 16 \text{ mU mg}^{-1}$) (A). Enzyme kinetics at varied L-lysine levels, a saturating concentration of 2 mM NAD⁺ and different pH values: pH 7.8 ($k_{M, LYS} = 3,130 \pm 200 \mu\text{M}$, $v_{max} = 316 \pm 7 \text{ mU mg}^{-1}$) and pH 10.0 ($k_{M, LYS} = 486 \pm 18 \mu\text{M}$, $v_{max} = 1002 \pm 11 \text{ mU mg}^{-1}$) (B). The crude cell extract for analysis was obtained from *C. glutamicum* PIA-1A during the exponential growth phase. All assays were performed at 30 °C. The data represent mean values and standard errors from three biological replicates.

Towards improved enzymatic activity, the option of protein engineering of LysDH was evaluated next. As the crystal structure of the LysDH from *R. pomeroyi* was not available, 3D structures of LysDH variants from related organisms were investigated (UniProt Reference Clusters (Steinegger & Soding, 2018; Suzek et al, 2015)) to reconstruct the structure of the used LysDH using homology modelling (Adindla et al, 2004). Organisms phylogenetically close to *R. pomeroyi* were additionally evaluated for their native environment. The microbes *Ruegeria denitrificans* (*R. denitrificans*) and *Pseudoruegeria aquimaris* (*R. aquimaris*) comprised a LysDH enzyme, while preferring a neutral pH of 7.6 for growth (Ruldeekulthamrong et al, 2008), matching the envisioned optimum for LysDH activity. Their 3D structures were taken from UniProt database using AlphaFold structure prediction (Acc. No. A0A0P1II55 and Acc. No. A0A1Y5TAF1 (The UniProt Consortium, 2023; Jumper et al, 2021; Varadi et al, 2022)).

Homology modelling of the LysDH from *R. denitrificans*, *R. aquimaris* and *R. pomeroyi* identified four potential mutation sites that suggested to lower the pH optimum of the LysDH enzyme of interest. The two variants LysDH^{I81K} and LysDH^{Q114D} were predicted to improve substrate binding at neutral pH, while LysDH^{S228A} and LysDH^{G286D} promised enhanced cofactor binding (Fig. S7).

Next, the encoding *lysDH* gene was modified using error-prone mutagenesis via specific primers. The newly generated gene variants were cloned upstream of the *proC* gene into the episomal vector *pClik5a* to replace the native gene in the initial implemented biosynthetic L-pipecolic acid operon. All variants were validated for correctness using Sanger sequencing. The two mutants that expressed the LysDH^{I81K} and LysDH^{Q114D}, respectively, were able to secrete 5.8 and 5.9 mM L-pipecolic – matching the value observed for the PIA-1A strain which expressed the native enzyme. The other mutants did not form any product. In summary, protein engineering at the level of LysDH did not provide superior enzyme variants.

Temperature highly impacts LysDH activity

Regarding temperature, LysDH exhibited optimum activity at 55 °C (Fig. 19) almost twice the growth temperature used for *C. glutamicum* (30 °C). Inspired by ectoine- and hydroxyectoine-producing *C. glutamicum* strains that had been cultivated up to 42 °C and exhibited maximum production of the extremolytes at 35 °C (Becker et al, 2013a; Giesselmann, 2018) and 37 °C (Jungmann et al, 2022), production at increased temperature was also tested here. Indeed, when grown at 34 °C (Fig. 19), PIA-1A produced L-pipecolic acid at a doubled yield (182 mmol mol⁻¹) and rate (0.62 g mol⁻¹ h⁻¹, Table 8); however, no growth was observed at 37 °C (Lamber, 2020). Because the parent strain LYS-12 was able to grow at 37 °C, this finding indicated that the producer faced extra stress, eventually caused by plasmid-burden (Wittmann & Becker, 2007) or inhibitory high levels of intracellular L-lysine (Wehrmann et al, 1998). In addition to the significant

improvement in production, the outcome underlined the importance of LysDH as a major factor in the pace of L-pipecolic acid biosynthesis.

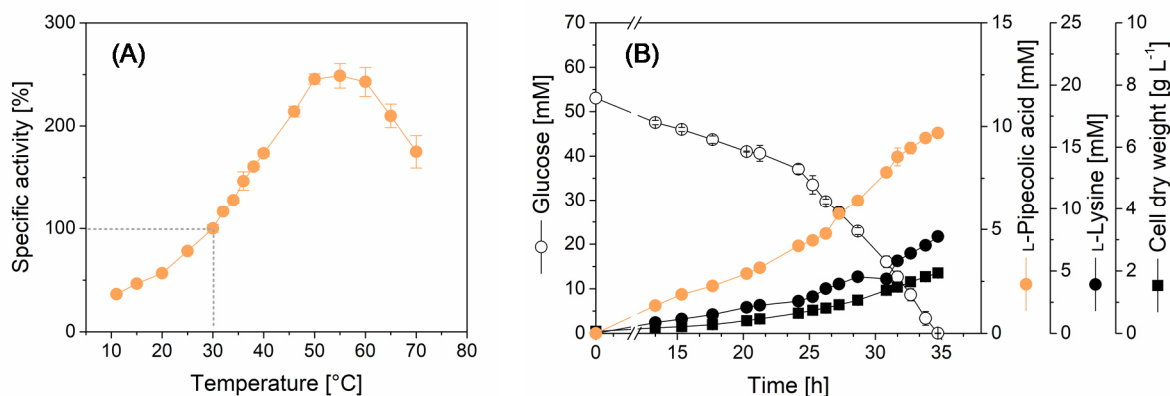


Fig. 19: Improved L-pipecolic acid production in *C. glutamicum* PIA-1A at increased temperature. Temperature dependence of the activity of L-lysine 6-dehydrogenase from *R. pomeroyi* (A). The assay was conducted at pH 10.0 with 30 mM L-lysine and 2 mM NAD⁺, using crude cell extract from *C. glutamicum* PIA-1A, harvested during the exponential growth phase (n = 3). Growth and L-pipecolic acid production of *C. glutamicum* PIA-1A at 34 °C (B). The cultivation was conducted in shake flasks on minimal glucose medium. The data represent mean values and standard errors from three biological replicates. Sampling during cultivation was partially covered by Jessica Lamber.

***In vivo* redox status massively influences LysDH activity**

Subsequently, redox requirements of LysDH were explored. The reaction of L-lysine 6-dehydrogenase additionally required NAD⁺ (Perez-Garcia et al, 2017), and the enzyme showed high affinity to the cofactor (Fig. 20). In addition, NADP⁺ was also accepted as a cofactor, and the copresence of NAD⁺ and NADP⁺ enabled a slightly faster reaction, whereas the activity with NADP⁺ was much lower (25 mU mg⁻¹) than the activity with NAD⁺ (950 mU mg⁻¹, Fig. 20).

Furthermore, the impact of NADH and NADPH was investigated. NADH was highly inhibitory (Fig. S8). Adding NADH to the same level as NAD⁺ (1:1 ratio) reduced the activity of LysDH by 50 %. When the ratio was further shifted toward NADH, the enzyme activity became even lower (Fig. 21A). Only a significant surplus of NAD⁺ could compensate for the presence of NADH. The same pattern emerged when assaying different mixtures of three reducing equivalents and all four compounds together (Fig. S8).

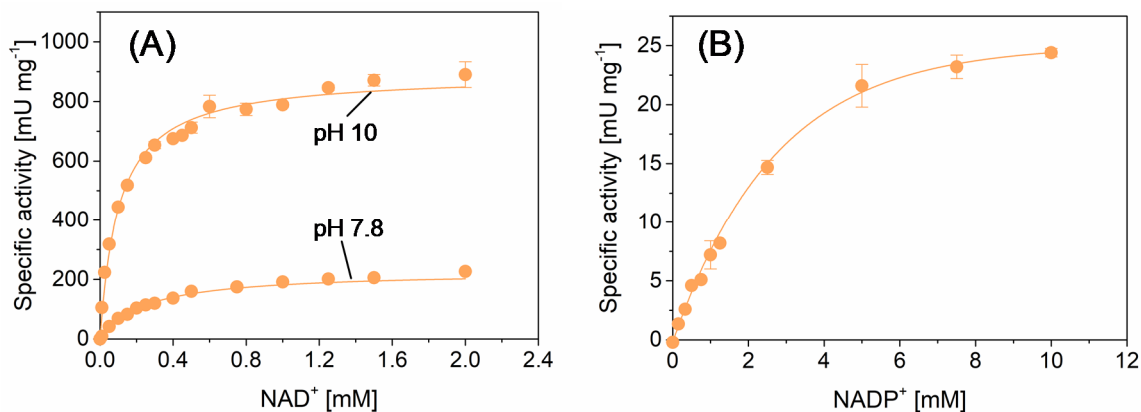


Fig. 20: Cofactor affinity of L-lysine 6-dehydrogenase from *R. pomeroyi* in crude cell extract of *C. glutamicum* PIA-1A. Enzyme kinetics at varied NAD⁺ levels, a saturating concentration of 30 mM L-lysine and different pH values: pH 7.8 ($K_{M, NAD^+} = 308 \pm 15 \mu\text{M}$, $v_{max} = 253 \pm 4 \text{ mU mg}^{-1}$) and pH 10.0 ($K_{M, NAD^+} = 104 \pm 9 \mu\text{M}$, $v_{max} = 892 \pm 16 \text{ mU mg}^{-1}$) (A). Enzyme kinetics using NADP⁺ as cofactor (B). The obtained kinetic parameters at pH 10.0 were $K_{M, NADP^+} = 2.5 \pm 0.69 \mu\text{M}$ and $v_{max} = 26.5 \pm 0 \text{ mU mg}^{-1}$. The assay at pH 7.8 did not yield measurable activity. The crude cell extract for analysis was obtained from *C. glutamicum* PIA-1A during the exponential growth phase. All assays were performed at 30 °C. The data represent mean values and standard errors from three biological replicates.

In comparison to NADH, the effect of NADPH was rather insignificant. NADH evidently competed with NAD⁺ for binding to the enzyme due to its structural similarity, thereby inhibiting the reaction. A similar mechanism has been observed for isocitrate dehydrogenase that uses NAD⁺ as cofactor and is inhibited by NADH by competition for the active site (Liu et al, 2018). This effect appeared more pronounced at neutral pH values, potentially strengthened by the reduced cofactor affinity under these conditions (Fig. 21A, Fig. S8). At pH 7.8 and in the presence of equal amounts of NADH and NAD⁺ (1:1), LysDH *in vitro* activity decreased by 40 % (Fig. 21A).

Next, the redox status *in vivo* was analyzed and the levels of NADH and NAD⁺ in PIA-1A cells ($\text{OD}_{660} = 4.0$) were quantified. The NADH to NAD⁺ ratio was estimated to be 0.74, indicating an unfavorably high abundance of NADH (Fig. 21B). In the original LYS-12 strain, the NADH to NAD⁺ ratio was only 0.20. It appeared that the NADH-generating L-pipecolic acid production pathway itself greatly perturbed the redox status and thus created an inhibitory reaction environment, as the formed NADH was not efficiently regenerated. Overall, the inhibiting redox environment and the unfavorable pH largely paralyzed the LysDH enzyme and appeared to be the major reason for the weak

production performance. The finding, furthermore, highlighted the great impact of sufficient supply of redox power on the efficiency of biosynthetic cell factories (Beckers et al, 2016; Borrero-de Acuna et al, 2014; Kiefer et al 2004; Lange et al, 2017; Wittmann et al, 2004a).

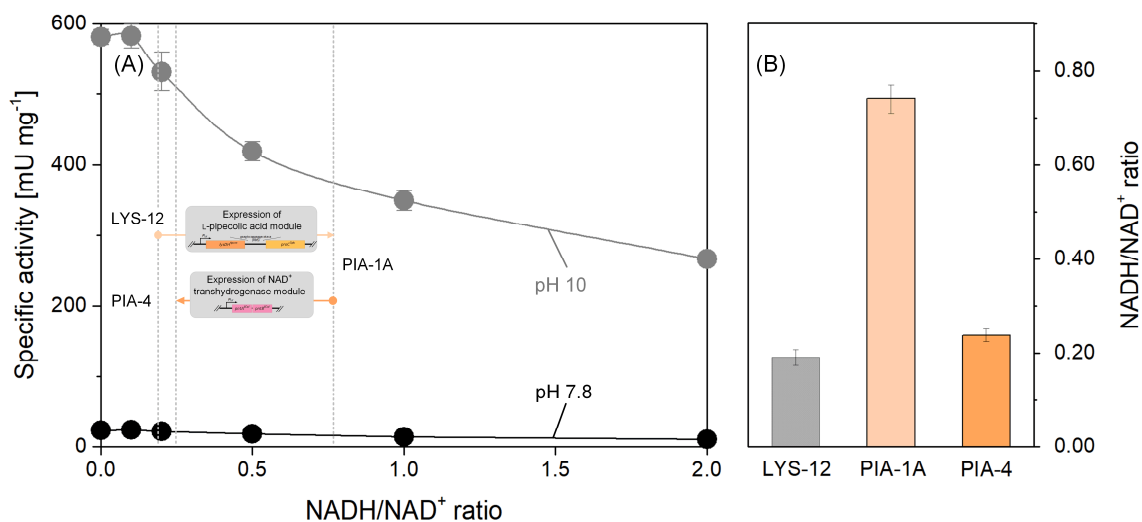


Fig. 21: Due to an unfavorable cellular environment, the expressed heterologous L-lysine 6-dehydrogenase exhibits ultralow activity *in vivo*, which limits L-pipecolic acid production in *C. glutamicum*. (A) Impact of the NADH to NAD⁺ ratio on the specific *in vivo* enzyme activity of L-lysine 6-dehydrogenase (A). The activity data were inferred from the *in vitro* activity of the enzyme at pH 10.0 and 7.8 (Fig. S8 and Fig. 18) at the intracellular level of L-lysine (Table 6). The *in vivo* analysis of the intracellular NADH to NAD⁺ ratio in *C. glutamicum* LYS-12, PIA-1A, and PIA-4 during the mid-exponential growth phase (B) enabled to infer the resulting *in vivo* enzyme activity of L-lysine 6-dehydrogenase for each producer. The data represent mean values and standard errors from three technical replicates.

Given the findings, modulation of redox metabolism emerged as a promising strategy to improve L-pipecolic acid production. With regard to optimizing the supply of NADPH, recombinant expression of the membrane-bound nicotinamide nucleotide transhydrogenase *pntAB* (Sauer et al, 2004) in *C. glutamicum* increased the production of L-lysine from glucose (Kabus et al, 2007; Sauer et al, 2004) and mannitol (Hoffmann et al, 2021), as well as the production of organic acids, under microaerobic conditions (Yamauchi et al, 2014). Driven by the proton motive force, the enzyme catalyzes the oxidation of NADH to NAD⁺, coupled to the reduction of NADP⁺ to NADPH (Fig. 22) (Jackson, 2003). In the context of strain PIA-1A, this activity appeared doubly attractive because it promised to recycle NADH, formed by LysDH, back into NAD⁺ and, furthermore, to supply NADPH (Hoffmann et al, 2018), of which 4 molecules are needed to synthesize L-lysine, the precursor of L-pipecolic acid (Wittmann & Heinzle, 2001b).

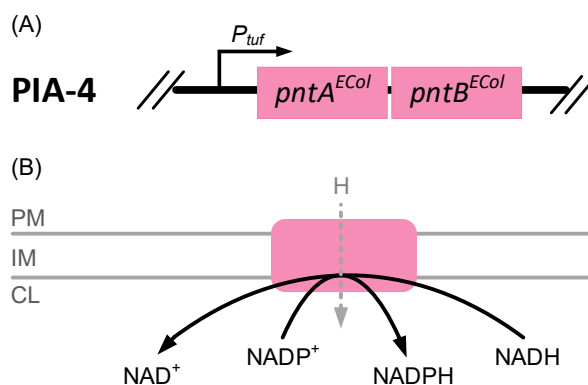


Fig. 22: Biosynthetic *pntAB* pathway for enhanced NAD^+ and $NADPH$ supply. (A) Biosynthetic module comprised of promoter *tuf* from *C. glutamicum* and *pntA* and *pntB* genes from *E. coli* K-12 for genome-based integration in the strain PIA-4. (B) Schematic illustration of membrane-integral nicotinamide nucleotide transhydrogenase complex in *E. coli*. PM = periplasm; IM = inner membrane; CL = cytosol; EC = *E. coli* (Sauer et al, 2004) (Bizouarn et al, 2000) (Johansson et al, 2005) (Francisco et al, 2018) (Hoffmann et al, 2021).

The newly constructed strain PIA-4 (PIA-1A P_{tuf} *pntAB*) harbored a genomic copy of the transhydrogenase gene from *E. coli*. When tested in batch culture at 30 °C, PIA-4 produced 6.1 mM L-pipecolic acid, 5 % more than PIA-1A (Fig. 23, Fig. S5). The strain also produced at an increased yield ($118 \text{ mmol mol}^{-1}$) (Table 8). The ratio of $NADH$ to NAD^+ was found to be readjusted to a value of 0.23 (Fig. 21B), streamlining the redox status and strongly promoting the activity of LysDH.

However, the implemented *pntAB* copy stimulated L-lysine production. The accumulation of L-lysine was increased by 75 % ($336 \text{ mmol mol}^{-1}$), much more than that of the desired product. This suggested that L-lysine production was enhanced too strongly by the increased $NADPH$ availability, so that only a fraction of the amino acid ended up in L-pipecolic acid, while the rest was excreted. When grown at 34 °C, the transhydrogenase mutant produced L-pipecolic acid at enhanced yield ($170 \text{ mmol mol}^{-1}$) but, once more, mainly secreted L-lysine ($295 \text{ mmol mol}^{-1}$) (Table 8). Unfavorably, the increased temperature negatively affected cell viability, as indicated by a reduction in the specific growth rate to 0.07 h^{-1} . Notably, the basic strain PIA-1A performed better at 34 °C, not only in terms of viability but also regarding L-pipecolic acid selectivity (Fig. 23).

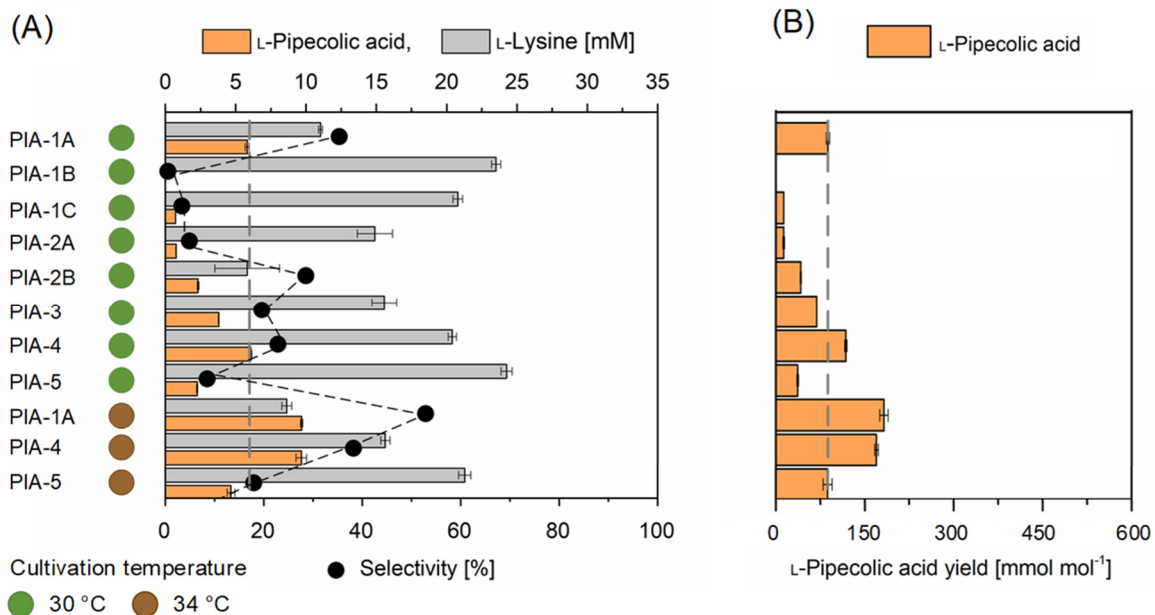


Fig. 23: Evaluation of basic and advanced L-pipecolic acid producers. The strains express biosynthetic modules each expressing a L-lysine 6-dehydrogenase from different donors, an additional RBS and Δ^1 -pyrroline 5-carboxylate reductase. Cultivation was performed in miniaturized bioreactor system using glucose minimal medium at 30 °C and 34 °C, respectively. Product titers and product selectivity (A) and corresponding L-pipecolic acid yields (B) are displayed. Mean values and standard deviation were calculated from three biological replicates.

Next, NADP-dependent glyceraldehyde-3-phosphate dehydrogenase from *S. mutans*, known for its influence on the supply of NADPH in *C. glutamicum* (Fig. 24) (Hoffmann et al, 2018; Hoffmann et al, 2021; Takeno et al, 2010), was introduced into the strain PIA-1A. Strain PIA-5, obtained through two rounds of recombination and validated by PCR and sequencing, expressed a genomic copy of *gapN*. Again, the modification mainly enhanced the formation of the byproduct L-lysine (Fig. 23, Fig. S5) to 427 mmol mol⁻¹, whereas the L-pipecolic acid yield remained low, even below that of PIA-1A (Table 8).

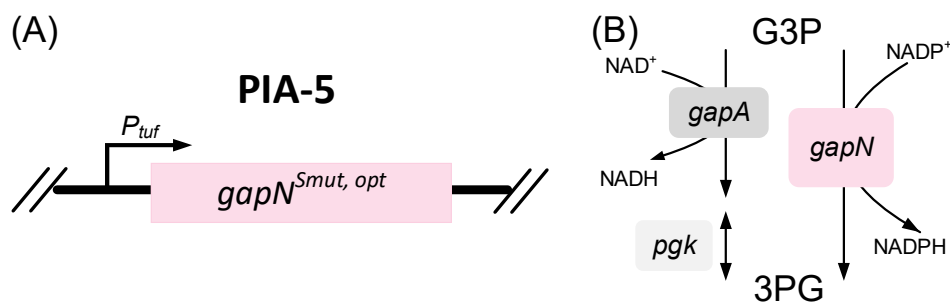


Fig. 24: NADP-dependent glyceraldehyde-3-phosphate dehydrogenase from *S. mutans* regenerates NADPH. (A) Pathway module of codon-optimized $gapN$ from *S. mutans* under control of the promoter tuf for stable genome-based integration into *C. glutamicum* PIA-1A yielding PIA-5. (B) Right: Natural formation of 3-phosphoglycerate (3PG) from glyceraldehyde 3-phosphate (G3P) in *C. glutamicum* mediated by NAD-dependent glyceraldehyde 3-dehydrogenase (encoded by $gapA$) and phosphoglycerate kinase (encoded by pgk). Left: NADP-dependent glyceraldehyde-3-phosphate dehydrogenase (encoded by $gapN$) from *S. mutans* mediated energy recovery. Smu = *S. mutans* (Hoffmann et al, 2021).

L-Pipecolic acid inhibits LysDH activity

As previously observed for 5-aminovalerate (Pauli, 2018) (Vandecasteele & Hermann, 1972), L-pipecolic acid was found to inhibit the first step of L-lysine degradation, catalyzed by LysDH (Fig. 25). As shown, enzymatic activity assays in crude cell extract, taken from exponentially growing strain PIA-1A, revealed 80 % reduced enzyme activity at an elevated level of L-pipecolic acid of 250 mM. Given the intracellular level of the compound 267 mM (Table 6), this suggested significant inhibitory effects *in vivo*. In contrast, L-lysine did not negatively the LysDH activity at higher concentration (Fig. 25).

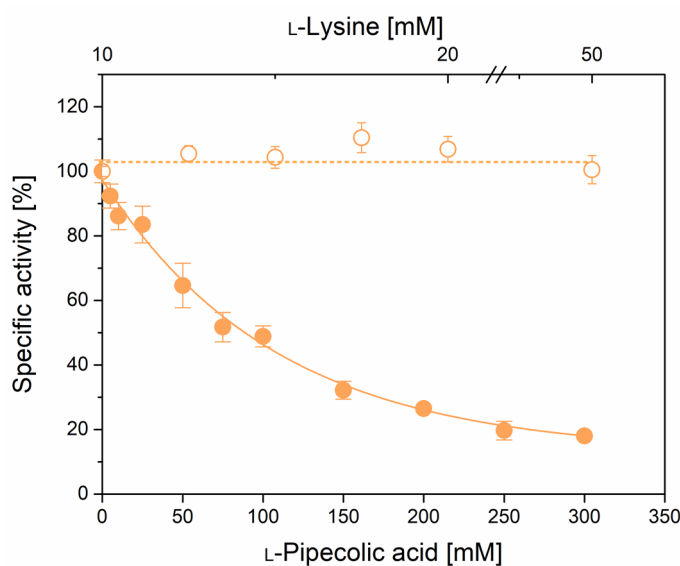


Fig. 25: Influence of L-pipecolic acid and L-lysine on LysDH activity. Inhibition of the enzymatic reaction by L-pipecolic acid (closed circles) and L-lysine (open circles) at pH 7.8. The crude cell extract for analysis was obtained from *C. glutamicum* PIA-1A during the exponential growth phase. All assays were performed at 30 °C. The data represent mean values and standard errors from three technical replicates.

Table 8: Kinetics and stoichiometry of growth and product formation in basic L-pipecolic acid-producing *C. glutamicum* strains. The producers were based on the expression of L-lysine 6-dehydrogenase from different donors and combined with different supporting modifications (Table 2, Fig. 22, Fig. 24). All strains were grown on glucose minimal medium in shake flasks at 30 °C and 34 °C. The data comprise rates of growth (μ), substrate consumption and product formation (q), as well as yields (Y). The data represent mean values and standard errors from three biological replicates. GLC = glucose; PIA = L-pipecolic acid, LYS = L-lysine, X = biomass. * n.d. = not detected.

	PIA-1A (30 °C)	PIA-2A (30 °C)	PIA-2C (30 °C)	PIA-4 (30 °C)	PIA-5 (30 °C)	PIA-1A (34 °C)	PIA-4 (34 °C)	PIA-5 (34 °C)
Rates								
μ [h ⁻¹]	0.18 ± 0.00	0.19 ± 0.00	0.18 ± 0.00	0.14 ± 0.00	0.19 ± 0.00	0.13 ± 0.00	0.07 ± 0.00	0.10 ± 0.00
q _{GLC} [mmol g ⁻¹ h ⁻¹]	3.58 ± 0.08	4.08 ± 0.17	4.27 ± 0.09	3.25 ± 0.11	4.00 ± 0.08	3.42 ± 0.27	2.59 ± 0.10	3.65 ± 0.11
q _{PIA} [mmol g ⁻¹ h ⁻¹]	0.31 ± 0.00	0.05 ± 0.01	n.d.*	0.38 ± 0.00	0.15 ± 0.00	0.63 ± 0.07	0.44 ± 0.01	0.32 ± 0.02
q _{LYS} [mmol g ⁻¹ h ⁻¹]	0.68 ± 0.06	1.20 ± 0.00	0.88 ± 0.09	1.09 ± 0.02	1.71 ± 0.03	0.53 ± 0.34	0.76 ± 0.03	1.47 ± 0.04
Yields								
Y _{X/GLC} [g mol ⁻¹]	48.9 ± 0.7	45.8 ± 1.0	41.0 ± 0.4	42.7 ± 0.9	46.8 ± 1.3	37.4 ± 0.9	28.8 ± 0.5	28.8 ± 0.8
Y _{PIA/GLC} [mmol mol ⁻¹]	88.1 ± 2.8	13.3 ± 1.5	n. d.	118.04 ± 1.8	37.0 ± 1.3	182.3 ± 7.0	169.8 ± 2.9	87.6 ± 7.5
Y _{LYS/GLC} [mmol mol ⁻¹]	191.8 ± 20.4	293.3 ± 17.3	204.9 ± 1.8	335.6 ± 9.2	427.0 ± 7.6	155.4 ± 1.2	294.5 ± 21.5	403.8 ± 13.9

In summary, systematic efforts to harness the L-lysine 6-dehydrogenase pathway for L-pipecolic acid production in *C. glutamicum* provided the desired product up to a yield of 182 mmol mol⁻¹. Even if some further improvement seemed possible, for example, through even stronger expression of the heterologous pathways, it was concluded from the limitations found for the created strain genealogy that the upper end of the expected performance had been approximated, which was admittedly still far from industrially attractive implementation (Becker et al, 2015; Becker & Wittmann, 2012a). At this point, the L-lysine 6-dehydrogenase pathway was dropped, although it had previously appeared to be the most promising route in *C. glutamicum*.

4.3 Evaluation of pathway alternatives for L-pipecolic acid biosynthesis

One step route via L-lysine cyclodeaminase

To improve performance, two alternative routes were considered. The first was taken from the biosynthesis of rapamycin (Khaw et al, 1998), an immunosuppressant macrolactone (Pan et al, 2012). Its biosynthetic pathway involves the incorporation of L-pipecolic acid, formed from L-lysine by a cyclodeamination reaction that involves a reversible oxidation at the α -amine; internal cyclization; and subsequent reduction of the cyclic Δ^1 -piperidine-2-carboxylate intermediate. All steps are catalyzed by a single enzyme, namely, L-lysine cyclodeaminase (*rapL*) (Gatto et al, 2006) (Poupin et al, 1999), which internally regenerates the redox cofactor (Fig. 26A). Here, *rapL* from *Streptomyces hygroscopicus*, also known as *S. rapamycinicus* (Gatto et al, 2006) was expressed with its native codon usage using the same plasmid under the control of P_{tur} as before (Fig. 26B).

The resulting mutant PIA-6 formed L-pipecolic acid, confirming successful expression of the enzyme, but the performance was very low ($12.5 \text{ mmol mol}^{-1}$) (Fig. 31, Table 9). The finding matched previous conclusions that the low catalytic performance of L-lysine cyclodeaminase is a major roadblock for enhanced L-pipecolic acid production (Wang et al, 2021a).

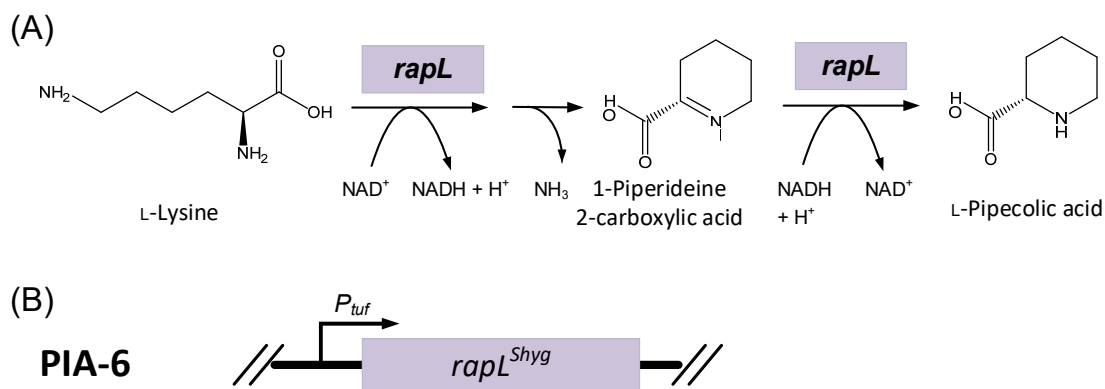


Fig. 26: L-lysine cyclodeaminase pathway. (A) RapL from *S. hygroscopicus* catalyzes complete degradation of L-lysine into L-pipecolic acid. (B) *rapL* module comprised of promoter *tuf* and *S. hygroscopicus* gene for plasmid-based expression in *C. glutamicum* LYS-12. Shyg = *S. hygroscopicus*. Adapted from Gatto et al., 2006.

Two-step route via L-lysine 6-aminotransferase

In a second attempt, L-lysine 6-aminotransferase (LAT) from the L-lysine degradation pathway of *Flavobacterium lutescens* was considered, where it transaminates L-lysine into α -amino adipic acid semialdehyde using the cofactor α -ketoglutarate (Fujii et al, 2000), followed by a spontaneous reaction into 1-piperideine 6-carboxylate and *proC*-mediated reduction to L-pipecolic acid (Fig. 27A) (Fujii et al, 2002b). The *lat* gene with its native codon usage was cloned together with *proC* into a *P_{tuf}*-controlled hybrid module (*P_{tuf} lat proC*), yielding *C. glutamicum* PIA-7 (Fig. 27B).

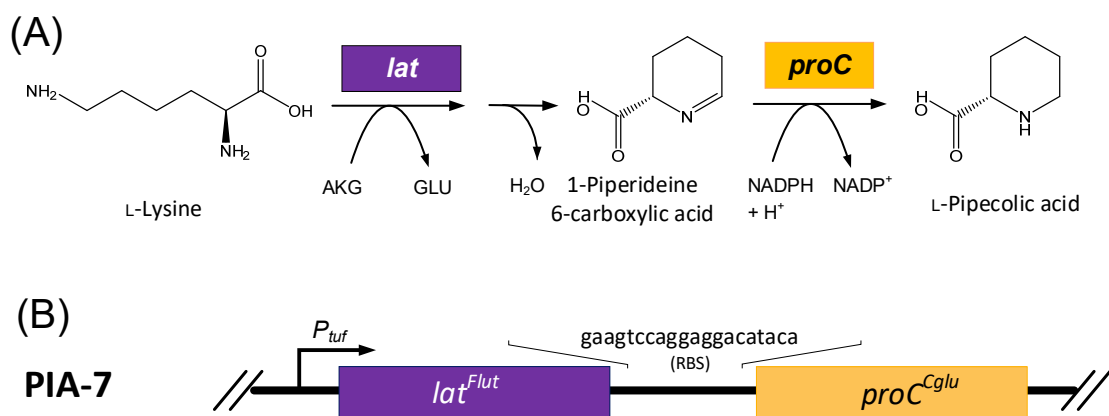


Fig. 27: LAT-mediated L-lysine degradation into L-pipecolic acid. (A) LAT from *F. lutescens* catalyzes the first degradation step towards α -amino adipic acid semialdehyde spontaneously hydrolyzed into 1-piperideine 6-carboxylic acid. ProC mediates further conversion into L-pipecolic acid. (B) Biosynthetic module for plasmid-based expression in *C. glutamicum* LYS-12 comprising promoter *tuf*, *lat* and *proC* gene, separated by an additional RBS. Flut = *F. lutescens*; Cglu = *C. glutamicum*. Adapted from Fujii et al, 2002.

When tested at miniaturized scale, the new producer *C. glutamicum* PIA-7 formed a tremendously increased amount of 8.5 mM L-pipecolic acid and exhibited improved selectivity, far better than that of all other strains (Fig. 31). In shake flasks at 30 °C, PIA-7 secreted 8 mM L-pipecolic acid at a 60 % increased yield and even had a doubled production rate compared to that of PIA-1A (Fig. 29, Table 9), outcompeting all previous efforts. This discovery was a surprise given that the L-lysine 6-aminotransferase-based route was not considered a promising metabolic pathway for L-pipecolic acid synthesis (Wang et al, 2021a).

Table 9: Kinetics and stoichiometry of growth and product formation in L-pipecolic acid-producing *C. glutamicum* strains. The producers were based on the expression of different L-pipecolic acid synthesis routes. All strains were grown on glucose minimal medium in shake flasks at 30 °C. The data comprise rates of growth (μ), substrate consumption and product formation (q), as well as yields (Y). The data represent mean values and standard errors from three biological replicates. GLC = glucose; PIA = L-pipecolic acid, LYS = L-lysine, X = biomass.

	PIA-1A (30 °C)	PIA-6 (30 °C)	PIA-7 (30 °C)
Rates			
μ [h^{-1}]	0.18 \pm 0.00	0.18 \pm 0.01	0.23 \pm 0.01
q_{GLC} [$\text{mmol g}^{-1} \text{h}^{-1}$]	3.58 \pm 0.08	3.86 \pm 0.08	4.14 \pm 0.08
q_{PIA} [$\text{mmol g}^{-1} \text{h}^{-1}$]	0.31 \pm 0.00	0.05 \pm 0.00	0.58 \pm 0.01
q_{LYS} [$\text{mmol g}^{-1} \text{h}^{-1}$]	0.68 \pm 0.06	1.03 \pm 0.02	0.32 \pm 0.01
Yields			
$Y_{\text{X/GLC}}$ [g mol^{-1}]	48.9 \pm 0.7	45.5 \pm 2.3	56.0 \pm 03.2
$Y_{\text{PIA/GLC}}$ [mmol mol^{-1}]	88.1 \pm 2.8	12.5 \pm 0.2	139.9 \pm 0.5
$Y_{\text{LYS/GLC}}$ [mmol mol^{-1}]	191.8 \pm 20.4	266.5 \pm 5.7	76.3 \pm 01.3

Comparative gene expression profiling of PIA-7 and PIA-0 revealed strong upregulation of L-lysine 6-aminotransferase, as desired (Table 10), plus a few other changes of apparently minor relevance that were also visible in PIA-1A. Accordingly, the transcriptomes of the two producers PIA-1A and PIA-7 showed no significant difference, except for the heterologous genes (data not shown).

Table 10: Transcription profiling of L-pipecolic acid-producing *C. glutamicum* PIA-7. The data comprise significantly up- and downregulated genes compared to *C. glutamicum* PIA-0 expressing the empty plasmid (\log_2 -fold change ≥ 1 and ≤ -1 , $p \leq 0.05$). The samples were taken from glucose-based cultures during mid-exponential growth. The statistical quality of the data was verified by PCA (Fig. S2). The data represent mean values and standard errors from three biological replicates.

Locus tag	Gene	Gene description	Log ₂ fold change
	<i>lat</i>	L-lysine 6-aminotransferase	+ 9.6
<i>CGL_RS02095</i>	<i>proC</i>	Δ^1 -pyrroline 5-carboxylate reductase	+ 4.6
<i>CGL_RS15485</i>	-	Hypothetical protein	+ 2.5
<i>CGL_RS03280</i>	<i>prpD2</i>	MmgE/PrpD family protein	+ 2.4
<i>CGL_RS14845</i>	<i>NCgl2877</i>	PadR family transcriptional regulator	+ 2.4
<i>CGL_RS03285</i>	<i>prpB2</i>	Methylisocitrate lyase	+ 2.3
<i>CGL_RS00835</i>	<i>NCgl0156</i>	Hypothetical protein	+ 2.3
<i>CGL_RS12550</i>	<i>ftn</i>	Ferritin	+ 2.3
<i>CGL_RS00840</i>	<i>msmA</i>	CoA-acylating methylmalonate-semialdehyde dehydrogenase	+ 2.2
<i>CGL_RS05910</i>	<i>narI</i>	Respiratory nitrate reductase subunit gamma	+ 1.6
<i>CGL_RS02010</i>	<i>mtrA</i>	HtaA domain-containing protein	- 4.8
<i>CGL_RS02015</i>	<i>mtrA</i>	HtaA domain-containing protein	- 4.4
<i>CGL_RS06520</i>	<i>NCgl1254</i>	Hypothetical protein	- 3.5
<i>CGL_RS01750</i>	<i>NCgl0329</i>	Iron-siderophore ABC transporter substrate-binding protein	- 3.4
<i>CGL_RS04925</i>	<i>ripA</i>	Helix-turn-helix transcriptional regulator	- 3.3
<i>CGL_RS02555</i>	<i>NCgl0483</i>	Iron chelate uptake ABC transporter family permease subunit	- 3.0
<i>CGL_RS02550</i>	<i>NCgl0482</i>	ABC transporter ATP-binding protein	- 2.9
<i>CGL_RS04045</i>	<i>NCgl0773</i>	Siderophore-interacting protein	- 2.9
<i>CGL_RS10120</i>	<i>NCgl1959</i>	Iron-siderophore ABC transporter substrate-binding protein	- 2.8
<i>CGL_RS03335</i>	<i>Irp1B</i>	Iron ABC transporter permease	- 2.7

Interestingly, the intracellular level of L-lysine in the new strain was 22 mM (Table 11). This value was significantly lower than in strain PIA-1A, indicating faster conversion into L-pipecolic acid. Decreased L-pipecolic acid concentration (222.3 mM) even suggests

more efficient secretion (Table 11). In summary, without doubt, the use of the *lat* enzyme promised a breakthrough.

Table 11 Intracellular amino acid pools in the *C. glutamicum* strains PIA-1A and PIA-7 compared control strain PIA-0. Samples were extracted from mid-exponentially on glucose growing cells. Based on the correlation factor of 1.95 ($\mu\text{L cytoplasm}$) $\text{mg}_{\text{CDW}}^{-1}$ intracellular concentration were determined (Krömer et al, 2004). Displayed data represent mean values and standard errors of three biological replicates.

Amino acid	PIA-1A [mM]	PIA-7 [mM]	PIA-0 [mM]
L-Lysine	35.3 ± 5.8	22.4 ± 3.8	63.5 ± 6.9
L-Aspartic acid	16.6 ± 0.8	13.5 ± 1.5	12.1 ± 1.3
L-Glutamic acid	227.4 ± 19.8	186.3 ± 21.3	238.2 ± 19.6
L-Asparagine	7.7 ± 0.5	6.5 ± 0.6	4.1 ± 0.4
L-Serine	7.7 ± 0.5	6.9 ± 0.6	4.9 ± 0.5
L-Glutamine	22.0 ± 1.0	16.6 ± 1.8	42.3 ± 5.8
L-Histidine	0.0 ± 0.0	0.0 ± 0.0	0.0 ± 0.0
Glycine	11.6 ± 1.2	10.9 ± 1.1	9.8 ± 1.1
L-Threonine	6.2 ± 0.5	6.1 ± 0.5	3.2 ± 0.4
L-Arginine	8.0 ± 0.5	6.9 ± 0.6	5.0 ± 5.0
L-Alanine	14.3 ± 0.9	11.4 ± 1.2	12.1 ± 1.1
L-Tyrosine	0.0 ± 0.0	0.0 ± 0.0	0.0 ± 0.0
L-Valine	32.3 ± 2.8	22.7 ± 2.4	28.4 ± 2.9
L-Methionine	4.5 ± 0.4	4.2 ± 0.4	1.7 ± 0.1
L-Phenylalanine	8.9 ± 0.7	7.5 ± 0.8	5.1 ± 0.5
L-Isoleucine	16.7 ± 1.3	12.5 ± 1.1	14.3 ± 1.5
L-Leucine	11.9 ± 0.8	10.0 ± 1.0	6.9 ± 0.6
L-Tryptophan	21.7 ± 1.4	18.0 ± 1.6	11.8 ± 1.0
L-Proline	49.9 ± 5.8	35.0 ± 4.3	59.1 ± 4.4
L-Pipecolic acid	266.9 ± 48.1	222.3 ± 26.2	0.0 ± 0.0

4.4 Systems metabolic engineering of *C. glutamicum* PIA-7

The two-step route via L-lysine 6-aminotransferase in the strain *C. glutamicum* PIA-7 appeared most promising for high-level L-pipecolic acid production. Further insights into the catalytic efficiency of the LAT enzyme and transporter engineering should demonstrate the potential of the novel production route.

4.4.1 L-lysine 6-aminotransferase exhibits high catalytic efficiency *in vivo*

To evaluate (and eventually further optimize) L-lysine 6-aminotransferase-based production, the newly introduced LAT enzyme was studied in more detail. PIA-7, sampled during the midexponential growth phase, exhibited an *in vitro* activity of 170 mU mg⁻¹ at 10 mM L-lysine, which was increased to 230 mU mg⁻¹ when assayed at 30 mM L-lysine and (cytoplasmic) pH 7.8 and to 500 mU mg⁻¹ at 30 mM L-lysine and pH 8.5 (Fig. 28). The metabolome data translated into an L-lysine-corrected flux capacity of approximately 200 mU mg⁻¹, i.e., 2.6 mmol g⁻¹ h⁻¹, offering high-efficiency production.

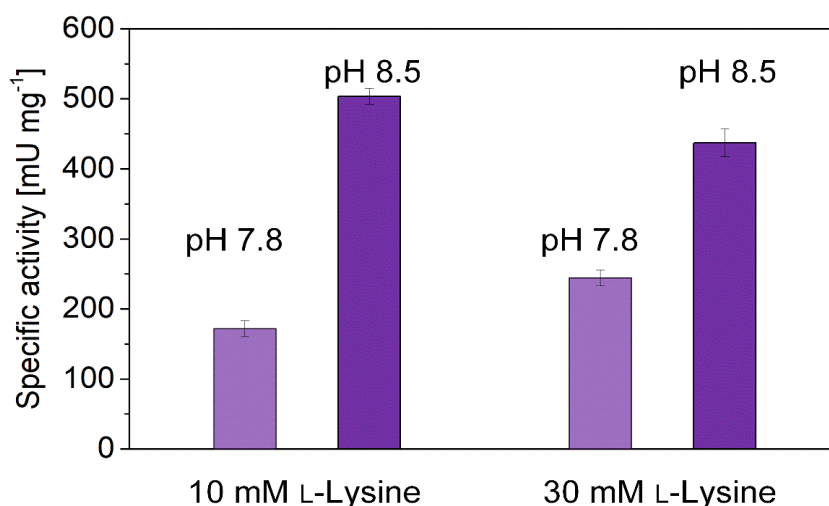


Fig. 28: Activity of L-lysine 6-aminotransferase from *F. lutescens* expressed in the advanced L-pipecolic acid producer *C. glutamicum* PIA-7. The assay was conducted at 30°C at different pH values and L-lysine concentrations using crude cell extract from exponentially growing *C. glutamicum* PIA-7. The data represent mean values and standard errors from three biological replicates.

4.4.2 PIA-7 exhibits optimal redox supply

As described before, the LAT enzyme required higher L-lysine levels to work fully saturated with substrate than LysDH. It was therefore aimed to increase the supply of L-lysine by modulating the redox status through genomic expression of *pntAB* (Fig. 22) and *gapN* (Fig. 24), respectively. As shown for the strains *C. glutamicum* PIA-4 and PIA-5 (Table 8), both genetic modifications were able to enhance the synthesis of L-lysine.

First, the membrane-bound nicotinamide nucleotide transhydrogenase *pntAB* from *E. coli* was genomically expressed in PIA-7. The correctness of the integration of the genetic

elements was verified by PCR (4316 bp integration mutant, 1184 bp original integration locus) and sequencing. The newly derived strain was designated PIA-8A. It exhibited a slightly increased L-pipecolic acid yield of 149 mmol mol⁻¹, 6 % higher than the parent strain under the same growth conditions – suggesting a mild effect of the *pntAB* expression. Again, the secretion of L-lysine enhanced, this time resulting in a yield of 183 mmol mol⁻¹.

The integration of a genomic copy of the NADP-dependent glyceraldehyde-3-phosphate dehydrogenase *gapN* from *S. mutans* in PIA-7 resulted in strain PIA-8B. The correctness of the modification was verified by colony PCR (2558 bp integration mutant, 1064 bp original integration locus) and Sanger sequencing. This modification was even found detrimental. At 30 °C, PIA-8B yielded 40 % less L-pipecolic acid (112 mmol mol⁻¹) than PIA-7 together with amounts of L-lysine (170.0 mmol mol⁻¹). Overall, engineering of the redox metabolism did not provide an extra benefit in LAT-based producers.

4.4.3 Metabolic engineering of product transport

As an alternative at this point, elimination of the L-lysine exporter and completely blocking L-lysine secretion was aimed at. Previously, the deletion of the encoding *lysE* gene enabled the selective formation of other L-lysine-based products at high yields, namely, 1,5-diaminopentane (Kind et al, 2014) and glutarate (Rohles et al, 2018). In all these cases, *lysE* deletion was conducted after heterologous production of the novel product of interest had been established to prevent the inhibition or even the lethal accumulation of L-lysine. As shown, successful deletion of the exporter without such an *escape* pathway was possible only in weak L-lysine overproducers (Giesselmann et al, 2019). Accordingly, the *lysE* deletion in the hyperproducing LYS-12-background required L-pipecolic acid formation to operate at a high level during strain construction (Kind et al, 2011).

It is important to note that the best-performing strain, PIA-7, carried the biosynthetic L-pipecolic acid pathway on a plasmid with kanamycin resistance. Because the integrative

plasmid *pClik int SacB* was based on the same selection marker (Becker et al, 2005), *kan^R* on the vector was replaced by the chloramphenicol acetyltransferase gene *cm^R* (Christmann et al, 2023) and inserted the two homology regions required for *lysE* deletion. However, after transformation of the plasmid into PIA-7, the desired second recombination event could not be observed, despite several repeated attempts. Likewise, a complementary strategy (involving *cm^R* on the episomal *pClik5a* vector and *kan^R* on the integrative *pClik int SacB* vector) was not successful. A higher temperature likewise did not enable the desired modification (data not shown). Notably, the additional use of chloramphenicol massively impaired cell vitality (Song et al, 2010), which could have negatively affected the overall cloning efficiency.

To demonstrate selective L-pipecolic acid production the previously created (weak) L-lysine overproducer *C. glutamicum lysC^{fbr} ΔlysE* was used, which already lacked the exporter (Giesselmann et al, 2019). The mutant was transformed with the *lat*-based plasmid. The obtained strain PIA-8C revealed L-lysine-free, selective L-pipecolic acid production (26 mmol mol⁻¹, Table 12). In this regard, it was proved that the deletion of the L-lysine exporter enabled selective L-pipecolic acid production in low-performing strains. However, it was not possible in LYS-12-based strains, where it appeared lethal.

In addition, it was aimed to potentially reduce or eliminate the import of L-pipecolic acid back into the cell. Interestingly, the ring-structured metabolite ectoine reveals high structural similarity to L-pipecolic acid (Becker et al, 2018b; Hara et al, 2019). It was therefore decided to evaluate the previously identified proline and ectoine importer ProP for its potential effect on L-pipecolic acid import (Perez-Garcia et al, 2019) and deleted the encoding *proP* gene in *C. glutamicum* PIA-7. The correctness of the modification was verified by colony PCR (1195 bp deletion mutant, 2667 bp original integration locus) and Sanger sequencing.

The new strain PIA-8D was evaluated in glucose medium in shake flask cultures. It showed a 7 % increase in L-pipecolic acid formation (150 mmol mol⁻¹), while the L-lysine formation

was increased by 46 % (111 mmol mol⁻¹), compared to the parent strain (Table 12). On the other hand, the strain used glucose slower. The specific L-pipecolic acid production rate remained unchanged. Obviously, the deletion of *proP* caused only minor changes. Notably, transcriptome analysis then revealed (Table 10), that *proP* was downregulated 24-fold in PIA-7 strain, eventually explain the weak effect of its deletion.

4.5 High-level fed-batch production of L-pipecolic acid

Findings from transcriptomics, proteomics, and metabolomics were translated into optimization strategies to develop PIA genealogy. Mainly based on the characterization of the L-lysine degradation enzymes and interplay with the *C. glutamicum* host, *de novo* L-pipecolic acid synthesis was pushed to economically attractive yields.

4.5.1 Optimization of process conditions

Interestingly, production was boosted by the addition of pyridoxal phosphate (10 mg L⁻¹), a stabilizing coenzyme of L-lysine 6-aminotransferase (Coque et al, 1991), previously proven to support other *C. glutamicum* cell factories (Kind et al, 2010). At 30 °C, the supply of the coenzyme (10 mg L⁻¹) increased the productivity of PIA-7 by 25 % to 0.73 mmol g⁻¹ h⁻¹, while the yield was even increased by 40 % - 140 mmol mol⁻¹ (Fig. 29B, Table 12). Higher concentrations of pyridoxal phosphate (25 mg L⁻¹, 50 mg L⁻¹) did not provide additional benefits (data not shown). The cultivation temperature beneficially stimulated strain PIA-7 (Fig. 29C). At 34 °C, the producer yielded L-pipecolic acid at 30 % yield and a production rate of 1.1 mmol g⁻¹ h⁻¹ (Fig. 31, Table 12). In contrast to the L-lysine 6-dehydrogenase-based strains, PIA-7 was able to grow at 37 °C. Under these conditions, for the first time, strain PIA-7 achieved almost completely selective production of L-pipecolic acid (96 %) (Fig. 31).

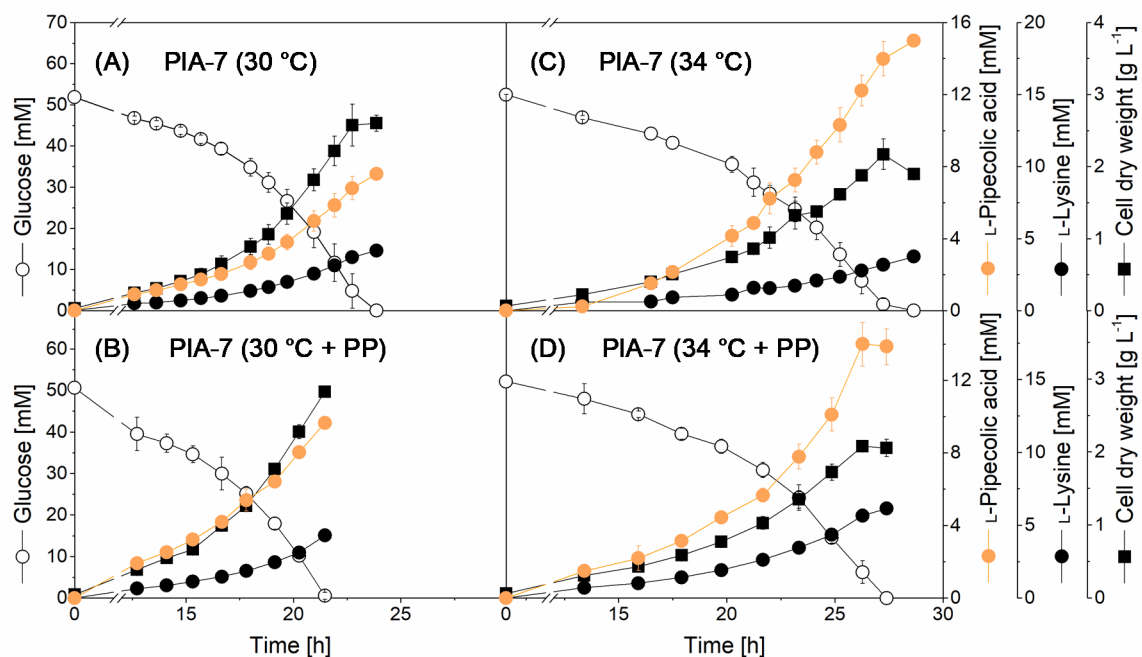


Fig. 29: Performance of the advanced L-pipecolic acid producer *C. glutamicum* PIA-7 in shake flask cultures Cultivation was conducted on glucose minimal medium at 30 °C (A) and 34 °C (C). Additionally, the medium was enriched with 10 mg L⁻¹ pyridoxal phosphate (PP), and the cells were incubated at 30 °C (B) and 34 °C (D). The data represent mean values and standard errors from three biological replicates.

In summary, the new producer *C. glutamicum* PIA-7 comprised several beneficial modifications. In batch mode at 37 °C, it exhibited an extraordinary L-pipecolic acid yield of 562 mmol mol⁻¹, more than sixfold more than that of the basic producer PIA-1A at the start (Table 12). The yield corresponded to 74 % of the theoretical maximum (Becker et al, 2011), demonstrating the high synthetic capability of the new cell factory. The L-lysine yield of the parent L-lysine-producer LYS-12, used to create PIA-7, was only 260 mmol mol⁻¹ when determined under similar conditions (Becker et al, 2011) PIA-7 surpassed this value by 216 %. This leap in performance impressively underlines how much extra carbon could be pushed and pulled through L-lysine biosynthesis toward the novel product. Notably, PIA-7 still formed minor shares of L-lysine when grown at temperatures below 37 °C (Fig. 31).

Table 12: Kinetics and stoichiometry of growth and product formation in superior L-pipecolic acid-producing *C. glutamicum* strains. The producing strain PIA-7 was based on LYS-12 and expressed the L-lysine 6-aminotransferase from *F. lutescens* and Δ^1 -pyrroline 5-carboxylate reductase (Table 2). PIA-8A and PIA-8B additionally expressed *pntAB* and *gapN* module. For PIA-8C *C. glutamicum lysC^{fb} Δ lysE* was transformed with the same plasmid. PIA-8D was based on PIA-7 where *proP* gene was deleted. The strains were cultivated in glucose minimal medium in shake flask at the temperatures specified, partially supplemented with pyridoxal phosphate (10 mg L⁻¹). The data comprise growth rates (μ), substrate consumption and product formation rate (q) and yields (Y). GLC = glucose; PIA = L-pipecolic acid, LYS = L-lysine, X = biomass, PP = pyridoxal phosphate. The data represent mean values and standard errors from three biological replicates. *n. d. = not detected.

	PIA-7 30 °C	PIA-7 34 °C	PIA-7 30 °C+ PP	PIA-7 34 °C + PP	PIA-7 37 °C	PIA-8A 30 °C	PIA-8B 30 °C	PIA-8C 30 °C	PIA-8D 30 °C
Rates									
μ [h ⁻¹]	0.23 ± 0.01	0.16 ± 0.01	0.24 ± 0.01	0.16 ± 0.01	0.10 ± 0.01	0.17 ± 0.00	0.20 ± 0.00	0.40 ± 0.01	0.22 ± 0.01
q_{GLC} [mmol g ⁻¹ h ⁻¹]	4.14 ± 0.08	3.63 ± 0.13	3.74 ± 0.33	3.59 ± 0.04	3.39 ± 0.14	3.74 ± 0.06	4.32 ± 0.29	4.56 ± 0.06	3.81 ± 0.07
q_{PIA} [mmol g ⁻¹ h ⁻¹]	0.58 ± 0.01	1.10 ± 0.05	0.73 ± 0.01	1.09 ± 0.12	1.91 ± 0.09	0.56 ± 0.01	0.49 ± 0.05	0.12 ± 0.01	0.57 ± 0.02
q_{LYS} [mmol g ⁻¹ h ⁻¹]	0.32 ± 0.01	0.31 ± 0.02	0.34 ± 0.03	0.44 ± 0.04	0.09 ± 0.00	0.68 ± 0.02	0.73 ± 0.04	n.d.*	0.42 ± 0.02
Yields									
$Y_{\text{X/GLC}}$ [g mol ⁻¹]	56.0 ± 3.2	42.9 ± 3.0	63.3 ± 6.5	41.4 ± 1.6	29.9 ± 0.6	45.9 ± 0.1	48.1 ± 3.0	87.0 ± 1.1	58.4 ± 3.7
$Y_{\text{PIA/GLC}}$ [mmol mol ⁻¹]	139.9 ± 0.5	304.3 ± 8.4	196.1 ± 12.4	304.1 ± 36.2	562.1 ± 2.8	149.0 ± 3.3	112.4 ± 3.6	26.0 ± 1.6	149.7 ± 6.4
$Y_{\text{LYS/GLC}}$ [mmol mol ⁻¹]	76.3 ± 1.3	84.8 ± 2.1	89.6 ± 0.2	123.0 ± 12.9	27.4 ± 1.0	182.6 ± 5.2	170.0 ± 4.4	n.d.	111.1 ± 7.0

4.5.2 Fed-batch process of *C. glutamicum* PIA-7

To assess performance under industrially relevant conditions, the PIA-7 strain was benchmarked in a fed-batch process on glucose medium at 34 °C (Fig. 30). During the batch phase, PIA-7 accumulated L-pipecolic acid at a yield of 0.24 mol mol⁻¹ (0.17 g g⁻¹) and reached a concentration of 12.9 g L⁻¹ (100 mM). The strain grew exponentially to a biomass concentration of 29.5 g L⁻¹ and revealed a favorable robustness in efficiently utilizing the high start level of the sugar (85 g L⁻¹) (Rohles et al, 2018; Rohles, 2021). After 16 h, the initially supplied glucose was depleted, and the feed phase was started. Triggered by a sudden rise in the DO signal, pulses of the concentrated feed were automatically added when the sugar was exhausted. Favorably, this DO-based control

worked highly robustly and allowed us to operate the process without external monitoring (Rohles, 2021). After 28 h, the maximum biomass concentration (32.9 g L^{-1}) was reached. The concentration of L-pipecolic acid continuously increased to a final titer of 82 g L^{-1} (635 mM) after 110 hours (Fig. 30).

During the feed phase, the L-pipecolic acid yield increased to 0.29 g g^{-1} ($405 \text{ mmol mol}^{-1}$) (Fig. 33). Although a slight overestimation cannot be excluded, due to small amounts of yeast extract added (below $3/100$ of sugar in feed), the created cell factory exhibited attractive synthetic performance. In addition to L-pipecolic acid, 18 g L^{-1} L-lysine was secreted. L-lysine accumulated mainly during the batch phase under glucose excess. Strikingly, after 34 h, L-lysine secretion stopped, roughly linked to the end of growth. Afterward, PIA-7 exclusively secreted L-pipecolic acid and maintained 100 % selectivity for the rest of the process (Fig. 33).

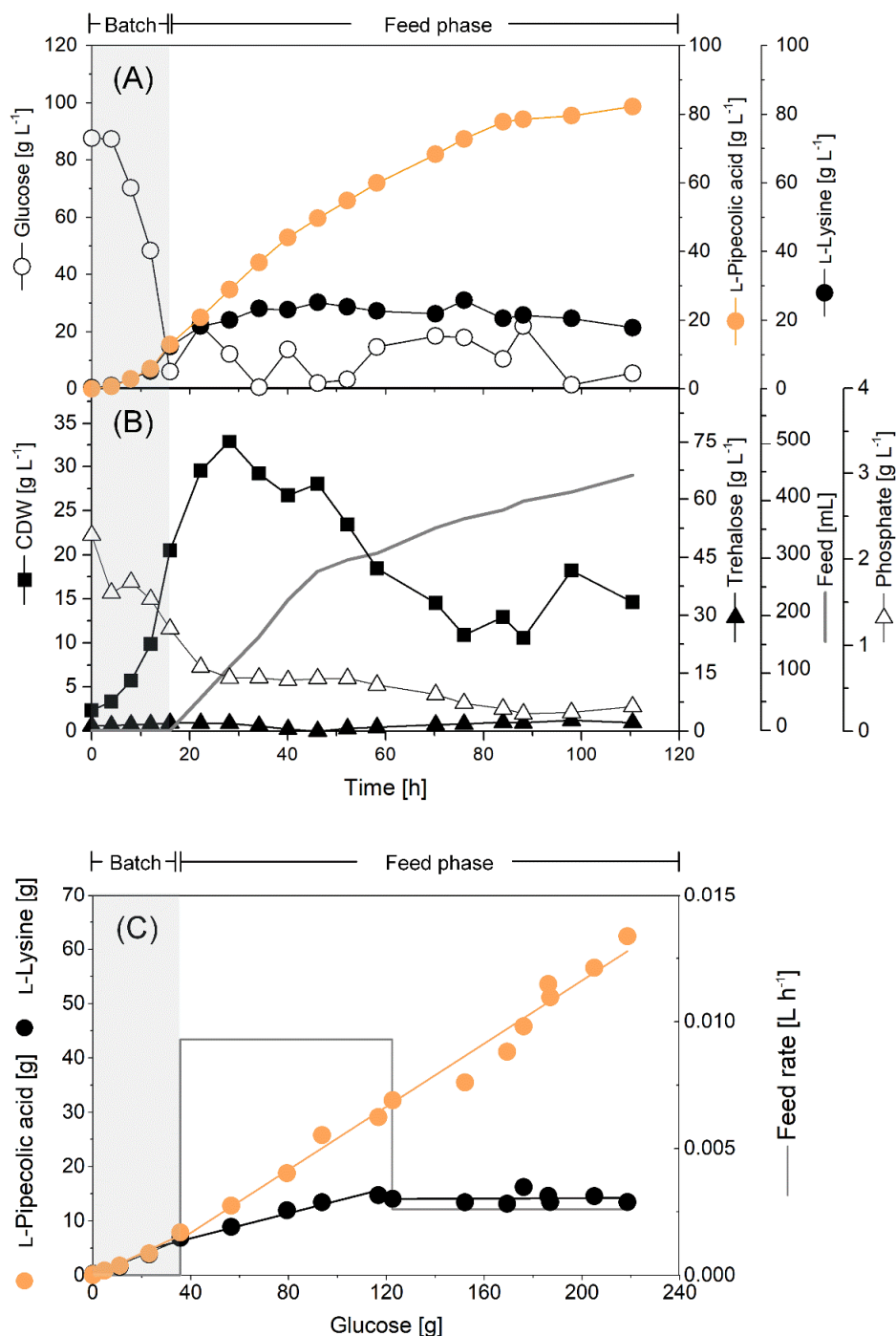


Fig. 30: Fed-batch production of L-pipecolic acid by metabolically engineered *C. glutamicum* PIA-7. The process was operated at 34 °C. After depletion of the initial sugar at the end of the batch phase, pulses of feed were added automatically, using an increase in the level of dissolved oxygen (DO) above 50 % as a trigger (A). The batch and feed phases are denoted by dotted lines in the culture profile. The batch medium contained glucose (85 g L⁻¹) and yeast extract (15 g L⁻¹) as carbon sources. The feed contained six-fold more glucose (500 g L⁻¹), while the yeast extract level (15 g L⁻¹) remained the same. The process was operated at 34 °C. Yield and selectivity of the L-pipecolic acid production improved during fermentation, which was linked to the limited availability of glucose during the feed phase (B). The volumetric productivity was 0.36 g L⁻¹ h⁻¹ during the batch phase and 0.97 g L⁻¹ h⁻¹ during the feed phase. The average volumetric productivity over the entire process was 0.80 g L⁻¹ h⁻¹. The key performance indicators of the production process are summarized in Fig. 33. The process was conducted as duplicate. The deviation between duplicates was in the range of 5 %.

4.6 Fine-tuning of *lat* expression towards maximized production

As shown, L-lysine secretion in growing cells during the initial batch phase remained an undesired feature of the developed strains (Fig. 31). The targeted limitation of cell growth by adaptation of the medium appeared not to be a useful approach to overcome this problem, as reaching a high number of cells early was in fact required to efficiently produce L-pipecolic acid. Likewise, it was decided to not reduce the batched sugar level and to shorten the batch phase because the chosen setup that included a high starting concentration of glucose appeared rather suitable. It provided a high biomass level within a few hours and, furthermore, minimized broth dilution by the later feed addition and, thereby, kept the product titer high. Therefore, it was decided to tackle the problem of undesired L-lysine secretion genetically.

4.6.1 Native promoter replacement for *lat* expression

Obviously, it was not possible to delete the L-lysine exporter in the LYS-12-based strains (shown above). Therefore, the fine-tuned balancing of glucose uptake, L-lysine biosynthesis and conversion into L-pipecolic acid appeared crucial to improve performance (Schwentner et al, 2019). Because the activity of L-lysine amino transferase still displayed a bottleneck in PIA-7, optimized expression of the *lat* gene was focused on. As an alternative to P_{tuf} , the promoter P_{sod} was selected first, which mediates the expression of the *sod* (superoxide dismutase) gene in *C. glutamicum* and was previously successfully used for constitutive overexpression in the microbe (Becker et al, 2005) (Becker et al, 2007; Becker & Wittmann, 2012b). To compare the expression strength between P_{sod} and P_{tuf} , both promoters were cloned in front of the *mCherry* gene into *pClik* and the two vectors were individually transformed into the LYS-12 strain. Then, the two reporter strains were monitored online for fluorescence and cell growth (Kohlstedt et al, 2018). The analysis revealed that P_{sod} expressed the reporter gene well, although 5-fold weaker than P_{tuf} (Fig. S9). Based on previous experience, the relative strength of both

promoters in the genome of *C. glutamicum* can vary, depending on the expressed gene and the expression locus (Becker et al, 2005; Lee et al, 2018). Beneficially, the newly created P_{sod} -based strain PIA-9 ($P_{sod} \text{ lat } proC$) produced significantly more L-pipecolic acid at 30 °C than PIA-7, while the formation of L-lysine was reduced by almost 50 % at 30 °C and 34 °C (Fig. 31).

4.6.2 Synthetic promoter variants enhance productivity

Inspired by this improvement, optimization of the expression level was further aimed. For this purpose, a library of synthetic variants of P_{sod} was created using random mutagenesis and cloned it into the *mCherry* reporter plasmid. The broad color spectrum of the obtained, plated clones showed that a library of promoters of different strengths could be generated. Two clones with intensive red color, presumably hosting strong promoters, were selected for further work. Sequencing revealed the mutations that mediated the increased expression strength in the new promoters (Fig. S9). The two variants were designated P_{sod}^{opt1} and P_{sod}^{opt2} and evaluated for expression strength. They were found to be 6.0- and 10.3-fold stronger than the native promoter P_{sod} , respectively. Compared to P_{tuf} , which is present in strain PIA-7, P_{sod}^{opt2} enabled 1.9-fold stronger *mCherry* expression.

Based on this development, two final producers were designed: PIA-10A ($P_{sod}^{opt1} \text{ lat } proC$) and PIA-10B ($P_{sod}^{opt2} \text{ lat } proC$). Both mutants significantly outperformed all previously created strains (Fig. 31). They formed 30 % more L-pipecolic acid than PIA-9 when tested at 30 °C and 34 °C. At 34 °C, strain PIA-10B achieved a remarkable yield of 525 mmol mol⁻¹. Furthermore, the use of the new promoters fully eliminated L-lysine secretion. The conversion of L-lysine into L-pipecolic acid inside the cell was efficient enough to obtain L-pipecolic acid at maximum selectivity.

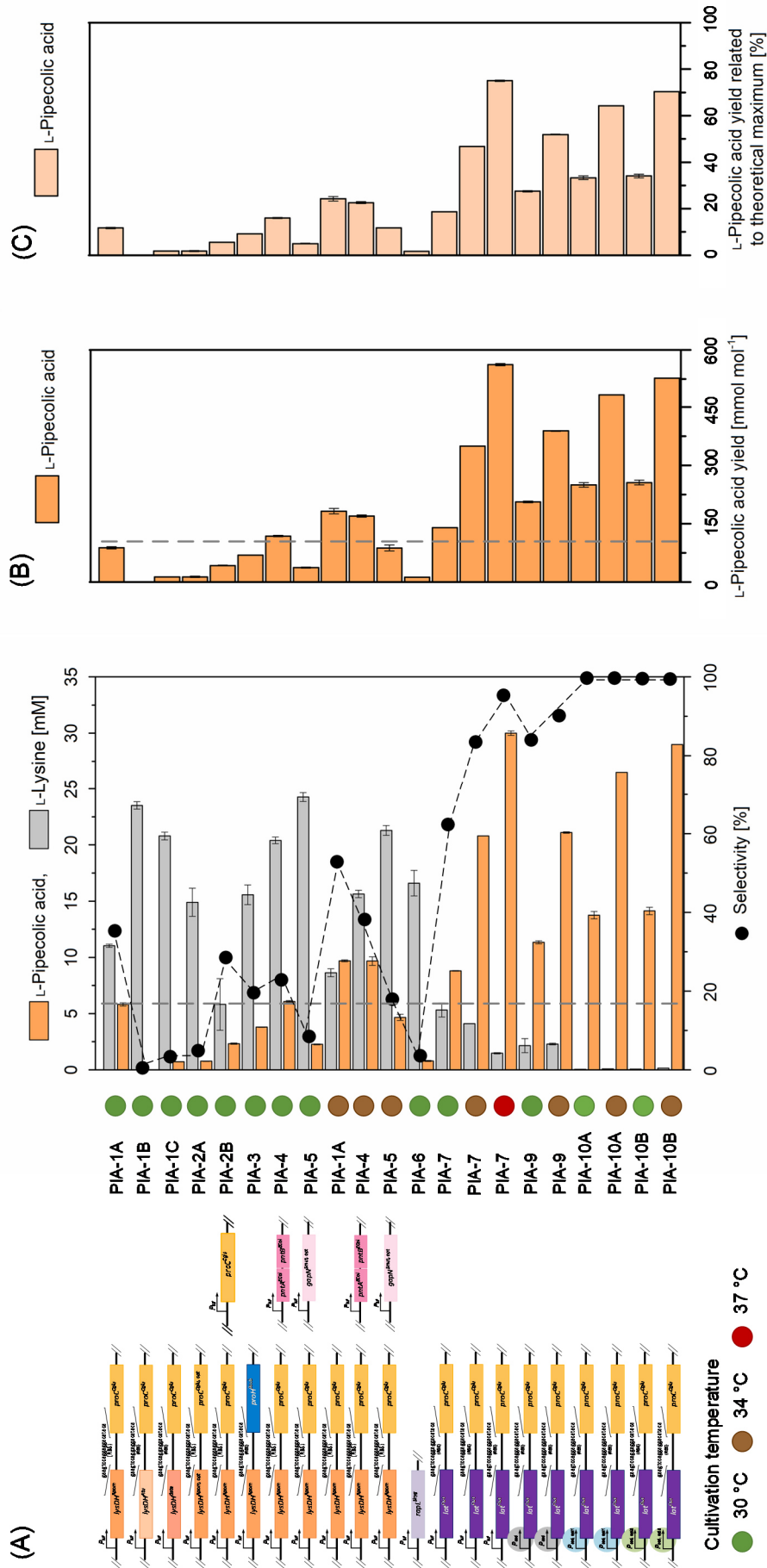


Fig. 31: Systems metabolic engineering of *C. glutamicum* for L-pipecolic acid production. During strain development, the production performance of the created overproducers was evaluated in batch processes at a miniaturized scale on glucose minimal medium using different temperatures (30 °C, 34 °C, 37 °C). The data show the improvement of the final titer of L-pipecolic acid, the reduction of L-lysine formation and the improvement in selectivity, the latter indicating the share of L-pipecolic acid in the sum of both products. The data represent mean values and standard errors from three biological replicates (A). In addition, the L-pipecolic acid yield for the different strains is given (B), also related to theoretical maximum (C). The genetic background of all overproducers can be taken from Table 2.

The improvement offered attractive economics: production at high yield and simplified, low-cost downstream processing. From the metabolic engineering viewpoint, the successfully implemented superior promoter variants nicely highlight the great impact of synthetic promoters on strain performance, even in advanced producers (Rytter et al, 2014; Shen et al, 2017; Yim et al, 2013; Zhang et al, 2018).

4.6.3 Benchmarking *C. glutamicum* PIA-10B in a fed-batch process

C. glutamicum PIA-10B was then selected to benchmark the developed strain family. Given the excellent performance at 30 °C and 34 °C (Fig. 31), the strain was tested in two different fed-batch configurations, one at a temperature of 30 °C and another that was operated at 30 °C during the batch phase and shifted to 34 °C at the beginning of the feed phase.

In the 30/34 °C two-temperature process, PIA-10B consumed almost all glucose within less than 20 h, which initiated the addition of the feed (Fig. 32). During the batch phase, the strain accumulated L-pipecolic acid at a yield of 293 mmol mol⁻¹ (0.21 g g⁻¹) and reached a product level of 15.2 g L⁻¹ (118 mM). Remarkably, L-lysine was not detected in the culture broth. After 20 h, the maximum biomass concentration (28.1 g L⁻¹) was reached. The concentration of L-pipecolic acid continuously increased to a final titer of 93 g L⁻¹ (720 mM) after 90 hours, the highest value reported thus far for *de novo* production of this chemical (Xu et al, 2022). Remarkably in terms of the yield (Fig. 33), the strain even achieved high-efficiency biotransformation processes that use L-lysine as a precursor (Han et al, 2020). Throughout the whole process, PIA-10B secreted L-pipecolic acid almost exclusively (Fig. 32). While L-lysine was not present at all, minor shares of trehalose were the only byproduct observed. The selective formation of the target product appeared highly beneficial toward straightforward, simplified downstream purification.

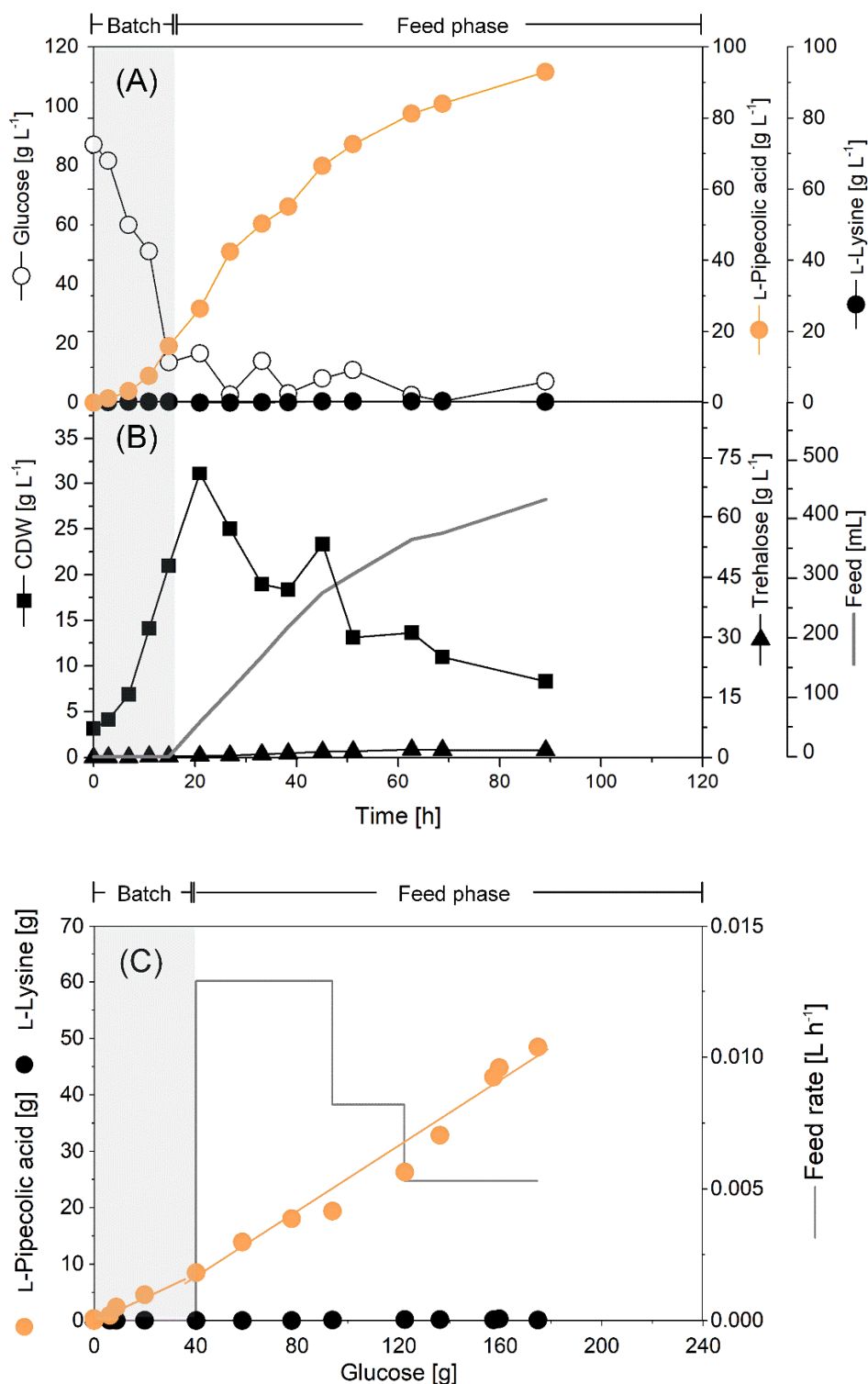


Fig. 32: Fed-batch production of L-pipecolic acid by metabolically engineered *C. glutamicum* PIA-10B. After depletion of the initial sugar at the end of the batch phase, pulses of feed were added automatically, using an increase in the level of dissolved oxygen (DO) above 50 % as a trigger (A). The batch and feed phases are denoted by dotted lines in the culture profile. The batch medium contained glucose (85 g L^{-1}) and yeast extract (15 g L^{-1}) as carbon sources. The feed contained six-fold more glucose (500 g L^{-1}), while the yeast extract level (15 g L^{-1}) remained the same. The process was operated at 30 °C during the batch phase and shifted to 34 °C at the beginning of the feed phase. Yield and selectivity of the L-pipecolic acid production improved during fermentation, which was linked to the modulated temperature and the limited availability of glucose during the feed phase (B). The volumetric productivity was 0.68 $\text{g L}^{-1} \text{h}^{-1}$ during the batch phase and 1.22 $\text{g L}^{-1} \text{h}^{-1}$ during the feed phase. The average volumetric productivity over the entire process was 1.08 $\text{g L}^{-1} \text{h}^{-1}$. The key performance indicators of the production process are summarized in Fig. 33. The process was conducted as duplicate. The deviation between duplicates was in the range of 5 %.

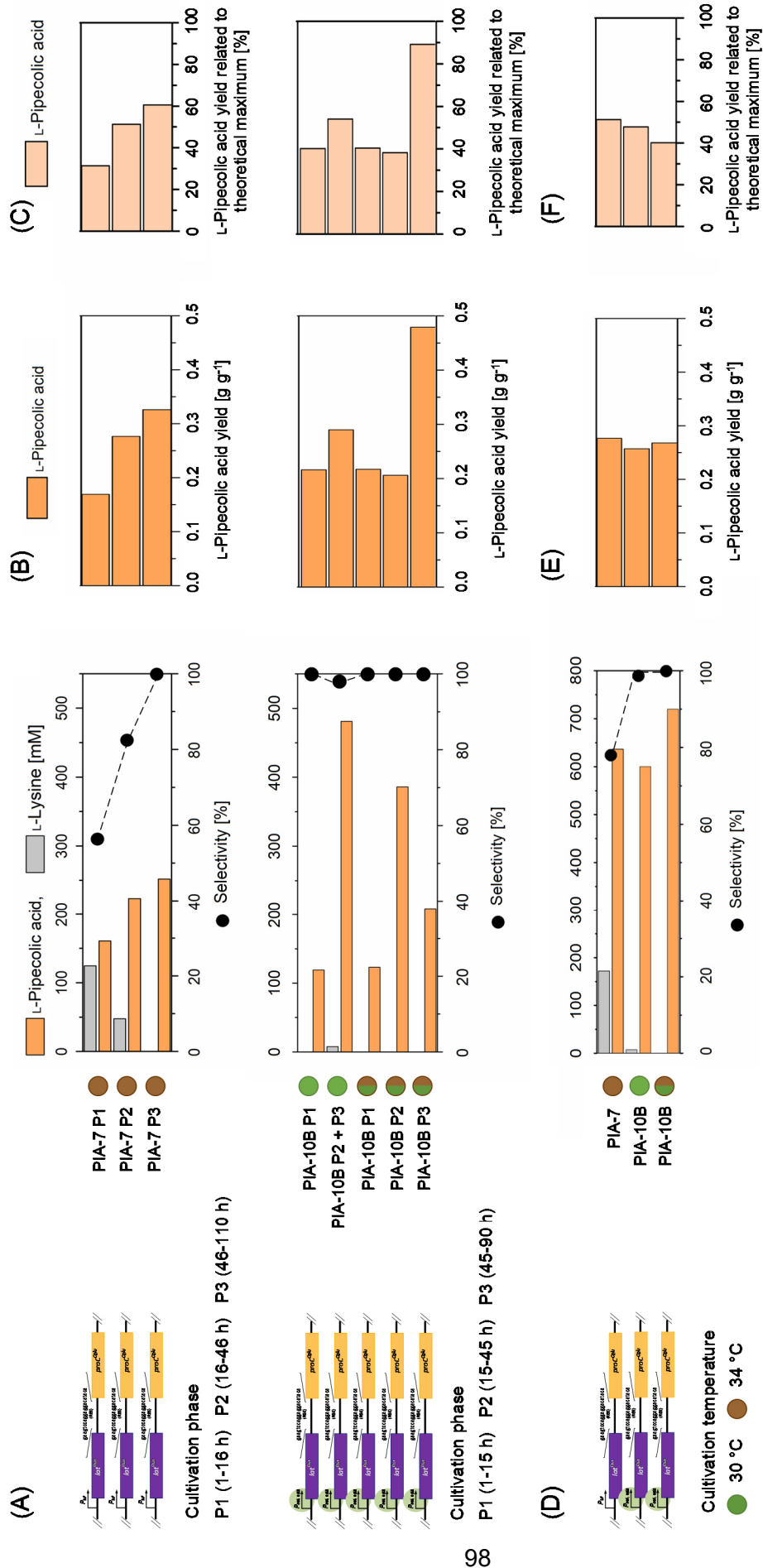


Fig. 33: Performance of the novel L-pipecolic acid production processes using *C. glutamicum*. The corresponding data are shown for the advanced producers C. *glutamicum* PIA-7 and PIA-10B, which were benchmarked in glucose-based fed-batch processes. Hereby, the data reflect the values from different process stages (A) and the average values from the entire processes (D). In addition, the total L-pipecolic acid yield (B, E) and the relative yield related to the theoretical maximum (C, F) for the different strains is given. The genetic background of all overproducers can be taken from Table 2. The processes were performed in duplicates, standard deviation was estimated 5 %.

The PIA-10B strain also performed very well at constantly 30 °C, although it did not fully achieve the same performance (Fig. S10). The final L-pipecolic acid titer (82 g L^{-1} , 635 mM) and the volumetric productivity was slightly lower under these conditions. However, the production was again highly selective (no L-lysine detected) (Fig. 33).

5 Conclusion and Outlook

The escalating scarcity and pricing volatility of fossil raw materials due to their environmentally damaging extraction and processing practices necessitate the exploration of alternative solutions (Kohlstedt et al, 2022; Becker et al, 2013a). Over the past few decades, the field of systems metabolic engineering has paved the way for the establishment of cell factory-based bioprocesses with significant industrial implications. These processes have not only managed to decrease the carbon footprint but have also lessened the overall impact on the environment (Becker et al, 2018b; Nielsen et al, 2019; Rohles et al, 2018). One noteworthy triumph in modern biotechnology lies in the realm of valuable molecule production through metabolically engineered *C. glutamicum* (Wittmann & Becker, 2007).

Amidst a wide array of natural and non-natural products, the synthesis of the essential amino acid L-lysine remains a pivotal biotechnologically provided compound (Eggeling & Bott, 2015; Wittmann & Becker, 2007). Remarkably, even after more than a decade, the strain *C. glutamicum* LYS-12 continues to stand as a premier producer, making it an exceptional chassis for the ongoing synthesis of L-lysine derivatives (Becker et al, 2011; Becker et al, 2018b; Kind et al, 2010; Rohles et al, 2016; Rohles et al, 2018).

In recent developments, *C. glutamicum* LYS-12 underwent metabolic engineering at various levels, encompassing precursor supply, biosynthesis, export, and the mitigation of undesired re-uptake. This comprehensive approach aimed at achieving the selective high-level production of 5-aminovalerate (Rohles, 2021). Intriguingly, monitoring intracellular metabolite concentrations revealed elevated product levels, indicating a deficiency in export mechanisms (Rohles, 2021). While one genomic copy of a heterologous exporter proved beneficial for the strain's performance, the expression of two copies appeared overly potent, potentially compromising cell viability (Wehrmann et al, 1998; Kind et al, 2011). In the context of *C. glutamicum* AVA-8, the additional transporter expression demonstrated a rather detrimental impact. This juncture suggests that the deployment of

other heterologous transporters, such as the GABA permeases from *Mycobacterium smegmatis* (Pavicet al, 2021) and *Escherichia coli* (Niegemann et al, 1993), could yield advantages over the use of two copies of the exporter from *P. putida*. Additionally, codon-optimization, contrary to the findings for the *davBA* operon (Pauli, 2018), could serve as a valuable tool to enhance transporter expression. Moreover, the existence of endogenous export mechanisms within *C. glutamicum* remains a puzzle, as comparisons with the heterologous GABA permease from *P. putida* only identified non-specific transporter candidates (Rohles, 2021). Thus, a broader exploration of export proteins from other organisms, like *Streptococcus* (Sakanaka et al, 2015), which handle structurally similar substrates such as N-acetyl-ornithine and L-ornithine (Wu et al, 2019b), could be a strategic approach.

Given the structural resemblance between γ -aminobutyrate and 5-aminovalerate, and the fact that the corynebacterial 4-aminobutyrate aminotransferase (*gabT*) accepts 5-aminovalerate as additional substrate (Rohles et al, 2016), the glutamate/ GABA antiporter *GadC* from *E. coli* emerges as another compelling candidate for exporter functionality (Ma et al, 2012). Lastly, the corynebacterial L-lysine translocator *LysE* stands out as a potential transporter candidate, demonstrated by its ability to accommodate the L-ornithine derivative L-citrulline as substrate (Lubitz et al, 2016; Perez-Garcia & Wendisch, 2018), which might facilitate the initial release of 5-aminovaleramide (Sommer, 2023).

However, based on current knowledge, the challenge of managing persistently high intracellular product concentrations necessitates alternative strategies. As demonstrated in earlier work, targeting the feedback inhibition of the key enzyme *DavB* presents an appealing avenue for optimization (Becker et al, 2005; Im et al, 2018). In this context, tracking the intracellular concentrations of the intermediate 5-aminovaleramide proves crucial, as it is anticipated to influence enzyme activity (Pauli, 2018; Vandecasteele & Hermann, 1972). Moreover, enzyme engineering at the level of the counteracting enzyme *ArgD* could potentially reduce its affinity for the non-native substrate

5-aminovalerate. Alternatively, attenuating the entire L-arginine/ornithine operon through overexpression of the native repressor ArgR (Yim et al, 2011; Wu et al, 2019b) might offer a route to achieve a glutarate-free culture supernatant without necessitating the deletion of *argD*.

In contrast to the fossil-based and low-yield chemical synthesis, which also entails intricate purification steps (Lemire & Charette, 2010), the biotechnological approach developed in this work, achieved remarkable L-pipecolic acid yields of up to 562 mmol mol⁻¹, accompanied by a notable 100 % product selectivity. Surpassing previous endeavors, the PIA-10B strain reached a milestone by attaining an impressive L-pipecolic acid titer of 93 g L⁻¹ within 90 hours of a fed-batch process, firmly advancing the goal of GRAS designated L-pipecolic acid production.

An all-encompassing scrutiny of the physiology of the newly developed L-pipecolic acid producing strains, including transcriptomics, metabolomics, and enzymatic analysis, revealed the intricate interplay of cellular components and conditions. The initially favored route involving L-Lysine 6-dehydrogenase, despite its theoretical appeal, proved to be incompatible with the intracellular milieu of the *C. glutamicum* host. Challenges arose, including inadequate redox availability for the key enzyme, feedback inhibition by L-pipecolic acid, and the influence of physiological parameters such as pH and temperature, collectively reducing enzyme activity to a mere 1 % of its theoretical capacity. While computational pH adaptation of LysDH did not yield improvements, a comprehensive resolution of the enzyme's crystal structure holds promise to address these bottlenecks. In a manner similar to GapN from *S. mutans* (Hoffmann et al, 2018), adjusting LysDH cofactor affinity to NADP⁺ may provide a solution, potentially creating a cyclic redox recovery system (Gatto et al, 2006) to circumvent the inhibitory effects of NADH. Modulation of L-pipecolic acid binding sites, akin to the strategy employed for aspartokinase (Becker et al, 2005), could also alleviate feedback inhibition.

Interestingly, an initially overlooked avenue was the synthesis of L-pipecolic acid via L-Lysine 6-aminotransferase (Wang et al, 2021a). In the present study, this enzyme alternative led to a breakthrough. Unlike the previous setup where it was expressed in *E. coli* for the conversion of externally fed L-lysine (Fujii et al, 2002a), the enzyme was introduced into *C. glutamicum* for the *de novo* L-pipecolic acid production. *C. glutamicum* appeared to provide a conducive environment for the new enzyme. Elevated cultivation temperatures, up to 37 °C, exhibited positive effects on high-level production. Additionally, a stimulatory impact attributed to pyridoxal 5'-phosphate was observed. Instead of external supplementation, upregulation of the endogenous coenzyme pathway could prove advantageous (Jochmann et al, 2011). The co-expression of LysDH and LAT enzymes represents another promising optimization strategy, albeit less efficient than doubling the amount of LAT, to potentially compensate for cofactor utilization.

At the scale of bioreactor fermentation, *C. glutamicum* PIA-7 achieved a notable final L-pipecolic acid titer of 82 g L⁻¹ after 110 hours, with L-lysine secretion persisting for the initial 50 hours. Incorporating an inducible L-lysine re-import mechanism after several hours of fermentation presents an advantageous strategy. While the endogenous importer LysI mandates an alkaline pH and L-lysine auxotrophy (Broer & Krämer, 1990), the L-lysine importer (LysP) from *E. coli* emerges as a prime optimization target (Steffes et al, 1992; Fujii et al, 2002a; Li et al, 2016; Xiao et al, 2020). Notably, the deletion of *lysE* was ineffective in PIA-7. Thus, focusing on engineering at the level of the transcription regulator LysG could indirectly mitigate L-lysine secretion (Bellmann et al, 2001).

However, precise modulation of the *lat* expression through promoter replacement eventually yielded optimal selectivity. In the context of a fed-batch process, the most refined and definitive strain accomplished an impressive titer of 93 g L⁻¹ yielding 0.27 g g⁻¹. During a subsequent phase of the temperature-shifted process, *C. glutamicum* PIA-10B achieved a remarkable 90 % of the theoretical maximum, with a yield of 0.48 g g⁻¹. This observation is likely attributed to the fermentation temperature of 34 °C, which was

identified as pivotal determinant influencing the strain's performance. The implementation of adapted feeding strategies holds promise for potentially yielding even higher outputs, particularly in the context of prolonged fermentation processes. Elevating the fermentation temperature further, to 37°C or even 40 °C during the feed-phase could conceivably lead to heightened titers, as demonstrated with the extremolyte ectoine (Becker et al, 2013b). While not directly contributing to an elevation in product selectivity during the initial phase, the overexpression of *gapN* in *C. glutamicum* PIA-10B could potentially maximize L-lysine provisioning, particularly under elevated cultivation temperatures.

Beyond the adjustment of process parameters like temperature, several cellular-level targets could be addressed to enhance overall strain performance. Notably, the identification and potential modification of a product exporter presents a particularly intriguing avenue for optimization. Similar to molecules with structural resemblance such as L-proline and ectoine (Giesselmann, 2018; Zhang et al, 2017a), the transport mechanism for export remains unclear, as does the mechanism of action of extremolytes, which are anticipated to act intracellularly (Perez-Garcia & Wendisch, 2018; Perez-Garcia et al, 2019). Understanding these mechanisms would contribute significantly to this optimization endeavor.

For a comprehensive grasp of the physiological shifts occurring at temperatures above 30 °C, monitoring intracellular metabolite concentrations and aligning them with the current characteristics of key enzymes could prove beneficial. This approach could provide insights into the level of the cofactor α -ketoglutarate (Fujii et al, 2002b) and the potentially feedback inhibitory metabolite L-pipecolic acid, shedding light on the *in vivo* activity of LAT. Additionally, since the ProC enzyme typically participates in L-proline synthesis from L-glutamate (Ankri et al, 1996), monitoring metabolite levels could reveal changes in the second conversion step towards L-pipecolic acid. Eliminating interfering pathways, as demonstrated in 5-aminovalerate synthesis (Rohles, 2021), could also be of interest. Consider the acetylmethionine aminotransferase ArgD, which originally mediates L-ornithine

and L-arginine synthesis (Zhang et al, 2017a; Sakanyan et al, 1996), and is known to downregulate ProC activity in *E. coli* (Deutch et al, 1982). Consequently, attenuating *argD* might serve to increase Δ^1 -pyrroline 5-carboxylate reductase activity. Moreover, a strategy involving cyclodeaminase-coupled L-proline biosynthesis via L-ornithine emerges as a viable option (Jensen & Wendisch, 2013), potentially avoiding L-proline auxotrophy while simultaneously freeing ProC from the native substrate Δ^1 -pyrroline 5-carboxylate (Fujii et al, 2002b).

In a broader context, the novel production processes showcased a notable level of plasmid stability. Even though the L-pipecolic acid modules were expressed episomal, a continuous secretion of L-pipecolic acid was observed. Notably, the *C. glutamicum* strains PIA-7 and PIA-10B can effectively compete with other cell factories that genomically express their production modules (Rohles et al, 2018; Kind et al, 2014).

Furthermore, the fermentative broth derived from PIA-7 and PIA-10B delivers L-pipecolic acid in high degree of purity, serving as an ideal starting point for subsequent applications as a precursor. Similar to its counterpart L-proline, L-pipecolic acid can be directly purified from the culture broth. It is imperative to optimize downstream processes for efficiency and environmental compatibility while avoiding extraction techniques that might impede future pharmaceutical applications. Although the use of organic solvents raises environmental and human health concerns, chromatographic techniques (De Luca et al, 2021) such as ion-exchange resins and reversed phase chromatography combined with crystallization methods (Hanko & Rohrer, 2004; Klein & Hüttel, 2011), are predominantly favored for separating biopharmaceutical molecules from culture broth, largely supplanting alcohol-based extraction techniques (Bowden et al, 2018). Recently, liquid-phase adsorption has been expanded to selectively separate L-lysine using activated carbons as adsorbents, offering a cost-effective alternative to the conventional downstream processes for amino acid isolation from fermentative broth (Deischer et al, 2020). Further utilization of the culture broth for the direct production of more intricate molecules like rapamycin

(Gatto et al, 2006; Park et al, 2010) is also entirely feasible. Additionally, the transformation of L-pipecolic acid into hydroxylated formulations for the application in plants and other organisms presents an intriguing avenue (Klein & Hüttel, 2011; Luo et al, 2022).

The preceding fermentation processes undoubtedly mark a significant milestone towards achieving GRAS (Generally Recognized As Safe) designation for L-pipecolic acid production, with expansive future applications in the pharmaceutical and chemical markets, and beyond (Roura Padrosa et al, 2020; Becker & Wittmann, 2020a; Westman et al, 2019). Furthermore, the comparatively modest investment in terms of effort and cost for *de novo* synthesis renders this process compelling for potential large-scale industrial implementation (Becker et al, 2011; Buschke et al, 2011; Rohles et al, 2018), extending beyond simple biotransformation approaches (Han et al, 2020).

6 Appendix

6.1 Abbreviations and symbols

Abbreviations

1,3BPG	1,3-bisphosphoglycerate
¹³ C	Carbon-13
2D	Two-dimensional
2OG	2-Oxoglutarate
2PG	2-phosphoglycerate
3PG	3-phosphoglycerate
A	Adenine
<i>A. thaliana</i>	<i>Arabidopsis thaliana</i>
<i>A. tumefaciens</i> , Atum	<i>Agrobacterium tumefaciens</i>
AcCoA	Acetyl Coenzyme A
<i>aceE</i>	Gene, encoding pyruvate dehydrogenase E1
<i>acn</i>	Gene, encoding aconitase
Add.	Addendum
AKG	α -ketoglutarate
<i>alaT</i>	Gene, encoding alanine aminotransferase
ALD	Aminotransferase AGD2-like defense response protein
<i>amtR</i>	Gene, encoding nitrogen regulator
<i>amyA</i>	Gene, encoding α-amylase
<i>argD</i>	Gene, encoding acetylornithine aminotransferase
ArgD	Acetylornithine aminotransferase
ArgR	Repressor of L-arginine/ ornithine operon
Asa	Aspartate semialdehyde
Ascl	Restriction enzyme: <i>Arthrobacter</i> species
Aspp	Aspartyl phosphate
ATCC	American Type Culture Collection
ATP	Adenosine triphosphate
AVA	5-aminovalerate
<i>avtA</i>	Gene, encoding valine-pyruvate aminotransferase
<i>B. subtilis</i> , Bsub	<i>Bacillus subtilis</i>
<i>betP</i>	Gene, encoding glycine betaine transporter
BHI(S)	Brain heart infusion (sorbitol)

<i>bioA</i>	Gene, encoding adenosylmethionine-8-amino-7-oxononanoate aminotransferase
bioD	Gene, encoding ATP-dependen dethiobiotin synthetase
bp	Base pair
C	Cytosin
<i>C. glutamicum</i> , Cglu	<i>Corynebacterium glutamicum</i>
Cas	CRISPR-associated
<i>catA</i>	Gene, encoding catechol 1,2-dioxygenase
(c)DNA	(Complementary) desoxiribunucleic acid
CDW	Cell dry weight
CICC	China Center of Industrial Culture Collection
Cit	Citrate
CL	cytosol
<i>cm^R</i>	Chloramphenicol resistance
CoA	Coenzyme A
Cpf1	CRISPR-associated endonuclease in <i>Prevotella</i> and <i>Francisella</i> 1
CRISPR	Clustered regularly interspaced short palindromic repeats
<i>crtB</i>	Gene, encoding phytoene synthase
<i>crtI2</i>	Gene, encoding phytoene desaturase
Cy3	Cyanine Dye 3
<i>dapB</i>	Gene, encoding 4-hydroxy-tetrahydrodipicolinate reductase
<i>dapD</i>	Gene, encoding tetrahydrodipicolinate succinylase
<i>davA</i>	Gene, encoding 5-aminovaleramide amidase
DavA	5-aminovaleramide amidase
<i>davB</i>	Gene, encoding L-lysine 2-monooxygenase
DavB	L-lysine 2-monooxygenase
<i>davBA</i>	Gene operon encoding L-lysine 2-monooxygenase and 5-aminovaleramide amidase
DavD	Glutarate semialdehyde dehydrogenase
DavT	5-aminovalerate transaminase
<i>ddh</i>	Gene, encoding meso-diaminopimelate dehydrogenase
DHAP	Dihydroxyacetone phosphate
DHB	3,4-Dihydroxybenzoic acid
dNTP	Desoxynucleosid triphosphate
DMSO	Dimethyl sulfoxide

DO	Dissolved oxygen
DpkA	Δ^1 -pyrroline 2-carboxylate reductase
DSM(Z)	German Collection of Microorganisms and Cell Cultures
DTT	Dithiothreitol
e. g.	Exempli gratia
<i>E. coli</i> , Ecol	Escherichia coli
E4P	Erythrose 4-phosphate
EcDH DPR	Dihydrodipicolinate reductase from <i>E. coli</i>
EDTA	Ethylenediamine tetraacetic acid
EMP	Embden-Meyerhof-Parnas Pathway
ESI	Electrospray ionisation
ex	exported
<i>exeR</i>	Gene, encoding extracellular nuclease
<i>F. lutescens</i> , Flut	<i>Flavobacterium lutescens</i>
F1,6BP	Fructose 1,6 bisphosphate
F1P	Fructose 1-phosphate
F6P	Fructose 6-phosphate
FADH	Flavin adenine dinucleotide semiquinone
Fbp	Fructose 1,6-bisphosphatase
fbr	Feedback resistant
Fig.	Figure
Fmoc	fluorenylmethoxycarbonyl
Frc	Fructose
<i>ftn</i>	Gene, encoding Ferritin
Fum	Fumarate
G	Guanine
<i>G. stearothermophilus</i> ,	<i>Geobacillus stearothermophilus</i>
Gste	
G3P	Glyceraldehyde 3-phosphate
G6P	Glucose 6-phosphate
GABA	Gamma-aminobutyric acid
<i>gabD</i>	Gene, encoding glutarate semialdehyde dehydrogenase
<i>gabP</i> , PP2911	Gene, encoding GABA-permease-III
GabP-III	GABA-permease-III
<i>gabT</i>	Gene, encoding 5-aminovalerate transaminase
<i>gabTDP</i>	Gene, encoding GABA Operon
GadC	Glutamate/ GABA antiporter

<i>gapA</i>	Gene, encoding glyceraldehyde-3-phosphate dehydrogenase
<i>gapC</i>	Gene, encoding glyceraldehyde-3-phosphate dehydrogenase, cytosolic
<i>gapN</i>	Gene, encoding NAD(P)-dependent glyceraldehyde-3-phosphate-dehydrogenase
GC	Gas Chromatography
GELFrEE	Gel-eluted Liquid Fraction Entrapment Electrophoresis
GEO	Gene expression omnibus
<i>glaA</i>	Gene, encoding α -1,3-galactosidase A
GLC/ Gluc	Glucose
<i>glk</i>	Gene, encoding glucokinase
<i>gltA</i>	Gene, encoding citrate synthase
GLU	L-glutamate
Glx	Glyoxylate
GRAS	Generally regarded as safe
gRNA	guiding RNA
GTA	Glutarate
<i>hmuT</i>	Gene, encoding hemin-binding periplasmic protein
<i>hom</i>	Gene, encoding homoserine dehydrogenase
HPLC	High pressure liquid chromatography
i. e.	Id est
<i>icd</i>	Gene, encoding isocitrate dehydrogenase
Ici	Isocitrate
<i>ilvN</i>	Gene, encoding acetolactate synthase isozyme
IM	inner membrane
<i>ioiT</i>	Gene, encoding myo-inositol transporter
<i>kan^R</i> , Kan	Kanamycine resistance
kDA	Kilo Dalton
KEGG	Kyoto Encyclopedia of Genes and Genomes
<i>KpnI</i>	Restriction enzyme from <i>Klebsiella pneumoniae</i>
L-2,3-Dhd	L-2,3 dihydrodipicolinate
L-Asp	L-Aspartate
LAT	Protein: L-lysine 6-aminotransferase
LC	Liquid chromatography
LdcC	Protein: L-lysine decarboxylase
<i>ldhA</i>	Gene, encoding L-Lactate dehydrogenase A chain

<i>leuD</i>	Gene, encoding 3-isopropylmalate dehydratase
L-Lys	L-Lysine
<i>Irp1B</i>	Gene, encoding low-density lipoprotein receptor-related protein
LYS	L-Lysine
<i>lysA</i>	Gene, encoding meso-diaminopimelate decarboxylase
<i>lysC</i>	Gene, encoding aspartokinase
<i>lysDH</i>	Gene, encoding L-lysine 6-dehydrogenase
LysDH	L-lysine 6-dehydrogenase
<i>lysE</i>	Gene, encoding L-lysine translocator
LysG	Transcription regulator of <i>lysE</i>
LysP	L-lysine importer
L- Δ^1 -Tdhhd	L- Δ^1 -Tetrahydrodipicolinate
<i>mak</i>	Gene, encoding maltokinase
Mal	Malate
MALDI-TOF	Matrix-assisted laser desorption/ ionization- time-of-flight mass spectrometry
MCS	Multiple cloning site
<i>mdh</i>	Gene, encoding malate dehydrogenase
meso-Dap	meso-Diaminopimelate
<i>mgo</i>	Gene, encoding malate:quinone oxidoreductase
mRNA	Messenger ribonucleic acid
MS	Mass spectrometry
MSD	Mass spectrometry detector
<i>msmA</i>	Gene, encoding putative methylmalonate-semialdehyde dehydrogenase
<i>mtlR</i>	Gene, encoding DeoR-type repressor
<i>mtrA</i>	Gene, encoding DNA-binding response regulator
<i>murE</i>	Gene, encoding UDP-N-acetylmuramoyl-L-alanyl-D-glutamate-2,6-diaminopimelate ligase
n.d.	Not detected
<i>narI</i>	Gene, encoding respiratory nitrate reductase subunit gamma
NAD(H)	Nicotinamide adenine dinucleotide
NADP(H)	Nicotinamide adenine dinucleotide phosphate
<i>narG</i>	Gene, encoding nitrate reductase
<i>narJ</i>	Gene, encoding nitrate reductase delta subunit

<i>NdeI</i>	Restriction enzyme from <i>Neisseria denitrificans</i>
<i>ndh</i>	Gene, encoding NADH dehydrogenase
NMR	Nuclear magnetic resonance
Oaa	Oxaloacetate
OD	Optical density
<i>odx</i>	Gene, encoding oxaloacetate decarboxylase
<i>opcA</i>	Gene, encoding glucose 6-phosphate dehydrogenase
opt	(Codon-)optimized
ORI	Origin of replication
P	promotor
p	plasmid
<i>P. putida</i> , Pput	<i>Pseudomonas putida</i>
P2C	1-piperideine 2-carboxylic acid
P5P	Pentose 5-phosphate
P6C	1-piperideine 6-carboxylic acid
PA	Polyamide
PaASPDH	aspartate dehydrogenase from <i>Pseudomonas aeruginosa</i>
PAGE	Polyacrylamide gel electrophoresis
PatA	Protein: cadaverine transaminase
PatD	Protein: 4-aminobuyraldehyde dehydrogenase
PCA	Principal component analysis
<i>pck</i>	Gene, encoding phosphoenolpyruvate carboxykinase
PCR	Polymerase chain reaction
PEG	Polyethyleglucol
PEP	Phosphoenolpyruvate
<i>pgk</i>	Gene, encoding phosphoglycerate kinase
<i>pgl</i>	Gene, encoding 6-phosphogluconolactonase
pH	Power/ potential of hydrogen
PIA	L-pipecolic acid
<i>pipA</i>	Gene, encoding L-lysine cyclodeaminase
PM	periplasm
PMF	Peptide mass fingerprint
<i>pntAB</i>	Gene, encoding membrane-integral nicotinamide nucleotide transhydrogenase
PP	Pyridoxal 5'phosphate
<i>ppc</i>	Gene, encoding phosphoenolpyruvate carboxylase
<i>ppgK</i>	Gene, encoding polyphosphate glucokinase

<i>proC</i>	Δ^1 -pyrroline 5-carboxylate reductase
ProC	Protein: Δ^1 -pyrroline 5-carboxylate reductase
<i>proH</i>	Δ^1 -pyrroline 5-carboxylate reductase
ProH	Protein: Δ^1 -pyrroline 5-carboxylate reductase
<i>proP</i>	Gene, encoding ectoine/ proline transporter
ProP	Protein: Ectoine/ proline transporter
<i>prpB2</i>	Gene, encoding probale 2-methylisocitrate lysase 1
<i>P_{tac}</i>	Hybrid promotor combining promoter from tryptophane and lactose operon
<i>P_{trc}</i>	Optimization of <i>P_{tac}</i>
<i>pTS</i>	Phosphotransferase system
<i>ptsF</i>	Gene, encoding fructose-specific transporter subunit II
<i>ptxDPst</i>	Gene, encoding phosphite oxidoreductase
<i>ptsG</i>	Gene encoding glucose transporter
<i>pycA</i>	Gene, encoding pyruvate carboxylase
Pyr	Pyruvate
(q)PCR	(quantitative) Polymerase chain reaction
<i>R. pomeryoi</i> , Rpom	<i>Ruegeria pomeroiy</i>
<i>rAIP</i>	Gene, encoding apoptosis-inducing protein
<i>rapL</i>	Gene, encoding L-lysine cyclodeaminase
RBS	Ribosomal binding site
RID	Refractive index detector
RIN	RNA integrity number
<i>ripA</i>	Gene, encoding HTH-type transcriptional regulator
rRNA	(Ribosomal) ribonucleic acid
<i>S. hygrosopicus</i> , Shyg	<i>Streptomyces hygrosopicus</i>
<i>S. mutans</i> , Smut	<i>Streptococcus mutans</i>
S7P	Sedoheptulose 7-phosphate
<i>sacB</i>	Gene, encoding levansucrase from <i>B. subtilis</i>
SARD	Protein: Systemic acquired resistance- deficient
<i>scrK</i>	Gene, encoding fructokinase
<i>sdhA</i>	Gene encoding succinate-ubiquinone oxidoreductase
<i>sdhB</i>	Gene, encoding succinate dehydrogenase subunit B
<i>sdhC</i>	Gene, encoding succinate dehydrogenase subunit C
SDS	Sodium dodecyl sulfate
SFU	Specific fluorescence unit
<i>Smal</i>	Restriction enzyme from <i>Serratia marcescens</i>

<i>sod</i>	Gene, encoding superoxide dismutase
Suc	Succinate
Suc-CoA	Succinyl Coenzyme A
T	Thymine
TAE	Tris-acetate-EDTA
<i>tal</i>	Gene, encoding transaldolase
<i>taq</i>	DNA polymerase from <i>Thermus aquaticus</i>
TCA	Trichloroacetic acid cycle
<i>tet^R</i>	Tetracycline resistance
<i>tkt</i>	Gene, encoding transketolase
TmASADH	aspartate-semialdehyde dehydrogenase from <i>Tistrella mobilis</i>
<i>tuf</i>	Gene, encoding elongation factor <i>tu</i>
UTR	5'-untranslated regions
UV	ultraviolet
X	biomass
<i>Xba</i> I	Restriction enzyme from <i>Xanthomonas badrii</i>
<i>xy</i> IAB	Genes encoding xylose kinase
<i>zwf</i>	Gene, encoding glucose 6-phosphate dehydrogenase

Symbols

k_M	Michaelis Menten konstant	$[\mu\text{mol mol}^{-1}]$
μ	Specific growth rate	$[\text{h}^{-1}]$
p-value	Probabilitas value	$[\%]$
q-value	Minimum false discovery rate	$[\%]$
q_s	Specific substrate uptake rate	$[\text{mmol g}^{-1} \text{h}^{-1}]$
q_p	Specific production rate	$[\text{mmol g}^{-1} \text{h}^{-1}]$
rpm	Revolutions per minute	$[\text{min}^{-1}]$
T	Temperature	$[\text{°C}]$
t	Time	$[\text{h}]$
U	Unit	$[\mu\text{mol min}^{-1}]$
v_{max}	Maximal velocity	$[\text{mU mg}^{-1}]$
$Y_{P/S}$	Product yield	$[\text{mmol mol}^{-1}]$
$Y_{X/S}$	Biomass yield	$[\text{g mol}^{-1}]$
Δ	Delta, deletion	-

6.2 Molecular tools

PCR setup and primers

The reaction mixture and thermos cycler program used for PCR are listed in the tables below (Table S1, Table S2). Site-specific primers designed for fragment amplification and sequencing are listed in Table S3.

Table S1: Reaction mixture for PCR.

Component	[μ L]
Master mix Phusion/ Phire Green (2x)	25
DMSO	1.6
Primer sense [10 μ M]	1.25
Primer antisense [10 μ M]	1.25
Template plasmid DNA [5 - 500 ng]	3.75
Water	17.15
	50

Table S2: Thermo cycler program for PCR. Annealing temperature and elongation times were adjusted to primers and polymerase used. Denaturation, annealing, and elongation steps were repeated thirty times.

Step	Temperature [$^{\circ}$ C]	Time
Lid heating	98	automatically
Cell disruption	98	3 min OR 15 min (for colony PCR)
Denaturation	98	30 s
Annealing	depends on primers	30 s
Elongation	72	depends on fragment size/ polymerase
End elongation	72	5 min

} 30x

Table S3: Primers used in this work.

Primer	Sequence	Use	
pClik5a_seqF	GTGGCCGACAATCAATGAAGCTATG	Sequencing	
pClik5a_seqR	CCGGAGAACCTGCGTGCAATCCAT	<i>pClik5a</i>	
RB06_Seq_antisense	ATTGTCTGTTGTGCCAGTCATAG	Sequencing <i>pClik</i>	
SK_pClik_int_sacB sense	AATAATAGTGAACGGCAGGT	<i>int SacB</i>	
Pr_pClik_eftu_Sma_fwd	ATTGGGATCCTCTAGACCCTGGCCGT TACCCTGCGAATG	Amplification for episomal <i>lysDH</i> <i>proC</i> operon	
Pr_eftu_lysdh_rev	CGACACAAATGTTCCAGCGCATTGTAT GTCCTCCTGGACTTC		
Pr_lysdh_eftu_fwd	GAAGTCCAGGAGGACATAACAATGCGC TGGAACATTTGTGTCG		
Pr_lysdh_RBS_rev	TGTATGTCCTCCTGGACTTCTCAAGCG GCCTTGTTTTGGG		
Pr_RBS_proC_fwd	GAAGTCCAGGAGGACATAACAATGACA ACAATTGCTGTAATC		
Pr_proC_pClik_Sma_rev	CCGCTAGCGATTTAAATCCCCTAGCG CTTTCCGAGTTC		
PR_Peftu_pClik5aMCS	CCTGACGTCGGGCCCGGTACTGGCC GTTACCCTGCGAATG		
LysDH_I81K_fwd	GGCCGCCTTGGCGATCTTCGGAGTCA GAAAGA		Amplification for <i>lysDH</i> to introduce point mutations
LysDH_I81K_rev	TCTTTCTGACTCCGAAGATCGCCAAG GCGGCC		
LysDH_Q114D_fwd	GGCATGAAGGCGGTATCGCTGTCTTC GGCCA		
LysDH_Q114D_rev	TGGCCGAAGACAGCGATACCGCCTTC ATGCC		
LysDH_S228A_fwd	GGTACGAGACCGCGCGCCTTGCC		
LysDH_S228A_rev	GGCAAGGCGCGCGCGGTCTCGTACC		
LysDH_G286D_fwd	CGCAGCTGGCCATCGATCCGCCCTT		
LysDH_G286D_rev	AAGGGCGGATCGATGGCCAGCTGCG		
PR_Peftu_proC_rev	ATTACAGCAATTGTTGTCATTGTATGT CCTCCTGGACTTC	Amplification for second <i>proC</i> copy	
PR_Peftu_proC_fwd	GAAGTCCAGGAGGACATAACAATGACA ACAATTGCTGTAAT		
PR_proC_pClik5aMCS_rev	AACTAGTCATATGACGCGTGCTAGCG CTTTCCGAGTTCTT		

Continuation of table S3.

PR_RBS_proH_fwd	GAAGTCCAGGAGGACATACAATGCGA ACAAAAAAGCGAAC	Amplification for <i>proH</i>
PR_proH_rev	TAGCGGATCATTTAAATCCCTCACTTT ATCACTCCTGATAG	
PR1_TS1 BioA_nat_fwd	AATTGGGATCCTCTAGACCCGCTTGC GCGAGCTTGATCAC	Fragment amplification for integrative <i>lysDH</i> <i>proC</i> operon
PR2_TS1 BioA_nat_rev	CATTCGCAGGGTAACGGCCAGCGCAG GTACTCGGAAATCG	
PR3_BioA_Operon nat_fwd	CGATTTCCGAGTACCTGCGCTGGCCG TTACCCTGCGAATG	
PR4_BioA_Operon nat_rev	CAGTGGCAATTTTCATCGACGCTAGCG CTTTCCGAGTTCTTC	
PR5_TS2 BioA_nat_fwd	GAAGAACTCGGAAAGCGCTAGCGTCC ATGAAATTGCCACTG	
PR6_TS2 BioA_nat_rev	CCGCTAGCGATTTAAATCCCTTATTTC CCTTTAACTGCAGC	
Pr1_pClik5A_eftu_fwd	GACTAGTTTCGACCTAGGGATTGGCC GTTACCCTGCGAATG	Fragment amplification for <i>rapL</i>
Pr2_eftu_rapL_rev	CACAGAACCTTGGTCTGCATTGTATGT CCTCCTGGACTTC	
Pr3_eftu_rapL_fwd	GAAGTCCAGGAGGACATACAATGCAG ACCAAGGTTCTGTG	
Pr4_rapL_pClik5A_rev	GAAGAGCATCGATGTCGACGATCTAC AGCGAGTACGGATCGAGG	
ProC_rev_CM	CGGGGCTGATCCCCGGCCCCCTAGC GCTTTCGGAGTTC	Fragment amplification for chloramphenicol cassette
CM_fwd	TGGGATCCTCTAGACCCGGGGCCGG GGATCAGCCCCGGAT	
Cm_rev	ACCGGGCCGGCCGGCGCGCCTTACG CCCCGCCCTGCCACT	
ProP_del_up_fwd	AATTGGGATCCTCTAGACCCCAGACT GGTGGAGCCAAC	Fragment amplification for <i>proP</i> deletion
ProP_del_up_rev	GTCGATGACGTCAACGTTGCATATGC CGTTTCCTGATGAG	
ProP_del_down_fwd	CTCATCAGGAAACGGCATATGCAACG TTGACGTCATCGAC	
ProP_del_down_rev	TAGCGGATCATTTAAATCCCCGGATGA TTGAAGCGCTC	

Continuation of table S3.

SH53_PR_Fusion_eftu_pnta b_fw	GAAGTCCAGGAGGACATACAATGCGA ATTGGCATACCAAG	
SH54_PR_Fusion_eftu_pnta b_rev	CTTGGTATGCCAATTCGCATTGTATGT CCTCCTGGACTTC	
SH55_PR_Fusion_pClik_TS 1(crtB)	AATTGGGATCCTCTAGACCCGGTAGTA GGCGGTGTCACTG	
SH56_PR_Fusion_pntab_TS 2(crtB) fw	CAATCCTGAAAGCTCTGTAATGAAGGT CTCGACTAAAACCT	Fragment amplification for integrative <i>pntAB</i> construct
SH57_PR_Fusion_pntab_TS 2(crtB) rev	AGTTTTAGTCGAGACCTTCATTACAGA GCTTTCAGGATTG	
SH58_PR_Fusion_TS1(crtB) _eftu fw	TACCAGAAGCAGCCTCAGCTTGGCCG TTACCCTGCGAATG	
SH59_PR_Fusion_TS1(crtB) _eftu rev	CATTCGCAGGGTAACGGCCAAGCTGA GGCTGCTTCTGGTA	
SH60_PR_Fusion_TS2(crtB) _pClik rev	CCGCTAGCGATTTAAATCCCTTAGGAT CTGGCGCAACACC	
Delta lysE up_fwd	ACTAGTTCGGACCTAGGGATATCGTTG GGTGGAGGAACCG	
Delta lysE up_rev	CTTTTACTGTCCATCGGACCGTCCAGC CCCAAGGTGTGGC	Fragment amplification for <i>lysE</i> deletion
Delta lysE down_fwd	GCCACACCTTGGGGCTGGACGGTCCG ATGGACAGTAAAAG	
Delta lysE down_rev	AGAGCATCGATGTTCGACGATACGCCG CAGCAAGGATAATG	
PRmCherry_1	GGGCCCGGTACCACGCGTCACATATG GTGAGCAAGGGCGAGGA	Fragment amplification for <i>mCherry</i>
PRmCherry_2	CTAGGTCCGAAGTACTAGTCATATTA TACAGCTCGTCCA	
PRSOD_FOR	TAGTGCCAATTATTCCGGG	
PRSOD_REV	GGGTAAAAAATCCTTTCGTA	Fragment amplification for promotor <i>sod</i>
PRSOD_mCherry_FOR	GCCCGGTACCACGCGTCACATATAGC TGCCAATTATTCCGGG	
PRSOD_mCherry_REV	TCCTCGCCCTTGCTCACCATGGGTAAA AAATCCTTTCGTA	
PRTUF_mCherry_FOR	GCCCGGTACCACGCGTCACATGGCCG TTACCCTGCGAATG	Fragment amplification for promotor <i>tuf</i>
PRTUF_mCherry_REV	TCCTCGCCCTTGCTCACCATATGTATG TCCTCCTGGACTTC	

Continuation of table S3.

PR1_PSOD_lat_FOR	AATTGGGATCCTCTAGACCCTAGCTGC CAATTATTCCGGG	Fragment amplification for promoter exchange
PR2_PSOD_lat_REV	GCGGGGCAAGAAGGGACATGGGTAAA AAATCCTTTTCGTA	
PR3_PSOD_lat_FOR	CTACGAAAGGATTTTTTACCCATGTCC CTTCTTGCCCCGCT	
PR3_PSOD_lat_REV	TAGCGGATCATTAAATCCCCTAGCGC TTTCCGAGTTC	
PR5_PP2911_fwd	AATTGGGATCCTCTAGACCCGCACTG ACAGCGGTGATTGG	Fragment amplification for integration of the second copy of <i>gabP</i> -III, replacing <i>crtI2</i>
PR6_PP2911_rev	CATTCGCAGGGTAACGGCCAATTTTGA TCCCTATCATCGA	
Cglu_PR196	TGGCCGTTACCCTGCGAATGTCC	
PR7_PP2911_rev	TCTACAGAAAGAATTCGTGATCAGGCG CCCTGCCCTACGC	
PR8_PP2911_fwd	GCGTAGGGCAGGGCGCCTGATCACG AATTCTTTCTGTAGA	
PR9_PP2911_rev	TAGCGGATCATTAAATCCCCAAGAGC ATGTAATAGCCTTC	

Gibson assembly enzyme master mix

Table S4: Composition of Gibson assembly enzyme master mix. dGTP = deoxyguanosine triphosphate; dCTP = deoxycytidine triphosphate; dATP = deoxyadenosine triphosphate; dTTP = deoxythymidine triphosphate; DTT = dithiothreitol; PEG = polyethylene glycol.

Enzyme master mix	1.2 mL
5x Gibson assembly buffer	320 μ L
T5 exonuclease [10 U μ L ⁻¹]	0.64 μ L
Phusion DNA polymerase [2 U μ L ⁻¹]	20 μ L
Taq DNA ligase [40 U μ L ⁻¹]	160 μ L
Water	Add. 1.2 mL

5x Gibson assembly buffer	6000 μL
Tris-HCl pH 7.5 [1 M]	3 mL
MgCl ₂ [1 M]	300 μ L
dGTP [100 mM]	60 μ L
dCTP [100 mM]	60 μ L
dATP [100 mM]	60 μ L
dTTP [100 mM]	60 μ L
DTT [1 M]	300 μ L
PEG-8000	1.5 g
NAD	20 mg
Water	Add. 6 mL

6.3 Supplementary data

Validation of PIA production via GC/MS

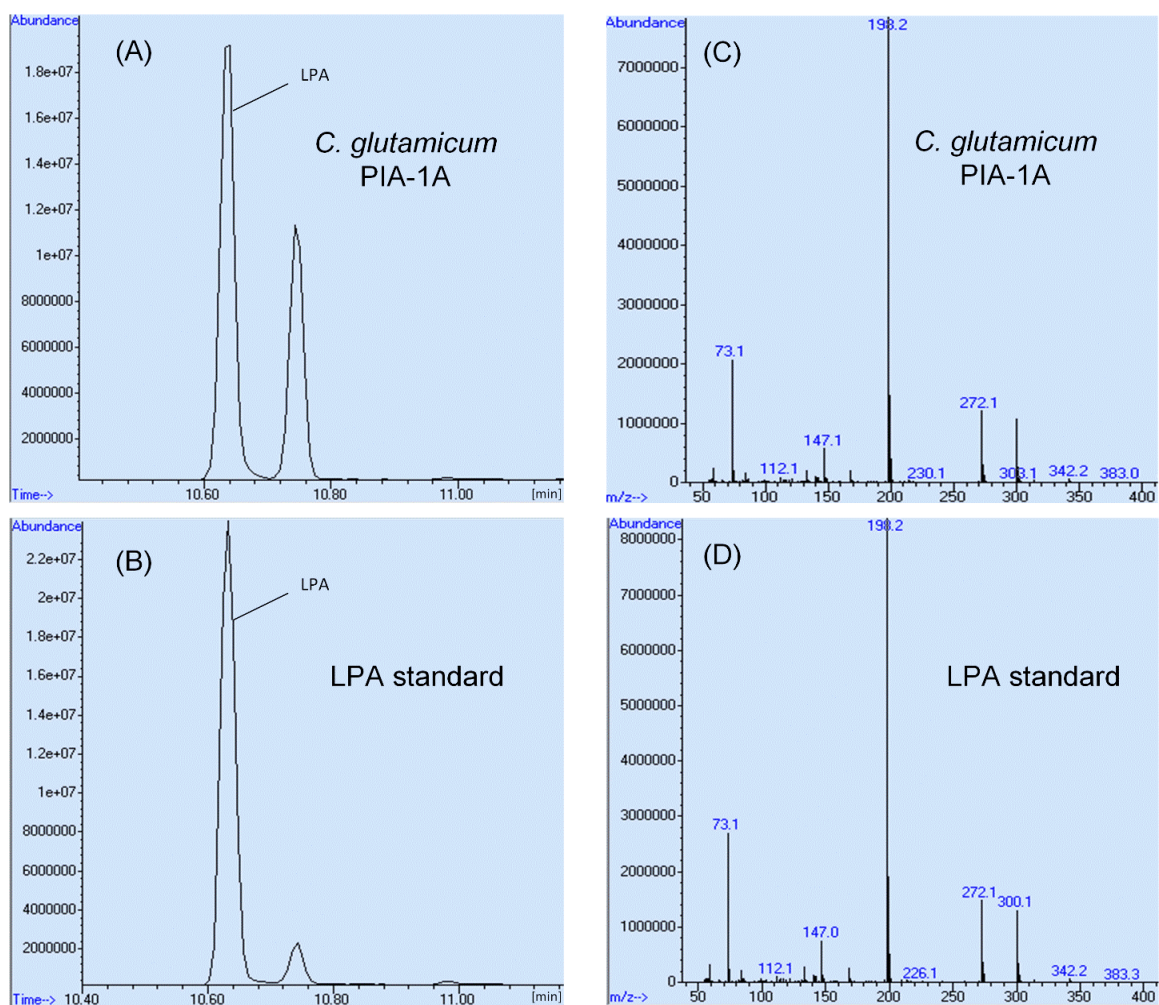


Fig. S1: Validation of L-pipecolic acid (PIA) production in *C. glutamicum* using GC/MS analysis of the TBDMS-derivative. The data comprise the total ion chromatograms of culture supernatant from *C. glutamicum* PIA-1A (A) and a pure L-pipecolic acid standard (B), as well as the corresponding mass spectra (C, D).

Principal component analysis of gene expression data sets

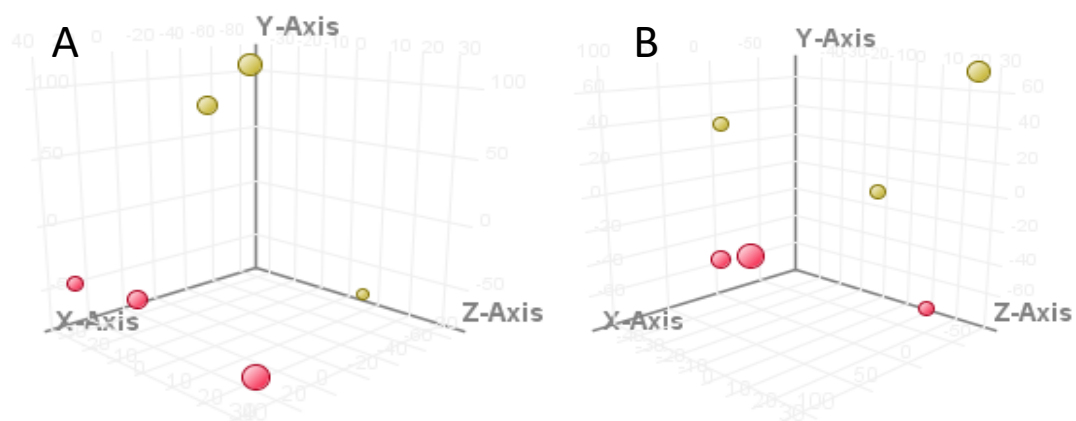


Fig. S2: Principal component analysis of the gene expression data sets of L-pipecolic acid producing and non-producing *C. glutamicum* strains. *C. glutamicum* PIA-1A and PIA-0 (A), *C. glutamicum* PIA-7 and PIA-0 (B).

Codon-optimization of the *lysDH* and *proC* genes

lysDH native	1	ATGCGCTGGAACATTTGTGTCGT	CGGGGCCGGGAAGATCGGTCAGATGAT	50
lysDH opt	1	ATGCGCTGGAACATCTGCGTCGT	TGGTGC TGGTAAGATCGGTCAGATGAT	50
lysDH native	51	CGCCGCTTTGCTCAAGACTTTCATCCA	ACTACTC GGT CACCGTGGCCGATC	100
lysDH opt	51	TGCAGCGCTGTGAAAACCTCCTCCA	ACTACTC CGT GACCGT TGCAGACC	100
lysDH native	101	ACGATCTGGCCGCGCTGGCGGTGCTGAA	CCGGATGGGTGTTGCCACCAAG	150
lysDH opt	101	ACGATCTGGCGGCCCTCGCAGT	GCTGAATCGCATGGGC GTT GCCACCAAG	150
lysDH native	151	CAGGTGGATGCCAAGGACGAAGCCGG	GTTGGCCAAAGGCGCTGGCCGGGTT	200
lysDH opt	151	CAAGTGGATGCAAAGGATGAGGCCAG	CCCTCGCCAAAGCACTCGGTGGCTT	200
lysDH native	201	CGATGCGGTGATTTGCGCGCGCC	TTCTTTCTGACTCCGATCATCGCCA	250
lysDH opt	201	CGATGCGGTCACTCAGCAGCCCA	TTCTTCTGACTCCGATTATCGCTA	250
lysDH native	251	AGGCGGCCAAGGCCGCGGGCGCC	CACTATTTTGACCTGACCGAGGATGTG	300
lysDH opt	251	AAGCTGCGAAAGCAGCAGGTGCT	CACTACTTCGACCTTACCGAGGATGTA	300
lysDH native	301	GCCGCCACAATGCGGTGCGCGCACT	TGGCCGAAGACAGCCAGACC	350
lysDH opt	301	GCAAGCCACGAATGCGGTT	CGTGCATTGGCTGAGGACTCTCAGACTGCCTT	350
lysDH native	351	CATGCCGCAATGCGGTTTGGCACCG	GGCTTTGTGGTATCGCAGGGGCCGG	400
lysDH opt	351	TATGCCCCAATGTGGTCTGGCCCA	AGGCTTTGTGGCATCGCTGGTGTG	400
lysDH native	401	CGCTGGCGGGCTGAGTTGACGAGAT	CGACAGCCTGCATATGCGGGTGGGG	450
lysDH opt	401	CACTGGCTGCGGAGTTGACGAA	AATCGACTCGTTGCACATGCGGGT TGG A	450
lysDH native	451	GCGCTGCCGCTCTATCCGACCAAT	GCGCTGAAATACAACCTGACCTGGTC	500
lysDH opt	451	GCACTTCCGTTGTACCCAACTA	AATGCGCTGAAGTACAACCTGACCTGGTC	500
lysDH native	501	CACCGACGGGCTGATCAACGAGTAT	TGCAACCCCTGCGACGCCATCGTGA	550
lysDH opt	501	AACAGACGGCCTGATCAACGA	ATACTGCAACCCCTGTGACGCCGATCGTGA	550
lysDH native	551	ATGGAGAGCGGGTCAAGACCGCGCC	GCTGGAGGATTACGAGATCCTCGGC	600
lysDH opt	551	ATGGCGAACGCGTCAAGACCGCC	CTCTTGAGGACTACGAATCCTGGGA	600

Fig. S3: Sequence alignment of the native and codon-optimized *lysDH* genes. The nucleotide substitutions are highlighted in red. The codon-optimized sequence was provided by Eurofins. opt = codon-optimized.

Continuation of fig. S3

lysDH native	601	CATGACGGGGTTGAATACGAATGCTTCAACACCTCGGGCGG-GTTGGGCA	649
lysDH opt	601	CATGATGGGGTCGAGTATGAGTGCCTTCAACACCTCTGGAGGTCTTGGG-A	649
lysDH native	650	CGCTGCCCGAGACGCTGGATGGCAAGGCGCGCTCGGTCTCGTACCGCTCG	699
lysDH opt	650	CGCTTCCGGAAACCCTGGATGGCAAGGCTCGCTCCGTCTCTACCGCTCC	699
lysDH native	700	ATCCGCTATCCGGGGCACCGCGATATCCTGCGCCTGCTGCTGAACGATCT	749
lysDH opt	700	ATTTCGCTATCCTGGACATCGCGACATTTCTCCGCCTCCTTCTCAACGACCT	749
lysDH native	750	GGGGCTGGAGCGTCGCCGCGACCTGCTCAAGGACATTTTCGAAACTGCGC	799
lysDH opt	750	CGGTCTTGAACGTCGTCGGATCTGCTGAAAGATATCTTCGAAACCCTGTT	799
lysDH native	800	TGCCGCGCACCGATCAGGACGTGGTGCTGGTCTATTGCACCGCCAAAGGG	849
lysDH opt	800	TGCCACGTACCGACCAGGATGTGGTACTCGTCTACTGCACCGCCGAAAGGC	849
lysDH native	850	CGGATCGGTGGCCAGCTGCGTGAAAAGAGCCTGATCAACAAGTCTATTTC	899
lysDH opt	850	CGGATTGGAGGGCAACTGCGCGAAAAGAGCCTGATCAACAAGTCTGTATAG	899
lysDH native	900	CCGCGTCATCGACGGCCAGGCTGGAGCGCGATCCAGGTCACCACCGCCG	949
lysDH opt	900	CCGTGTGATCGATGGCCAGGTTTGGTCTGCCATTACAGGTAACCACAGCTG	949
lysDH native	950	CCGGTGTGCTGGGCGTGGTTCGACCTGATGCGTGCCGGAACGCTGCCCGCC	999
lysDH opt	950	CCGGAGTCTTGGGCGTGTGGATCTCATGCGAGCTGGCACTCTGCCTGCA	999
lysDH native	1000	AAGGGGTTTGTTCGGCAAGAGCAGGTCAGTTTCGCGGATTTCTCGAAAC	1049
lysDH opt	1000	AAGGGCTTTGTGCGTCAGGAACAGGTTGAAGTTTCGCGGATTTCTTGAGAC	1049
lysDH native	1050	CGAATTCGGCCGCTTTATCGGGCGGGCGATCTGACCGCCCAAACAAGG	1099
lysDH opt	1050	GGAGTTTGGCGCTTGTATCGAGCAGGTGACCTTACTGCTCAGAACAAAGG	1099
lysDH native	1100	CCGCTTGA	1107
lysDH opt	1100	CTGCGTAA	1107

Fig. S3: Sequence alignment of the native and codon-optimized *lysDH* genes. The nucleotide substitutions are highlighted in red. The codon-optimized sequence was provided by Eurofins. opt = codon-optimized.

proC native	1	ATGACAAACAATTGCTGTAATCGGCGGGCGGACAAATCGGCGAGGCTTTAGT	50
proC opt	1	ATGACCACCATTGCGGTGATTGGTGGTGGCCAGATTGGGGAAGCACTGGT	50
proC native	51	CTCAGGTTTGATCGCGGCCAACATGAATCCACAAAATATTCGCGTCACCA	100
proC opt	51	ATCTGGTCTGATTGCGGCCAACATGAACCCTCAGAAACATCCGTGTGACCA	100
proC native	101	ACCGTTCGGAAGAGCGCGGCCAAGAGCTGCGTGACCGCTACGGCATCCTC	150
proC opt	101	ATCGCTCCGAAGAACGTGGTCAAGAGCTGCGCGATCGCTATGGCATCCTG	150
proC native	151	AACATGACGGATAATTCCCAAGCCGCGAGACGAAGCCGACGTGGTGTTCCT	200
proC opt	151	AATATGACGGACAACCTCCCAAGCTGCGGATGAAGCGGATGTCTGTGTTTCT	200
proC native	201	GTGCGTGAAGCCGAAATTTATCGTCGAAGTGCTCTCCGAAATCACCGGCA	250
proC opt	201	CTGCGTAAAGCCCAAGTTCATCGTCGAGGTCCTGTCCGAGATCACCGGAA	250
proC native	251	CTTTGGATAACAACCTCCGCACAAAGT-----GTTGTGGTTCAGCATGGCCG	295
proC opt	251	CCTTGGACAACAACCTCCGCAC--AGTCCGTCTGTTGT-GTC--CATGGCGG	295
proC native	296	CAGGCATCAGCATCGCTGCCATGGAAGAAAGCGCCTCTGCGGGGCTCCCC	345
proC opt	296	CGGGCATCTCAATCGCAGCTATGGAGGAAAGCGCATCAGCAGGACTTCCC	345
proC native	346	GTCTGTCGCGTCAATGCCGAACACTCCAATGCTCGTGGGCAAGGGCATGTC	395
proC opt	346	GTTGTTCGGGTGATGCCGAATACCCCGATGCTGGTGGGAAAGGCATGTC	395
proC native	396	GACTGTCACCAAAGGCCGCTACGTTGACGCGGAAACAGTTGGAACAAGTCA	445
proC opt	396	CACAGTCACGAAAGGCCGCTACGTAGACGCTGAACAGCTCGAACAGGTGA	445
proC native	446	AGGACTTGTGAGCACCGTTGGAGACGTCCTCGAAGTCGCGGAATCAGAC	495
proC opt	446	AGGATCTCTCAGCACAGTGGGTGACGTCCTGGAGGTTGCTGAGTCGGAC	495
proC native	496	ATCGACGCGAGTCACCGCGATGTCCGGATCCTCCCTGCATACCTGTTTCT	545
proC opt	496	ATCGATGCCGTTACTGCCATGAGCGGATCGTCTCCAGCATACCTGTTTCT	545
proC native	546	TGTGACCGAAGCGCTCATTGAGGCGAGGTTAATCTAGGCCTGCCCCGCG	595
proC opt	546	CGTGACCGAAGCGTTGATCGAAGCAGGCGTGAACCTGGGACTTCCACGGG	595

Fig. S4: Sequence alignment of the native and codon-optimized *proC* genes. The nucleotide substitutions are highlighted in red. The codon-optimized sequence was provided by Eurofins. The shifts that occur can be attributed to the format of the local alignment (Smith-Waterman), but do not affect the resulting amino acid sequence. opt = codon-optimized.

Continuation of fig. S4

proC native	596	CGACCGCTAAAAGCTCGCTGTGGCCTCATTTCGAAGGTGCTGCAACCATG	645
proC opt	596	CAACTGCCAAGAAGCTTGCCTCGCTTCGTTTCGAAGGTGCTGCTACCATG	645
proC native	646	ATGAAGGAAACCGGCAAAGAACCTCAGAATTGCGCGCAGGCGTTTCCTC	695
proC opt	646	ATGAAGGAGACTGGCAAAGAGCCTTCTGAATTGCGAGCTGGGCGTTTCCTC	695
proC native	696	ACCCGCGAGGCACCACCGTCGCAGCCATCCGAGAACTCGAAGAAAGCGGAA	745
proC opt	696	CCCAGCCGGCACTACCGTCGCAGCTATCCGCGAAGCTTGAGGAGTCAGGCA	745
proC native	746	TCCGAGGCGCTTTCTACCGCGCAGCCCAAGCTTGCGCCGACCGATCTGAA	795
proC opt	746	TTCGCGGAGCCTTTACCGCGCAGCACAGGCTTGTCGGATCGTTCCGAG	795
proC native	796	GAACTCGGAAAGCGCTA	812
proC opt	796	GAGCTGGGTAAGCGTTA	812

Fig. S4: Sequence alignment of the native and codon-optimized *proC* genes. The nucleotide substitutions are highlighted in red. The codon-optimized sequence was provided by Eurofins. The shifts that occur can be attributed to the format of the local alignment (Smith-Waterman), but do not affect the resulting amino acid sequence. opt = codon-optimized.

Cultivation profiles of basic PIA producing strains

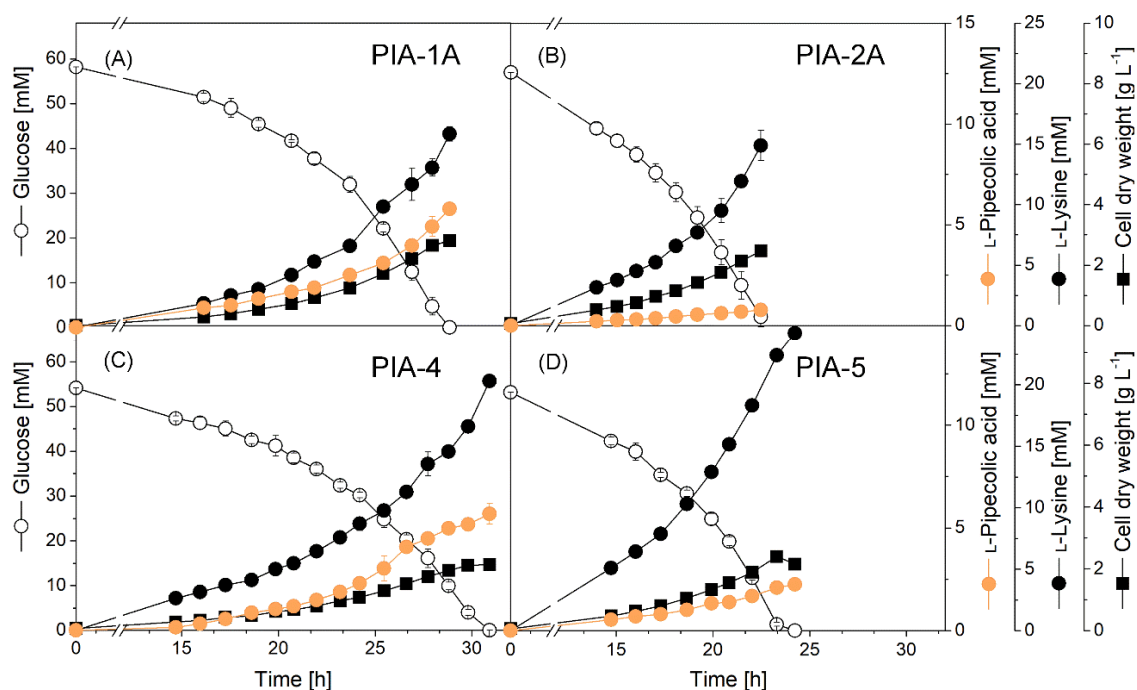


Fig. S5: Performance of basic L-pipecolic acid-producing *C. glutamicum* strains. All strains were based on episomal expression of *lysDH* from *R. pomeroyi* and *proC* from *C. glutamicum* (Table 2). Cultivations were performed in shake flasks at 30 °C using minimal using glucose medium. The data represent mean values and standard errors from three biological replicates.

Protein sequence alignment of the Δ^1 -pyrroline 5-carboxylate reductases ProC and

ProH

ProC	4	I A V I G G G Q I G E A L V S G L I A A N M N P - Q N I R V T N R S E - E R G Q	41
ProH	19	V A F I G A G S M A E G M I S G I V R A N K I P K Q N I C V T N R S N T E R L T	58
ProC	42	E L R D R Y G I L N M T D N S Q A A D E A D V V F L C V K P K F I V E V L S E I	81
ProH	59	E L E L Q Y G I K G A L P N Q L C I E D M D V L I L A M K P K D A E N A L S S L	98
ProC	82	T G T L D N N S A Q S V V V S M A A G I S I A A M E E S A S A G L P V V R V M P	121
ProH	99	K S R I - - - Q P H Q L I L S V L A G I T T S F I E Q S L L N E Q P V V R V M P	135
ProC	122	N T P M L V G K G M S T V T K G R Y V D A E Q L E Q V K D L L S T V G D V L E V	161
ProH	136	N T S S M I G A S A T A I A L G K Y V S E D L K K L A E A L L G C M G E V Y T I	175
ProC	162	A E S D I D A V T A M S G S S P A Y L F L V T E A L I E A G V N L G L P R A T A	201
ProH	176	Q E N Q M D I F T G I A G S G P A Y F Y Y L M E F I E K T G E E A G L D K Q L S	215
ProC	202	K K L A V A S F E G A A T M M K E T G K E P S E L R A G V S S P A G T T V A A I	241
ProH	216	R S I G A Q T L L G A A K M L M E T G E H P E I L R D N I T S P N G T T A A G L	255
ProC	242	R E L E E S G I R G A F Y R A A Q A C A D R S E E L G K	269
ProH	256	Q A L K K S G G G E A I S Q A I K H A A K R S K E I S E	283

Fig. S6: Protein sequence alignment of the Δ^1 -pyrroline 5-carboxylate reductases ProC (*C. glutamicum*) and ProH (*B. subtilis*). The data are given as local Smith-Waterman alignment, created with SnapGene 5.3.2 (GSL Biotech, Chicago, IL, USA). Identical residues are shown in black, similar residues are shown in blue, differing residues are shown in red. The overall sequence identity between the two proteins was 35.07 %. The corresponding similarity was 56.72 %, while gaps accounted for 1.87 %.

Continuation of fig. S7

(B)

tr A0A1Y5TAF1 A0A1Y5TAF1_9RHOB	P--GVQV-RQVDGSDAAGVAAVLAD--CDAAISAAPFFLTPSIAEGARRAGAHYFDLTE	97
tr Q5LX24 Q5LX24_RUEPO	M--GVAT-KQVDAKDEAGLAKALGG--FDAVISAAPFFLTPIIAKAAKAAGAHYFDLTE	98
tr A0A0P1II55 A0A0P1II55_9RHOB	Q--SIAT-RQIDVGEAQLTQGLSG--FDAVISAAPFFLTPKIAKAAKTAGAHYFDLTE	98
	K	
tr A0A1Y5TAF1 A0A1Y5TAF1_9RHOB	DVAATEAVRSLAEEAD--TAFMPQCGLAPGFVGIAGADLARRFDRLDTLSLRVGLPQFP	155
tr Q5LX24 Q5LX24_RUEPO	DVAATNAVRALAEDSQ--TAFMPQCGLAPGFVGIAGAALAAEFDEIDSLHMRVGLPLYP	156
tr A0A0P1II55 A0A0P1II55_9RHOB	DVAATNAVRELAEDSD--TAFMPQCGLAPGFVGIAGASLAAEFDELDSLHMRVGLPLYP	156
	D	
tr A0A1Y5TAF1 A0A1Y5TAF1_9RHOB	TLAEALAG-KARQVYRIRYPGHRDVVKKLLQLQLA--SRRDLMKEIFEALPRTEQD	272
tr Q5LX24 Q5LX24_RUEPO	TLPETLDG-KARSVSYRSIRYPGHRDILRLLNLDLGLE--RRRDLLKDFETALPRTDQD	273
tr A0A0P1II55 A0A0P1II55_9RHOB	TLPETLEG-KARAVSYRSIRYPGHCDILKLLKDLGLE--RRRDLLKDFETALPRTDQD	273
	A	
tr A0A1Y5TAF1 A0A1Y5TAF1_9RHOB	VVIVHCTATGW-IDGAYREHSFLNKTYARQVGGAHMSAIQITTAAGVCGVVELMRRGALP	331
tr Q5LX24 Q5LX24_RUEPO	VVLVYCTAKGR-IGGQLREKSLINKSYSRVIDGQVWSAIQVTTAAGVLGVVDMRAGTLP	332
tr A0A0P1II55 A0A0P1II55_9RHOB	VVLVYCTAKGM-IDGTLREKSLINKSFARTLNGQVWSAIQVTTAAGVLGVVDMRTGGGLP	332
	D	

Fig. S7: Identification of potential modifications sites in the LysDH protein sequence. (A) The multiple protein sequence alignment was generated using ClustalOmega (Sievers et al, 2011) and demonstrates the sequence conservation of 88 LysDHs from organisms phylogenetically close to *R. pomeroyi* which were additionally evaluated for their native environment regarding pH. (B) The 3D homologous models of the LysDH from *R. denitrificans* (A0A0P1II55_9RHOB) and from *P. aquimaris* (A0A1Y5TAF1_9RHOB) served as template for the model of LysDH from *R. pomeroyi*. Final protein sequence alignment identified four potential mutation sites that suggested to lower the pH optimum of the LysDH enzyme of interest. The two variants LysDH^{I81K} and LysDH^{Q114D} were predicted to improve substrate binding at neutral pH, while LysDH^{S228A} and LysDH^{G286D} promised enhanced cofactor binding. Models and alignments were kindly provided by Michael Hutter.

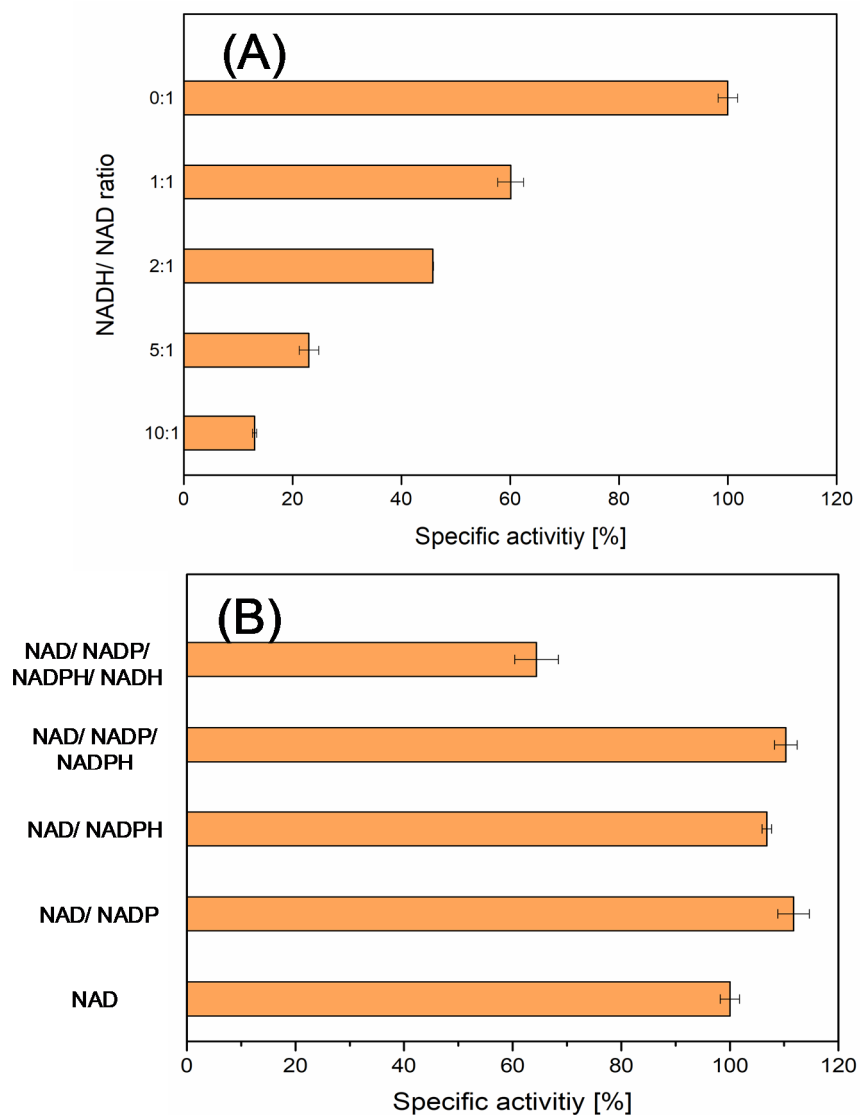
Characterization of L-lysine 6-dehydrogenase from *R. pomeroyi*

Fig. S8: Characterization of L-lysine 6-dehydrogenase form *R. pomeroyi* for L-pipecolic acid production. (A) Impact of the NADH / NAD⁺ ratio on the enzymatic activity, assayed at pH 10.0 and at 30 mM L-lysine. (B) Impact of different cofactor combinations (NAD⁺, NADP⁺, NADP⁺, and NADPH) (pH 10.0, 30 mM L-lysine). The crude cell extract for analysis was obtained from *C. glutamicum* PIA-1A during the exponential growth phase. All assays were performed at 30 °C. The data represent mean values and standard errors from three biological replicates.

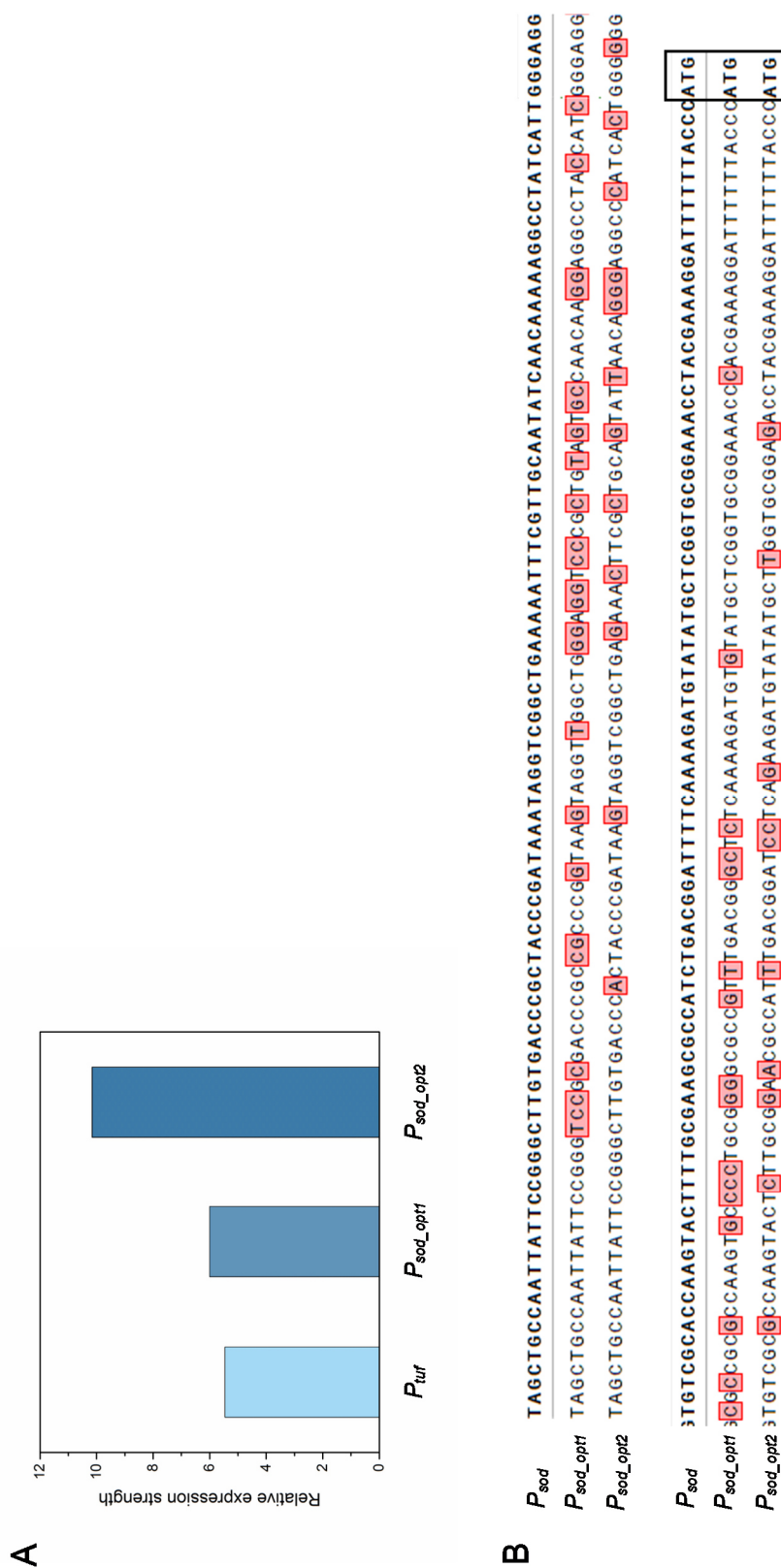
Evaluation of native and synthetic constitutive promoters in *C. glutamicum*

Fig. S9: Evaluation of native and synthetic promoters in *C. glutamicum*. The studied promoters included the *tuf* promoter, the *sod* promoter and two synthetic *sod* variants, namely P_{sod_opt1} and P_{sod_opt2} which were created by random mutagenesis, respectively. The promoters were evaluated and compared regarding the strength of expression of *mCherry* from a plasmid. For this purpose, the corresponding reporter strains were grown in a miniaturized culture system with online monitoring of cell growth and fluorescence. The obtained data were used to calculate the specific strength of each promoter. For comparison, the data display the relative strength of expression, normalized to P_{sod} as a reference (set to a value of 1) (A). Sequence analysis revealed the genetic origin of the modulated expression of P_{sod_opt1} and P_{sod_opt2} (B). The last in each sequence codon represents the translational start codon, and the red color indicates the identified mutations. The data represent mean values and standard errors from three biological replicates.

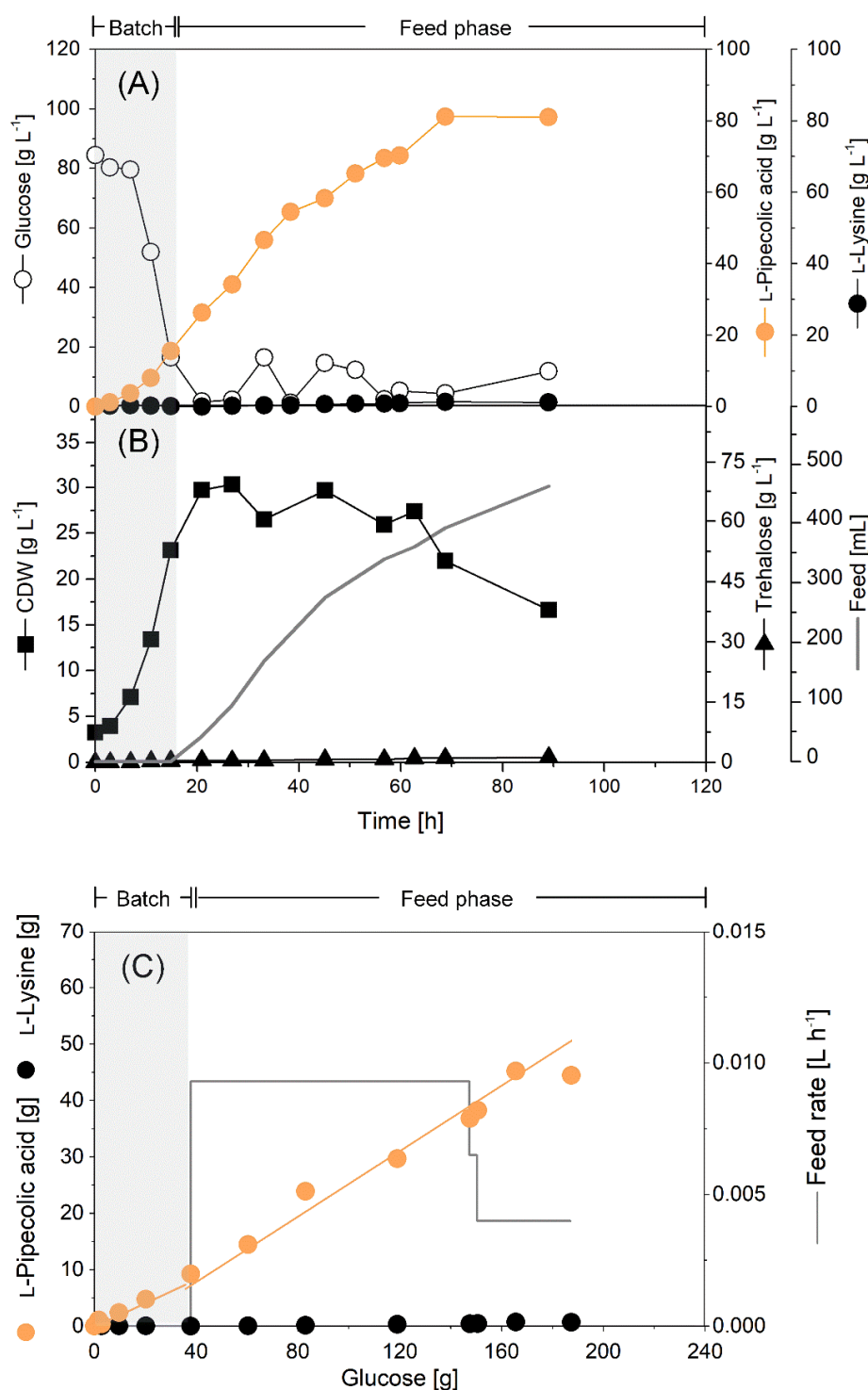
Fed-batch fermentation of *C. glutamicum* PIA-10B

Fig. S10: Fed-batch production of L-pipecolic acid by metabolically engineered *C. glutamicum* PIA-10B. After depletion of the initial sugar at the end of the batch phase, pulses of feed were added automatically, using an increase in the level of dissolved oxygen (DO) above 50 % as a trigger (A). The batch and feed phases are denoted by dotted lines in the culture profile. The batch medium contained glucose (85 g L⁻¹) and yeast extract (15 g L⁻¹) as carbon sources. The feed contained six-fold more glucose (500 g L⁻¹), while the yeast extract level (15 g L⁻¹) remained the same. The process was operated at 30 °C. The yield and selectivity of L-pipecolic acid production improved during fermentation, which was linked to the limited availability of glucose during the feed phase (B). The volumetric productivity was 0.65 g L⁻¹ h⁻¹ during the batch phase and 1.31 g L⁻¹ h⁻¹ during the feed phase. The average volumetric productivity over the entire process was 1.14 g L⁻¹ h⁻¹. The key performance indicators of the production process are summarized in Fig. 33. The data represent mean values from two biological replicates.

7 References

- Adger B, Dyer U, Hutton G, Woods M (1996). Stereospecific Synthesis of the Anaesthetic Levobupivacaine. *Tetrahedron Lett.* **37**: 6399-6402.
- Adindla S, Guruprasad K, Guruprasad L (2004). Three-dimensional models and structure analysis of corynemycolyltransferases in *Corynebacterium glutamicum* and *Corynebacterium efficiens*. *Int. J. Biol. Macromol.* **34**: 181-189.
- Adkins J, Jordan J, Nielsen DR (2013). Engineering *Escherichia coli* for renewable production of the 5-carbon polyamide building-blocks 5-aminovalerate and glutarate. *Biotechnol. Bioeng.* **110**: 1726-1734.
- Adkins J, Pugh S, McKenna R, Nielsen DR (2012). Engineering microbial chemical factories to produce renewable "biomonomers". *Front. Microbiol.* **3**: 313.
- Akermann A, Weiermüller J, Christmann J, Guirande L, Glaser G, Knaus A, Ulber R (2020). Brewers' spent grain liquor as a feedstock for lactate production with *Lactobacillus delbrueckii subsp. lactis*. *Eng. Life Sci.* **20**: 168-180.
- Anaya-Reza O, Lopez-Arenas T (2017). Comprehensive assessment of the L-lysine production process from fermentation of sugarcane molasses. *Bioprocess Biosyst. Eng.* **40**: 1033-1048.
- Andrady AL, Neal MA (2009). Applications and societal benefits of plastics. *Philos. Trans. R. Soc. Lond. B. Biol. Sci.* **364**: 1977-1984.
- Ankri S, Serebrijski I, Reyes O, Leblon G (1996). Mutations in the *Corynebacterium glutamicum* proline biosynthetic pathway: a natural bypass of the *proA* step. *J. Bacteriol.* **178**: 4412-4419.
- Atakav Y, Pinar O, Kazan D (2021). Investigation of the physiology of the obligate alkaliphilic *Bacillus marmarensis* GMBE 72(T) considering its alkaline adaptation mechanism for poly(3-hydroxybutyrate) synthesis. *Microorganisms* **9**.
- Barton N, Horbal L, Starck S, Kohlstedt M, Luzhetskyy A, Wittmann C (2018). Enabling the valorization of guaiacol-based lignin: Integrated chemical and biochemical production of *cis,cis*-muconic acid using metabolically engineered *Amycolatopsis sp* ATCC 39116. *Metab. Eng.* **45**: 200-210.
- Becker J, Buschke N, Bückner R, Wittmann C (2010). Systems level engineering of *Corynebacterium glutamicum* - Reprogramming translational efficiency for superior production. *Eng. Life Sci.* **10**: 430-438.
- Becker J, Klopprogge C, Herold A, Zelder O, Bolten CJ, Wittmann C (2007). Metabolic flux engineering of L-lysine production in *Corynebacterium glutamicum*—over expression and modification of G6P dehydrogenase. *J. Biotechnol.* **132**: 99-109.
- Becker J, Klopprogge C, Schroder H, Wittmann C (2009). Metabolic engineering of the tricarboxylic acid cycle for improved lysine production by *Corynebacterium glutamicum*. *Appl. Environ. Microbiol.* **75**: 7866-7869.
- Becker J, Klopprogge C, Wittmann C (2008). Metabolic responses to pyruvate kinase deletion in lysine producing *Corynebacterium glutamicum*. *Microb. Cell. Fact.* **7**: 8.
- Becker J, Klopprogge C, Zelder O, Heinzle E, Wittmann C (2005). Amplified expression of fructose 1,6-bisphosphatase in *Corynebacterium glutamicum* increases *in vivo* flux through the pentose phosphate pathway and lysine production on different carbon sources. *Appl. Environ. Microbiol.* **71**: 8587-8596.
- Becker J, Kuhl M, Kohlstedt M, Starck S, Wittmann C (2018a). Metabolic engineering of *Corynebacterium glutamicum* for the production of *cis, cis*-muconic acid from lignin. *Microb. Cell. Fact.* **17**: 115.
- Becker J, Lange A, Fabarius J, Wittmann C (2015). Top value platform chemicals: bio-based production of organic acids. *Curr. Opin. Biotechnol.* **36**: 168-175.

- Becker J, Reinefeld J, Stellmacher R, Schäfer R, Lange A, Meyer H, Lalk M, Zelder O, von Abendroth G, Schröder H, Haefner S, Wittmann C (2013a). Systems-wide analysis and engineering of metabolic pathway fluxes in bio-succinate producing *Basfia succiniciproducens*. *Biotechnol. Bioeng.* **110**: 3013-3023.
- Becker J, Rohles CM, Wittmann C (2018b). Metabolically engineered *Corynebacterium glutamicum* for bio-based production of chemicals, fuels, materials, and healthcare products. *Metab. Eng.* **50**: 122-141.
- Becker J, Schäfer R, Kohlstedt M, Harder BJ, Borchert N. S., Stöveken N, Bremer E, Wittmann C (2013b). Systems metabolic engineering of *Corynebacterium glutamicum* for production of the chemical chaperone ectoine. *Microb. Cell. Fact* **12**: 110.
- Becker J, Wittmann C (2012a). Bio-based production of chemicals, materials and fuels - *Corynebacterium glutamicum* as versatile cell factory. *Curr. Opin. Biotechnol.* **23**: 631-640.
- Becker J, Wittmann C (2012b). Systems and synthetic metabolic engineering for amino acid production - the heartbeat of industrial strain development. *Curr. Opin. Biotechnol.* **23**: 718-726.
- Becker J, Wittmann C (2014). GC-MS-based ¹³C metabolic flux analysis. *Methods Mol. Biol.* **1191**: 165-174.
- Becker J, Wittmann C (2015). Advanced biotechnology: metabolically engineered cells for the bio-based production of chemicals and fuels, materials, and health-care products. *Angew. Chem. Int. Ed. Engl.* **54**: 3328-3350.
- Becker J, Wittmann C (2018). From systems biology to metabolically engineered cells-an omics perspective on the development of industrial microbes. *Curr. Opin. Microbiol.* **45**: 180-188.
- Becker J, Wittmann C (2019a). A field of dreams: Lignin valorization into chemicals, materials, fuels, and health-care products. *Biotechnol. Adv.* **37**: 107360.
- Becker J, Wittmann C (2019b). Pathways at Work: Metabolic flux analysis of the industrial cell factory *Corynebacterium glutamicum*. In: Yukawa H, Inui M (eds) *Corynebacterium glutamicum. Microbiology Monographs*, vol **23**. Springer, Berlin, Heidelberg.
- Becker J, Wittmann C (2020a). Microbial production of extremolytes - high-value active ingredients for nutrition, health care, and well-being. *Curr. Opin. Biotechnol.* **65**: 118-128.
- Becker J, Wittmann C (2020). Pathways at Work: Metabolic flux analysis of the industrial cell factory *Corynebacterium glutamicum*. In: Inui M, Toyoda K (eds) *Corynebacterium glutamicum. Microbiology Monographs*, vol **23**. Springer, Cham.
- Becker J, Zelder O, Hafner S, Schröder H, Wittmann C (2011). From zero to hero--design-based systems metabolic engineering of *Corynebacterium glutamicum* for L-lysine production. *Metab. Eng.* **13**: 159-168.
- Beckers V, Poblete-Castro I, Tomasch J, Wittmann C (2016). Integrated analysis of gene expression and metabolic fluxes in PHA-producing *Pseudomonas putida* grown on glycerol. *Microb. Cell Fact.* **15**: 73.
- Belitsky BR, Brill J, Bremer E, Sonenshein AL (2001). Multiple genes for the last step of proline biosynthesis in *Bacillus subtilis*. *J. Bacteriol.* **183**: 4389-4392.
- Bellmann A, Vrljic M, Patek M, Sahn H, Krämer R, Eggeling L (2001). Expression control and specificity of the basic amino acid exporter LysE of *Corynebacterium glutamicum*. *Microbiology (Reading)* **147**: 1765-1774.
- Bermudez LE (2000). Operation Smile: plastic surgery with few resources. *Lancet* **356** Suppl: s45.
- Bernasconi R, Jones RS, Bittiger H, Olpe HR, Heid J, Martin P, Klein M, Loo P, Braunwalder A, Schmutz M (1986). Dose pipicolinic acid interact with the central GABA-ergic system. *J. Neural Transm.* **67**: 175-189.

- Bernsdorff F, Döring AC, Gruner K, Schuck S, Bräutigam A, Zeier J (2016). Pipecolic acid orchestrates plant systemic acquired resistance and defense priming via salicylic acid-dependent and -independent pathways. *Plant Cell* **28**: 102-129.
- Binder S, Schendzielorz G, Stabler N, Krumbach K, Hoffmann K, Bott M, Eggeling L (2012). A high-throughput approach to identify genomic variants of bacterial metabolite producers at the single-cell level. *Genome Biol.* **13**: R40.
- Bizouarn T, Fjellstrom O, Meuller J, Axelsson M, Bergkvist A, Johansson C, Goran Karlsson B, Rydstrom J (2000). Proton translocating nicotinamide nucleotide transhydrogenase from *E. coli*. Mechanism of action deduced from its structural and catalytic properties. *Biochim. Biophys. Acta.* **1457**: 211-228.
- Blombach B, Riestler T, Wieschalka S, Ziert C, Youn JW, Wendisch VF, Eikmanns BJ (2011). *Corynebacterium glutamicum* tailored for efficient isobutanol production. *Appl. Environ. Microbiol.* **77**: 3300-3310.
- Bolten CJ, Heinzle E, Müller R, Wittmann C (2009). Investigation of the central carbon metabolism of *Sorangium cellulosum*: metabolic network reconstruction and quantification of pathway fluxes. *J. Microbiol. Biotechnol.* **19**: 23-36.
- Bolten CJ, Kiefer P, Letisse F, Portais JC, Wittmann C (2007). Sampling for metabolome analysis of microorganisms. *Anal. Chem.* **79**: 3843-3849.
- Borrero-de Acuna JM, Bielecka A, Haussler S, Schobert M, Jahn M, Wittmann C, Jahn D, Poblete-Castro I (2014). Production of medium chain length polyhydroxyalkanoate in metabolic flux optimized *Pseudomonas putida*. *Microb. Cell Fact.* **13**: 88.
- Bott M (2007). Offering surprises: TCA cycle regulation in *Corynebacterium glutamicum*. *Trends Microbiol.* **15**: 417-425.
- Bowden NA, Sanders JPM, Bruins ME (2018). Solubility of the Proteinogenic alpha-amino acids in water, ethanol, and ethanol-water mixtures. *J. Chem. Eng. Data* **63**: 488-497.
- Briki A, Kabore K, Olmos E, Bosselaar S, Blanchard F, Fick M, Guedon E, Fournier F, Delaunay S (2020). *Corynebacterium glutamicum*, a natural overproducer of succinic acid. *Engineering in Life Sciences* **20**: 205-215.
- Broer S, Krämer R (1990). Lysine uptake and exchange in *Corynebacterium glutamicum*. *J. Bacteriol.* **172**: 7241-7248.
- Buschke N, Becker J, Schäfer R, Kiefer P, Biedendieck R, Wittmann C (2013a). Systems metabolic engineering of xylose-utilizing *Corynebacterium glutamicum* for production of 1,5-diaminopentane. *Biotechnol. J.* **8**: 557-570.
- Buschke N, Schäfer R, Becker J, Wittmann C (2013b). Metabolic engineering of industrial platform microorganisms for biorefinery applications--optimization of substrate spectrum and process robustness by rational and evolutive strategies. *Bioresour. Technol.* **135**: 544-554.
- Buschke N, Schröder H, Wittmann C (2011). Metabolic engineering of *Corynebacterium glutamicum* for production of 1,5-diaminopentane from hemicellulose. *Biotechnol. J.* **6**: 306-317.
- Chae TU, Kim WJ, Choi S, Park SJ, Lee SY (2015). Metabolic engineering of *Escherichia coli* for the production of 1,3-diaminopropane, a three carbon diamine. *Sci. Rep.* **5**: 13040.
- Chang YF, Adams E (1974). D-lysine catabolic pathway in *Pseudomonas putida*: interrelations with L-lysine catabolism. *J. Bacteriol.* **117**: 753-764.
- Chen A, Yin B (2020). A brief overview of renewable plastics. *Mater. Today Sustain.* **7-8**: 100031.
- Chen R, Yang H (2000). A highly specific monomeric isocitrate dehydrogenase from *Corynebacterium glutamicum*. *Arch. Biochem. Biophys.* **383**: 238-245.
- Chen Z, Liu G, Zhang J, Bao J (2019). A preliminary study on L-lysine fermentation from lignocellulose feedstock and techno-economic evaluation. *Bioresour. Technol.* **271**: 196-201.

- Cheng J, Chen P, Song A, Wang D, Wang Q (2018a). Expanding lysine industry: industrial biomanufacturing of lysine and its derivatives. *J. Ind. Microbiol. Biotechnol.* **45**: 719-734.
- Cheng J, Huang Y, Mi L, Chen W, Wang D, Wang Q (2018b). An economically and environmentally acceptable synthesis of chiral drug intermediate L-pipecolic acid from biomass-derived lysine via artificially engineered microbes. *J. Ind. Microbiol. Biotechnol.* **45**: 405-415.
- Cheng J, Tu W, Luo Z, Gou X, Li Q, Wang D, Zhou J (2021). A high-efficiency artificial synthetic pathway for 5-aminovalerate production from biobased L-lysine in *Escherichia coli*. *Front. Bioeng. Biotechnol.* **9**: 633028.
- Christmann J, Cao P, Becker J, Desiderato CK, Goldbeck O, Riedel CU, Kohlstedt M, Wittmann C (2023). High-efficiency production of the antimicrobial peptide pediocin PA-1 in metabolically engineered *Corynebacterium glutamicum* using a microaerobic process at acidic pH and elevated levels of bivalent calcium ions. *Microb. Cell. Fact.* **22**: 41.
- Clemente-Jimenez JM, Martinez-Rodriguez S, Rodriguez-Vico F, Heras-Vazquez FJ (2008). Optically pure alpha-amino acids production by the "Hydantoinase Process". *Recent. Pat. Biotechnol.* **2**: 35-46.
- Conrath U, Beckers GJ, Langenbach CJ, Jaskiewicz MR (2015). Priming for enhanced defense. *Annu. Rev. Phytopathol.* **53**: 97-119.
- Copeland MF, Politz MC, Pfleger BF (2014). Application of TALEs, CRISPR/Cas and sRNAs as trans-acting regulators in prokaryotes. *Curr. Opin. Biotechnol.* **29**: 46-54.
- Coque JJ, Liras P, Laiz L, Martin JF (1991). A gene encoding lysine 6-aminotransferase, which forms the beta-lactam precursor alpha-aminoadipic acid, is located in the cluster of cephamycin biosynthetic genes in *Nocardia lactamdurans*. *J. Bacteriol.* **173**: 6258-6264.
- Dairo TO, Nelson NC, Slowing II, Angelici RJ, Woo LK (2016). Aerobic oxidation of cyclic amines to lactams catalyzed by ceria-supported nanogold. *Catal. Lett.* **146**: 2278-2291.
- De Luca C, Lievore G, Bozza D, Buratti A, Cavazzini A, Ricci A, Macis M, Cabri W, Felletti S, Catani M (2021). Downstream processing of therapeutic peptides by means of preparative liquid chromatography. *Molecules* **26**.
- Deischer J, Wolter N, Palkovits R (2020). Tailoring activated carbons for efficient downstream processing: selective liquid-phase adsorption of lysine. *ChemSusChem* **13**: 3614-3621.
- Deutch A, Smith C, Rushlow K, Kretschmer P (1982). *Escherichia coli* delta1-pyrroline-5-carboxylate reductase: gene sequence, protein overproduction and purification. *Nucleic acids res.* **10**: 7701-7714.
- Ding P, Reikhter D, Ding Y, Feussner K, Busta L, Haroth S, Xu S, Li X, Jetter R, Feussner I, Zhang Y (2016). Characterization of a pipecolic acid biosynthesis pathway required for systemic acquired resistance. *Plant Cell* **28**: 2603-2615.
- Eggeling L, Bott M (2015). A giant market and a powerful metabolism: L-lysine provided by *Corynebacterium glutamicum*. *Appl. Microbiol. Biotechnol.* **99**: 3387-3394.
- Eggeling L, Oberle S, Sahm H (1998). Improved L-lysine yield with *Corynebacterium glutamicum*: use of *dapA* resulting in increased flux combined with growth limitation. *Appl. Microbiol. Biotechnol.* **49**: 24-30.
- Eggeling L, Sahm H (1999). L-Glutamate and L-lysine: traditional products with impetuous developments. *Appl. Microbiol. Biotechnol.* **52**: 146-153.
- Encarnacion S, Hernandez M, Martinez-Batallar G, Contreras S, Vargas Mdel C, Mora J (2005). Comparative proteomics using 2-D gel electrophoresis and mass spectrometry as tools to dissect stimulons and regulons in bacteria with sequenced or partially sequenced genomes. *Biol. Proced. Online* **7**: 117-135.
- European Bioplastics n.l. (2022). Bioplastics facts and figures. Nova-Institute (2022), European Bioplastics e.V. (EUBP), Berlin.

- Follmann M, Ochrombel I, Krämer R, Trotschel C, Poetsch A, Rückert C, Hüser A, Persicke M, Seiferling D, Kalinowski J, Marin K (2009). Functional genomics of pH homeostasis in *Corynebacterium glutamicum* revealed novel links between pH response, oxidative stress, iron homeostasis and methionine synthesis. *BMC Genomics* **10**: 621.
- Forlani G, Nocek B, Chakravarthy S, Joachimiak A (2017). Functional characterization of four putative delta¹-pyrroline-5-carboxylate reductases from *Bacillus subtilis*. *Front. Microbiol.* **8**: 1442.
- Francisco A, Ronchi JA, Navarro CDC, Figueira TR, Castilho RF (2018). Nicotinamide nucleotide transhydrogenase is required for brain mitochondrial redox balance under hampered energy substrate metabolism and high-fat diet. *J. Neurochem.* **147**: 663-677.
- Fujii T, Aritoku Y, Agematu H, Tsunekawa H (2002a). Increase in the rate of L-pipecolic acid production using *lat*-expressing *Escherichia coli* by *lysP* and *yeiE* amplification. *Biosci. Biotechnol. Biochem.* **66**: 1981-1984.
- Fujii T, Mukaihara M, Agematu H, Tsunekawa H (2002b). Biotransformation of L-lysine to L-pipecolic acid catalyzed by L-lysine 6-aminotransferase and pyrroline-5-carboxylate reductase. *Biosci. Biotechnol. Biochem.* **66**: 622-627.
- Fujii T, Narita T, Agematu H, Agata N, Isshiki K (2000). Characterization of L-lysine 6-aminotransferase and its structural gene from *Flavobacterium lutescens* IFO3084. *J. Biochem.* **128**.
- Gatto GJ, Boyne MT, Kelleher NL, Walsh CT (2006). Biosynthesis of pipecolic acid by RapL, a lysine cyclodeaminase encoded in the rapamycin gene cluster. *J. Am. Chem. Soc.* **128**: 3838-3847.
- Georgi T, Rittmann D, Wendisch VF (2005). Lysine and glutamate production by *Corynebacterium glutamicum* on glucose, fructose and sucrose: roles of malic enzyme and fructose-1,6-bisphosphatase. *Metab. Eng.* **7**: 291-301.
- Germann UA, Shlyakhter D, Mason VS, Zelle RE, Duffy JP, Galullo V, Armistead DM, Saunders JO, Boger J, Harding MW (1997). Cellular and biochemical characterization of VX-710 as a chemosensitizer: reversal of P-glycoprotein-mediated multidrug resistance *in vitro*. *Anticancer Drugs* **8**: 125-140.
- Gerstmeir R, Wendisch VF, Schnicke S, Ruan H, Farwick M, Reinscheid D, Eikmanns BJ (2003). Acetate metabolism and its regulation in *Corynebacterium glutamicum*. *J. Biotechnol.* **104**: 99-122.
- Gibson DG, Young L, Chuang RY, Venter JC, Hutchison CA, 3rd, Smith HO (2009). Enzymatic assembly of DNA molecules up to several hundred kilobases. *Nat. Methods* **6**: 343-345.
- Giesselmann G (2018). Systems metabolic engineering of *Corynebacterium glutamicum* for the production of L-lysine and ectoine. Dissertation, Faculty of Science and Technology, Saarland University, Saarland University.
- Giesselmann G, Dietrich D, Jungmann L, Kohlstedt M, Jeon EJ, Yim SS, Sommer F, Zimmer D, Mühlhaus T, Schroda M, Jeong KJ, Becker J, Wittmann C (2019). Metabolic engineering of *Corynebacterium glutamicum* for high-level ectoine production: design, combinatorial assembly, and implementation of a transcriptionally balanced heterologous ectoine pathway. *Biotechnol. J.* **14**: e1800417.
- Goldbeck O, Desef DN, Ovchinnikov KV, Perez-Garcia F, Christmann J, Sinner P, Crauwels P, Weixler D, Cao P, Becker J, Kohlstedt M, Kager J, Eikmanns BJ, Seibold GM, Herwig C, Wittmann C, Bar NS, Diep DB, Riedel CU (2021). Establishing recombinant production of pediocin PA-1 in *Corynebacterium glutamicum*. *Metab. Eng.* **68**: 34-45.
- Gouffi K, Bernard T, Blanco C (2000). Osmoprotection by pipecolic acid in *Sinorhizobium meliloti*: specific effects of D and L isomers. *Appl. Environ. Microbiol.* **66**: 2358-2364.

- Gourdon P, Baucher MF, Lindley ND, Guyonvarch A (2000). Cloning of the malic enzyme gene from *Corynebacterium glutamicum* and role of the enzyme in lactate metabolism. *Appl. Environ. Microbiol.* **66**: 2981-2987.
- Graf M, Haas T, Muller F, Buchmann A, Harm-Bekbenbetova J, Freund A, Niess A, Persicke M, Kalinowski J, Blombach B, Takors R (2019). Continuous adaptive evolution of a fast-growing *Corynebacterium glutamicum* strain independent of protocatechuate. *Front. Microbiol.* **10**: 1648.
- Guo X, Wang J, Xie X, Xu Q, Zhang C, Chen N (2013). Enhancing the supply of oxaloacetate for L-glutamate production by *pyc* overexpression in different *Corynebacterium glutamicum*. *Biotechnol. Lett.* **35**: 943-950.
- Gutierrez MC, Delgado-Coello BA (1989). Influence of pipercolic acid on the release and uptake of [3H]GABA from brain slices of mouse cerebral cortex. *Neurochem. Res.* **14**: 405-408.
- Han YH, Choi TR, Park YL, Park JY, Song HS, Kim HJ, Lee SM, Park SL, Lee HS, Bhatia SK, Gurav R, Yang YH (2020). Enhancement of pipercolic acid production by the expression of multiple lysine cyclodeaminase in the *Escherichia coli* whole-cell system. *Enzyme Microb. Technol.* **140**: 109643.
- Hanko VP, Rohrer JS (2004). Determination of amino acids in cell culture and fermentation broth media using anion-exchange chromatography with integrated pulsed amperometric detection. *Anal. Biochem.* **324**: 29-38.
- Hara R, Nishikawa T, Okuhara T, Koketsu K, Kino K (2019). Ectoine hydroxylase displays selective trans-3-hydroxylation activity towards L-proline. *Appl. Microbiol. Biotechnol.* **103**: 5689-5698.
- Hara R, Yamagata K, Miyake R, Kawabata H, Uehara H, Kino K (2017). Discovery of lysine hydroxylases in the clavaminic acid synthase-like superfamily for efficient hydroxylysine bioproduction. *Appl. Environ. Microbiol.* **83**.
- Hasegawa S, Suda M, Uematsu K, Natsuma Y, Hiraga K, Jojima T, Inui M, Yukawa H (2013). Engineering of *Corynebacterium glutamicum* for high-yield L-valine production under oxygen deprivation conditions. *Appl. Environ. Microbiol.* **79**: 1250-1257.
- Hashiro S, Yasueda H (2018). Plasmid copy number mutation in *repA* gene encoding RepA replication initiator of cryptic plasmid *pHM1519* in *Corynebacterium glutamicum*. *Biosci. Biotechnol. Biochem.* **82**: 2212-2224.
- Hauptka C, Delépine B, Irla M, Heux S, Wendisch VF (2020). Flux enforcement for fermentative production of 5-aminovalerate and glutarate by *Corynebacterium glutamicum*. *Catalysts* **10**: 1065.
- He M (2006). Pipercolic acid in microbes: biosynthetic routes and enzymes. *J. Ind. Microbiol. Biotechnol.* **33**: 401-407.
- Heider SA, Peters-Wendisch P, Wendisch VF (2012). Carotenoid biosynthesis and overproduction in *Corynebacterium glutamicum*. *BMC Microbiol.* **12**: 198.
- Heinzle E, Yuan Y, Kumar S, Wittmann C, Gehre M, Richnow HH, Wehrung P, Adam P, Albrecht P (2008). Analysis of ¹³C labeling enrichment in microbial culture applying metabolic tracer experiments using gas chromatography-combustion-isotope ratio mass spectrometry. *Anal. Biochem.* **380**: 202-210.
- Henke NA, Frohwitter J, Peters-Wendisch P, Wendisch VF (2018). Carotenoid production by recombinant *Corynebacterium glutamicum*: strain construction, cultivation, extraction, and quantification of carotenoids and terpenes. *Methods Mol. Biol.* **1852**: 127-141.
- Herbert KR, Williams GM, Cooper GJ, Brimble MA (2012). Synthesis of glycosylated 5-hydroxylysine, an important amino acid present in collagen-like proteins such as adiponectin. *Org. Biomol. Chem.* **10**: 1137-1144.
- Hermann T, Finkemeier M, Pfefferle W, Wersch G, Kramer R, Burkovski A (2000). Two-dimensional electrophoretic analysis of *Corynebacterium glutamicum* membrane fraction and surface proteins. *Electrophoresis* **21**: 654-659.

- Heydari M, Ohshima T, Nunoura-Kominato N, Sakuraba H (2004). Highly stable L-lysine 6-dehydrogenase from the thermophile *Geobacillus stearothermophilus* isolated from a Japanese hot spring: characterization, gene cloning and sequencing, and expression. *Appl. Environ. Microbiol.* **70**: 937-942.
- Hirao T, Nakano T, Azuma A, Sugimoto M, Nakanishi T (1989). L-Lysine production in continuous culture of an L-lysine hyperproducing mutant of *Corynebacterium glutamicum*. *Appl. Microbiol. Biotechnol.* **32**: 269-273.
- Hoffmann SL, Jungmann L, Schiefelbein S, Peyriga L, Cahoreau E, Portais JC, Becker J, Wittmann C (2018). Lysine production from the sugar alcohol mannitol: Design of the cell factory *Corynebacterium glutamicum* SEA-3 through integrated analysis and engineering of metabolic pathway fluxes. *Metab. Eng.* **47**: 475-487.
- Hoffmann SL, Kohlstedt M, Jungmann L, Hutter M, Poblete-Castro I, Becker J, Wittmann C (2021). Cascaded valorization of brown seaweed to produce L-lysine and value-added products using *Corynebacterium glutamicum* streamlined by systems metabolic engineering. *Metab. Eng.* **67**: 293-307.
- Holmes EC, Chen YC, Sattely ES, Mudgett MB (2019). An engineered pathway for N-hydroxy-pipecolic acid synthesis enhances systemic acquired resistance in tomato. *Sci. Signal* **12**.
- Hong YG, Moon YM, Hong JW, No SY, Choi TR, Jung HR, Yang SY, Bhatia SK, Ahn JO, Park KM, Yang YH (2018). Production of glutaric acid from 5-aminovaleric acid using *Escherichia coli* whole cell bio-catalyst overexpressing GabTD from *Bacillus subtilis*. *Enzyme Microb. Technol.* **118**: 57-65.
- Ikeda M (2012). Sugar transport systems in *Corynebacterium glutamicum*: features and applications to strain development. *Appl. Microbiol. Biotechnol.* **96**: 1191-1200.
- Ikeda M (2017). Lysine Fermentation: History and Genome Breeding. *Adv Biochem. Eng. Biotechnol.* **159**: 73-102.
- Ikeda M, Katsumata R (1998). A novel system with positive selection for the chromosomal integration of replicative plasmid DNA in *Corynebacterium glutamicum*. *Microbiology (Reading)* **144 (Pt 7)**: 1863-1868.
- Ikeda M, Katsumata R (1999). Hyperproduction of tryptophan by *Corynebacterium glutamicum* with the modified pentose phosphate pathway. *Appl Environ Microbiol* **65**: 2497-2502.
- Ikeda M, Mizuno Y, Awane S, Hayashi M, Mitsuhashi S, Takeno S (2011). Identification and application of a different glucose uptake system that functions as an alternative to the phosphotransferase system in *Corynebacterium glutamicum*. *Appl. Microbiol. Biotechnol.* **90**: 1443-1451.
- Ikeda M, Nakagawa S (2003). The *Corynebacterium glutamicum* genome: features and impacts on biotechnological processes. *Appl. Microbiol. Biotechnol.* **62**: 99-109.
- Ikeda M, Takeno S (2013). Amino acid production by *Corynebacterium glutamicum*. In: Yukawa H, Inui M (eds) *Corynebacterium glutamicum*. Microbiology Monographs, vol **23**. Springer, Berlin, Heidelberg.
- Im D, Matsui D, Arakawa T, Isobe K, Asano Y, Fushinobu S (2018). Ligand complex structures of l-amino acid oxidase/monooxygenase from *Pseudomonas* sp. AIU 813 and its conformational change. *FEBS Open. Bio.* **8**: 314-324.
- Inderwildi OR, King DA (2009). Quo vadis biofuels? *Energy Environ. Sci.* **2**: 343.
- Inoue H, Nojima H, Okayama H (1990). High efficiency transformation of *Escherichia coli* with plasmids. *Gene* **96**: 23-28.
- Inui M, Murakami S, Okino S, Kawaguchi H, Vertes AA, Yukawa H (2004). Metabolic analysis of *Corynebacterium glutamicum* during lactate and succinate productions under oxygen deprivation conditions. *J. Mol. Microbiol. Biotechnol.* **7**: 182-196.

- Inui M, Suda M, Okino S, Nonaka H, Puskas LG, Vertes AA, Yukawa H (2007). Transcriptional profiling of *Corynebacterium glutamicum* metabolism during organic acid production under oxygen deprivation conditions. *Microbiology (Reading)* **153**: 2491-2504.
- Ireland RE, Gleason JL, Gegnas LD, Highsmith TK (1996). A Total Synthesis of FK-506¹. *J. Org. Chem.* **61**: 6856-6872.
- Jackson JB (2003). Proton translocation by transhydrogenase. *FEBS Lett* **555**: 176-177.
- Jäger W, Schäfer A, Pühler A, Labes G, Wohlleben W (1992). Expression of the *Bacillus subtilis* *sacB* gene leads to sucrose sensitivity in the gram-positive bacterium *Corynebacterium glutamicum* but not in *Streptomyces lividans*. *J. Bacteriol.* **174**: 5462-5465.
- Jayarathna S, Andersson M, Andersson R (2022). Recent advances in starch-based blends and composites for bioplastics applications. *Polymers (Basel)* **14**.
- Jensen JV, Wendisch VF (2013). Ornithine cyclodeaminase-based proline production by *Corynebacterium glutamicum*. *Microb. Cell. Fact.* **12**: 63.
- Jiang Y, Huang MZ, Chen XL, Zhang B (2020). Proteome analysis guided genetic engineering of *Corynebacterium glutamicum* S9114 for tween 40-triggered improvement in L-ornithine production. *Microb. Cell. Fact.* **19**: 2.
- Jiang Y, Qian F, Yang J, Liu Y, Dong F, Xu C, Sun B, Chen B, Xu X, Li Y, Wang R, Yang S (2017). CRISPR-Cpf1 assisted genome editing of *Corynebacterium glutamicum*. *Nat. Commun.* **8**: 15179.
- Jin C, Bao J (2021). Lysine production by dry biorefining of wheat straw and cofermentation of *Corynebacterium glutamicum*. *J. Agric. Food Chem.* **69**: 1900-1906.
- Jochmann N, Gotker S, Tauch A (2011). Positive transcriptional control of the pyridoxal phosphate biosynthesis genes *pdxST* by the MocR-type regulator PdxR of *Corynebacterium glutamicum* ATCC 13032. *Microbiology (Reading)* **157**: 77-88.
- Johansson T, Oswald C, Pedersen A, Tornroth S, Okvist M, Karlsson BG, Rydstrom J, Kregel U (2005). X-ray structure of domain I of the proton-pumping membrane protein transhydrogenase from *Escherichia coli*. *J. Mol. Biol.* **352**: 299-312.
- Jojima T, Fujii M, Mori E, Inui M, Yukawa H (2010). Engineering of sugar metabolism of *Corynebacterium glutamicum* for production of amino acid L-alanine under oxygen deprivation. *Appl. Microbiol. Biotechnol.* **87**: 159-165.
- Jojima T, Noburyu R, Sasaki M, Tajima T, Suda M, Yukawa H, Inui M (2015). Metabolic engineering for improved production of ethanol by *Corynebacterium glutamicum*. *Appl. Microbiol. Biotechnol.* **99**: 1165-1172.
- Joo JC, Oh YH, Yu JH, Hyun SM, Khang TU, Kang KH, Song BK, Park K, Oh MK, Lee SY, Park SJ (2017). Production of 5-aminovaleric acid in recombinant *Corynebacterium glutamicum* strains from a *Miscanthus* hydrolysate solution prepared by a newly developed *Miscanthus* hydrolysis process. *Bioresour. Technol.* **245**: 1692-1700.
- Jorge JMP, Perez-Garcia F, Wendisch VF (2017). A new metabolic route for the fermentative production of 5-aminovalerate from glucose and alternative carbon sources. *Bioresour. Technol.* **245**: 1701-1709.
- Jumper J, Evans R, Pritzel A, Green T, Figurnov M, Ronneberger O, Tunyasuvunakool K, Bates R, Zidek A, Potapenko A, Bridgland A, Meyer C, Kohli SAA, Ballar AJ, Cowie A, Romera-Paredes B, Nikolov S, Jain R, Adler J, Back T, Petersen S, Reiman D, Clancy E, Zielinski M, Steinegger M, Pacholska M, Berghammer T, Bodenstein S, Silver D, Vinyals O, Senior AW, Kavukcuoglu K, Kohli P, Hassabis D (2021). Highly accurate protein structure prediction with AlphaFold. *Nature* **596**: 583-589.
- Jungmann L, Hoffmann SL, Lang C, De Agazio R, Becker J, Kohlstedt M, Wittmann C (2022). High-efficiency production of 5-hydroxyectoine using metabolically engineered *Corynebacterium glutamicum*. *Microb. Cell. Fact.* **21**: 274.

- Kabus A, Georgi T, Wendisch VF, Bott M (2007). Expression of the *Escherichia coli pntAB* genes encoding a membrane-bound transhydrogenase in *Corynebacterium glutamicum* improves L-lysine formation. *Appl. Microbiol. Biotechnol.* **75**: 47-53.
- Kalinowski J, Bathe B, Bartels D, Bischoff N, Bott M, Burkovski A, Dusch N, Eggeling L, Eikmanns BJ, Gaigalat L, Goesmann A, Hartmann M, Huthmacher K, Kramer R, Linke B, McHardy AC, Meyer F, Mockel B, Pfefferle W, Puhler A, Rey DA, Ruckert C, Rupp O, Sahm H, Wendisch VF, Wiegrabe I, Tauch A (2003). The complete *Corynebacterium glutamicum* ATCC 13032 genome sequence and its impact on the production of L-aspartate-derived amino acids and vitamins. *J. Biotechnol.* **104**: 5-25.
- Kalinowski J, Cremer J, Bachmann B, Eggeling L, Sahm H, Puhler A (1991). Genetic and biochemical analysis of the aspartokinase from *Corynebacterium glutamicum*. *Mol. Microbiol.* **5**: 1197-1204.
- Kamada N, Yasuhara A, Ikeda M (2003). Significance of the non-oxidative route of the pentose phosphate pathway for supplying carbon to the purine-nucleotide pathway in *Corynebacterium ammoniagenes*. *J. Ind. Microbiol. Biotechnol.* **30**: 129-132.
- Kang SB, Choi JI (2022). Production of cadaverine in recombinant *Corynebacterium glutamicum* overexpressing lysine decarboxylase (*ldcC*) and response regulator *dr1558*. *Appl. Biochem. Biotechnol.* **194**: 1013-1024.
- Kappelmann J, Klein B, Papenfuss M, Lange J, Blombach B, Takors R, Wiechert W, Polen T, Noack S (2020). Comprehensive analysis of *C. glutamicum* anaplerotic deletion mutants under defined D-glucose conditions. *Front. Bioeng. Biotechnol.* **8**: 602936.
- Kawasaki H, Martinac B (2020). Mechanosensitive channels of *Corynebacterium glutamicum* functioning as exporters of L-glutamate and other valuable metabolites. *Curr. Opin. Chem. Biol.* **59**: 77-83.
- Kendrick N, Darie CC, Hoelter M, Powers G, Johansen J (2019). 2D SDS PAGE in combination with western blotting and mass spectrometry is a robust method for protein analysis with many applications. *Adv. Exp. Med. Biol.* **1140**: 563-574.
- Khaw LE, Böhm GA, Metcalfe S, Staunton J, Leadlay PF (1998). Mutational biosynthesis of novel papamycins by a strain of *Streptomyces hygroscopicus* NRRL 5491 disrupted in *rapL*, encoding a putative lysine cyclodeaminase. *J. Bacteriol.* **180**: 809-814.
- Kiefer P, Heinzle E, Wittmann C (2002). Influence of glucose, fructose and sucrose as carbon sources on kinetics and stoichiometry of lysine production by *Corynebacterium glutamicum*. *J. Ind. Microbiol. Biotechnol.* **28**: 338-343.
- Kiefer P, Heinzle E, Zelder O, Wittmann C (2004). Comparative metabolic flux analysis of lysine-producing *Corynebacterium glutamicum* cultured on glucose or fructose. *Appl. Environ. Microbiol.* **70**: 229-239.
- Kim GY, Kim J, Park G, Kim HJ, Yang J, Seo SW (2023). Synthetic biology tools for engineering *Corynebacterium glutamicum*. *Comput. Struct. Biotechnol. J.* **21**: 1955-1965.
- Kind S, Becker J, Wittmann C (2013). Increased lysine production by flux coupling of the tricarboxylic acid cycle and the lysine biosynthetic pathway--metabolic engineering of the availability of succinyl-CoA in *Corynebacterium glutamicum*. *Metab. Eng.* **15**: 184-195.
- Kind S, Jeong WK, Schroder H, Wittmann C (2010). Systems-wide metabolic pathway engineering in *Corynebacterium glutamicum* for bio-based production of diamino-pentane. *Metab. Eng.* **12**: 341-351.
- Kind S, Kreye S, Wittmann C (2011). Metabolic engineering of cellular transport for overproduction of the platform chemical 1,5-diamino-pentane in *Corynebacterium glutamicum*. *Metab. Eng.* **13**: 617-627.

- Kind S, Neubauer S, Becker J, Yamamoto M, Volkert M, Abendroth G, Zelder O, Wittmann C (2014). From zero to hero - production of bio-based nylon from renewable resources using engineered *Corynebacterium glutamicum*. *Metab. Eng.* **25**: 113-123.
- Kinoshita S, Udaka S, Shimono M (2004). Studies on the amino acid fermentation. Part 1. Production of L-glutamic acid by various microorganisms. *J. Gen. Appl. Microbiol.* **50**: 331-343.
- Kirchner O, Tauch A (2003). Tools for genetic engineering in the amino acid-producing bacterium *Corynebacterium glutamicum*. *J. Biotechnol.* **104**: 287-299.
- Klaffl S, Eikmanns BJ (2010). Genetic and functional analysis of the soluble oxaloacetate decarboxylase from *Corynebacterium glutamicum*. *J. Bacteriol.* **192**: 2604-2612.
- Klein C, Hüttel W (2011). A simple procedure for selective hydroxylation of L-proline and L-pipecolic acid with recombinantly expressed proline hydroxylases. *ASC* **353**: 1375-1383.
- Ko YS, Kim JW, Lee JA, Han T, Kim GB, Park JE, Lee SY (2020). Tools and strategies of systems metabolic engineering for the development of microbial cell factories for chemical production. *Chem. Soc. Rev.* **49**: 4615-4636.
- Kohlstedt M, Sappa PK, Meyer H, Maass S, Zapras A, Hoffmann T, Becker J, Steil L, Hecker M, van Dijk JM, Lalk M, Mader U, Stulke J, Bremer E, Volker U, Wittmann C (2014). Adaptation of *Bacillus subtilis* carbon core metabolism to simultaneous nutrient limitation and osmotic challenge: a multi-omics perspective. *Environ. Microbiol.* **16**: 1898-1917.
- Kohlstedt M, Starck S, Barton N, Stolzenberger J, Selzer M, Mehlmann K, Schneider R, Pleissner D, Rinkel J, Dickschat JS, Venus J, van Duuren JBJH, Wittmann C (2018). From lignin to nylon: Cascaded chemical and biochemical conversion using metabolically engineered *Pseudomonas putida*. *Metab. Eng.* **47**: 279-293.
- Kohlstedt M, Weimer A, Weiland F, Stolzenberger J, Selzer M, Sanz M, Kramps L, Wittmann C (2022). Biobased PET from lignin using an engineered *cis*, *cis*-muconate-producing *Pseudomonas putida* strain with superior robustness, energy and redox properties. *Metab. Eng.* **72**: 337-352.
- Krömer JO, Bolten CJ, Heinzle E, Schröder H, Wittmann C (2008). Physiological response of *Corynebacterium glutamicum* to oxidative stress induced by deletion of the transcriptional repressor McbR. *Microbiology (Reading)* **154**: 3917-3930.
- Krömer JO, Fritz M, Heinzle E, Wittmann C (2005). *In vivo* quantification of intracellular amino acids and intermediates of the methionine pathway in *Corynebacterium glutamicum*. *Anal. Biochem.* **340**: 171-173.
- Krömer JO, Sorgenfrei O, Klopprogge K, Heinzle E, Wittmann C (2004). In-depth profiling of lysine-producing *Corynebacterium glutamicum* by combined analysis of the transcriptome, metabolome, and fluxome. *J. Bacteriol.* **186**: 1769-1784.
- Krömer JO, Wittmann C, Schröder H, Heinzle E (2006). Metabolic pathway analysis for rational design of L-methionine production by *Escherichia coli* and *Corynebacterium glutamicum*. *Metab. Eng.* **8**: 353-369.
- Kuhl M, Glaser L, Rebets Y, Rückert C, Sarkar N, Hartsch T, Kalinowski J, Luzhetskyy A, Wittmann C (2020). Microparticles globally reprogram *Streptomyces albus* toward accelerated morphogenesis, streamlined carbon core metabolism, and enhanced production of the antituberculosis polyketide pamamycin. *Biotechnol. Bioeng.* **117**: 3858-3875.
- Kuhnert P, Scholten E, Haefner S, Mayor D, Frey J (2010). *Basfia succiniciproducens* gen. nov., sp. nov., a new member of the family *Pasteurellaceae* isolated from bovine rumen. *Int. J. Syst. Evol. Microbiol.* **60**: 44-50.
- Lamber J (2020). Synthese des Schutzmoleküls Pipecolinsäure in *Corynebacterium glutamicum*. Bachelor Thesis, Faculty of Natural Sciences and Technology and Faculty of Medicine, Saarland University, Saarbrücken, Germany.

- Lange A, Becker J, Schulze D, Cahoreau E, Portais JC, Haefner S, Schröder H, Krawczyk J, Zelder O, Wittmann C (2017). Bio-based succinate from sucrose: High-resolution ^{13}C metabolic flux analysis and metabolic engineering of the rumen bacterium *Basfia succiniciproducens*. *Metab. Eng.* **44**: 198-212.
- Lee HN, Shin WS, Seo SY, Choi SS, Song JS, Kim JY, Park JH, Lee D, Kim SY, Lee SJ, Chun GT, Kim ES (2018). *Corynebacterium* cell factory design and culture process optimization for muconic acid biosynthesis. *Sci. Rep.* **8**: 18041.
- Lei M, Peng X, Sun W, Zhang D, Wang Z, Yang Z, Zhang C, Yu B, Niu H, Ying H, Ouyang P, Liu D, Chen Y (2021). Nonsterile L-lysine fermentation using engineered phosphite-grown *Corynebacterium glutamicum*. *ACS Omega* **6**: 10160-10167.
- Lemire A, Charette AB (2010). Stereoselective syntheses of L-pipecolic acid and (2S,3S)-3-hydroxypipecolic acid from a chiral N-imino-2-phenyl-1,2-dihydropyridine intermediate. *J. Org. Chem.* **75**: 2077-2080.
- Leuchtenberger W, Huthmacher K, Drauz K (2005). Biotechnological production of amino acids and derivatives: current status and prospects. *Appl. Microbiol. Biotechnol.* **69**: 1-8.
- Li CL, Ruan HZ, Liu LM, Zhang WG, Xu JZ (2022). Rational reformation of *Corynebacterium glutamicum* for producing L-lysine by one-step fermentation from raw corn starch. *Appl. Microbiol. Biotechnol.* **106**: 145-160.
- Li Y, Ai Y, Zhang J, Fei J, Liu B, Wang J, Li M, Zhao Q, Song J (2020). A novel expression vector for *Corynebacterium glutamicum* with an auxotrophy complementation system. *Plasmid* **107**: 102476.
- Li Z, Xu J, Jiang T, Ge Y, Liu P, Zhang M, Su Z, Gao C, Ma C, Xu P (2016). Overexpression of transport proteins improves the production of 5-aminovalerate from L-lysine in *Escherichia coli*. *Sci. Rep.* **6**: 30884.
- Litsanov B, Brocker M, Bott M (2012). Toward homosuccinate fermentation: metabolic engineering of *Corynebacterium glutamicum* for anaerobic production of succinate from glucose and formate. *Appl. Environ. Microbiol.* **78**: 3325-3337.
- Liu J, Xu JZ, Rao ZM, Zhang WG (2022). Industrial production of L-lysine in *Corynebacterium glutamicum*: Progress and prospects. *Microbiol. Res.* **262**: 127101.
- Liu N, Zhang TT, Rao ZM, Zhang WG, Xu JZ (2021). Reconstruction of the diaminopimelic acid pathway to promote L-lysine production in *Corynebacterium glutamicum*. *Int. J. Mol. Sci.* **22**.
- Liu P, Zhang H, Lv M, Hu M, Li Z, Gao C, Xu P, Ma C (2014). Enzymatic production of 5-aminovalerate from L-lysine using L-lysine monooxygenase and 5-aminovaleramidase. *Sci. Rep.* **4**: 5657.
- Liu Y, Hu L, Ma T, Yang J, Ding J (2018). Insights into the inhibitory mechanisms of NADH on the alphasigma heterodimer of human NAD-dependent isocitrate dehydrogenase. *Sci. Rep.* **8**: 3146.
- Lohnes K, Quebbemann NR, Liu K, Kobzeff F, Loo JA, Ogorzalek Loo RR (2016). Combining high-throughput MALDI-TOF mass spectrometry and isoelectric focusing gel electrophoresis for virtual 2D gel-based proteomics. *Methods* **104**: 163-169.
- Loos A, Glanemann C, Willis LB, O'Brien XM, Lessard PA, Gerstmeir R, Guillouet S, Sinskey AJ (2001). Development and validation of *Corynebacterium* DNA microarrays. *Appl. Environ. Microbiol.* **67**: 2310-2318.
- Lubitz D, Jorge JM, Perez-Garcia F, Taniguchi H, Wendisch VF (2016). Roles of export genes *cgmA* and *lysE* for the production of L-arginine and L-citrulline by *Corynebacterium glutamicum*. *Appl. Microbiol. Biotechnol.* **100**: 8465-8474.
- Luo Z, Wang Z, Wang B, Lu Y, Yan L, Zhao Z, Bai T, Zhang J, Li H, Wang W, Cheng J (2022). An artificial pathway for N-hydroxy-pipecolic acid production from L-lysine in *Escherichia coli*. *Front. Microbiol.* **13**: 842804.

- Ma D, Lu P, Yan C, Fan C, Yin P, Wang J, Shi Y (2012). Structure and mechanism of a glutamate-GABA antiporter. *Nature* **483**: 632-636.
- Maddess ML, Tackett MN, Ley SV (2008). Total synthesis studies on macrocyclic pipercolic acid natural products: FK506, the antascomicins and rapamycin. *Prog. Drug Res.* **66**: 13, 15-186.
- Mager M (2022). Production of L-lysine derivatives in cell factories of *Corynebacterium glutamicum*. Bachelor Thesis, Institute of Systems biotechnology, Saarland University, Saarbrücken.
- Malla S, van der Helm E, Darbani B, Wieschalka S, Forster J, Borodina I, Sommer MOA (2022). A novel efficient L-lysine exporter Identified by functional metagenomics. *Front. Microbiol.* **13**: 855736.
- Martin JF, Barreiro C, Gonzalez-Lavado E, Barriuso M (2003). Ribosomal RNA and ribosomal proteins in corynebacteria. *J. Biotechnol.* **104**: 41-53.
- Melo RM, de Souza JMF, Williams TCR, Fontes W, de Sousa MV, Ricart CAO, do Vale LHF (2023). Revealing *Corynebacterium glutamicum* proteoforms through top-down proteomics. *Sci. Rep.* **13**: 2602.
- Melzer G, Esfandabadi ME, Franco-Lara E, Wittmann C (2009). Flux design: *In silico* design of cell factories based on correlation of pathway fluxes to desired properties. *BMC Syst. Biol.* **3**: 120.
- Mihalik SJ, Moser HW, Watkins PA, Danks DM, Poulos A, Rhead WJ (1989). Peroxisomal L-pipercolic acid oxidation is deficient in liver form Zellweger syndrome patients. *Pediatr. Res.* **25**: 548-552.
- Misono H, Hashimoto H, Uehigashi H, Nagata S, Nagasaki S (1989). Properties of L-lysine epsilon-dehydrogenase from *Agrobacterium tumefaciens*. *J. Biochem.* **105**: 1002-1008.
- Mohd Kamal K, Mahamad Maifiah MH, Abdul Rahim N, Hashim YZH, Abdullah Sani MS, Azizan KA (2022). Bacterial metabolomics: sample preparation methods. *Biochem. Res. Int.* **2022**: 9186536.
- Moker N, Brocker M, Schaffer S, Kramer R, Morbach S, Bott M (2004). Deletion of the genes encoding the MtrA-MtrB two-component system of *Corynebacterium glutamicum* has a strong influence on cell morphology, antibiotics susceptibility and expression of genes involved in osmoprotection. *Mol. Microbiol.* **54**: 420-438.
- Molnar I, Aparicio JF, Haydock SF, Khaw LE, Schwecke T, Konig A, Staunton J, Leadlay PF (1996). Organisation of the biosynthetic gene cluster for rapamycin in *Streptomyces hygroscopicus*: analysis of genes flanking the polyketide synthase. *Gene* **169**: 1-7.
- Moon MW, Park SY, Choi SK, Lee JK (2007). The phosphotransferase system of *Corynebacterium glutamicum*: features of sugar transport and carbon regulation. *J. Mol. Microbiol. Biotechnol.* **12**: 43-50.
- Moritz B, Striegel K, De Graaf AA, Sahm H (2000). Kinetic properties of the glucose-6-phosphate and 6-phosphogluconate dehydrogenases from *Corynebacterium glutamicum* and their application for predicting pentose phosphate pathway flux *in vivo*. *Eur J. Biochem.* **267**: 3442-3452.
- Moritz B, Striegel K, de Graaf AA, Sahm H (2002). Changes of pentose phosphate pathway flux *in vivo* in *Corynebacterium glutamicum* during leucine-limited batch cultivation as determined from intracellular metabolite concentration measurements. *Metab. Eng.* **4**: 295-305.
- Mormann S, Lomker A, Ruckert C, Gaigalat L, Tauch A, Puhler A, Kalinowski J (2006). Random mutagenesis in *Corynebacterium glutamicum* ATCC 13032 using an IS6100-based transposon vector identified the last unknown gene in the histidine biosynthesis pathway. *BMC Genomics* **7**: 205.
- Muramatsu H, Mihara H, Yasuda M, Ueda M, Kurihara T, Esaki N (2006). Enzymatic synthesis of L-pipercolic acid by delta1-piperideine-2-carboxylate reductase from *Pseudomonas putida*. *Biosci. Biotechnol. Biochem.* **70**: 2296-2298.

- Nakamura Y, Nishio Y, Ikeo K, Gojobori T (2003). The genome stability in *Corynebacterium* species due to lack of the recombinational repair system. *Gene* **317**: 149-155.
- Nakano T, Azuma T, Kuratsu Y. (1994). Process for producing L-lysine by iodothyronine resistant strain of *Mucorynebacterium glutamicum*. Kyowa Hakko Kogyo Co., Ltd., Japan. US5302521A
- Navarova H, Bernsdorff F, Doring AC, Zeier J (2012). Pipecolic acid, an endogenous mediator of defense amplification and priming, is a critical regulator of inducible plant immunity. *Plant Cell* **24**: 5123-5141.
- Neshich IA, Kiyota E, Arruda P (2013). Genome-wide analysis of lysine catabolism in bacteria reveals new connections with osmotic stress resistance. *Isme. J.* **7**: 2400-2410.
- Nešvera J, Pátek M (2011). Tools for genetic manipulations in *Corynebacterium glutamicum* and their applications. *Appl. Microbiol. Biotechnol.* **90**: 1641-1654.
- Niegemann E, Schulz A, Bartsch K (1993). Molecular organization of the *Escherichia coli* gab cluster: nucleotide sequence of the structural genes gabD and gabP and expression of the GABA permease gene. *Arch. Microbiol.* **160**: 454-460.
- Nielsen J (2017). Systems biology of metabolism. *Annu. Rev. Biochem.* **86**: 245-275.
- Nielsen TD, Hasselbalch J, Holmberg K, Stripple J (2019). Politics and the plastic crisis: A review throughout the plastic life cycle. *WIREs Energy and Environment* **9**.
- Ohnishi J, Ikeda M (2006). Comparisons of potentials for L-lysine production among different *Corynebacterium glutamicum* strains. *Biosci. Biotechnol. Biochem.* **70**: 1017-1020.
- Okino S, Suda M, Fujikura K, Inui M, Yukawa H (2008). Production of D-lactic acid by *Corynebacterium glutamicum* under oxygen deprivation. *Appl. Microbiol. Biotechnol.* **78**: 449-454.
- Pan Y, Nishida Y, Wang M, Verdin E (2012). Metabolic regulation, mitochondria and the life-prolonging effect of rapamycin: a mini-review. *Gerontology* **58**: 524-530.
- Papenfort K, Vanderpool CK (2015). Target activation by regulatory RNAs in bacteria. *FEMS Microbiol. Rev.* **39**: 362-378.
- Parise MTD, Parise D, Aburjaile FF, Pinto Gomide AC, Kato RB, Raden M, Backofen R, Azevedo VAC, Baumbach J (2021). An integrated database of small RNAs and their interplay with transcriptional gene regulatory networks in *Corynebacteria*. *Front. Microbiol.* **12**: 656435.
- Park SH, Kim HU, Kim TY, Park JS, Kim SS, Lee SY (2014a). Metabolic engineering of *Corynebacterium glutamicum* for L-arginine production. *Nat. Commun.* **5**: 4618.
- Park SJ, Kim EY, Noh W, Park HM, Oh YH, Lee SH, Song BK, Jegal J, Lee SY (2013). Metabolic engineering of *Escherichia coli* for the production of 5-aminovalerate and glutarate as C5 platform chemicals. *Metab. Eng.* **16**: 42-47.
- Park SJ, Oh YH, Noh W, Kim HY, Shin JH, Lee EG, Lee S, David Y, Baylon MG, Song BK, Jegal J, Lee SY, Lee SH (2014b). High-level conversion of L-lysine into 5-aminovalerate that can be used for nylon 6,5 synthesis. *Biotechnol. J.* **9**: 1322-1328.
- Park SR, Yoo YJ, Ban YH, Yoon YJ (2010). Biosynthesis of rapamycin and its regulation: past achievements and recent progress. *J. Antibiot. (Tokyo)* **63**: 434-441.
- Patek M, Nesvera J, Guyonvarch A, Reyes O, Leblon G (2003). Promoters of *Corynebacterium glutamicum*. *J. Biotechnol.* **104**: 311-323.
- Pauli S (2018). Systems biology of 5-aminovalerate and glutarate producing *Corynebacterium glutamicum*. Master of Science Thesis, Institute of Systems Biotechnology, Saarland University, Saarbrücken.

- Pavic A, Ji Y, Serafini A, Garza-Garcia A, McPhillie MJ, Holmes AOM, de Carvalho LPS, Wang Y, Bartlam M, Goldman A, Postis VLG (2021). Functional characterization of the gamma-aminobutyric acid transporter from *Mycobacterium smegmatis* MC(2) 155 reveals sodium-driven GABA transport. *J. Bacteriol.* **203**.
- Perez-Garcia F, Brito LF, Wendisch VF (2019). Function of L-pipecolic acid as compatible solute in *Corynebacterium glutamicum* as basis for its production under hyperosmolar conditions. *Front. Microbiol.* **10**: 340.
- Perez-Garcia F, Max Risse J, Friehs K, Wendisch VF (2017). Fermentative production of L-pipecolic acid from glucose and alternative carbon sources. *Biotechnol. J.* **12**.
- Perez-Garcia F, Peters-Wendisch P, Wendisch VF (2016). Engineering *Corynebacterium glutamicum* for fast production of L-lysine and L-pipecolic acid. *Appl. Microbiol. Biotechnol.* **100**: 8075-8090.
- Perez-Garcia F, Wendisch VF (2018). Transport and metabolic engineering of the cell factory *Corynebacterium glutamicum*. *FEMS Microbiol. Lett.* **365**.
- Peter H, Weik B, Burkovski A, Krämer R, Morbach S (1998). *Corynebacterium glutamicum* is equipped with four secondary carriers for compatible solutes: identification, sequencing, and characterization of the proline/ectoine uptake system, ProP, and the ectoine/proline/glycine betaine carrier, EctP. *J. Bacteriol.* **180**: 6005-6012.
- Pfeifer-Sancar K, Mentz A, Ruckert C, Kalinowski J (2013). Comprehensive analysis of the *Corynebacterium glutamicum* transcriptome using an improved RNAseq technique. *BMC Genomics* **14**: 888.
- Plecko B, Hikel C, Korenke GC, Schmitt B, Baumgartner M, Baumeister F, Jakobs C, Struys E, Erwa W, Stockler-Ipsiroglu S (2005). Pipecolic acid as a diagnostic marker of pyridoxine-dependent epilepsy. *Neuropediatrics* **36**: 200-205.
- Poblete-Castro I, Hoffmann SL, Becker J, Wittmann C (2020). Cascaded valorization of seaweed using microbial cell factories. *Curr. Opin. Biotechnol.* **65**: 102-113.
- Poupin P, Ducrocq V, Hallier-Soulier S, Truffaut N (1999). Cloning and characterization of the genes encoding a cytochrome P450 (PipA) involved in piperidine and pyrrolidine utilization and its regulatory protein (PipR) in *Mycobacterium smegmatis* mc(2)155. *J. Bacteriol.* **181**: 3419-3426.
- Prasad S, Ingle A (2019). Chapter 12 -impacts of sustainable biofuels production from biomass. In: Rai M, Ingle AP (eds) Sustainable Bioenergy, vol. **2019**. Elsevier.
- Prell C, Busche T, Ruckert C, Nolte L, Brandenbusch C, Wendisch VF (2021). Adaptive laboratory evolution accelerated glutarate production by *Corynebacterium glutamicum*. *Microb. Cell Fact.* **20**: 97.
- Prell C, Vonderbank S-A, Meyer F, Pérez-García F, Wendisch VF (2022). Metabolic engineering of *Corynebacterium glutamicum* for de novo production of 3-hydroxycadaverine. *CRBIOT* **4**: 32-46.
- Qi B, Zhang Y, Xu B, Fei G, Lin L, Li Q (2022). Metabolomic characterization of acute ischemic stroke facilitates metabolomic biomarker discovery. *Appl. Biochem. Biotechnol.* **194**: 5443-5455.
- Qiu YY, Chang QC, Gao JF, Bao MJ, Luo HT, Song JH, Hong SJ, Mao RF, Sun YY, Chen YY, Liu MY, Wang CR, Liu XL (2022). Multiple biochemical indices and metabolomics of *Clonorchis sinensis* provide a novel interpretation of biomarkers. *Parasit Vectors* **15**: 172.
- Rao VV, Chang YF (1990). L-pipecolic acid metabolism in human liver: detection of L-pipecolate oxidase and identification of its reaction product. *Biochim. Biophys. Acta.* **1038**: 295-299.
- Revelles O, Espinosa-Urgel M, Fuhrer T, Sauer U, Ramos JL (2005). Multiple and interconnected pathways for L-lysine catabolism in *Pseudomonas putida* KT2440. *J. Bacteriol.* **187**: 7500-7510.

- Riedel C, Rittmann D, Dangel P, Mockel B, Petersen S, Sahm H, Eikmanns BJ (2001). Characterization of the phosphoenolpyruvate carboxykinase gene from *Corynebacterium glutamicum* and significance of the enzyme for growth and amino acid production. *J. Mol. Microbiol. Biotechnol.* **3**: 573-583.
- Rohles C (2021). Systems metabolic engineering of *Corynebacterium glutamicum* for the production of five-carbon platform chemicals. Dissertation, Faculty of Science and Technology, Saarland University, Saarbrücken, Germany.
- Rohles CM, Giesselmann G, Kohlstedt M, Wittmann C, Becker J (2016). Systems metabolic engineering of *Corynebacterium glutamicum* for the production of the carbon-5 platform chemicals 5-aminovalerate and glutarate. *Microb. Cell Fact.* **15**: 154.
- Rohles CM, Gläser L, Kohlstedt M, Giesselmann G, Pearson S, del Campo A, Becker J, Wittmann C (2018). A bio-based route to the carbon-5 chemical glutaric acid and to bionylon-6,5 using metabolically engineered *Corynebacterium glutamicum*. *Green Chem.* **20**: 4662-4674.
- Roura Padrosa D, Benítez-Mateos AI, Calvey L, Paradisi F (2020). Cell-free biocatalytic syntheses of L-pipecolic acid: a dual strategy approach and process intensification in flow. *Green Chem.* **22**: 5310-5316.
- Ruldeekulthamrong P, Maeda S, Kato S, Shinji N, Sittipraneed S, Packdibamrung K, Misono H. (2008). Molecular characterization of lysine 6-dehydrogenase from *Achromobacter denitrificans*. *BMB Rep.* **41**: 790-795.
- Rytter JV, Helmark S, Chen J, Lezyk MJ, Solem C, Jensen PR (2014). Synthetic promoter libraries for *Corynebacterium glutamicum*. *Appl. Microbiol. Biotechnol.* **98**: 2617-2623.
- Sahm H, Eggeling L, de Graaf AA (2000). Pathway analysis and metabolic engineering in *Corynebacterium glutamicum*. *Biol. Chem.* **381**: 899-910.
- Sahm H, Eggeling L, Eikmanns BJ, Krämer R (1995). Metabolic design in amino acid producing bacterium *Corynebacterium glutamicum*. *FEMS Microbiol. Rev.* **16**: 243-252.
- Sakai S, Tsuchida Y, Nakamoto H, Okino S, Ichihashi O, Kawaguchi H, Watanabe T, Inui M, Yukawa H (2007). Effect of lignocellulose-derived inhibitors on growth of and ethanol production by growth-arrested *Corynebacterium glutamicum* R. *Appl. Environ. Microbiol.* **73**: 2349-2353.
- Sakanaka A, Kuboniwa M, Takeuchi H, Hashino E, Amano A (2015). Arginine-Ornithine Antiporter ArcD Controls Arginine Metabolism and Interspecies Biofilm Development of *Streptococcus gordonii*. *J. Biol. Chem.* **290**: 21185-21198.
- Sakanyan V, Petrosyan P, Lecocq M, Boyen A, Legrain C, Demarez M, Hallet JN, Glansdorff N (1996). Genes and enzymes of the acetyl cycle of arginine biosynthesis in *Corynebacterium glutamicum*: enzyme evolution in the early steps of the arginine pathway. *Microbiology (Reading)* **142 (Pt 1)**: 99-108.
- Sassi AH, Deschamps AM, Lebeault JM (1996). Process analysis of L-lysine fermentation with *Corynebacterium glutamicum* under different oxygen and carbon dioxide supplies and redox potentials. *Process Biochem.* **31**: 493-497.
- Sauer U, Canonaco F, Heri S, Perrenoud A, Fischer E (2004). The soluble and membrane-bound transhydrogenases UdhA and PntAB have divergent functions in NADPH metabolism of *Escherichia coli*. *J. Biol. Chem.* **279**: 6613-6619.
- Sauer U, Eikmanns BJ (2005). The PEP-pyruvate-oxaloacetate node as the switch point for carbon flux distribution in bacteria. *FEMS Microbiol. Rev.* **29**: 765-794.
- Saxena RK, Anand P, Saran S, Isar J (2009). Microbial production of 1,3-propanediol: Recent developments and emerging opportunities. *Biotechnol. Adv.* **27**: 895-913.
- Schäfer R (2016). Improvement of *Corynebacterium glutamicum* for production of lysine and ectoine from industrial raw materials. Dissertation, Faculty of Chemistry, Pharmacy, Bio- and Material Sciences, Faculty of Science and Technology, Saarland University, Saarbrücken, Germany.

- Schilling O, Frick O, Herzberg C, Ehrenreich A, Heinzle E, Wittmann C, Stulke J (2007). Transcriptional and metabolic responses of *Bacillus subtilis* to the availability of organic acids: transcription regulation is important but not sufficient to account for metabolic adaptation. *Appl. Environ. Microbiol.* **73**: 499-507.
- Schneider J, Niermann K, Wendisch VF (2011). Production of the amino acids L-glutamate, L-lysine, L-ornithine and L-arginine from arabinose by recombinant *Corynebacterium glutamicum*. *J. Biotechnol.* **154**: 191-198
- Schröder J, Tauch A (2010). Transcriptional regulation of gene expression in *Corynebacterium glutamicum*: the role of global, master and local regulators in the modular and hierarchical gene regulatory network. *FEMS Microbiol. Rev.* **34**: 685-737.
- Schroeter R, Hoffmann T, Voigt B, Meyer H, Bleisteiner M, Muntel J, Jurgen B, Albrecht D, Becher D, Lalk M, Evers S, Bongaerts J, Maurer KH, Putzer H, Hecker M, Schweder T, Bremer E (2013). Stress responses of the industrial workhorse *Bacillus licheniformis* to osmotic challenges. *PLoS One* **8**: e80956.
- Schrumpf B, Eggeling L, Sahm H (1992). Isolation and prominent characteristics of an L-lysine hyperproducing strain of *Corynebacterium glutamicum*. *Appl Microbiol. Biotechnol.* **37**: 566-571.
- Schwarzer A, Pühler A (1991). Manipulation of *Corynebacterium glutamicum* by gene disruption and replacement. *Biotechnology (N Y)* **9**: 84-87.
- Schwechheimer SK, Becker J, Wittmann C (2018). Towards better understanding of industrial cell factories: novel approaches for ¹³C metabolic flux analysis in complex nutrient environments. *Curr. Opin. Biotechnol.* **54**: 128-137.
- Schwentner A, Feith A, Munch E, Stiefelmaier J, Lauer I, Favilli L, Massner C, Ohrlein J, Grund B, Huser A, Takors R, Blombach B (2019). Modular systems metabolic engineering enables balancing of relevant pathways for L-histidine production with *Corynebacterium glutamicum*. *Biotechnol. Biofuels* **12**: 65.
- Shan L, He P (2018). Pipped at the post: pipercolic acid derivative identified as SAR regulator. *Cell* **173**: 286-287.
- Shen J, Chen J, Jensen PR, Solem C (2017). A novel genetic tool for metabolic optimization of *Corynebacterium glutamicum*: efficient and repetitive chromosomal integration of synthetic promoter-driven expression libraries. *Appl. Microbiol. Biotechnol.* **101**: 4737-4746.
- Sheng Q, Wu XY, Xu X, Tan X, Li Z, Zhang B (2021). Production of L-glutamate family amino acids in *Corynebacterium glutamicum*: Physiological mechanism, genetic modulation, and prospects. *Synth. Syst. Biotechnol.* **6**: 302-325.
- Shetty S, Kusminski CM, Scherer PE (2009). Adiponectin in health and disease: evaluation of adiponectin-targeted drug development strategies. *Trends Pharmacol. Sci.* **30**: 234-239.
- Shi F, Luan M, Li Y (2018). Ribosomal binding site sequences and promoters for expressing glutamate decarboxylase and producing gamma-aminobutyrate in *Corynebacterium glutamicum*. *AMB Express* **8**: 61.
- Shin JH, Park SH, Oh YH, Choi JW, Lee MH, Cho JS, Jeong KJ, Joo JC, Yu J, Park SJ, Lee SY (2016). Metabolic engineering of *Corynebacterium glutamicum* for enhanced production of 5-aminovaleric acid. *Microb. Cell Fact.* **15**: 174.
- Sievers F, Wilm A, Dineen D, Gibson TJ, Karplus K, Li W, Lopez R, McWilliam H, Remmert M, Soding J, Thompson JD, Higgins DG (2011). Fast, scalable generation of high-quality protein multiple sequence alignments using Clustal Omega. *Mol. Syst. Biol.* **7**: 539.
- Silva-Rocha R, Martinez-Garcia E, Calles B, Chavarria M, Arce-Rodriguez A, de Las Heras A, Paez-Espino AD, Durante-Rodriguez G, Kim J, Nikel PI, Platero R, de Lorenzo V (2013). The standard european vector architecture (SEVA): a coherent platform for the analysis and deployment of complex prokaryotic phenotypes. *Nucleic acids res.* **41**: D666-675.

- Smith KM, Cho KM, Liao JC (2010). Engineering *Corynebacterium glutamicum* for isobutanol production. *Appl. Microbiol. Biotechnol.* **87**: 1045-1055.
- Sommer A (2023). Production of 5-aminovaleramide using *Corynebacterium glutamicum*. Bachelor Thesis, Faculty of biotechnology, Mannheim University of Applied Sciences, Mannheim, Germany.
- Song C, Gao NY, Gao HW (2010). Transmembrane distribution of kanamycin and chloramphenicol: insights into the cytotoxicity of antibacterial drugs. *Mol. Biosyst.* **6**: 1901-1910.
- Steffes C, Ellis J, Wu J, Rosen BP (1992). The *lysP* gene encodes the lysine-specific permease. *J. Bacteriol.* **174**: 3242-3249.
- Steger R, Weinand M, Krämer R, Morbach S (2004). LcoP, an osmoregulated betaine/ectoine uptake system from *Corynebacterium glutamicum*. *FEBS Lett* **573**: 155-160.
- Steinegger M, Soding J (2018). Clustering huge protein sequence sets in linear time. *Nat. Commun.* **9**: 2542.
- Stincone A, Prigione A, Cramer T, Wamelink MM, Campbell K, Cheung E, Olin-Sandoval V, Gruning NM, Kruger A, Tauqeer Alam M, Keller MA, Breitenbach M, Brindle KM, Rabinowitz JD, Ralser M (2015). The return of metabolism: biochemistry and physiology of the pentose phosphate pathway. *Biol. Rev. Camb. Philos. Soc.* **90**: 927-963.
- Suzek BE, Wang Y, Huang H, McGarvey PB, Wu CH (2015). UniRef clusters: a comprehensive and scalable alternative for improving sequence similarity searches. *Bioinformatics* **31**: 926-932.
- Suzuki N, Okai N, Nonaka H, Tsuge Y, Inui M, Yukawa H (2006). High-throughput transposon mutagenesis of *Corynebacterium glutamicum* and construction of a single-gene disruptant mutant library. *Appl. Environ. Microbiol.* **72**: 3750-3755.
- Takeo S, Hori K, Ohtani S, Mimura A, Mitsunashi S, Ikeda M (2016). L-Lysine production independent of the oxidative pentose phosphate pathway by *Corynebacterium glutamicum* with the *Streptococcus mutans gapN* gene. *Metab. Eng.* **37**: 1-10.
- Takeo S, Murata R, Kobayashi R, Mitsunashi S, Ikeda M (2010). Engineering of *Corynebacterium glutamicum* with an NADPH-generating glycolytic pathway for L-lysine production. *Appl. Environ. Microbiol.* **76**: 7154-7160.
- Takeo S, Takasaki M, Urabayashi A, Mimura A, Muramatsu T, Mitsunashi S, Ikeda M (2013). Development of fatty acid-producing *Corynebacterium glutamicum* strains. *Appl. Environ. Microbiol.* **79**: 6776-6783.
- Tani Y, Miyake R, Yukami R, Dekishima Y, China H, Saito S, Kawabata H, Mihara H (2015). Functional expression of L-lysine alpha-oxidase from *Scomber japonicus* in *Escherichia coli* for one-pot synthesis of L-pipecolic acid from DL-lysine. *Appl. Microbiol. Biotechnol.* **99**: 5045-5054.
- Tauch A, Homann I, Mormann S, Ruberg S, Billault A, Bathe B, Brand S, Brockmann-Gretza O, Ruckert C, Schischka N, Wrenger C, Hoheisel J, Mockel B, Huthmacher K, Pfefferle W, Puhler A, Kalinowski J (2002). Strategy to sequence the genome of *Corynebacterium glutamicum* ATCC 13032: use of a cosmid and a bacterial artificial chromosome library. *J. Biotechnol.* **95**: 25-38.
- The Uniprot Consortium (2023). UniProt: the Universal Protein Knowledgebase in 2023. *Nucleic acids res.* **51**: D523-D531.
- Thompson MG, Pearson AN, Barajas JF, Cruz-Morales P, Sedaghatian N, Costello Z, Garber ME, Incha MR, Valencia LE, Baidoo EEK, Martin HG, Mukhopadhyay A, Keasling JD (2020). Identification, characterization, and application of a highly sensitive lactam biosensor from *Pseudomonas putida*. *ACS Synth. Biol.* **9**: 53-62.

- Tsotsou GE, Barbirato F (2007). Biochemical characterisation of recombinant *Streptomyces pristinaespiralis* L-lysine cyclodeaminase. *Biochimie* **89**: 591-604.
- Tsuge Y, Yamaguchi A (2021). Physiological characteristics of *Corynebacterium glutamicum* as a cell factory under anaerobic conditions. *Appl. Microbiol. Biotechnol.* **105**: 6173-6181.
- Turk SC, Kloosterman WP, Ninaber DK, Kolen KP, Knutova J, Suir E, Schurmann M, Raemakers-Franken PC, Muller M, de Wildeman SM, Raamsdonk LM, van der Pol R, Wu L, Temudo MF, van der Hoeven RA, Akeroyd M, van der Stoel RE, Noorman HJ, Bovenberg RA, Trefzer AC (2016). Metabolic engineering toward sustainable production of nylon-6. *ACS Synth. Biol.* **5**: 65-73.
- Vandecasteele JP, Hermann M (1972). Regulation of a catabolic pathway. Lysine degradation in *Pseudomonas putida*. *Eur. J. Biochem.* **31**: 80-85.
- Varadi M, Anyango S, Deshpande M, Nair S, Natassia C, Yordanova G, Yuan D, Stroe O, Wood G, Laydon A, Zidek A, Green T, Tunyasuvunakool K, Petersen S, Jumper J, Clancy E, Green R, Vora A, Lutfi M, Figurnov M, Cowie A, Hobbs N, Kohli P, Kleywegt G, Birney E, Hassabis D, Velankar S (2022). AlphaFold Protein Structure Database: massively expanding the structural coverage of protein-sequence space with high-accuracy models. *Nucleic acids res.* **50**: D439-D444.
- Vardon DR, Franden MA, Johnson CW, Karp EM, Guarnieri MT, Linger JG, Salm MJ, Strathmann TJ, Beckham GT (2015). Adipic acid production from lignin. *Energy Environ. Sci.* **2015**: 617.
- Vranova V, Lojkova L, Rejsek K, Formanek P (2013). Significance of the natural occurrence of L- versus D-pipecolic acid: a review. *Chirality* **25**: 823-831.
- Vrljic M, Sahm H, Eggeling L (1996). A new type of transporter with a new type of cellular function: L-lysine export from *Corynebacterium glutamicum*. *Mol. Microbiol.* **22**: 815-826.
- Wang J, Gao C, Chen X, Liu L (2021a). Chapter one - Expanding the lysine industry: biotechnological production of L-lysine and its derivatives. *Advances in Appl. Microbiol.* **115**: 1-33.
- Wang Q, Zhang J, Al Makishah NH, Sun X, Wen Z, Jiang Y, Yang S (2021b). Advances and perspectives for genome editing tools of *Corynebacterium glutamicum*. *Front. Microbiol.* **12**: 654058.
- Wang X, Cai P, Chen K, Ouyang P (2016). Efficient production of 5-aminovalerate from L-lysine by engineered *Escherichia coli* whole-cell biocatalysts. *J. Mol. Catal. B Enzym.* **134**: 115-121.
- Wehrmann A, Phillipp B, Sahm H, Eggeling L (1998). Different modes of diamino-pomelate synthesis and their role in cell wall integrity: a study with *Corynebacterium glutamicum*. *J. Bacteriol.* **180**: 3159-3165.
- Weighill D, Tschaplinski TJ, Tuskan GA, Jacobson D (2019). Data integration in poplar: 'omics layers and integration strategies. *Front. Genet.* **10**: 874.
- Weiland F, Barton N, Kohlstedt M, Becker J, Wittmann C (2023). Systems metabolic engineering upgrades *Corynebacterium glutamicum* to high-efficiency *cis, cis*-muconic acid production from lignin-based aromatics. *Metab. Eng.* **75**: 153-169.
- Weiland F, Kohlstedt M, Wittmann C (2022). Guiding stars to the field of dreams: Metabolically engineered pathways and microbial platforms for a sustainable lignin-based industry. *Metab. Eng.* **71**: 13-41.
- Weixler D, Berghoff M, Ovchinnikov KV, Reich S, Goldbeck O, Seibold GM, Wittmann C, Bar NS, Eikmanns BJ, Diep DB, Riedel CU (2022). Recombinant production of the lantibiotic nisin using *Corynebacterium glutamicum* in a two-step process. *Microb. Cell Fact.* **21**: 11.

- Wendisch VF, Spies M, Reinscheid DJ, Schnicke S, Sahm H, Eikmanns BJ (1997). Regulation of acetate metabolism in *Corynebacterium glutamicum*: transcriptional control of the isocitrate lyase and malate synthase genes. *Arch. Microbiol.* **168**: 262-269.
- Westman SM, Kloth KJ, Hanson J, Ohlsson AB, Albrechtsen BR (2019). Defence priming in *Arabidopsis* - a meta-analysis. *Sci. Rep.* **9**: 13309.
- Wittmann C, Becker J (2007). The L-lysine story: from metabolic pathways to industrial production. In: Wendisch VF (eds) Amino Acid Biosynthesis ~ Pathways, Regulation and Metabolic Engineering. *Microbiology Monographs*, vol **5**. Springer, Berlin, Heidelberg.
- Wittmann C, Heinzle E (2001a). Application of MALDI-TOF MS to lysine-producing *Corynebacterium glutamicum*: a novel approach for metabolic flux analysis. *Eur. J. Biochem.* **268**: 2441-2455.
- Wittmann C, Heinzle E (2001b). MALDI-TOF MS for quantification of substrates and products in cultivations of *Corynebacterium glutamicum*. *Biotechnol. Bioeng.* **72**: 642-647.
- Wittmann C, Heinzle E (2002). Genealogy profiling through strain improvement by using metabolic network analysis: metabolic flux genealogy of several generations of lysine-producing *Corynebacteria*. *Appl. Environ. Microbiol.* **68**: 5843-5859.
- Wittmann C, Kiefer P, Zelder O (2004a). Metabolic fluxes in *Corynebacterium glutamicum* during lysine production with sucrose as carbon source. *Appl. Environ. Microbiol.* **70**: 7277-7287.
- Wittmann C, Kim HM, Heinzle E (2004b). Metabolic network analysis of lysine producing *Corynebacterium glutamicum* at a miniaturized scale. *Biotechnol. Bioeng.* **87**: 1-6.
- Wolf S, Becker J, Tsuge Y, Kawaguchi H, Kondo A, Marienhagen J, Bott M, Wendisch VF, Wittmann C (2021). Advances in metabolic engineering of *Corynebacterium glutamicum* to produce high-value active ingredients for food, feed, human health, and well-being. *Essays Biochem.* **65**: 197-212.
- Wood JM, Bremer E, Csonka LN, Kraemer R, Poolman B, van der Heide T, Smith LT (2001). Osmosensing and osmoregulatory compatible solute accumulation by bacteria. *Comp. Biochem. Physiol. A. Mol. Integr. Physiol.* **130**: 437-460.
- Wu W, Zhang Y, Liu D, Chen Z (2019a). Efficient mining of natural NADH-utilizing dehydrogenases enables systematic cofactor engineering of lysine synthesis pathway of *Corynebacterium glutamicum*. *Metab. Eng.* **52**: 77-86.
- Wu XY, Guo XY, Zhang B, Jiang Y, Ye BC (2019b). Recent advances of L-ornithine biosynthesis in metabolically engineered *Corynebacterium glutamicum*. *Front. Bioeng. Biotechnol.* **7**: 440.
- Xiao J, Wang D, Wang L, Jiang Y, Xue L, Sui S, Wang J, Guo C, Wang R, Li N, Fan H, Lv M (2020). Increasing L-lysine production in *Corynebacterium glutamicum* by engineering amino acid transporters. *Amino Acids* **52**: 1363-1374.
- Xu J, Han M, Zhang J, Guo Y, Zhang W (2014). Metabolic engineering *Corynebacterium glutamicum* for the L-lysine production by increasing the flux into L-lysine biosynthetic pathway. *Amino Acids* **46**: 2165-2175.
- Xu JZ, Ruan HZ, Chen XL, Zhang F, Zhang W (2019a). Equilibrium of the intracellular redox state for improving cell growth and L-lysine yield of *Corynebacterium glutamicum* by optimal cofactor swapping. *Microb. Cell Fact.* **18**: 65.
- Xu JZ, Ruan HZ, Yu HB, Liu LM, Zhang W (2020). Metabolic engineering of carbohydrate metabolism systems in *Corynebacterium glutamicum* for improving the efficiency of L-lysine production from mixed sugar. *Microb. Cell. Fact.* **19**: 39.
- Xu JZ, Wu ZH, Gao SJ, Zhang W (2018a). Rational modification of tricarboxylic acid cycle for improving L-lysine production in *Corynebacterium glutamicum*. *Microb. Cell Fact.* **17**: 105.

- Xu JZ, Yang HK, Liu LM, Wang YY, Zhang WG (2018b). Rational modification of *Corynebacterium glutamicum* dihydrodipicolinate reductase to switch the nucleotide-cofactor specificity for increasing L-lysine production. *Biotechnol. Bioeng.* **115**: 1764-1777.
- Xu JZ, Yu HB, Han M, Liu LM, Zhang WG (2019b). Metabolic engineering of glucose uptake systems in *Corynebacterium glutamicum* for improving the efficiency of L-lysine production. *J. Ind. Microbiol. Biotechnol.* **46**: 937-949.
- Xu X, Rao ZM, Xu JZ, Zhang WG (2022). Enhancement of L-pipecolic acid production by dynamic control of substrates and multiple copies of the *pipA* gene in the *Escherichia coli* genome. *ACS Synth. Biol.* **11**: 760-769.
- Yamauchi Y, Hirasawa T, Nishii M, Furusawa C, Shimizu H (2014). Enhanced acetic acid and succinic acid production under microaerobic conditions by *Corynebacterium glutamicum* harboring *Escherichia coli* transhydrogenase gene *pntAB*. *J. Gen. Appl. Microbiol.* **60**: 112-118.
- Yang P, Liu W, Chen Y, Gong AD (2022). Engineering the glyoxylate cycle for chemical bioproduction. *Front. Bioeng. Biotechnol.* **10**: 1066651.
- Yim SH, Jung S, Lee SK, Cheon CI, Song E, Lee SS, Shin J, Lee MS (2011). Purification and characterization of an arginine regulatory protein, ArgR, in *Corynebacterium glutamicum*. *J. Ind. Microbiol. Biotechnol.* **38**: 1911-1920.
- Yim SS, An SJ, Kang M, Lee J, Jeong KJ (2013). Isolation of fully synthetic promoters for high-level gene expression in *Corynebacterium glutamicum*. *Biotechnol. Bioeng.* **110**: 2959-2969.
- Ying H, Tao S, Wang J, Ma W, Chen K, Wang X, Ouyang P (2017). Expanding metabolic pathway for de novo biosynthesis of the chiral pharmaceutical intermediate L-pipecolic acid in *Escherichia coli*. *Microb. Cell Fact.* **16**: 52.
- Yoneda K, Fukuda J, Sakuraba H, Ohshima T (2010). First crystal structure of L-lysine 6-dehydrogenase as an NAD-dependent amine dehydrogenase. *J. Biol. Chem.* **285**: 8444-8453.
- Yu X, Shi F, Liu H, Tan S, Li Y (2021). Programming adaptive laboratory evolution of 4-hydroxyisoleucine production driven by a lysine biosensor in *Corynebacterium glutamicum*. *AMB Express* **11**: 66.
- Zahoor A, Lindner SN, Wendisch VF (2012). Metabolic engineering of *Corynebacterium glutamicum* aimed at alternative carbon sources and new products. *Comput Struct. Biotechnol. J.* **3**: e201210004.
- Zemanova M, Kaderabkova P, Patek M, Knoppova M, Silar R, Nesvera J (2008). Chromosomally encoded small antisense RNA in *Corynebacterium glutamicum*. *FEMS Microbiol. Lett.* **279**: 195-201.
- Zhang B, Yu M, Zhou Y, Li Y, Ye BC (2017a). Systematic pathway engineering of *Corynebacterium glutamicum* S9114 for L-ornithine production. *Microb. Cell Fact.* **16**: 158.
- Zhang B, Zhou N, Liu YM, Liu C, Lou CB, Jiang CY, Liu SJ (2015). Ribosome binding site libraries and pathway modules for shikimic acid synthesis with *Corynebacterium glutamicum*. *Microb. Cell Fact.* **14**: 71.
- Zhang J, Barajas JF, Burdu M, Wang G, Baidoo EE, Keasling JD (2017b). Application of an acyl-CoA ligase from *Streptomyces aizunensis* for lactam biosynthesis. *ACS Synth. Biol.* **6**: 884-890.
- Zhang S, Liu D, Mao Z, Mao Y, Ma H, Chen T, Zhao X, Wang Z (2018). Model-based reconstruction of synthetic promoter library in *Corynebacterium glutamicum*. *Biotechnol. Lett.* **40**: 819-827.
- Zhao Z, Cai M, Liu Y, Hu M, Yang F, Zhu R, Xu M, Rao Z (2022). Genomics and transcriptomics-guided metabolic engineering *Corynebacterium glutamicum* for *Biotechnology Letters* L-arginine production. *Bioresour. Technol.* **364**: 128054.